Integrated simulation and multi-site optimisation of wind-operated alkaline water electrolysis for green hydrogen production in Kuwait

A Thesis Submitted for the Degree of Doctor of Philosophy

By

Abdulrahman M H A H Alhajeri

Department of Mechanical and Aerospace Engineering, Brunel University London

2026

Abstract

Diversification of energy mix to meet Vision 2035 sustainability goals is a main challenge facing Kuwait. Green hydrogen production is expected to be one of the solutions. Therefore, this research investigates the technical and economic feasibility of using alkaline water electrolysis to convert intermittent wind resources into green hydrogen, focusing on three strategic sites: Airport, Wafra, and Abdaly.

The methodology includes utilisation of a multi-stage modeling framework. A mathematical model was developed in Excel, using semi-empirical equations (Hug and Ulleberg models) to characterise the non-linear relationships between current density, cell voltage, and Faraday efficiency. The Excel model was integrated with TRNSYS for transient system analysis and optimised using HOMER Pro to determine the Levelised Cost of Hydrogen (LCOH).

The results show significant differences in site potential and performance. The Airport site appeared as the most feasible, achieving an annual hydrogen production of 469.8 kg (Excel) and 162.65 kg (TRNSYS), with Specific Energy Consumption (SEC) of 52.9 kWh/kg. The Abdaly site showed an efficiency cliff, where low current densities during winter months decreased Faraday efficiency and increased SEC to 407.4 kWh/kg. The comparative analysis reveals that static models (Excel) tend to overpredict energy penalties at Wafra and Abdaly sites by up to 69% compared to dynamic simulations (TRNSYS), which benefit from control logic and battery buffering.

HOMER Pro techno-economic analysis results show that system at the Airport site achieved lowest Levelised Cost of Energy (LCOE) of $1.14/kWh and LCOH of $9.03/kg. Irrespective of the high initial capital investment ($103,652), the system demonstrates strategic feasibility for decentralised, zero-emission applications. The study concludes that off-grid wind-operated systems at the Wafra and Abdaly sites are technically inefficient and economically unfeasible without hybridisation with solar arrays. These findings provide a critical roadmap for Kuwaiti policymakers to develop site-specific renewable clusters and adopt encouraging subsidy amendments to evolve competitive local hydrogen systems.

Keywords: Green Hydrogen, Alkaline Electrolyser, Wind Energy, Kuwait, Techno-Economic Assessment, TRNSYS, HOMER Pro, LCOH.

Declaration

No part of this thesis has been submitted in support of an application for any degree or qualification of Brunel University London or any other University or Institute of learning.

Acknowledgments

First, I would like to express my deep gratitude to my supervisor Professor Hussam Jouhara, for his guidance, support, and passion for sustainable energy research. His expertise, advice, and encouragement directed my research toward successful completion.

I am also grateful to Dr. Bertrand Delpech for his help, support and advice, which were helpful for the successful completion of this work.

Special recognitions are also due to Dr. Heba Ghazal and Dr. Valentina Olabi for their time, constructive feedback, and the contributions they offered during the various stages of my research.

I would also like to extend my sincere thanks to my researcher development advisor, Dr. Jurgita Malinauskaite, for her support and for providing the professional development tools required to navigate the journey of my research.

My research journey would not have been possible without the support and encouragement of this exceptional supervisory team. Their guidance has helped me complete this thesis and greatly impacted my development as a researcher interested in green hydrogen technology advancements.

Beyond the academic supervision, I also express my sincere gratitude to my parents, brothers and sisters, family and friends for their unconditional love and patience throughout my long years of study. Their constant help and support charged me with strength I needed to continue challenging the difficulties I have experienced during my research.

Finally, I would like to acknowledge Brunel University staff for providing the resources and facilities that made this work possible. To everyone who contributed to my research, whether through a brief conversation or years of support: thank you for being part of my achievement.

Publications

Alhajeri, A., Ghazal, H., Olabi, V. and Jouhara, H. (2025). Technical assessment of green hydrogen production in Kuwait. *International Journal of Hydrogen Energy*, Vol. 144, pp. 924-931.

Jouhara, H., Kodresko, A., Alhajeri, A., Olabi, V. and Ghazal, H. (2025). Cutting-edge advances in hydrogen applications for the medical and pharmaceutical industries. *International Journal of Hydrogen Energy*, Vol. 189, Article: 152181.

Olabi, V., Alhajeri, A. and Jouhara, H. (2025). Designing a sustainable hydrogen supply chain network in the Gulf Cooperation Council (GCC) region: Multi-objective optimisation using a Kuwait case-study. *International Journal of Hydrogen Energy*, Vol. 142, No. 1, pp. 994-1013.

Olabi, V., Alhajeri, A., Ghazal, H. and Jouhara, H. (2026). Dynamic multi-objective, multi-period optimisation of a hydrogen supply chain in the Gulf Cooperation Council (GCC) region: A Saudi Arabia case study. *International Journal of Hydrogen Energy*, Vol. 231, Article: 154838.

Nomenclatures

Symbols

Symbol	Meaning	Units
a	Constant	---
A	Electrolyser surface area	m^2
A	Diode ideality factor	---
A_{rotor}	Turbine rotor swept area	m^2
b	Volume of hydrogen gas molecules	m^3
B	Constant	K/m
C_{ann}	Annualised cost	$
C_{Com}	Component capital cost	$
C_{Fuel}	Fuel cost	$
$C_{O\&M}$	Operation and maintenance cost	$
C_{Rep}	Replacement cost	$
C_{Sal}	Salvage value	$
CO_2	Carbon dioxide	---
C_p	Turbine power coefficient	---
E_{def}	Deferrable load	kWh
$E_{grid,sales}$	Energy sold to the grid	kWh
$E_{prim,AC}$	Primary AC electrical load	kWh
$E_{prim,DC}$	Primary DC electrical load	kWh
E_{served}	Served electrical load	kWh
f	Annual inflation rate	%
f_1	Constant	A^2/m^4
f_2	Constant	---
F	Faraday constant	C/mol
G	Solar radiation	W/m^2
G	Gibbs energy	J/kg
GHI	Global horizontal irradiance	$kWh/m^2/day$
G_{ref}	Reference solar irradiance	W/m^2
h	Rotor hub height	m
H	Enthalpy	J/kg
H_2	Hydrogen gas	---
i'	Nominal interest rate	%
i_d	Discount rate	%
I	Current	A
$I_{density}$	Current density of each cell	A
I_{ely}	Electrolyser cell current	A
I_L	Photocurrent	A

Symbol	Meaning	Units
I_o	Reverse saturation current	A
I_{sc}	Short circuit current	A
$I_{sc,ref}$	Reference short circuit current	A
k	Boltzmann constant	J/K
M_{H_2}	Hydrogen mass	kg
n	Project lifetime	Years
n	Number of electrons	---
n_{H_2}	Number of hydrogen moles	mol
n_{O_2}	Number of oxygen moles	mol
$N_{cells}; N_s$	Number of series cells	---
O_2	Oxygen gas	---
p	Pressure	Pa
p_{cr}	Critical pressure	Pa
P	Power	W
q	Electron charge	coulomb
R	Gas constant	J/kgK
R_{ohm}	Ohmic resistance	Ohm
R_s	Series resistance	Ohm
s	Constant loss parameter	---
s	Tafel slope constant	V
S	Constant	---
S	Entropy	J/kgK
t	Constant loss parameter	---
t_1	Empirical temperature coefficient	m^2/A
t_2	Empirical temperature coefficient	m^2 °C/A
t_3	Empirical temperature coefficient	m^2 $°C^2/A$
T	Temperature	K
T_{cr}	Critical temperature	K
T_{atm}	Atmospheric temperature	°C
T_{ref}, T_o	Reference temperature	°C, K
U_{act}	Activation overvoltage	V
U_{cell}	Electrloyser cell voltage	V
U_L	Heat loss coefficient	W/m^2K
U_{Ohm}	Ohmic voltage	V
U_{rev}	Reversible cell voltage	V
U_s	Set point of the electrolyser cell voltage	V
U_{therm}	Enthalpic volt	V
U_{tn}	Thermonutral voltage	V
v_{elec}	Electricity price	$/kWh
v_g	Wind speed at 10 m from the ground	m/s
v_w	Wind speed at the hub height	m/s

Symbol	Meaning	Units
V	Voltage	V
V_{oc}	Open circuit voltage	V
$V_{oc,ref}$	Reference open circuit voltage	V
W_{el}	Electric energy	kWh
w_{poly}	Polytropic compression work	J/kg
Z	Number of exchanged electrons	---
Z_0	Roughness length	m

Greek Symbols

Symbol	Meaning	Units
α	Reflectance; Power law exponent	---
α_L	Factor	---
γ	Parameter related to ohmic resistance	---
δ_d	Daily perturbation factor	---
δ_h	Hourly perturbation factor	---
Δ	Change	---
ρ_{air}	Air density	kg/m^3
τ	Transmittance	---
η_F	Faraday efficiency	%
η_{HHV}	Higher heating value efficiency	%
η_{PV}	Conversion efficiency	%
η_{volt}	Voltage efficiency	%
$\mu_{I_{sc}}$	Temperature coefficient of short circuit current	A/°C
$\mu_{V_{oc}}$	Temperature coefficient of open circuit voltage	V/°C

Abbreviations

Abbreviation	Meaning
AEM	Anion Exchange Membrane
AFC	Alkaline Fuel Cell
AWE	Alkaline Water Electrolyser
BESS	Electricity Storage Battery
CAPEX	Capital Expenditure
CF	Capacity Factor
CI	Clearness Index
CRF	Capital Recovery Factor
DC	Direct Current
DoD	Depth of Charge
ELE	Electrolyser
FC	Fuel Cell
GCC	Gulf Cooperation Council
GEIF	Grid Energy Interaction Factor

Abbreviation	Meaning
GHG	Greenhouse gas
HER	Hydrogen Evolution Reaction
HHV	Higher Heating Value (J/kg)
HOMER	Hybrid Optimization Model for Electrical Renewables
INV	Inverters
IRENA	International Renewable Energy Agency
KISR	Kuwait Institute for Scientific Research
LCOE	Levelised Cost of Energy ($/kWh)
LCOH	Levelised Cost of Hydrogen ($/kg H_2)
LHV	Lower Heating Value (J/kg)
MAPE	Mean Absolute Percentage Error
NA	Not Available
NASA	National Aeronautics and Space Administration
NG	Natural Gas
NPC	Net Present Cost ($)
NREL	National Renewable Energy Laboratory
O&M	Operation and Maintenance
OER	Oxygen Evolution Reaction
OPEX	Operating Expenditure
PEM	Proton Exchange Membrane; Polymer Electrolyte Membrane
PFSA	PerFluroSulfonated Acid
PPS	PolyPhenilene Sulphide
PV	Photovoltaic
QAPS	Quaternary Ammonia PolySulfone
R&D	Research and Development
RE	Renewable Energy
SB	Storage Battery
SEC	Specific Energy Consumption (kWh/kg H_2)
SLF	Satisfied Load Fraction
SOC	State of charge
SOEC	Solid Oxide Electrolyser Cell
ST	Storage Tank
STP	Standard Temperature and Pressure
TRNSYS	TRaNsient SYstems Simulation tool
UF	Utilisation Factor
WP	Wind Power
WT	Wind Turbine
YSZ	Yttria-Stabilised Zirconia

Table of Contents

List of Figures

List of Tables

Chapter 1: Introduction

1.1 Background

The energy sectors all over the globe are now considering significant shifts toward emission reduction and decarbonisation. These shifts are mainly driven by critical needs for a quick intervention to mitigate climate change and comply with the strict environmental laws and regulations. As many countries are requesting energy-secure transition from fossil fuels, alterative green fuels are proposed. Among the alternatives of growing interest is the green hydrogen, which is produced using renewable energy sources. Green hydrogen produced using water electrolysis, operated by renewable energy, has been proposed as a key route for future sustainability of energy (Algburi et al., 2025; Elegbeleyeet al., 2025). Compared with traditional grey and blue hydrogen, green has a lifecycle of low carbon footprint. Therefore, it is a necessary solution for economy sectors experiencing technical difficulties to mitigate carbon emissions, particularly the transport sector (Roy et al., 2025).

Governments of Gulf Cooperation Council (GCC) countries such as Kuwait are now paying increased attention to the transition toward hydrogen economy. Their efforts and initiatives are driven by the impact of hydrogen economy on environment and strategic diversification of energy sources (Sanfilippo et al., 2024). For Kuwait, the adoption of renewable energy (RE) mega projects and the development of RE infrastructure are essential for the national development plan known as New Kuwait Vision 2035. Kuwaiti government is targeting 15% increase of RE share in the national energy mix by 2030 (Hamed et al., 2026). During the past few decades, renewable energy plans in Kuwait has mainly focused on the utility-scale (large-scale) renewable energy mega-projects such as Shagaya Renewable Energy Park. At present, more attention is paid to the small-scale and decentralised green energy systems to achieve the 7.4% target reduction in carbon emissions by 2035 (Kuwait Solar News, 2026).

Among the green hydrogen production technologies, water electrolysis is well-established and commonly used. Compared to other technologies, Alkaline Water Electrolysers (AWEs) are the most mature and commercially available equipment for green hydrogen production (Al Dhahri et al., 2026). Therefore, they are suitable for green hydrogen production systems operated by renewable energy systems (Shehzad et al., 2026). AWEs characterise by robust designs, reliable operation, extended service life, and relatively low capital cost relative to

other electrolysis systems such as Proton Exchange Membrane (PEM) (Vedrtnamet al., 2025). However, the use of AWEs for off-grid renewable energy systems has characteristic technical barriers, especially when operated by wind power of intermittent nature (Nguyen et al., 2024). In arid countries such as Kuwait, these systems operate under harsh weather conditions such as frequent occurrence of sandstorms and high ambient temperatures. Under harsh conditions, these systems may experience low stack efficiency, short service life, increased auxiliary cooling energy, and high maintenance cost (Awad et al., 2024).

Nowadays, large-scale green hydrogen production systems are well-documented, with lack of research on the applications of small-scale production systems. At present, techno-economic feasibility of small-scale systems operated using wind and solar energy remains under investigation. These systems are suitable for on-site green hydrogen production, which limits the costs and logistical needs of gas transportation (Arpino et al., 2024). They can be used for seasonal energy storage to store excess summer renewable energy for winter use. They can also be used to fuel small-scale combined heat and power systems to generate both electricity and heat for residential and commercial buildings (Tatti et al., 2024; Yaici and Longo, 2025). Moreover, these systems are promising for transportation sector by producing fuel in local hydrogen stations for fuelling bus fleets and/or light-duty vehicles (Simunovic et al., 2022; Caponi et al., 2025).

In Kuwait, there are noticeable variations in wind speeds and accordingly in wind energy potential between the coastal urban areas (such as Kuwait Airport) and the remote inland areas such as Wafra and Abdaly (Alsaffar et al., 2025). Usually, coastal sites such as Kuwait Airport have high wind speeds sufficient to annually produce about 300 metric tonnes of green hydrogen via wind-operated electrolysers (Alawadhi, 2023; Alhajeri et al., 2025). On the other hand, remote inland sites like Wafra and Abdaly have moderate wind speeds, but still suitable to annually produce about 172 and 145 metric tonnes of green hydrogen (Kamel et al., 2024; Alhajeri et al., 2025).

The strategic energy transition in Kuwait necessitates searching for sustainable alternative fuels of low-carbon footprint, such as green hydrogen, to fulfil the needs of domestic and industrial sectors. Therefore, using wind energy to operate alkaline water electrolysers is an important solution aligning with Kuwait energy strategy. Despite the relatively high costs of hydrogen production using wind-operated electrolysis systems, the technical and economic feasibility studies for potential sites in Kuwait become a central research area. Installation

of small-scale wind-operated hydrogen production systems at different sites is expected to boost the governmental efforts for achieving carbon neutrality in Kuwait. Thu, building up knowledge on the performance of small-scale wind-operated systems at various sites is essential for producing hydrogen at low cost to ensure sustainable and reliable decentralised source of green fuel.

Studying the performance and economics of wind-operated electrolysis systems can be accomplished using experiments and/or software simulation. For the present study, software simulation was selected over experimental trials as it offers cost-effective, time saving, and safe research method to evaluate green hydrogen systems operating under the harsh weather of Kuwait. Also, software simulation eliminates the need for large capital of wind turbine, electrolyser, and other equipment. Using simulation tools such as TRNSYS and HOMER software enable fast and risk-free modelling, which remarkably suits multi-site comparison. Thus, studying the dynamic system performance using TRNSYS simulations and optimising system economics using HOMER software were adopted in the present research to achieve a benchmark, technically and financially, for small-scale wind-operated localised green hydrogen production systems.

1.2 Research Problem

Decreasing carbon footprint, by expanding the use of green energy, in Kuwait is currently challenging the lack of infrastructure of small-scale green hydrogen production systems. The large-scale projects such as Shagaya Renewable Energy Park are focusing on large capacity production. There is therefore a noticeable gap of research on the technical and financial feasibility of small-scale off-grid hydrogen production systems.

The models proposed in previous research are not adequate (Daoudi and Bounahmidi, 2024) to identify the regional placement sites for best performance and economics. These models overlook the way with which the change in wind speeds, particularly at Kuwait Airport area against remote areas such as Wafra and Abdaly, significantly affect the hydrogen production costs in off-grid renewable energy systems.

In the absence of robust techno-economic studies that balances the intermittent nature of wind energy with the requirements and storage of small-scale green hydrogen production systems, it remains high level of uncertainty about the way with which the off-grid systems at these sites may achieve practicality and feasibility in the harsh and arid environment.

Therefore, key problem to address in the present research is the lack of economic frameworks for the promising installation sites of small-scale off-grid hydrogen production systems in Kuwait. Reaching at such economic frameworks helps to explain the method with which the geographical location of installation site affects the operational and financial achievement of small-scale off-grid green hydrogen production systems.

1.3 Research Significance

The novelty of the present study lies in its concentration on decentralised, small-scale green hydrogen production systems, a departure from the models focusing on large-scale high-capacity systems which dominate the present literature in Gulf Cooperation Council (GCC) area. The large-scale systems produce bulk power; but they do not successfully deal with the challenge of decreasing emissions in various applications. By concentrating on small-scale systems, this research offers a technical and economic investigation of small-scale systems, which are very important for Kuwait.

The small-scale wind-operated green hydrogen production systems allow for:

- Development of integrated systems to prove that small-scale off-grid production systems can successfully operate away from Kuwait national grid, which can decrease the initial capital costs for small and private investors.
- Identification of the installation site advantage, such as the Airport site, which offers a benchmark for urban-installed systems over systems installed at remote areas such as Wafra and Abdaly.
- Determination of the feasibility of off-grid hydrogen production system as a reliable source of green fuels for local, remote, and light-duty applications needed for regional and industrial logistics in Kuwait.
- Granting novelty of research methodology by integrating the physics of mathematical model, dynamic simulation of TRNSYS software, and economic and optimisation of HOMER Pro software.

1.4 Aim and Objectives

1.4.1 Aim

The aim of this study is to investigate the techno-economic feasibility of a small-scale off-grid wind-operated green hydrogen production system in Kuwait.

1.4.2 Objectives

To achieve the research aim, the objectives are:

Objective 1: Development of a physical mathematical model using Microsoft Excel software to characterise the electrochemical response of alkaline water electrolysers.

Objective 2: Simulation of the hourly performance of small-scale green hydrogen production system using TRNSYS software to assess system reliability under intermittent wind profiles in Kuwait.

Objective 3: Use TRNSYS software to conduct a comparative multi-site analysis for the geographically distinct sites Airport, Wafra, and Abdaly, to assess the effect of local weather conditions on hydrogen production capacity and cost.

Objective 4: Optimise the system design using HOMER Pro software to find out the lowest hydrogen production cost and identify optimum size and capacity of system components.

Objective 5: Perform sensitivity analysis on green hydrogen demand scaling and wind power variability to evaluate hydrogen production costs.

1.5 Research Questions

The research questions were formulated as follows:

Q1) How does Kuwait's weather conditions affect the operational efficiency and hydrogen production cost of a small-scale off-grid alkaline water electrolysis system?

Q2) Which geographical site in Kuwait offers the highest technical reliability and lowest hydrogen cost for small-scale hydrogen demand?

Q3) What is the effect of wind intermittency on hydrogen storage capacity for a small-scale off-grid hydrogen production system?

Q4) What is the lowest achievable hydrogen production cost for a small-scale off-grid wind-operated green hydrogen production system, and how does the system components change with HOMER Pro optimisation?

1.6 Study Scope and Limitations

1.6.1 Study Scope

The research scope comprises multi-stage methodology including mathematical modelling, dynamic simulation, and techno-economic optimisation.

Mathematical modelling

Development of mathematical model, using Microsoft Excel, for alkaline water electrolysis system, concentrating on hydrogen production rate and Faraday efficiency, under various wind power inputs.

System dynamic simulation

Conducting hourly TRNSYS dynamic simulation of green hydrogen production system. The simulation is conducted using small-scale (10 kW Bergey DC) wind turbine. The simulation includes assessment of the electrolyser's response to wind intermittency and pressure-based state of charge (SOC) of the hydrogen storage tank.

Techno-economic optimisation

Performing cost analysis, using HOMER software, focusing on determination of hydrogen production cost. The optimisation study includes sensitivity analysis of the daily average hydrogen production rate, to assess the effect on the Net Present Cost (NPC) of the system for Airport, Wafra, and Abdaly sites.

1.6.2 Study Limitations

The present study is subjected to technical and geographical constraints as follows:

a) Specificity of the simulated technology

The investigation is limited to Alkaline Water Electrolysis (AWE) and does not consider other technologies such as Proton Exchange Membrane (PEM) or solid oxide electrolysers.

b) Generation capacity constraints

The wind power generation equipment is solely limited to a small-scale 10 kW Bergey DC wind turbine. Hybridisation of power generation equipment using solar PV panels or grid-connected operation is beyond the current research scope.

c) Geographical installation sites

The analysis is conducted only for Airport site, Wafra site, and Abdaly site. The analysis cannot be generalised to other sites without local wind profile changes.

1.7 Report Structure

The report of this study is arranged into five chapters to describe the logical progress of the work from theoretical modelling to dynamic simulation to economic optimisation of small-scale wind-operated hydrogen production system.

Chapter 1 starts with research background, followed by problem statement, and aim and objectives. This chapter also includes the significance, scope and limitations of the research, and description of report structure.

Chapter 2 includes comprehensive review of literature on alkaline electrolysis, potential of wind power in Kuwait, and the challenges facing small-scale off-grid hydrogen production system integration. It also includes literature review on previous research on using TRNSYS software for hourly performance simulation of energy system. This chapter also includes review of previous studies on using HOMER software to optimise the components of green hydrogen production systems.

Chapter 3 includes description of the research methodology such as method of developing the mathematical model using Microsoft Excel software and selection of the investigated geographic sites. It also includes description of the method of TRNSYS and HOMER Pro simulations.

Chapter 4 includes mathematical model result and TRNSYS dynamic simulation findings showing production system performance assessment and hourly production profiles for each site. This chapter also includes the techno-economic optimisation results of HOMER Pro, focusing on hydrogen production costs and results of sensitivity analysis. Chapter 4 also provides synthesis of the results, analyses and discussions of the site(s) of best performance and lowest hydrogen production cost. This chapter also includes discussion of the practical implications of renewable energy infrastructure in Kuwait for green hydrogen production.

Finally, chapter 5 concludes the research by presenting the main research findings and the recommendations that can be proposed for future research and Kuwaiti government.

Chapter 2: Literature Review

2.1 Introduction

The present chapter provides a review of the literature on the simulation of green hydrogen production using renewable energy. It includes a review of the literature on the production methods and the advances in hydrogen production using water alkaline electrolysers operating using wind and solar energy. Also, the significance of using green hydrogen as alternative to fossil fuels is explained. This chapter also explores the previous research on simulation of green hydrogen production systems using solar and wind energy including studies conducted using TRNSYS and HOMER Pro software. The existing literature was considered in the context of applications in Kuwait.

2.2 Significance of Hydrogen as a Fuel

The world's population has grown with a notable acceleration during the last few centuries, which is usually associated with increased energy consumption so that there is a need for more energy. For decades, the traditional and conventional primary sources of energy have been fossil fuels such as natural gas (NG), petroleum, oil and coal. However, the excessive use of fossil fuels produces huge amounts of emissions, which harm the environment and increase the rate of global warming.

Global warming, a main challenge, is a direct result of the excessive production of emissions and greenhouse gases (GHG) including carbon dioxide (CO_2). Transportation and power production sectors are the main CO_2 producers along with other industries (Dincer et al., 2018; Ferrer and Thome, 2023). The CO_2 produced by transportation sector worldwide, for instance, is about one quarter of the total global carbon emissions (Fan et al., 2023). Thus, replacing fossil fuel operated vehicles with electric and hydrogen operated versions is expected to be a promising solution for decreasing CO_2 emissions. The vehicles with green power drives can save the environment from about 40 tonnes of CO_2 emissions per car (Geotab Team, 2024). The most promising method for producing green electricity and hydrogen for vehicular applications and industrial needs is the use of renewable energy resources. Therefore, the hydrogen to be produced from green electricity generated using renewables i.e. solar and wind power, is termed green hydrogen.

Hydrogen has made a remarkable contribution to sustainable development relative to traditional energy resources (Akpasi et al., 2025; Algburi et al., 2025). With the increased concerns about the impact of carbon emissions on environment and the depletion of fossil fuel resources, hydrogen fuel has become a better alternative, especially when produced using electricity from renewable resources (Qazi, 2022; Bhuiyan and Siddique, 2025). As an energy source and alternative to fossil fuels, hydrogen has superior properties. Compared with gasoline (petrol) fuel of lower heating value (LHV) 44 J/kg, hydrogen has about a three times higher heating value (120 MJ/kg) on mass basis (Hamedani et al., 2024). Other hydrogen physicochemical properties are shown in Table 2.1, and the properties of hydrogen fuel are compared with other fuels as shown in Table 2.2.

Table 2.1 Physicochemical properties of hydrogen (Massarweh et al., 2023)

Property	Value	Units
Density @ 25°C and 1.01325 bar	0.089	kg/m^3
Molecular weight	2.016	g/mol
Viscosity @ 25°C and 1.01325 bar	0.89×10^{-5}	Pa s
Diffusion coefficient in air	6.1×10^{-5}	m^2/s
Diffusion coefficient in water	5.13×10^{-9}	m^2/s
Boiling point	–252.95	°C
Critical pressure	13.0	bar
Critical temperature	–239.95	°C
Flammability limits	4% to 75%	by volume in air
Adiabatic flame temperature	2044.85	°C
Minimum spark ignition energy	0.02	Milli Joules
Thermal conductivity	182.0×10^{-3}	W/m K
Research octane number	> 130	dimensionless

Table 2.2 Hydrogen properties compared with other fuels (Hamedani et al., 2024)

Property	Hydrogen	Methane	Gasoline	Diesel
Molecular weight	2.016	16.043	About 110	About 170
Carbon content	0	75% mass	84% mass	86% mass
HHV (MJ/kg)	141.7	55.5	47.3	44.8
LHV (MJ/kg)	119.9	50	44.5	42.5
Autoignition temp. (K)	853	813	About 623	About 523
Density (kg/m^3) @STP	0.089	0.72	730 to 780	830
Theoretical air/fuel ratio	34.4	17.2	14.7	14.5

HHV = Higher Heating Value; LHV = Lower heating Value; STP = Standard pressure (1 bar) and temperature (273K)

As shown in Table 2.2, hydrogen is a promising alternative to traditional fuels especially from the environmental point of view. Compared with other fuels, there is no carbon content in hydrogen, so that no carbon emissions are produced during hydrogen combustion, which makes hydrogen applications in good compliance with stricter environmental regulations. Based on these advantages, the future could be hydrogen fuel cells for vehicular powering applications, which produce zero carbon emissions (Verma and Taneja, 2024). Based on the expected benefits of hydrogen as an alternative fuel, it is important to understand and compare the various production methods, as presented in the next section.

2.3 Hydrogen Colours and Production Methods

2.3.1 Overview

Hydrogen is the most plentiful element on Earth. It is the most promising renewable energy carrier from environmental opinions (Vincent and Bessarabov, 2018; Bhuiyan and Siddique, 2025). The hydrogen atom has a single proton and a single electron; thus, it is the lightest element of outstanding properties. As shown in Table 2.2, hydrogen has superior mass-based energy content of about 120 MJ/kg with a significantly lower volume-based energy intensity of only about 8 MJ/L (Cai, 2025).

However, hydrogen does not directly exist in nature as a gas because it is usually found in the form of combinations with other elements. For instance, it combines with oxygen to form water (Sadeq et al., 2024). Thus, the true challenge is to efficiently and economically extract hydrogen from its natural compounds such as water (Dawood et al., 2020; Kumar and Lim, 2022). At present, there are various methods of hydrogen production such as methane reformation; methane partial oxidation; methane pyrolysis; fermentative production method; electrolytic processes, etc. (Stenina and Yaroslavtsev, 2023; Nnabuife et al., 2022; Dash et al., 2023).

In their study, Milani et al. (2020) reported that about 87 million tonnes of hydrogen are annually produced using conventional and renewable energy sources. They highlighted that about 95% of the produced hydrogen, as of 2020, was obtained using traditional fossil fuels, specifically through steam reformation of methane (from natural gas). However, this annual production of hydrogen is responsible for generating more than 830 million tonnes of carbon dioxide. The remaining 5% of the annually produced hydrogen, as of 2020, was obtained via water electrolysis using renewable energy sources (Mosca et al., 2020; Franco et al., 2025).

Hydrogen is needed by many energy-intensive sectors such as transportation and other applications. In addition to transportation needs, hydrogen is important for other industries, and it is important to fulfil the energy needs of commercial and residential users (Bhuiyan and Siddique, 2025). Also, hydrogen is used as a feedstock for industrial applications such as ammonia and methanol manufacturing, food processing, crude oil and petroleum refining, glass and textile, treatment of metals and metallic alloys, etc. (Rambhujun et al., 2020).

The demand for hydrogen varies from one country to another. There are countries with high hydrogen demand such as the USA, China, European countries such as the UK, Germany, France, Italy, etc., South Korea, Japan, India. The countries of high hydrogen demand have therefore adopted their own strategies and invested to develop and deploy fuel cell expertise. Other countries are on the road as hydrogen exporters, especially for hydrogen produced with lower carbon emissions including Morocco, Namibia, etc. Meanwhile, fossil fuel exporters in the Gulf area such as Kuwait, Saudi Arabia, United Arab Emirates (UAE) are considering expanding their production and utilisation of green hydrogen for diversifying their energy mixes and strengthening their economies (Massarweh et al., 2023). To identify the hydrogen production technology and the energy sources used for production, various hydrogen colours are utilised, as shown in Table 2.3.

Table 2.3 Common colours of produced hydrogen

Colour	Technology and Source	Cost ($/kg H_2)	CO_2 emissions
Brown	Gasification of brown coal (Lignite)	1.2 to 2.1	High
Black	Gasification of black coal (Bituminous)	1.2 to 2.1	High
Blue	Reforming of natural gas with carbon capture technologies	1.5 to 2.9	Low
Grey	Reforming of natural gas or coal without carbon capture	1.0 to 2.1	Medium
Green	Electrolysis of water	3.6 to 5.8	Minimal

As listed in Table 2.3, hydrogen is described using colours such as blue, grey, brown, black, and green(Ajanovic et al., 2022). Also, there is pink hydrogen that is produced using water electrolysers operated by nuclear energy (Arcos and Santos, 2023). Moreover, there is white hydrogen that is naturally found underground and yellow hydrogen that can be produced using water electrolysers operated using a mix of solar energy and fossil fuel (Sayer et al., 2024; Bhuiyan and Siddique, 2025). More details on the hydrogen colours are explained in the next sections.

2.3.2 Brown Hydrogen

Currently, brown hydrogen is the most produced type of hydrogen. It is usually produced via gasification processes of brown coal or methane as they are very rich in hydrocarbons. Thus, high CO_2 emissions are produced during the manufacture of this hydrogen type at a rate of about 10–12 tonnes CO_2/tonne of hydrogen (Hosseini et al., 2024).

2.3.3 Black Hydrogen

Black hydrogen is usually produced through coal gasification processes. During gasification, syngas is produced and accordingly the hydrogen gas can be obtained by its separation from the syngas via membranes or other forms of absorbents. The remaining gases after hydrogen separation are then released and emitted to the atmosphere (Hosseini et al., 2024).

2.3.4 Blue Hydrogen

Blue hydrogen is produced from natural gas through steam methane reforming (SMR) processes, as shown in Figure 2.1.

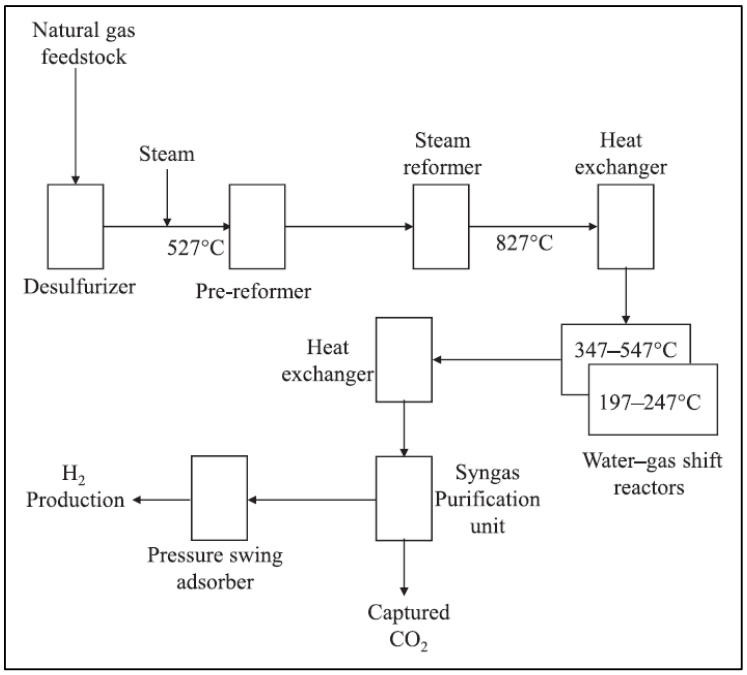

Figure 2.1 Hydrogen production via SMR process (Massarweh et al., 2023)

In the SMR process shown in Figure 2.1, the natural gas (NG) stream is reformed using high temperature steam to be separated into streams of hydrogen (H_2) and carbon dioxide (CO_2). Most of the CO_2 generated in this process (about 85 to 95%) is captured via a carbon capture system, but some is difficult to capture. Thus, the CO_2 which escapes from these processes negatively impact the environment and people's health (Ajanovic et al., 2022).

2.3.5 Grey Hydrogen

Grey hydrogen is produced through steam reforming of fossil fuels such as natural gas or coal. The production process of grey hydrogen is similar to that of blue hydrogen, although the CO_2 produced is directly released and emitted to the atmosphere, and no carbon capture technology is utilised (Roy et al., 2025). Most of the globally produced grey hydrogen (76%) is obtained from steam reforming of natural gas whereas the remaining 23% is obtained from coal gasification (Hermesmann and Muller, 2022). Grey hydrogen production usually takes place in petrochemical manufacturing facilities, and it is used to make ammonia (Ansari et al., 2025). The main drawback of the grey hydrogen production method is the excessive amount of carbon dioxide emitted to the atmosphere. Thus, the production of hydrogen turns out to be environmentally friendly if renewable energy is used for producing what is called green hydrogen. The technologies for producing grey and green hydrogen are compared in Figure 2.2. More details on the green hydrogen production are given in the next section.

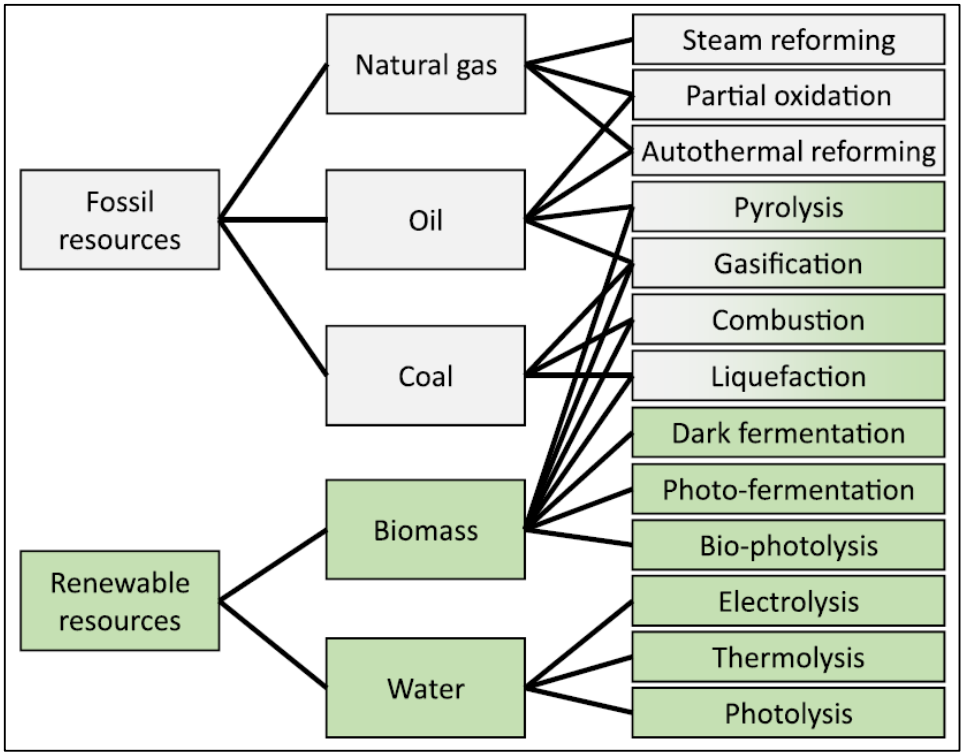

Figure 2.2 Grey and green production technologies (Hermesmann and Muller, 2022)

2.3.6 Green Hydrogen

Green hydrogen is produced, as shown in Figure 2.2, from water using electrolysers that operate using renewable (green) electricity. During the production using an electrolyser, electrical energy is used to split water into hydrogen (H_2) and oxygen (O_2). The production process is termed as green as it takes place without producing carbon emissions. In most of

green hydrogen production facilities, solar and wind energies are the commonly utilised renewable energy sources (Muller and Eichhammer, 2023; Leon et al., 2023; Reda et al., 2024; Nnabuife et al., 2025). Compared with other methods of hydrogen production, water-splitting using electrolysers is the preferred technology due to its improved efficiency, reduced production costs, and minimised negative impact on the environment (Nasser et al., 2022a; El-Shafie, 2023; Riaz et al., 2025). More details on the use of electrolysers to produce hydrogen are given in the next section.

2.4 Hydrogen Production using Water Electrolysis

2.4.1 Development of Electrolysers

Electrolysis of water is the technology utilised for splitting water to produce hydrogen using electricity, which when obtained from renewable resource produces green hydrogen (Leon et al., 2023; Maka and Mehmood, 2024). To suit the various industrial applications, water electrolysers have been notably developed over previous decades into the five generations shown in Figure 2.3.

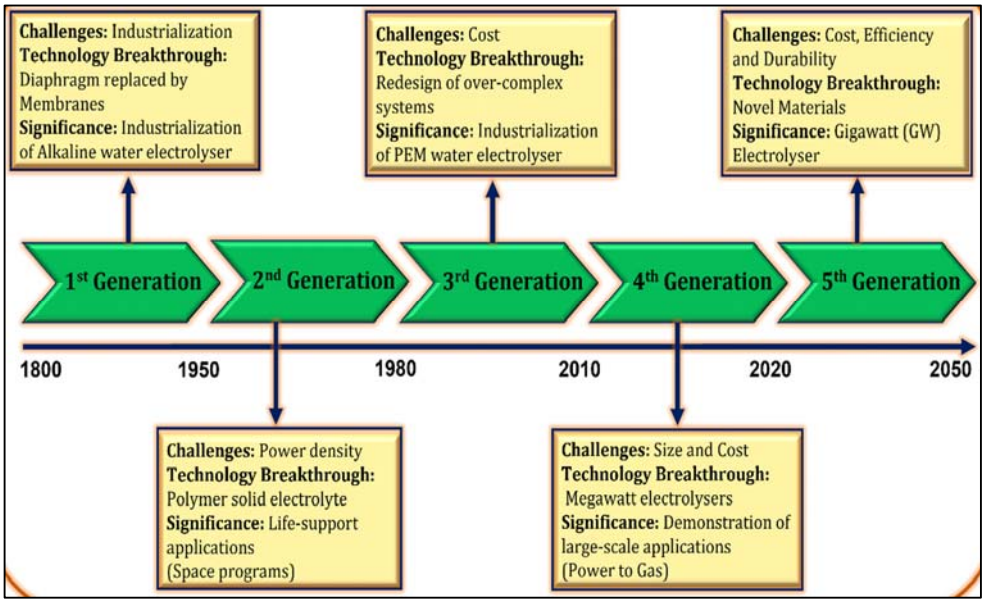

Figure 2.3 Various generations of water electrolysers (Kumar and Lim, 2022)

Figure 2.3 presents water electrolysing systems according to the type of electrolyte, the operating parameters, and the ionic agents. As shown, water electrolysers of the same operational idea include alkaline water electrolysers; polymer electrolyte membrane (PEM); Solid Oxide Electrolyser Cell (SOEC); and anion exchange membrane (AEM) electrolysers (IRENA, 2020; Sebbahi et al., 2024). A comparison between the various water electrolyser types is given in Table 2.4.

Table 2.4 Comparison of water electrolysers (El-Shafie, 2023)

Specification	Alkaline	PEM	SOEC	AEM
Technology maturity	Mature	Commercial	R&D	R&D
Cell temperature, °C	65–100	70–90	900–1000	50–70
Cell pressure, bar	25–30	30–80	<30	20–30
Current density, mA/cm^2	200–500	800–2500	300–1000	200–500
Cell voltage, V	1.8–2.4	1.8–2.2	0.95–1.3	1.8–2.2
Voltage efficiency, %	50–70.8	48.5–65.5	81–86	39.7
Energy consumption, kWh/Nm^3	4.5–7.5	5.8–7.5	2.5–3.5	4.8–5.2
Hydrogen production, Nm^3/hr	<760	0.265–30	----	0.25–1
Stack lifetime, hr	10,000	<20,000	<40,000	NA
Electrolyte	20–30% KOH	PFSA[1]	YSZ[2]	Polymer with KOH or $NaHCO_3$
Separator	Asbestos, NiO, ZrO with mesh	PFSA[1]	Solid electrolyte	QAPS[3]
Charge carrier	OH^-	H^+	O_2^-	OH^-
OER[4] catalyst	Ni-coated stainless	Ir/Ru oxide	Perovskite-type	CO_3O_4
HER[5] catalyst	Ni	Platinum	Ni/YSZ	Ni
Hydrogen purity, (vol%)	99.3–99.9	99.999	----	99.99
Capital cost (€/kW_{el})	1000–1200	1860–2320	>2000	NA

PFSA[*] = Perflurosulfonated acid; YSZ[2] = Yttria-stabilised zirconia; QAPS[3] = quaternary ammonia polysulfone; OER[4] = oxygen evolution reaction; HER[5] = hydrogen evolution reaction

Among the electrolysers compared in Table 2.4, the Alkaline Water Electrolyser (AE) is widely used because of its mature technology. The Polymer Electrolyte Membrane (PEM) types are of diverse commercial applications (Qayoom et al., 2024). For both types i.e. AE and PEM, the electrolysis cell is differentiated by the electrolyte used, the type of electrodes, and the barrier component type (Xu et al., 2022; Sahin, 2024; Qayoom et al., 2024). The electrolyte is the ionic substance needed to supply the positive ions (cations) and negative ions (anions) to the water splitting process. The ions in the splitting reaction are usually produced and oxidised by the electrodes. According to the type, the electrolyte can be liquid or solid. For instance, the electrolyte is 20–30% potassium hydroxide (KOH) in the alkaline electrolyser. In contrast, the electrolyte is a polymer with KOH or sodium bicarbonate i.e. baking soda ($NaHCO_3$) in the PEM type (Sahin, 2024).

In a water electrolyser, there are two electrodes, i.e. cathode and anode, utilised to attract ions during the water splitting reaction, and the hydrogen produced is collected at the cathode side of the cell. The operating efficiency and the effectiveness of the electrolyser electrodes are significantly improved by using electrocatalysts (Qayoom et al., 2024). Most water electrolysers operate with barriers. The barrier is the diaphragm permeable to the ions, or the polymer membrane needed for separating the hydrogen produced from the oxygen (Xu et al., 2022). More details on alkaline and PEM electrolysers are given in the next sections.

2.4.2 Alkaline Water Electrolysis

Alkaline water electrolysers are usually utilised for hydrogen production on an industrial scale (Sebbahi et al., 2024). A large-scale alkaline water electrolyser of hydrogen production capacity 10,000 m^3/hour was the first to operate, in 1939 (Santos et al., 2013; Kumar and Lim, 2022). An alkaline electrolyser functions using a high concentration alkaline solution (KOH/NaOH). In this type, Nickel (Ni) coated stainless steel electrodes are used with a separator diaphragm (Kumar and Lim, 2022), as shown in Figure 2.4.

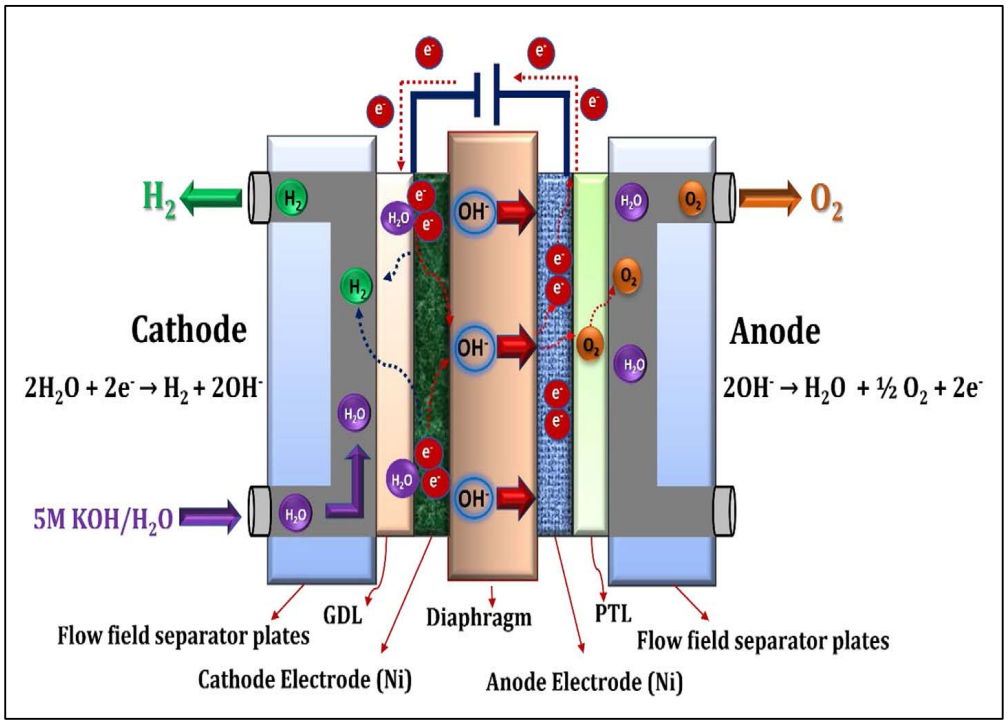

Figure 2.4 Components of alkaline water electrolyser (Kumar and Lim, 2022)

In the alkaline water electrolyser shown in Figure 2.4, hydroxyl ions (OH^-) are used as the ionic charge carrier. During operation, the alkaline solution and water passing through porous diaphragm enables the electrochemical reaction to happen (Brauns et al., 2021; Tuysuz, 2024).

The key challenge of alkaline water electrolysers is the limited current density, which varies from 100 to 500 mA/cm^2. The current density limitation is related to the restricted mobility of the hydroxyl ions (OH^-) and the higher corrosion rates caused by the increased liquid alkalinity (IRENA, 2020; Kumar and Lim, 2022). Also, the accumulation of salt (potassium carbonate, K_2CO_3) near to the pores of the electrolyser anode hinders the ion movement through the diaphragm, which decreases the hydrogen production rates. Moreover, the gases (hydrogen and oxygen) obtained by alkaline electrolysers are of low purity (about 99.9%) because the diaphragm does not effectively stop the gas crossover from one side of the cell to the other (Henkensmeier et al., 2024).

A commonly utilised electrolyte for the alkaline electrolyser is the saltwater solution of potassium hydroxide (KOH) or sodium hydroxide (NaOH). The usual concentration of the salt in water is in the range from 25% to 30% to ensure fastest ion transportation between the electrodes (Niblett et al., 2024). Alkaline electrolysers are characterised by their technology maturity, high hydrogen production yield (exceeding 650 m^3/hour), and long operating hours (tens of thousands) at an efficiency of about 70% (Abdelhaleem et al., 2024; Alhajeri et al., 2025).

Normally, alkaline electrolysers operate at atmospheric pressure and a moderate temperature of about 80ºC to produce about 50 to 485 m^3/hour of hydrogen (of purity 99.9%) using 25% concentration KOH electrolyte solution with energy consumption 4.1 to 4.3 kWh/m^3 (Ding et al., 2024). However, the electrolyser efficiency can decrease during operation with an increase of the applied current density. A better operating efficiency of electrolysers can be achieved, as suggested by Phillips (2019), using a current density of about 300 mA/cm^2, but most of the industrial electrolysers operate at higher current density about 400 mA/cm^2 or more when coated diaphragms are used (Demnitz et al., 2025).

Increasing the operating temperature of alkaline electrolysers may improve the performance, but the system service life decreases significantly due to the corrosion of the electrodes (Jang et al., 2023). Therefore, novel materials such potassium titanate (K_2TiO_3) and polyphenilene sulphide (PPS) are usually used for limiting the corrosion rates and extending the operating hours of the electrolyser (Abdelhaleem et al., 2024; Alhajeri et al., 2025).

2.4.3 PEM Water Electrolysis

In Polymer (Proton) Electrolyte Membrane (PEM) water electrolysers, the polymer membrane is normally utilised as a solid electrolyte. The main components and operating principles of PEM electrolysers are described in Figure 2.5.

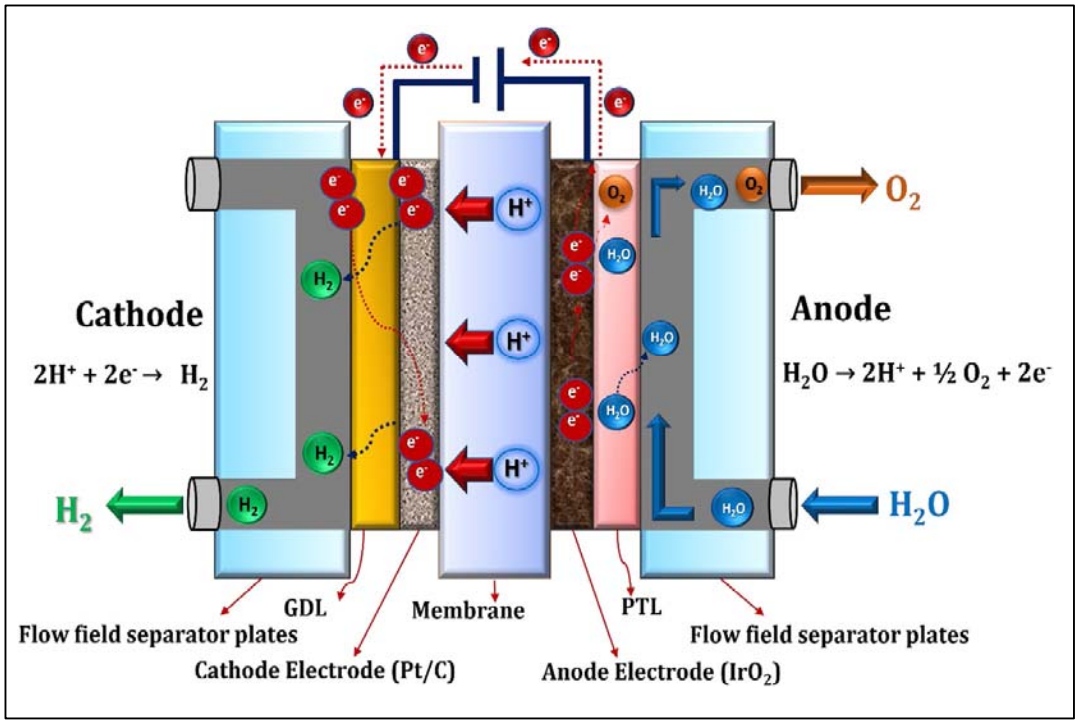

Figure 2.5 Typical components of PEM electrolyser (Kumar and Lim, 2022)

In the PEM electrolyser shown in Figure 2.5, a solid polymer (known as Nafion) is used instead of the liquid electrolyte used in a conventional alkaline electrolyser (Phillips, 2019). PEM electrolysers normally operate at low temperature (ranging from 30 to 80°C) at a higher current density (ranging from 1000 to 2000 mA/cm^2). PEM electrolysers can produce high purity (99.999%) hydrogen and oxygen gases, as reported by Kumar and Lim (2022).

Relative to the traditional alkaline water electrolyser, PEM technology is characterised by fast hydrogen reaction kinetics. This advantage is attributed to the increased active surface area of the electrolyser electrodes and to the lower pH of the electrolyser electrolyte (El-Shafie, 2023; Wallnofer-Ogris et al., 2024). Moreover, PEM electrolysers are characterised by fast hydrogen and oxygen reactions; thus, PEM electrolysers are highly recommended for several industrial applications because of their stable operation and consistent hydrogen production (Wang et al., 2022; Mucci et al., 2023). However, PEM electrolysers are expensive when compared with other technologies due to the high prices of its components

(Kumar and Himabindu, 2019; Krishnan et al., 2023). A comparison between the alkaline electrolysers and PEM electrolysers is shown in Table 2.5 and their leading manufacturers are listed in Table 2.6.

Table 2.5 Comparisons between alkaline and PEM electrolysers

	Alkaline electrolysers	PEM electrolysers
Advantages	Advanced technology	Fast and dynamic response
	Low cost (cost-effective)	Increased current density
	Long-term stability	Improved hydrogen gas purity
	Available in MW range	Improved voltage efficiency
	Needs non-noble catalysts	Has compact design
Disadvantages	Low current density	Expensive components
	Low operating pressures	Acid corrosive environment
	Low purity gases @ partial load	Possible decreased durability
	Corrosive liquid electrolyte	Available below MW range

Table 2.6 Leading manufacturers of electrolysers (Kumar and Lim, 2022)

	Manufacture	Country	Generic name	H_2 rate (m^3/h)	Pressure (bar)	Energy (kWh/m^3)
AE	Nel.	Norway	A3880	2400–3880	200	3.8–4.4
	Cummins	Canada	HySTAT	100	10	5.0–5.4
	John Cockerill	Belgium	DQ-500	500	30	4.0–4.3
	McPhy	France	MeLyzer	800	30	4.5
	Sunfire	Germany	HyLink Alkaline	2230	30	4.7
	Nuberg PERIC	China India	ZDQ-600	600	20	4.6
	TIANJIN Mainland	China	FDQ800	1000	5	4.4
	GreenHydrogen	Denmark	HyProvide	90	35	4.3
PEM	Nel.	Norway	M5000	5000	30	4.5
	Cummins	Canada	HyLYZER	4000	30	4.3
	Siemens	Germany	Silyzer 300	100–2000	35	NA
	Proton onsite	USA	M400	417	30	N/A
	ITM Power	UK	HGASXMW	110–1900	20	N/A
	Plug Power	USA	GenFuel 5 MW	1000	40	5.2
	Elogen	France	ELYTE 260	260	30	4.9

2.4.4 Reactions of the Electrolysis Process

The overall reaction of the electrolysis process is expressed as:

$$H_2O \rightarrow \frac{1}{2}O_2 + H_2 \tag{2.1}$$

During the process, the reaction describing hydrogen formation is termed as the hydrogen evolution reaction (HER) whereas the reaction describing oxygen formation is known as the oxygen evolution reaction (OER). To enhance HER reaction, electrocatalysts are used such as platinum catalysts, phosphides nitrides, carbides, etc. (Qadeer et al., 2024). However, the reaction rates significantly change with the electrolyser type (Gebremariam et al., 2023).

For alkaline electrolysers, the process reactions (Akpasi et al., 2025) are:

Anode reaction (OER): $4OH^-(g) \rightarrow 2H_2O(l) + 4e^- + O_2(g)$ (2.2)

Cathode reaction (HER): $2H_2O(l) + 4e^- \rightarrow 4OH^-(g) + 2H_2(g)$ (2.3)

For the PEM electrolysers, the reactions (Akpasi et al., 2025) are:

Anode reaction (OER): $2H_2O(l) \rightarrow O_2(g) + 4H^+(aq) + 4e^-$ (2.4)

Cathode reaction (HER): $4H^+(aq) + 4e^- \rightarrow 2H_2(g)$ (2.5)

For these electrolysers, the reaction mechanisms (IRENA, 2020) are shown in Figure 2.6.

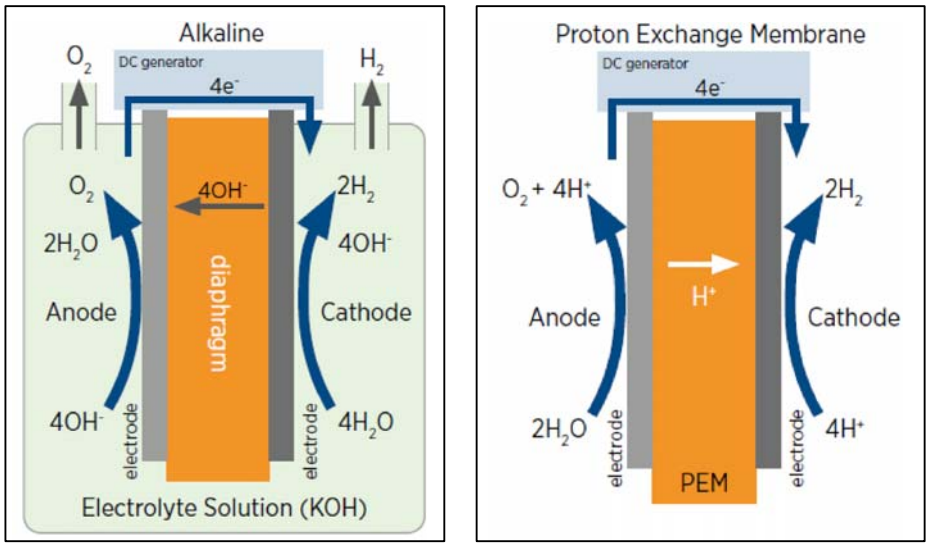

Figure 2.6 Reaction mechanisms of AE and PEM electrolysers (IRENA, 2020)

During the alkaline water electrolyser operation, it is crucial to use a barrier, such as a diaphragm, to ease the separation process of the gases produced. Without a barrier within the electrolyser body, the hydrogen produced at the cathode can migrate and then mix with

the oxygen produced at the anode forming an unwanted mixture. In PEM electrolysers, barriers are not required as the polymer solid electrolyte acts as a barrier, as illustrated in Figure 2.5.

Energy (heat and/or electricity) is required during water splitting process. It should be noted that an increased utilisation of heat decreases the need for electricity, but it increases the temperature and accordingly increases the corrosion rates of electrodes, especially for alkaline water electrolysers (Allebrod, 2013; Franco and Giovannini, 2023). The reaction of water splitting in the electrolysis process was described (Kumar and Lim, 2022) as:

$$H_2O + Electricity\left(237.2\,\frac{kJ}{mol}\right) + Heat\left(48.6\,\frac{kJ}{mole}\right) \xrightarrow{yields} H_2 + \frac{1}{2}O_2 \tag{2.6}$$

Based on Equation (2.6), Kumar and Lim (2022) reported that efficient water splitting into hydrogen and oxygen at room temperature requires the application of 1.48 volts between the electrodes, but Hou and Yang (2025) show that the lowest voltage to be applied is only 1.229V, at standard conditions of atmospheric pressure (1.01325 bar) and temperature 25°C. This voltage is the reversible voltage (U_{rev}) to be applied between the electrodes when direct current electricity is used.

The water splitting reactions initiated when sufficient voltage is implemented. The energy needed to split water is known as the standard molar enthalpy or the reaction enthalpy (ΔH), as reported by Gebremariam et al. (2023). It is the energy required for splitting each mole of water into a half mole of oxygen and one mole of hydrogen. According to El-Shafie (2023), the reaction enthalpy (ΔH) is the sum of an electrical part and a thermal part as follows:

$$\Delta H = \Delta G - T\Delta S \tag{2.7}$$

In the above Equation,

ΔG is the Gibbs energy required for the water splitting process

ΔS is the entropy change during the water splitting process

T is the water splitting process temperature

Gibbs energy (ΔG) is the lowest electric energy needed to split the water molecule whereas the entropy change (ΔS) is the lowest thermal energy needed for the process. The lowest voltage required to initiate the splitting reaction is the thermodynamic reversible theoretical voltage (U_{rev}) and the other voltage is the enthalpic voltage (U_{therm}). These voltages are defined by (Hou and Yang, 2025) as:

$$U_{rev} = \Delta G\ nF \tag{2.8}$$

$$U_{therm} = \Delta H\ nF \tag{2.9}$$

In the above equations:

n is the number of electrons (n = 2)

F is the Faraday constant (F = 96,485 C/mol)

At the standard operating temperature of 25°C, the electrolysis reactions happen using the standard Gibbs energy of 273.22 kJ/mole and enthalpy change 285.8 kJ/mole. Therefore, the required voltages are assessed as $U_{rev} \approx 1.229\ V$. However, the total reaction enthalpy is usually supplied solely as electricity, which results in a thermo-neutral voltage of the electrolyser cell termed as $U_{therm} \approx 1.48\ V$. The difference between these voltages is nearly 0.25 V, but the values of these voltages vary with other reaction parameters such as the operating temperature (El-Shafie, 2023).

The required reaction energy (ΔH) and electrical energy drop sharply with an increase in process temperature until it reaches 100°C. Beyond 100°C, these energies gradually increase with temperature due to the change of the water state from liquid to gas (Jiao et al., 2024). In practice, the actual electrolyser cell voltage (U_{cell}) is much higher, which is termed cell overpotential, to account for the activation voltage losses at the electrodes, mass transport restrictions, and ohmic resistances (Carmo and Stolten, 2018). Accordingly, the reaction of water splitting cells changes as:

- When $U_{cell} < U_{rev}$, no water splitting takes place
- When $U_{rev} < U_{cell} < U_{therm}$, more thermal energy is required for reaction initiation
- When $U_{therm} < U_{cell}$, an exothermic reaction takes place

When the water splitting reaction happens, the ratio between the actual electrolyser cell voltage and the thermo-neutral voltage defines the cell voltage efficiency η_{volt} as reported by Hermesmann and Muller (2022). The voltage efficiency is expressed as:

$$\eta_{volt} = \frac{U_{therm}}{U_{cell}} \tag{2.10}$$

One other method to assess the electrolyser efficiency is to calculate the ratio between the energy content of the hydrogen produced by the system and the electricity used for hydrogen production process. Therefore, the higher heating value (HHV) efficiency of the hydrogen production system can be evaluated as:

$$\eta_{HHV} = \frac{HHV}{W_{el}} = \frac{3.54\left(\frac{kWh}{m^3}\right)}{W_{el}\left(\frac{kWh}{m^3}\right)} \quad \text{water fed electrolysers} \quad (2.11)$$

$$\eta_{LHV} = \frac{LHV}{W_{el}} = \frac{3.00\left(\frac{kWh}{m^3}\right)}{W_{el}\left(\frac{kWh}{m^3}\right)} \quad \text{steam fed electrolysers} \quad (2.12)$$

2.5 Green Hydrogen Production Systems

Green hydrogen, as the name implies, is hydrogen produced without carbon emissions. Nowadays, green hydrogen is produced using water electrolysers operated by renewable energy sources such as solar and/or wind energy (Squadrito et al., 2023). Green hydrogen has an outstanding potential as an energy storage medium during the use of renewable energy such as solar and wind, which is characterised by an intermittent nature (Saadat et al., 2024). The demand for green hydrogen has substantially increased with the globally increased interest in limiting carbon emissions. The green hydrogen market was about USD 3.2 billion in 2021, which is expected to grow by about 40% by 2030 (Mohsen et al., 2026).

Green hydrogen production by water electrolysers operated using renewable energy has been the subject for research aiming to improve system performance and to further develop the technology. Green hydrogen production systems are usually studied using single or multiple sources of renewable energy. Utilising hybrid renewable energy sources such as solar and wind, for example, results in an improvement of the hydrogen production system efficiency and lowers hydrogen production costs, as shown in Table 2.7.

Table 2.7 Hydrogen production systems using hybrid renewables

Authors	RE Inputs	Tool	LCOH ($/kg H_2)	LCOE ($/kWh)
Abdin and Merida (2019)	PV[1] & WT[2] & SB[3]	HOMER Pro	NA	0.50–0.78
Nasser et al. (2022a)	PV & WT	Review	NA	NA
Nasser et al. (2022b)	PV & WT	Matlab/Simulink	4.54 to 7.48	NA
Hussam et al. (2024)	PV & WT & Grid PV & WT &SB	HOMER Pro	6.85 > 8	0.539 0.517
Ramadan and Gabbar (2024)	PV WT	TRNSYS 16	1.5 0.55	NA
Zhou et al. (2024)	PV & WT & SB	HOMER Pro	2.33	NA
Al-Rbaihat (2025)	PV & WT	TRNSYS	4.94	0.102
Haholu et al. (2025)	PV & WT & SB	HOMER Pro	10.3	NA
Munther et al. (2025)	PV & WT	HOMER Pro	1.98 to 2.72	NA

PV[1] = Photovoltaic panels; WT[2] = Wind Turbine; SB[3] = Storage Battery; NA = Not Available

As shown in Table 2.7, variations of hydrogen production capacity with system operating parameters have been mostly investigated using software packages such as Matlab/Simulink; Excel models; TRNSYS; HOMER Pro; etc. The use of software enables better opportunities for studying system performance under various operating and design parameters in shorter times with lower costs. The hydrogen production system, see Table 2.7, can operate as grid-connected or off-grid. Research efforts have been conducted to study the performance of systems operated by electricity from off-grid renewable energy (RE) sources to expand the use of green hydrogen production systems, as shown in Table 2.8.

Table 2.8 Examples of off-grid hydrogen production systems

Authors	Location; Study tool	PV (MW)	Wind (MW)	SB (MWh)	Electrolyser (MW)	LCOH ($/kg)
Abdin and Merida (2019)	Canada; NA	0.99	1.5	0.67	0.35	22.7
	LA, USA; NA	0.67	1.5	0.57	0.35	20.0
	CO, USA; NA	0.42	1.5	0.77	0.35	17.6
	Australia; NA	0.35	1.5	0.50	0.35	16.7
Yates et al. (2020)	Australia; NA	1.5	----	----	1.00	3.9
	Japan; NA	1.5	----	----	1.00	4.7
	Chile; NA	1.5	----	----	1.00	3.6
	Spain; NA	1.5	----	----	1.00	4.1
Temiz and Dincer (2021)	Canada; NA	2.2	----	----	0.90	4.8
Sorgulu and Dincer (2022)	Turkey; HOMER Pro	0.69	0.85	----	0.30	52.9
Zghaibeh et al. (2022)	Oman; NA	5	----	----	2.4	6.2
Al-Ghussain et al. (2023)	Estonia; NA	270	194k	14k	193k	1.42
Hassan et al. (2023)	Iraq; MATLAB	0.01	----	----	0.01	3.2
Shin et al. (2023)	S. Korea; NA	100	----	----	100	13.4
		----	100	----	100	8.5
Srettiwat et al. (2023) HOMER Pro	Belgium	899	----	375	375	12.2
	Morocco	402	----	287	287	9.7
	Namibia	418	----	299	299	7.8
Ram et al. (2024)	Fiji; HOMER Pro	0.56	0.50	0.39	0.75	13.0

Table 2.8 Continued

Authors	Location; Study tool	PV (MW)	Wind (MW)	SB (MWh)	Electrolyser (MW)	LCOH ($/kg)
Roy et al. (2024)	India; NA	0.31	0.69	0.17	0.15	22.3
Akdag (2025)	Turkey; NA	----	13.2	----	13.2	6.8
		6.6	6.6	----	13.2	6.4
Haholu et al. (2025)	Turkey; HOMER Pro	0.30	0.01	0.82	0.25	10.3
Guven (2024)	Turkey; NA	----	8	----	7	4.4
Osei et al. (2024)	Ghana; NA	5	----	----	5	9.5

As shown in Tables 2.7 and 2.8, most of the research to assess the performance of hydrogen production systems operated using renewable energy are carried out using software packages such as TRNSYS, Matlab, HOMER Pro. The use of software enables the input energy configurations to be changed and allows various process parameters to be examined. Hence, software simulations were selected to investigate the opportunity of producing green hydrogen in Kuwait. Using simulations enables the effect of design and operating parameters on the system performance to be studied under Kuwaiti weather conditions. The parameters affecting green hydrogen production rates and electrolyser efficiency are diverse. These parameters include the electrolyte type; electrode materials and coatings; applied voltage, current density, cell surface area; etc. Thus, previous research on green hydrogen production system performance, conducted using TRNSYS simulation software and HOMER Pro optimisation software, are reviewed in the next sections.

2.6 Simulation of Green Hydrogen Production System

2.6.1 Significance of System Simulation

Global concerns over carbon emissions from energy systems and the need to decrease them have demonstrated that green hydrogen is a promising sustainable solution (Algburi et al., 2025). However, the design of green hydrogen production systems using renewable energy faces complications such as the intermittent nature of renewable energy and the technological variations of electrolysis systems (Nnabuife et al., 2024), which necessitates accurate optimisation (Mukelabai et al., 2024). Thus, simulating the performance of green hydrogen production systems become essential as an accurate, fast and cheap design tool to assess system performance, evaluate the system economics and productivity, and approve the system safety measures (Criollo et al., 2024). Simulations help to examine the effect of

renewable energy fluctuations on electrolyser performance and efficiency, which helps to develop robust control measures for stable operation and consistent productivity (Zhu et al., 2024). Also, simulations help to accurately size system components to ensure better system operation and to maximise the system returns (Shash et al. 2025).

Simulation of system performance and the optimisation of system components are essential for analysing system feasibility. Simulations enable a techno-economic evaluation to be conducted to predict hydrogen production costs under different conditions, expressed as Levelised Cost of Hydrogen (LCOH) (Lebepe et al., 2025; Pinheiro et al., 2025). In practice, simulation of green hydrogen production includes the development of computational models to describe system components and their relationships during system operation (Superchi et al., 2023). The required models are the mathematical models describing the renewable energy (RE) sources such as solar, wind, etc.; water splitting electrolysers such as alkaline, PEM, etc.; storage facilities such as storage tanks, batteries, etc.; compression equipment such as hydrogen gas compressors; etc. The integration of these models enables examination of various outlines, operating parameters, marketing opportunities before the construction of hydrogen production systems. A review of selected simulation efforts and optimisation studies is given in the next sections.

2.6.2 TRNSYS Simulation of System Performance

Several studies have been conducted to assess the performance of green hydrogen production systems operating by solar energy, wind energy or hybrid solar/wind energy. For instance, Chen et al. (2022) used the TRNSYS model to investigate the transient performance of a hydrogen production system operated using solar power in the city of Izmir in Turkey. The simulated system comprised PV solar panels to produce green electricity, operating an alkaline electrolyser producing hydrogen to be stored in a tank. The authors developed a TRNSYS model as shown in Figure 2.7 to study the effect of the storage tank on system performance via parametric assessment. The simulation time step was set at 1 hour and the simulation was carried out over a whole year. The storage tank, of volume initially taken to be 5 m^3, has an initial pressure level assumed as 0.5 bar, whereas the volumetric hydrogen discharge from the tank was assumed constant at 1.1 m^3/h. The results indicated a significant relationship between hydrogen production rates and the seasonal variations of climatic conditions at the simulation site. The results of Chen et al. (2022) showed the highest

hydrogen production rates during summer and spring seasons due to the increased solar intensity and accordingly higher electrical power generation by the PV solar panels.

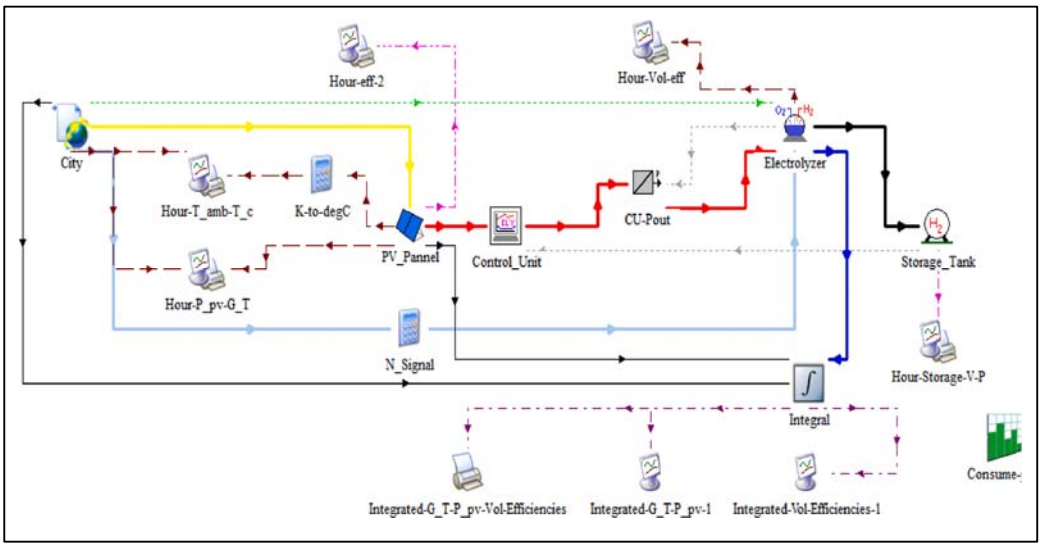

Figure 2.7 TRNSYS model of hydrogen production system (Chen et al., 2022)

For the system modelled in Figure 2.7, the monthly hydrogen production was highest at 1137 m^3 and 1110 m^3 during April and May, respectively. The annual power developed by the solar panels of the simulated system was 46.67 MWh, which resulted in an annual hydrogen production of 9600 m^3. The simulation results showed that the hydrogen rates were constrained by the tank volume. Therefore, increasing the tank volume from 5 to 20 m^3 increased the annual hydrogen production potentially by about 9%.

Mazzeo et al. (2022) conducted dynamic simulations using TRNSYS software to compare green hydrogen production systems operated by renewable energy. Three grid-connected large scale hydrogen production systems were investigated. The first system used 100 MW of PV solar panels to operate a 24 MW alkaline water electrolyser. The second system used wind turbines generating 100 MW, and the third case used a hybrid system of 50MW of PV solar panels and 50MW of wind energy to operate same electrolyser. The weekly, monthly and annual performance of each system were assessed for 28 locations using TRNSYS models. Three dimensionless indicators Satisfied Load Fraction (SLF), Utilization Factor (UF) and Grid Energy Interaction Factor (GEIF) were used by Mazzeo et al. (2022) to standardise the performance assessment. SLF was the ratio of the energy produced by the WT and the PV to the energy needed by the electrolyser. UF was the ratio of the energy passed to the electrolyser from the PV/WT system to the energy generated by the PV/WT system. GEIF described the interaction with the electricity grid. Both SLF and UF vary

between zero and one. A value of one for SLF means that all electricity to the electrolyser comes from solar PV and WT, and a value of one for UF means that no excess electricity goes to the grid from the hybrid system. The results of Mazzeo et al. (2022) show an annual SLF of 0.27–0.70 for the hybrid system, 0.22–0.40 for the PV system and 0.06–0.71 for the WT system. For all systems at any location, UF varied from 0.43 to 0.97 and GEIF varied from 0.63 to 1.21. The authors recommended the addition of a hydrogen storage facility to improve the system performance.

Izadi et al. (2022) integrated solar/wind hybrid renewable energy systems to develop a zero-energy building. The simulation was conducted using TRNSYS 18 software to develop a model comprising PV solar panels, a wind turbine, water alkaline electrolyser, hydrogen gas compressor, hydrogen storage tank, fuel cell, and controller. The authors assessed the system performance under the climatic condition of the cities Tehran, Yazd, Tabriz, and Bandar Abbas in Iran. The results show the ability of solar panels and wind turbines to supply between 35% and 49% of the electricity required by the building. The authors reported the significance of adding a hydrogen storage facility, which increased the renewable energy proportions to between 70% and 80% of the building needs.

Wei et al. (2022) used TRNSYS software for simulating the potential of solar and wind energy systems to produce hydrogen using a given land area in the city of Saskatoon in Canada. The transient performance of each system was assessed to compare the electrical energy and hydrogen production rates, and the energy extracted from converting hydrogen to electricity using fuel cells. The authors considered a fixed land area of 10,000 m^2 for each system. For the first system, 3842 PV solar panels were mounted on 70% of the land to avoid shading. For the second system, 324 wind turbines were installed with a separation 2.5 of rotor diameters between turbines to eliminate streamline interactions.

To develop the TRNSYS model, as shown in Figure 2.8, Wei et al. (2022) used weather data to supply the PV panels with hourly values of solar radiation and ambient temperature and to supply the wind turbines with wind speeds and ambient temperature. The power delivered by the panels or wind turbines were used to operate an alkaline electrolyser for hydrogen production. As shown, the authors utilised the power to the current converter unit before the electrolyser to ensure that the voltage required for best operation was received at each simulation step. This enabled an evaluation of the hourly hydrogen production rates of both systems. Also, the hydrogen produced by the electrolyser was used to operate the fuel cell to

produce electricity. The use of fuel cells was required to ensure consistent supply of electricity to overcome the intermittent nature of solar and wind renewable energy sources.

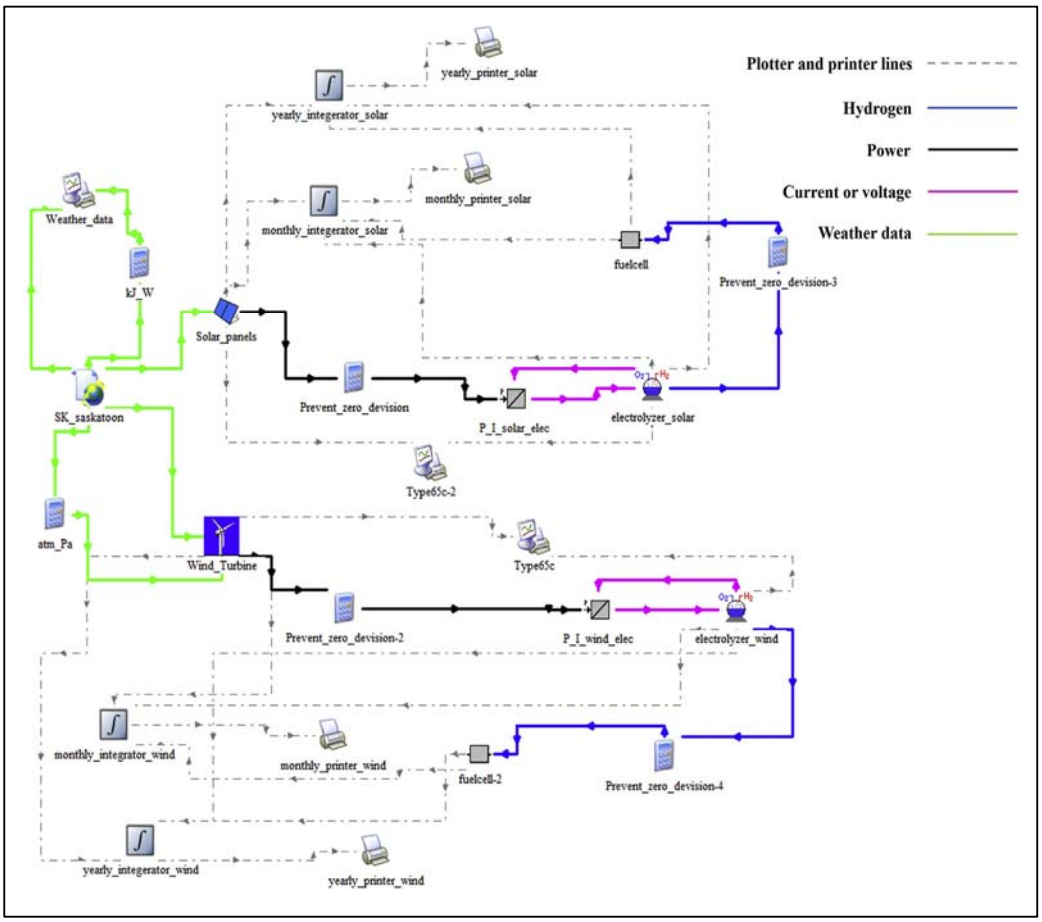

Figure 2.8 TRNSYS model of hydrogen production system of Wei et al. (2022)

The simulation results of the model shown in Figure 2.8 show the ability of the solar panels to generate 310 MWh electricity, 65,000 m^3 of hydrogen, and 100 MWh of electricity from the fuel cell in summer. The wind turbines produced only 8 MWh electricity, 1300 m^3 of hydrogen, and 2.2 MWh of fuel cell electricity. Therefore, the simulation results show the superiority of PV solar panels over the wind turbines. This can be related to the high intensity of solar radiation with relatively low wind speeds at the site chosen for simulation.

Mansir et al. (2022) developed a TRNSYS model to investigate the transient performance of an energy system to supply heating, cooling, hot water, and electricity to a residential building in Saudi Arabia. The simulation was used for comparing energy storage via batteries with energy storage with a fuel cell which operated using hydrogen from an electrolyser. The simulation showed better performance when the energy was stored using large capacity

hydrogen storage. But the cost of such storage was more than double that of conventional batteries. The increased cost of the system was related to the expensive price of the fuel cell.

Abdolmaleki and Berardi (2023) proposed a TRNSYS model to simulate the performance of an off-grid energy system producing hydrogen for a small-size building in Toronto, Canada. The model of the simulated system, as shown in Figure 2.9, includes a PV solar system, an alkaline electrolyser, a hydrogen storage tank, and a fuel cell.

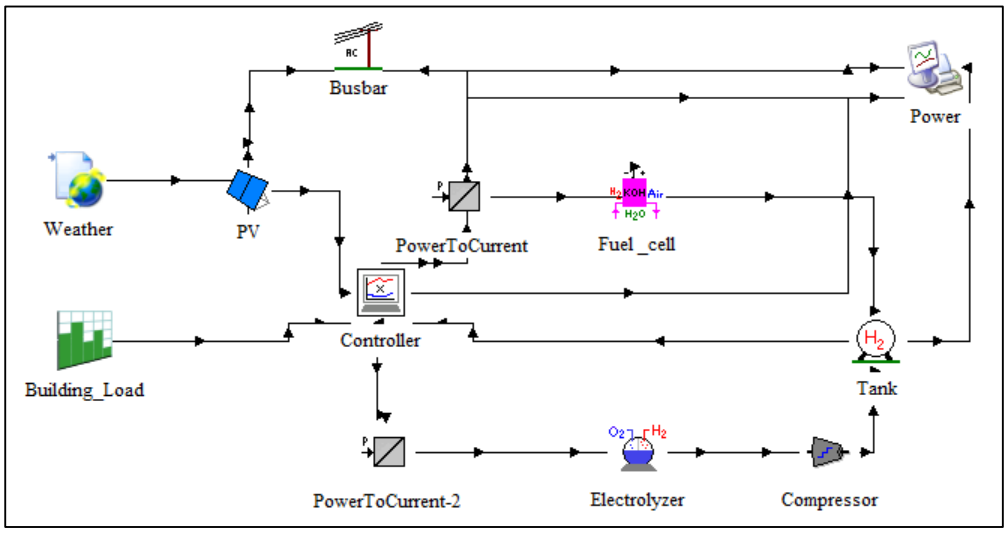

Figure 2.9 TRNSYS model of Abdolmaleki and Berardi (2023)

For the simulation model shown in Figure 2.9, the PV solar panels generate electricity for the building. When excess electricity is produced, it is used to operate the electrolyser to produce hydrogen which is stored in the tank. When the building needs electricity beyond the PV panels' capacity, the stored hydrogen is fed to operate the fuel cell to generate electricity. The system operation is monitored using a controller as shown in Figure 2.9. The authors reported the system capability of providing electricity during summer months due to high solar irradiance. Nevertheless, there was a supply shortage in winter months, which can be compensated by using hydrogen production and storage subsystems.

Saleem and Abas (2024) utilised the weather data of the city of Gujrat in Pakistan to investigate the potential of replacing fossil fuels by renewable energy resources. The authors designed an energy supply system comprising PV solar panels, wind turbines and a thermal energy source. The system also included a solar collector, fuel cell, alkaline water electrolyser, and absorption chiller. Saleem and Abas (2024) used TRNSYS software to optimise the system components and assess the system performance. The results show a maximum efficiency 52.2% for the wind power subsystem and 10.9% for the PV solar panel

sub system while generating 44.8 MWh of electrical power. As a part of the main system, there was a production subsystem used to produce hydrogen, which could be stored in a tank and used to operate the fuel cell to produce electricity. The authors also reported an annual production of 12700 m^3 of hydrogen from the electrolyser of 0.25 m^2 electrode area. The monthly peak hydrogen production was 1138 m^3 during summer.

Ramadan and Gabbar (2024) used TRNSYS software to simulate the dynamic performance of two green hydrogen production systems. In both systems, an alkaline electrolyser was used to produce hydrogen, which was powered first by PV solar panels (Figure 2.10a) and then by a wind turbine (Figure 2.10b) in Markham zone, Toronto, Canada.

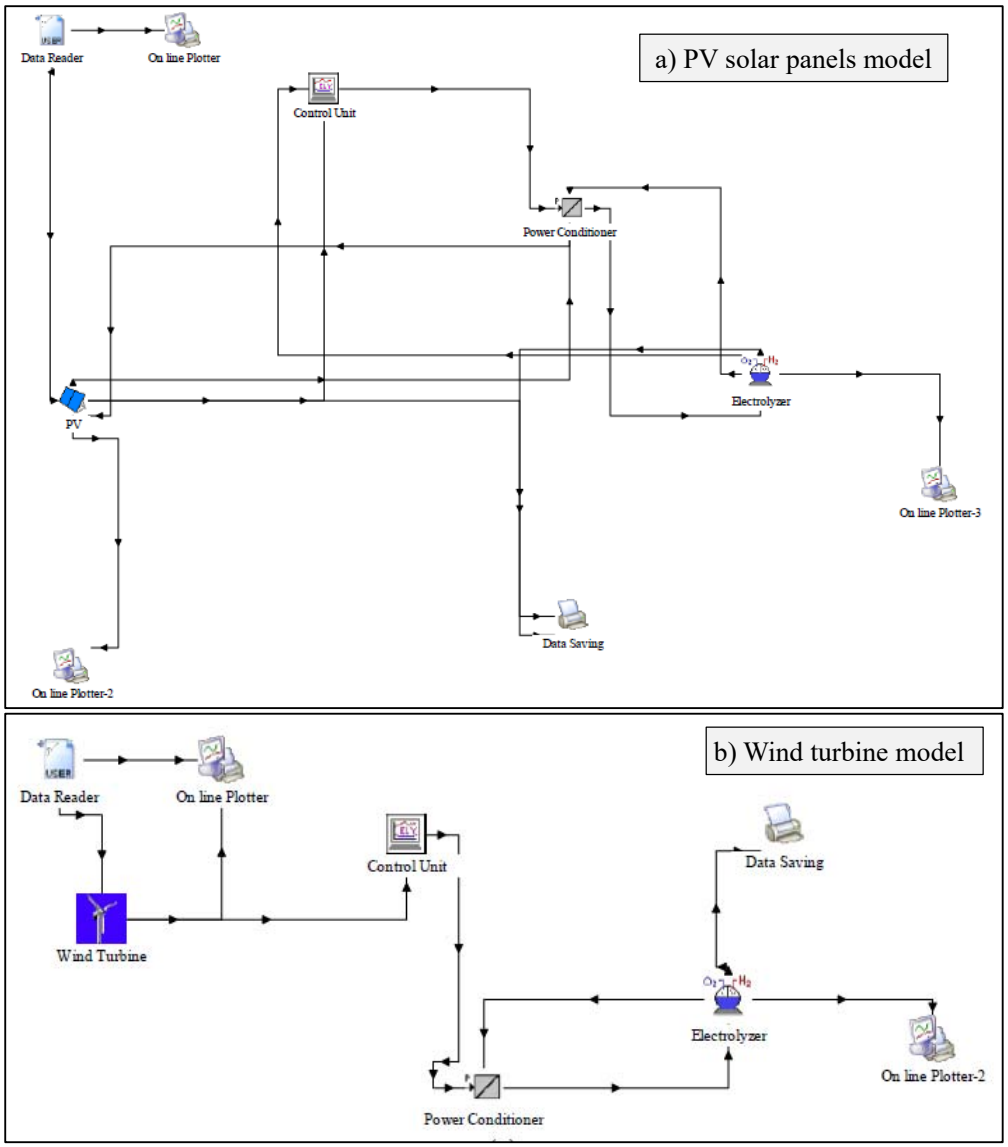

Figure 2.10 TRNSYS model of PV and WT systems (Ramadan and Gabbar, 2024)

Ramadan and Gabbar (2024) compared the performances of the systems shown in Figure 2.10. They reported that the wind operated system performed better than the system operated by the PV solar panels. The hydrogen production rate of the wind operated system was 9.03 kg/month whereas only 0.58 kg/month was produced by the PV operated system. Moreover, the LCOH were $0.55/kg for the wind powered system and $1.5/kg for the PV operated system. The superiority of the performance of the wind operated system could be attributed to increased wind speeds at the simulation site at the time the solar intensity was insufficient to operate the solar panels. Therefore, the outcomes from Ramadan and Gabbar (2024) showed a significant impact of weather conditions on the performance of green hydrogen production systems.

Haddad and Javani (2024) utilised a Python-based control algorithm and TRNSYS software to simulate the performance of a PV/WT hybrid renewable energy system. Part of the electricity produced by the RE system was used to produce green hydrogen to fulfil laboratory needs in the city of Diyarbakir, in Turkey. The TRNSYS model components of the hydrogen production subsystem, as shown in Figure 2.11, include an alkaline electrolyser, a compressor, a storage tank, a fuel cell, and controllers.

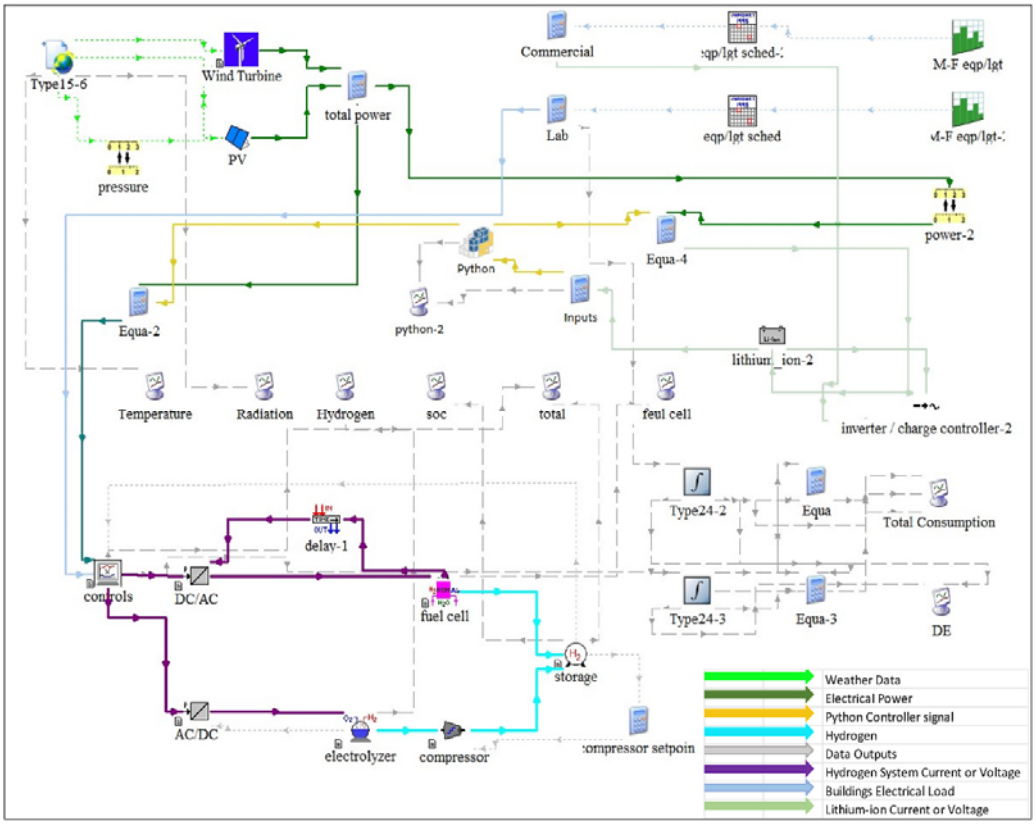

Figure 2.11 TRNSYS model of RE and hydrogen system (Haddad and Javani, 2024)

For the hydrogen production subsystem modelled in Figure 2.11, Haddad and Javani (2024) reported a peak electrolyser hydrogen production rate of 15.5 m^3/hr at an operating pressure of 1.3 bar. The total annual hydrogen production was reported as 75.8 tonnes. The authors claimed the system effectiveness would cut 34 tonnes of CO_2 emissions annually.

In another study, Haddad and Javani (2025) studied various hydrogen storage scenarios for a green hydrogen production system using an alkaline electrolyser operated by PV/WT hybrid renewable energy comprising a 3 MW wind turbine and 3.54 MW PV solar panels. The system simulation was conducted using the TRNSYS model shown in Figure 2.12.

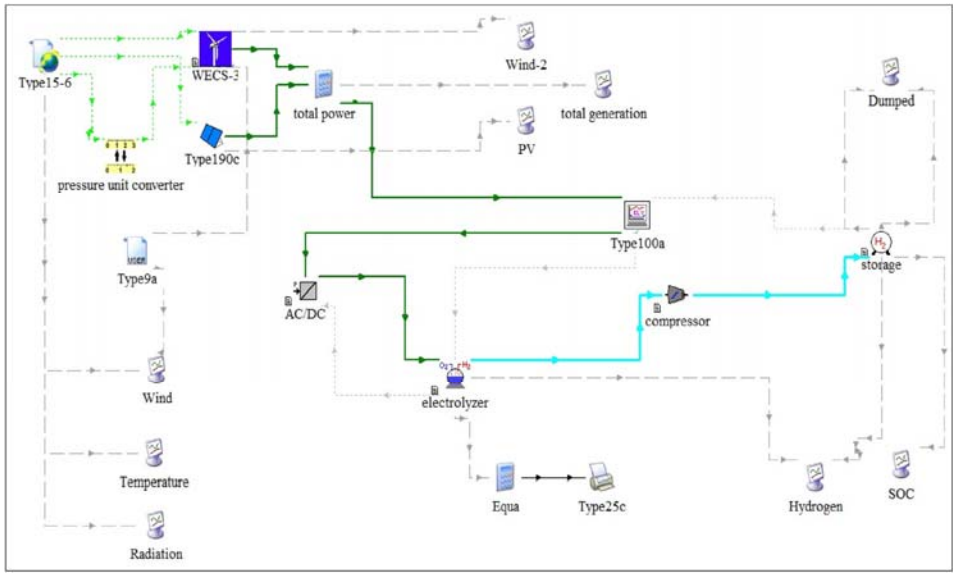

Figure 2.12 TRNSYS model of green hydrogen system (Haddad and Javani, 2025)

The components of the TRNSYS model shown in Figure 2.12 included weather data feeding the PV panels and wind turbine. The power from the RE system operated an alkaline electrolyser to produce hydrogen, which was compressed and stored. During the simulation, the authors changed the tank pressure from 200 and 350 bar for a hydrogen demand of 350 m^3/hour and studied the impact of the sale price of hydrogen. For low hydrogen prices, small size tanks were preferred compared with large tanks. The results show an opportunity of saving the environment from 6350 tonnes of CO_2 emissions annually with the system operating using renewable energy.

Al-Rbaihat (2025) used a TRNSYS simulation to assess a hydrogen production system operating using a PV/WT hybrid in Perth, Australia. The model, as shown in Figure 2.13, comprised PV solar panels, a wind turbine, controllers, an advanced alkaline electrolyser (ELE), online plotters, and an alkaline fuel cell (AFC).

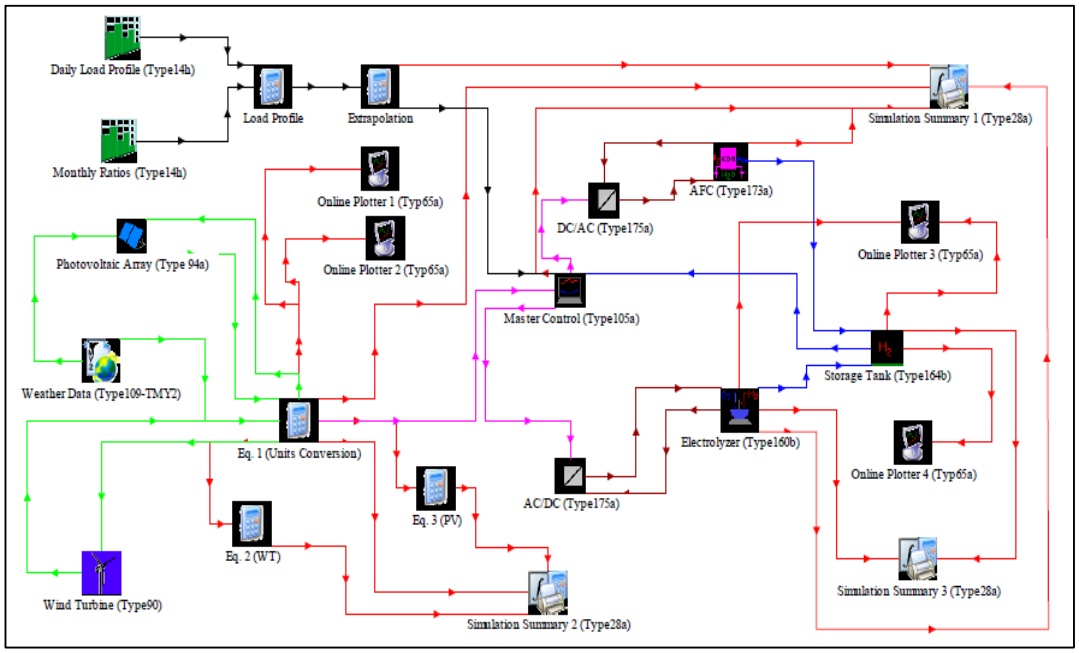

Figure 2.13 TRNSYS model of green hydrogen production system (Al-Rbaihat, 2025)

For the model shown in Figure 2.13, the annual electricity generation from the hybrid PV/WT system was 1898 MWh, and the annual hydrogen production was 253 m^3. The main parameters affecting system performance were the ambient conditions. The results of Al-Rbaihat (2025) show a system energy efficiency of 7.3% and an exergy efficiency of 5.2%. Also, the economic results show a levelised cost of energy (LCOE) of $0.102/kWh and a levelised cost of hydrogen (LCOH) of £4.94/kg with a payback period of 5.6 years. Moreover, the system operation benefitted the environment by cutting 55,777 tonnes of CO_2 emissions annually.

Hamdi and El Alimi (2025) used a TRNSYS model to simulate the performance of a green hydrogen alkaline electrolyser operated by PV solar panels in Tunisia. The electrolyser power was 24 kW, and the pressure of the hydrogen produced was 7 bar, which was pressurised to 200 bar before being stored and used to make green ammonia. The PV solar power was 24 kW and the electrolyser power taken from the grid when idle was 5 kW. The green hydrogen subsystem, as shown in Figure 2.14, comprised PV solar panels, an alkaline electrolyser, a hydrogen gas compressor and a hydrogen storage tank. During the TRNSYS model development, the electrolyser parameters were set as an electrode area of 0.25 m^2, the number of cells in series was 21, the number of stacks in parallel was 1, the maximum allowable current density was 300 mA/cm^2, the maximum allowable operating temperature was 353.15 K, and the minimum allowable cell voltage was set at 1.4 V.

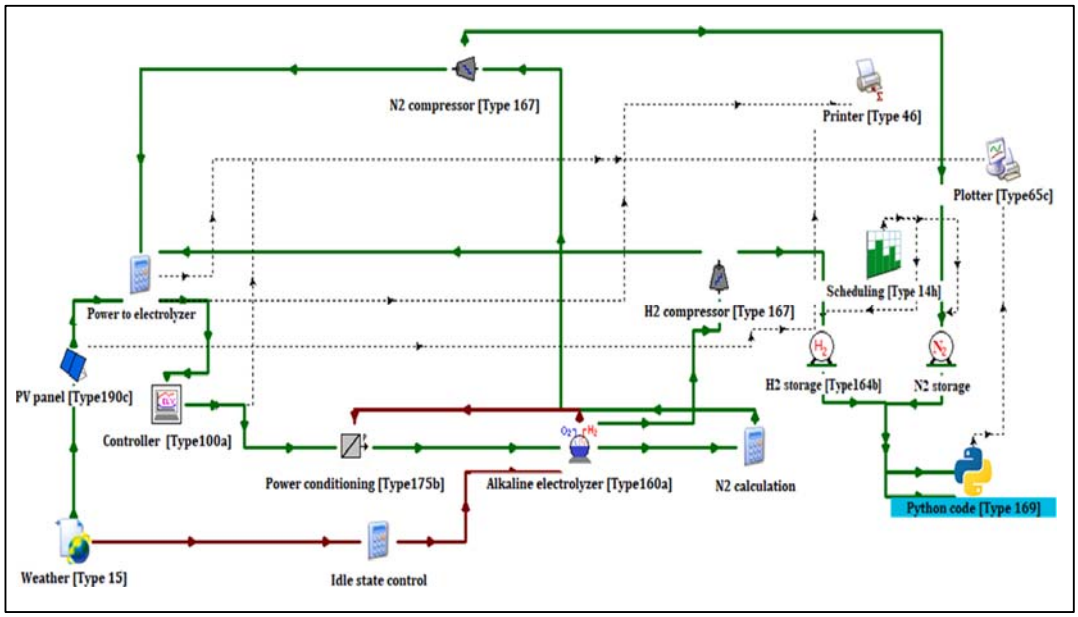

Figure 2.14 TRNSYS model of Hamdi and El Alimi (2025)

For the system modelled in Figure 2.14, the best operation was during summer months from March to June. The daily green hydrogen production during these months was 1.175, 1.304, 1.464, and 1.676 m^3, respectively. The simulation of Hamdi and El Alimi (2025) was developed mainly to produce green ammonia. As shown in Figure 2.14, part of the system's renewable power was used to produce low pressure (7 bar) nitrogen, which was compressed to high pressure (200 bar) before being stored in a nitrogen storage tank. Then, the ammonia was formed by the reaction between the hydrogen and nitrogen.

Hu et al. (2025) designed a green hydrogen production system and simulated its performance. The simulated system operated off-gid, independently of the electricity grid, using wind power (WP). The green hydrogen production system comprised an alkaline water electrolyser, a hydrogen fuel cell, a hydrogen gas compressor, a hydrogen storage tank, a controller, and hydrogen load to be fulfilled. The simulation to assess the system performance was conducted using the TRNSYS model as shown in Figure 2.15. The model also includes electricity storage battery (BESS) to store the excess power produced by the wind turbine, which is used to operate the electrolyser when the wind power is insufficient along with the electricity produced by the fuel cell operated from the pressurised nitrogen from the storage tank. The system was designed to study the opportunities of decreasing the hydrogen production costs and to assess the feasibility of using off-grid wind power to produce green hydrogen. During the simulation, the authors used the wind farm data obtained in Ordos, China, as a system input.

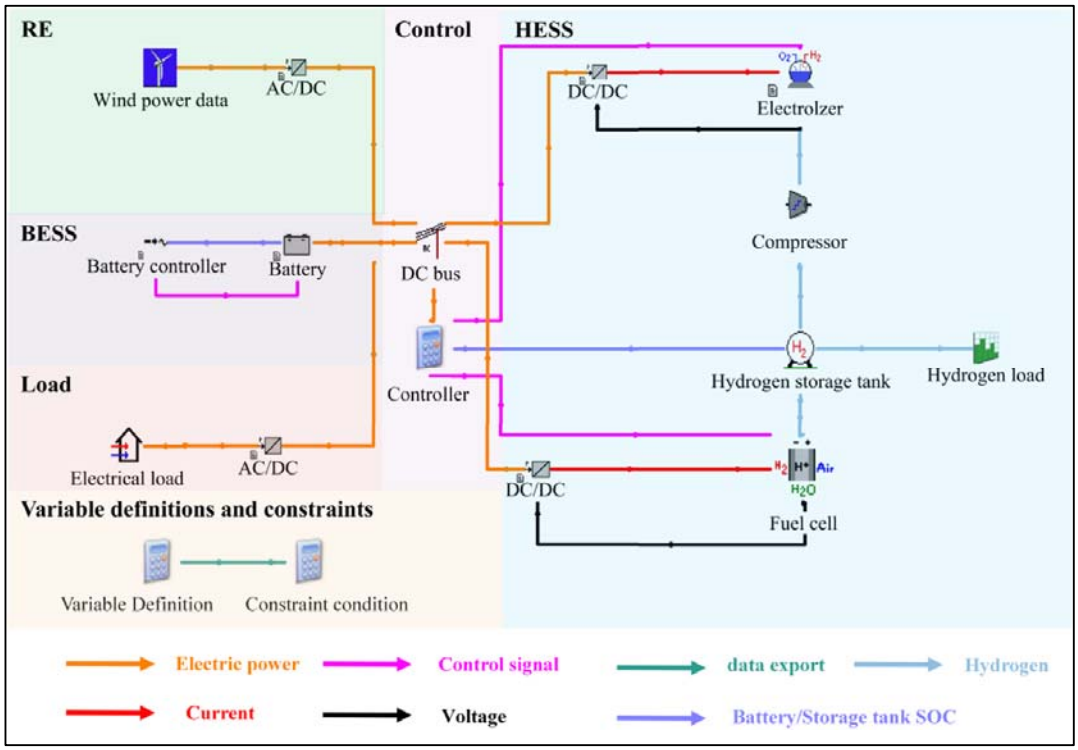

Figure 2.15 Off-grid TRNSYS green hydrogen model of Hu et al. (2025)

In their conclusions, Hu et al. (2025) reported the significance of adding a storage battery for supplying the required electric load so that it was able to fulfil 73% to 99% of the load gap and improve the system reliability. The authors also highlighted the role of stored green hydrogen in improving the overall efficiency of the system. They claimed the system was able to convert about 40.9 to 42.5% of the wind power into hydrogen annually, which improved the economics of the system operation.

2.7 Mathematical Models of TRNSYS Components

TRNSYS models used for simulating the performance of green hydrogen production systems operated using renewable energy comprise several components. The mathematical models describing the operation of these components are described in the next sections.

2.7.1 PV Solar Panels

The model describing the operation of the PV solar module is explained by Duffie and Beckman (2013) and Goswami (2015). Based on the model, the temperature of the PV solar panel module (T, °C) is expressed as:

$$T = T_{atm} + \frac{G(\tau\,\alpha - \eta_{PV})}{U_L} \tag{2.13}$$

In the above equation:

T_{atm} is the atmospheric temperature (°C)

U_L is the heat loss coefficient of the PV module (W/m^{2}K)

τ is the PV module transmittance (dimensionless)

α is the PV module reflectance (dimensionless)

G is the solar radiation (W/m^2)

η_{PV} is the conversion efficiency (dimensionless)

The conversion efficiency (η_{PV}) is defined (Duffie and Beckman, 2013) as:

$$\eta_{PV} = \frac{\text{Panel output power}}{\text{Solar radiation} \times \text{Area}} = \frac{P_{out}}{G \times A} = \frac{I \times V}{G \times A} \tag{2.14}$$

where:

V is the solar cell voltage (V)

I is the solar cell output current (A)

Based on the model of Khezzar et al. (2014), the solar cell current (I) can be expressed as:

$$I = I_L - I_o \left[exp\left(q \, \frac{V + I \, R_S}{N_S \, A \, k \, T} \right) - 1 \right] \tag{2.15}$$

where:

I_L is the photocurrent (A)

I_o is the reverse saturation current (A)

q is the charge of an electron ($1.60217663 \times 10^{-19}$ coulombs)

R_s is the series resistance (Ω)

N_s the number of cells in series (dimensionless)

A is the diode ideality factor (dimensionless)

k is the Boltzmann constant (1.380649×10^{-23} J/K)

T is the temperature (K)

Hamdi and El Alimi (2025) reported that the short circuit current (I_{sc}) and the open circuit voltage (V_{oc}) of the PV solar cell are expressed as:

$$I_{sc} = I_{sc,ref} \times \left(\frac{G}{G_{ref}} \right) + \mu_{I_{sc}} \left(T - T_{ref} \right) \tag{2.16}$$

$$V_{oc} = V_{oc,ref} + \left[\left(\frac{N_S \, A \, k \, T}{q} \right) ln \left(\frac{G}{G_{ref}} \right) \right] + \mu_{V_{oc}} \left(T - T_{ref} \right) \tag{2.17}$$

where the constants are based on Khezzar et al. (2014) as follows:

$I_{sc,ref}$ is the reference short circuit current (4.8 A)

$V_{oc,ref}$ is the reference open circuit voltage (21.7 V)

G_{ref} is the reference solar irradiance (1000 W/m^2)

T_{ref} is the reference temperature (25°C)

$\mu_{I_{sc}}$ is the temperature coefficient of the short circuit current (A/°C)

$\mu_{V_{oc}}$ is the temperature coefficient of the open circuit voltage (V/°C)

2.7.2 Wind Turbine

Wind turbines are used to convert part of the wind energy into mechanical energy then to electricity. The power to harvest from wind can be evaluated from (Oueslat, 2021):

$$P = \frac{1}{2}\, C_p\, \rho_{air,h}\, A_{rotor}\, v_{w,h}^3 \tag{2.18}$$

where:

P is the wind turbine generated power (W)

C_p is the turbine power coefficient (0.25 to 0.45)

$\rho_{air,h}$ is the air density (kg/m^3) at the wind turbine hub height h

A_{rotor} is the turbine rotor swept area (m^2)

$v_{w,h}$ is the wind speed (m/s) at the wind turbine hub height h

The speed of the wind approaching the turbine hub height can be obtained using the power law (Shafiee et al., 2024) as follows:

$$v_{w,h} = v_g \left(\frac{h}{10}\right)^{0.16} \tag{2.19}$$

where:

v_g is the ground wind speed (m/s) recorded at 10 m from the ground

h is the height of the wind turbine rotor hub (m)

The air density at the wind turbine hub height (Oueslat, 2021) is evaluated from:

$$\rho_{air,h} = \frac{P_{amb,h}}{R\, T_{amb,h}} \tag{2.20}$$

where:

$P_{amb,h}$ is the ambient pressure at the turbine hub height (Pa)

$T_{amb,h}$ is the ambient temperature at the turbine hub height (K)

The ambient temperature at the turbine hub height (h) is obtained from:

$$T_{amb,h} = T_o - B\, h \tag{2.21}$$

where:

T_o is the reference temperature (288 K)

B is a constant (6.5×10^{-3} K/m)

2.7.3 Alkaline Water Electrolyser

Electrolysers use electrical energy to split water into hydrogen and oxygen. The water splitting reaction (Ulleberg, 2003; Hong, 2013) is as follows:

$$H_2O + Electric\ Energy \rightarrow H_2 + \frac{1}{2}O_2 \tag{2.22}$$

During simulations using TRNSYS software, specific subroutines are used to represent the operation of alkaline water electrolysers, which consider the effects of hydrogen loss during water splitting and current loss during the reaction. Therefore, the alkaline water electrolyser operation is usually described by low and high reaction temperatures and the relationship between current and voltage during the water splitting process (Hu et al., 2025).

According to Ulleberg (2003) and Brauns and Turek (2020), the thermodynamic model used for describing the Gibbs energy ($\Delta G, \mathrm{J}/kg$) of the water splitting reaction is:

$$\Delta G = \Delta H - T\,\Delta S \tag{2.23}$$

where:

ΔH is the change in enthalpy during the splitting reaction (J/kg)

T is the temperature of the reaction (K)

ΔS is the entropy change during the reaction ($J/$kg K)

A minimum voltage has to be implelemented at the electrodes of the eleectrolyser to initiate the water splitting reaction described by Equation (2.22). This particular voltage is known as the electrolyser reversible voltage, which can be evaluated using the water splitting Gibbs energy described by Equation (2.23). Taking into account the number of electrons to be exchanged during the reaction ($z = 2$), the reversible voltage (U_{rev}) of the electrolyser cell can be expressed as:

$$U_{rev} = -\frac{\Delta G}{z\ F} \tag{2.24}$$

where:

F is the Faraday constant (96,485 Coulombs/mol)

Therefore, at standard water splitting reaction conditions of pressure 1 bar and temperatue 25°C, the reversible electrolyser cell voltage is about 1.229 V (Ulleberg, 2003).

During the actual electrolyser operation, the required cell voltage is normally higher than the reversible cell voltage, needed for the reaction initiation, due to losses ensountered during the reaction. The losses for instance include ohmic losses ($I\ R_{ohm}$) and there are losses due

to the activation overvoltages (U_{act}) as reported by Brauns and Turek (2020). Thus, Hong (2013) highlighted the possibility of evaluating the electrolyser cell voltage (U_{cell}) from:

$$U_{cell} = U_{rev} + \left(\gamma \frac{I_{ely}}{A}\right) + \left[S\ log\left(\frac{t\ I_{ely}}{A} + 1\right)\right] \quad (2.25)$$

where:

U_{cell} is the cell voltage of the water alkaline electrolyser (V)

U_{rev} is the reversible voltage (V)

γ is an electrolyser ohmic resistance dependent variable

I_{ely} is the current passing through the electrolyser cell (A)

A is the surface area of the electrolyser cell (m^2)

S, t are constant loss parameters

The main product of the alkaline electrolyser water splitting reaction is hydrogen gas. The total amount of hydrogen (Haddad and Javani, 2024) to be produced by the electrolyser is expressed as:

$$n_{H_2} = \eta_F\ N_{cells}\ I_{ely}\ F \quad (2.26)$$

where:

n_{H_2} is the number of hydrogen moles (mol)

N_{cells} is the number of electrolyser cells in series

I_{ely} is the current of applied to each cell (A)

η_F is Faraday efficiency and F is the Faraday constant

The by-product of the alkaline electrolyser splitting reaction is oxygen gas Therefore, the amount of oxygen gas to be produced by the electrolyser is expressed as:

$$n_{O_2} = 0.5\ n_{H_2} \quad (2.27)$$

where: n_{O_2} is the number of hydrogen moles (mol)

The Faraday efficiency is defined by Muthiah et al. (2024) as the ratio between the actual applied current and the theoretical value. It also represents the ratio of actual to theoretical amounts of electrolyser produced hydrogen. Therefore, it can be expressed (Ulleberg, 2003) as:

$$\eta_F = \left[\frac{I_{density}^2}{f_1 + I_{density}^2}\right]\ f_2 \quad (2.28)$$

where:

$I_{density}$ is the current density of each electrolyser cell (A/m^2)

f_1 is a constant ranged from 150 to 250 mA/cm^2 (15,000 to 25,000 A/m^2)

f_2 is a constant ranged from 0.85 to 1.0

During the water splitting operation, heat (thermal energy) is produced with the decrease of the electrical efficiency. To indicate the electrolyser heat loss, voltage efficiency (η_{volt}) is introduced (Elminshawy et al., 2024; Muthiah et al., 2024) as follows:

$$\eta_{volt} = \frac{U_{therm}}{U_{cell}} \tag{2.29}$$

where:

U_{therm} is the thermoneutral voltage (V)

U_{cell} is the electrolyser cell voltage (V)

The overall electrolysis efficiency (η_{elec}) (Muthiah et al., 2024), can be expressed as:

$$\eta_{elec} = \eta_F \times \eta_{volt} \tag{2.30}$$

2.7.4 Electrolyser Controller

During a TRNSYS simulation, a controller is utilised to define the setpoint of the power generation system feeding the electrolyser such as the PV solar panels, wind turbine, or both. During a TRNSYS simulation, hydrogen is produced at an elevated pressure, compressed to a higher pressure, and then stored in the hydrogen storage tank. Thus, the state of charge (SOC) describing the tank condition is a key parameter for the controller operation.

According to Hu et al. (2025) and Al-Rbaihat (2025), the controller setpoint is essential for keeping the compressor in operation to charge the tank if the tank SOC is below 70%. The storage tank charging process continues until the tank SOC reaches 90% then the compressor stops.

Thus, the control algorithm describing the controller operation is:

- When SOC < 0.7: switch ON and operate the electrolyser at full power
- When SOC > 0.9: switch OFF and operate the electrolyser at idle power

Chen et al. (2022) demonstrated that the electrolyser continues hydrogen production if the SOC of the storage tank is below the 0.7 limit. The control unit stops the electrolyser operation when SOC exceeds the upper limit, and the electrolyser is at idle condition. With hydrogen consumption from the tank, the tank pressure level decreases to the lower setpoint and the control unit sends a signal to operate the electrolyser. Therefore, when the control code is OFF, the electrolyser power equals the idle power.

2.7.5 Power Conditioning

In a TRNSYS model of green hydrogen production, the utilisation of a power conditioner unit is essential. This unit converts the DC power (generated by PV solar panels and/or wind turbines) to a DC power suitable for electrolyser operation. In practice, electrolysers operate at a constant cell voltage whereas the cell current changes with the load. A change of electrolyser current changes the power loss experienced by the power conditioner. Haddad and Javani (2024) reported the power loss of the unit as:

$$P_{loss} = P_{in} - P_{out} = P_0 + \left(\frac{U_s}{U_{Out}}\right) P_{out} + \left(\frac{R_i}{U_{Out}^2}\right) P_{Out}^2 \tag{2.31}$$

where:

P_0 is the power loss (W), which is also known as the idle power (P_{idle})

U_s is the set point of the power conditioning unit voltage (V)

R_i is the power conditioner unit internal resistance (Ω)

P_{out} is the power conditioner output power (W)

U_{Out} is the power conditioner output voltage (V)

2.7.6 Storage Tank

In TRNSYS modelling, the tank unit evaluates the pressure using van der Waals equation for real gases. Therefore, the tank pressure (p, Pa) can be evaluated (Eté et al., 2008) as:

$$p = \frac{n\,R\,T_{gas}}{V_{tank} - n\,b} - a\left(\frac{n^2}{V_{tank}^2}\right) \tag{2.32}$$

where:

n is the number of hydrogen moles (mol)

R is the universal gas constant (8.314 J/mole K)

T_{gas} is the hydrogen gas temperature (K)

V_{tank} is the volume of the hydrogen storage tank (m^3)

b is the volume of hydrogen gas molecules (m^3)

a is a constant varying with the intermolecular attraction forces of the hydrogen gas

The constants a and b (Sharifian and Harasek, 2013; Haddad and Javani, 2024) are:

$$a = \frac{27\ R^2\ T_{cr}^2}{64\ p_{cr}} \qquad \text{and} \qquad b = \frac{R\ T_{cr}}{8\ p_{cr}} \tag{2.33}$$

where:

T_{cr} is the critical temperature of the hydrogen (K)

p_{cr} is the critical pressure of the hydrogen (Pa)

2.8 HOMER Optimisation of Green Hydrogen Systems

2.8.1 HOMER Software

HOMER (Hybrid Optimization of Multiple Energy Resources) is a simulation tool that can be used to optimise energy systems by comparing various available scenarios. HOMER helps to examine various scenarios and enable technical and economical comparisons amongst these scenarios. HOMER was developed by National Renewable Laboratory (NREL) in the USA to support small energy system design and to investigate the feasibility of these systems by comparing the system technologies and considering their technical specifications and costs over their service life. HOMER enables changes in the simulation time step for comparison and analysis of off-grid and grid-connected renewable energy systems (Groppi et al., 2018; Lebepe et al., 2025).

For each simulated scenario, via techno-economic analysis, HOMER enables the evaluation of the overall Net Present Cost (NPC) of the scenario, which means the present costs over the service life minus its present value. Also, HOMER enables the evaluation of the Levelised Cost of Energy (LCOE) as an economic indicator. After comparison and reaching the best-case scenario, HOMER enables a sensitivity analysis to be conducted to assess the effect of specific parameters on system performance (Ram et al., 2024; Munther et al., 2025).

There are key input parameters to be entered to HOMER to start the simulation. These parameters include the annual electricity demand (kWh/year) for the application to which the simulation is conducted and weather conditions. The main weather conditions include solar irradiance, ambient temperature, and wind speed. The software is connected to a library having weather conditions for various locations; otherwise, data files can be used to enter the data (Maestre et al., 2024). To optimise the renewable energy system designed, costs and prices are needed as input parameters as well. For renewable energy operated green hydrogen production, the main components are PV panels (PV), wind turbines (WT), fuel cells (FC), storage batteries (SB), electrolysers (ELE), inverters (INV), hydrogen storage tanks (ST), etc. Using HOMER for simulation and optimisation requires entering prices of each component per unit power termed as Capital Expenditure (CAPEX), the lifetime of the component, the replacement cost of the component, operation and maintenance (O&M) also known as the operating expenditure (OPEX), fuel costs, etc. Examples of component prices and costs as input data needed for the system to perform simulations are listed in Table 2.9.

Table 2.9 Component costs for green hydrogen systems (Maestre et al., 2024)

Component	CAPEX	Replacement ($/kW)	OPEX ($/kW)	Lifetime
PV Solar panels: (Derating factor: 85%)	250–1050 $/kW	50% CAPEX	5% CAPEX	25 years
Wind turbines: Onshore	3,000–9,500 $/kW	60% CAPEX	5% CAPEX	25 years
Fuel Cells: (Efficiency: 54%)	1600–6000 $/kW	40% CAPEX	5% CAPEX	30,000 hours
Electrolysers: (50 kWh/kgH_2)	500–5600 $/kW	30% CAPEX	2% CAPEX	20 years
Hydrogen tanks:	700–1000 $/kg	85% CAPEX	1% CAPEX	25 years
DC/AC Inverters: (Efficiency: 95%)	300–900 $/kW	85% CAPEX	5% CAPEX	25 years
Storge battery: (Efficiency: 90%)	500–1000 $/kW	100% CAPEX	1% CAPEX	15 years

2.8.2 HOMER Optimisation and Techno-Economic Analysis

HOMER software was used by Groppi et al. (2018) to compare energy supply scenarios and to identify the optimal arrangement to power the island of Favignana, Italy. The system simulated is shown in Figure 2.15.

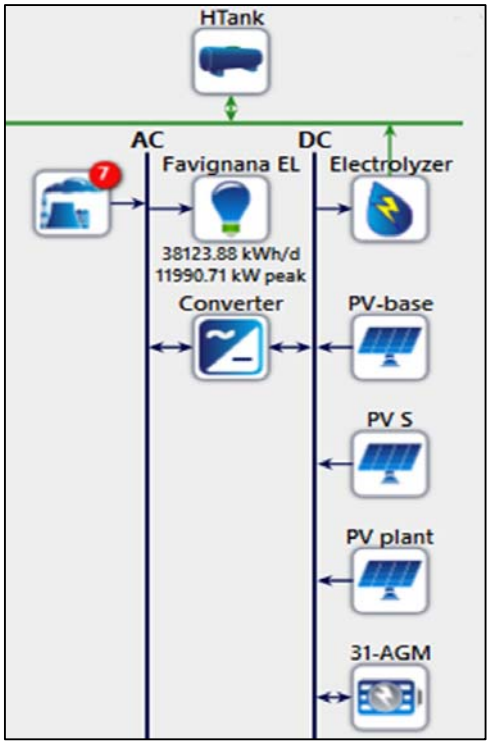

Figure 2.16 HOMER model developed and simulated by Groppi et al. (2018)

As shown in Figure 2.16, the system of Groppi et al. (2018) included diesel generators and PV solar panels for power generation. The system also included a storage system using electricity storage batteries and/or a hydrogen production system comprising an electrolyser and a storage tank. To perform the simulation, Groppi et al. (2018) utilised CAPEX (CAPital EXpenditure), replacement cost, O&M and technical lifetime for each component as economic inputs. The results show that the use of a hybrid storage system (electrical batteries and hydrogen) can be a sufficient and reliable solution to increase energy independency and support decarbonisation plans.

Abdin and Merida (2019) used HOMER Pro software for simulating and optimising the size of renewable energy system components to identify the most cost-effective arrangement. Energy production was ensured from PV solar panels (PV) and wind turbines (WT). Batteries and a hydrogen production system were considered for storage. The simulation was conducted using weather conditions at various locations including Squamish, Canada; Los Angeles, California, Golden, and Colorado, USA; Brisbane and Adelaide, Australia. Due to the lack of data for hydrogen production, the authors scaled the daily average to 70 kg of hydrogen. The simulation results show a minimum LCOE of 0.5 $/kWh at Golden, Colorado, USA for a system comprising PV, WT, battery, and hydrogen (electrolyser, fuel cell and storage tank). At same location, the minimum LCOE was increased to 0.78 $/kWh with the same system without a battery. Therefore, better economic performance was found when a hydrogen system was used for storage than batteries.

HOMER software was the preferred simulation tool by many researchers conducting techno-economic analyses of green hydrogen production systems using alkaline and PEM electrolysers operated using renewable energy sources. Also, HOMER has been widely used to conduct feasibility studies for hydrogen production systems operated by PV solar panels, wind turbines, or hybrid PV/WT power production systems. Storage batteries (SB) were added to some of the systems studied to overcome the intermittent nature of the power produced by PV or WT. Amongst several techno-economic analyses studies conducted using HOMER, there are various studies which considered a system of green hydrogen production (denoted H_2 in Table 2.10), using DC electricity to produce hydrogen, compressors to deliver the hydrogen produced to the hydrogen storage tanks, and fuel cells to be fed with hydrogen from the storage tank for conversion to electricity. A summary of techno-economic analyses studies is given in Table 2.10.

Table 2.10 Summary of techno-economic HOMER studies of hydrogen systems

Authors	Location	Power System	LCOE ($/kWh)	LCOH ($/kg)
Kalinci et al. (2015)	Bozcaada Island, Turkey	PV, WT & H_2	0.17	NA
Al-Sharafi et al. (2017)	Yanbu, Saudi Arabia	PV, WT & SB	0.609	NA
	Abha, Saudi Arabia	PV, WT, SB & H_2	1.208	43.1
Singh et al. (2017)	Building in India	PV & H_2	Meet the load	
Qolipour et al. (2017)	Hendijan, Iran	PV, WT & H_2	Feasible system	
Gokcek and Kale (2018)	Izmir-Cesme, Turkey	PV, WT & H_2	$0.146	7.5–7.87
Marino et al. (2019)	University, Italy	PV & H_2	0.80	NA
Okundamiya (2021)	University, Ekpoma	PV, Grid & H_2	0.0418	NA
Akarsu and Genc (2022)	Kayseri, Turkey	PV, WT & H_2	0.376	NA
Al-Badi et al. (2022)	Duqm, Oman	PV, WT & H_2	0.436	NA
		PV, WT & SB	0.273	NA
		PV, WT, SB & H_2	0.322	NA
Al-Orabi et al. (2023)	3 cities, Egypt	PV & H_2	0.4331	4.34
		WT & H_2	0.3239	4.13
		PV, WT & H_2	0.3803	4.79
Adedoja et al. (2024)	Nigeria	PV, WT, SB & H_2	0.34–0.41	NA
	South Africa		0.34–0.35	NA
Aktekin et al. (2024)	Mersin, Turkey	Nuclear, PV, WT & H_2	0.31	12.6
Al Saadi and Ghosh (2024)	Wadi Dayqah, Oman	PV & H_2	0.9704	29.7
Hussam et al. (2024)	Shagaya, Kuwait	PV, WT, Grid & H_2	0.539	6.85
		PV, WT, SB & H_2	0.365	8.0
Ram et al. (2024)	Fiji	PV, WT, Grid & H_2	0.1–0.19	9.1–27.6
		PV, WT, SB & H_2	1.15–4.28	13–49.7
Rizk-Allah et al. (2024)	Ostrava, Czech Republic	PV, WT, SB & H_2	NA	2.89

In a recent study, Haholu et al. (2025) utilised HOMER to analyse techno-economically an off-grid hybrid (PV/WT) system for green hydrogen production from surplus energy while meeting the energy demand for a residential community in Foca, Turkey. The weather data used for the system simulation and optimisation was obtained from the HOMER database of National Aeronautics and Space Administration (NASA). To assess the load profile, 100 houses were considered with an average daily demand of 10 kWh. The daily average consumption was evaluated as 574 kWh, and the peak load was 139 kW.

The HOMER database was used by Haholu et al. (2025) to select system components. For instance, the selected PV panel was the Canadian Solar MaxPower CS6U-330P of nominal maximum power 330 W. The panel slope was constant at 38.67 degrees without tracking. The selected wind turbine was the generic 3-blade upwind turbine of 3 kW rated capacity with hub height 17 m and lifetime 25 years. The selected battery storage was ABB PSBatME2 Li-ion of 90% Depth of Charge (DoD). Also, a generic system converter of 95% efficiency was selected. For hydrogen production components, a PEM electrolyser of capacity 250 kW, efficiency of 70 % and lifetime of 80,000 hours was selected. The HOMER model of the system is shown in Figure 2.17.

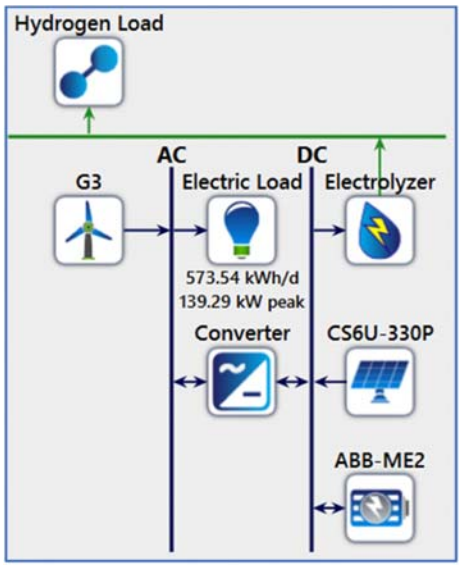

Figure 2.17 HOMER model developed by Haholu et al. (2025)

For the system shown in Figure 2.17, the optimal parameters were identified as 303 kW from the PV panels, 12 kW from the wind turbine, 822 kWh battery capacity, 250 kW PEM electrolyser with 225 kg storage tank and 146 kW converter. The hydrogen production rate of the system was 16.3 kg/day, and the specific energy needs were 56.3 kWh/kg. The LCOH was evaluated as 10.3 $/kg.

A techno-economic assessment of green hydrogen production systems from PEM and alkaline electrolysers was conducted by Munther et al. (2025). The input energy to the systems was obtained from PV solar, wind turbine, and a hybrid system. The simulation was conducted using weather data for four cities in Iraq. For each electrolyser type, three scenarios were compared using PV (of power 60 MW), WT (of power 30 MW), and a hybrid system. Therefore, there were six scenarios to compare for electrolysers of 17.5 MW capacity each. The results show that Anbar City was the location of best performance in terms of green hydrogen production where the PV solar panels were the best power generation option to decrease the LCOE to the lowest value of \$4.5/MWh. The LCOH was \$1.98/kg for alkaline electrolysers and \$2.72/kg for PEM electrolysers. The annual hydrogen production rate was 1.11×10^3 tonnes for the alkaline electrolyser and 1.19×10^3 tonnes for the PEM electrolysers.

A feasibility study of launching hydrogen refuelling stations was conducted by Okonkwo et al. (2025) in 5 cities in Oman using HOMER Pro software. For each city, 3 hybrid renewable energy systems were considered and compared: PV/SB, WT/SB, and hybrid PV/WT/SB, as shown in Figure 2.18.

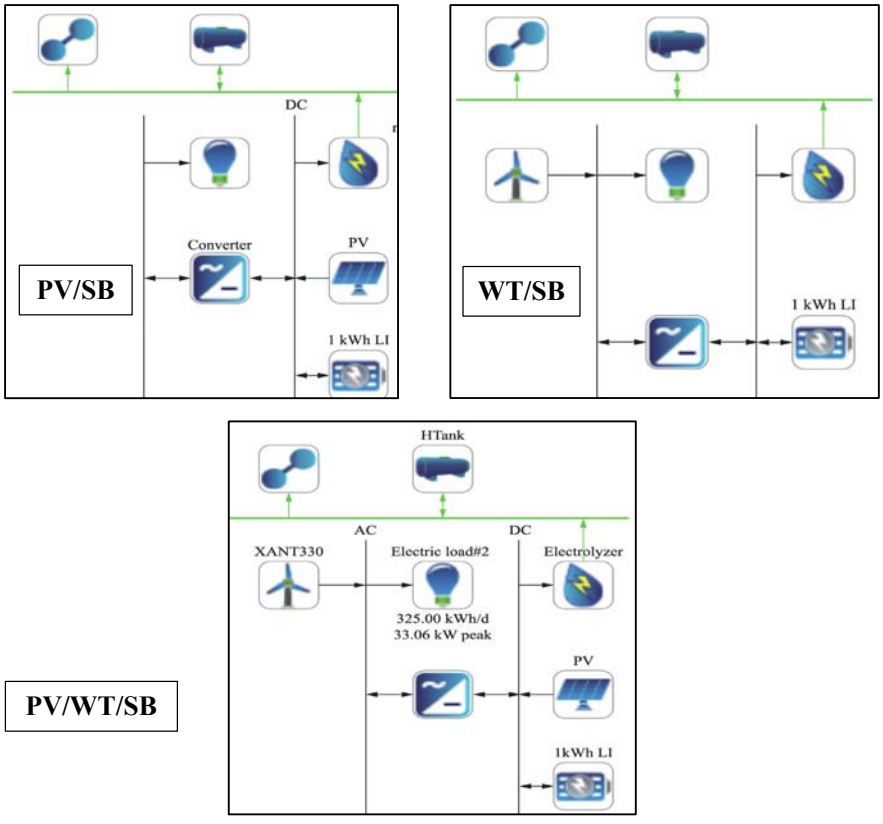

Figure 2.18 HOMER model developed by Okonkwo et al. (2025)

The simulation results of the system in Figure 2.18 indicated that the city with the most cost-effective outcomes was Duqm with LCOE of $0.0156/kWh and LCOH of $0.525/kg. The optimised system at this city included PV panels of 900 kW rated power, wind turbines of 660 kW capacity power, a converter of capacity 492 kW, an electrolyser of capacity 10 kW, and a 1,000 kg capacity hydrogen storage tank.

In a study to assess the potential of green hydrogen production on a large-scale, Prasetyo et al. (2025) used HOMER Pro to optimise a system operated by energy from the grid and renewable resources. The simulation was conducted in 5 cities in Indonesia using a grid-connected electricity production system comprising PV solar panels of power 50 MW and wind turbines of power 35 MW and a hybrid PV/WT system of power 45 MW. Two electrolysers were considered for hydrogen production, PEM and alkaline water. Three power arrangements were simulated Grid/PV, Grid/WT, and Grid/PV/WT. Therefore, six scenarios were compared assuming a project lifespan of 15 years and discount and inflation rates of 6.6% and 2.54%, respectively. A schematic diagram showing the system of hydrogen production is shown in Figure 2.19.

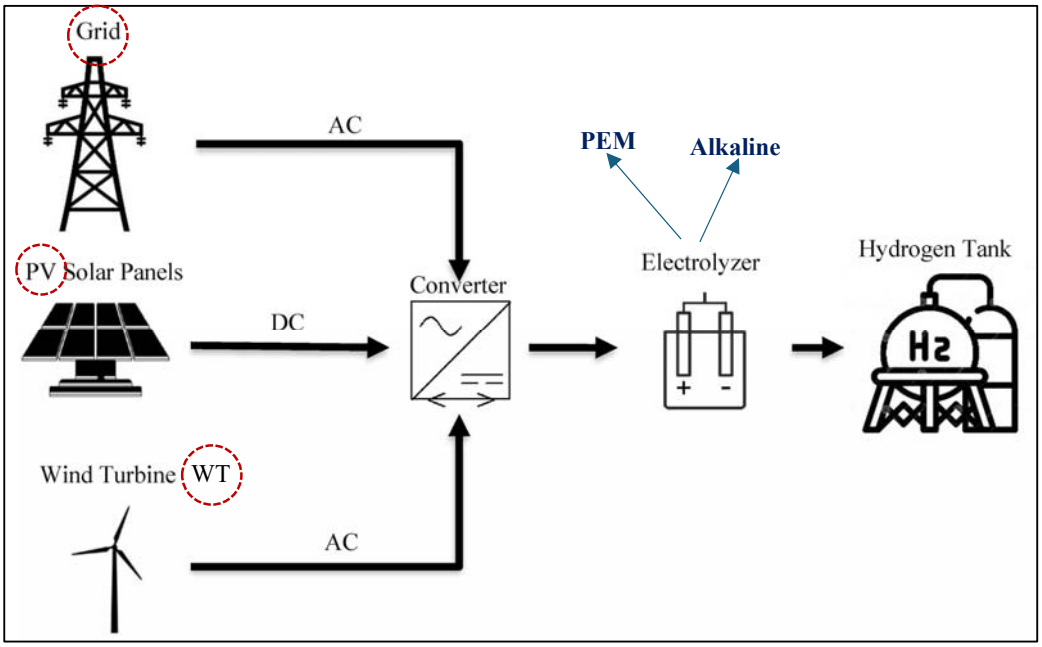

Figure 2.19 Schematic diagram of the system simulated by Prasetyo et al. (2025)

Fo the system in Figure 2.19, the compared scenarios were:

- Scenario-1: Alkaline electrolyser operated by Grid/PV
- Scenario-2: Alkaline electrolyser operated by Grid/WT
- Scenario-3: Alkaline electrolyser operated by Grid/PV/WT

– Scenario-4: PEM electrolyser operated by Grid/PV
– Scenario-5: PEM electrolyser operated by Grid/WT
– Scenario-6: PEM electrolyser operated by Grid/PV/WT

The simulation results demonstrated the highest annual hydrogen production of 1.9×10^3 tonnes at Bau-Bau city with scenario-2, with the lowest LCOH of $0.65/kg. The highest LCOH was $1.10/kg in Kupang city. In their conclusion, Prasetyo et al. (2025) highlighted the positive impact of using hybrid renewable energy systems on the efficiency of the hydrogen production systems in Indonesia.

With the significance of using HOMER software to simulate the configurations of green hydrogen production systems using electrolysers operated by renewable energy, the models describing the HOMER methods of estimating costs and system components are explained in more detail in the next sections.

2.8.3 HOMER Mathematical Approaches

a) PV solar array power calculation

To calculate the output power of a PV solar array during simulation, the HOMER help manual (HOMER ENERGY, 2015) reported the following equation:

$$P_{PV} = P_{PV,STC} \times f_{PV} \times \left[1 + \alpha_p\left(T_c - T_{c,STC}\right)\right] \times \left(\frac{G_T}{G_{T,STC}}\right) \quad (2.34)$$

where:

P_{PV} is the output power of the PV solar array (W

$P_{PV,STC}$ is the output power at standard testing conditions (kW)

f_{PV} is the derating factor of the PV solar array

α_p is the temperature coefficient of the output power (–0.39%/°C)

$T_{c,STC}$ is the standard temperature of the PV solar cell (25°C)

G_T is the solar radiation on the PV solar array at the simulation time step (W/m^2)

$G_{T,STC}$ is the solar radiation at standard testing conditions (1000 W/m^2)

T_c is the temperature of the PV cell at the simulation time step (°C)

The temperature of the PV cell at the simulation time step is evaluated from:

$$T_c = T_\infty + (7.8 \times 10^{-2} G_T) \quad (2.35)$$

where:

T_∞ is the ambient temperature at the simulation time step (°C)

b) Wind turbine power calculation

First, the wind speed at the turbine hub height is evaluated from the logarithmic law:

$$v_{hub} = v_{anem} \times \left[\frac{ln\left(\frac{Z_{hub}}{Z_o}\right)}{ln\left(\frac{Z_{anem}}{Z_o}\right)}\right] \tag{2.36}$$

where:

v_{hub} is the wind speed at the hub height (m/s)

v_{anem} is the wind speed at anemometer height, (m/s)

Z_{hub} is the hub height of the turbine rotor (m)

Z_{anem} is the anemometer height (usually 10 m)

Z_o is the ground roughness height (about 0.1 m)

HOMER can also calculate the wind speed at the hub height using the power law from:

$$v_{hub} = v_{anem} \times \left(\frac{Z_{hub}}{Z_{anem}}\right)^{\alpha} \tag{2.37}$$

where:

α is the power law exponent (1/7 or 0.143)

The wind speed at the hub height is then used by HOMER with the turbine power curve data to find the corresponding wind turbine power at standard temperature and pressure (STP) conditions ($P_{WT,STP}$) as illustrated in Figure 2.20.

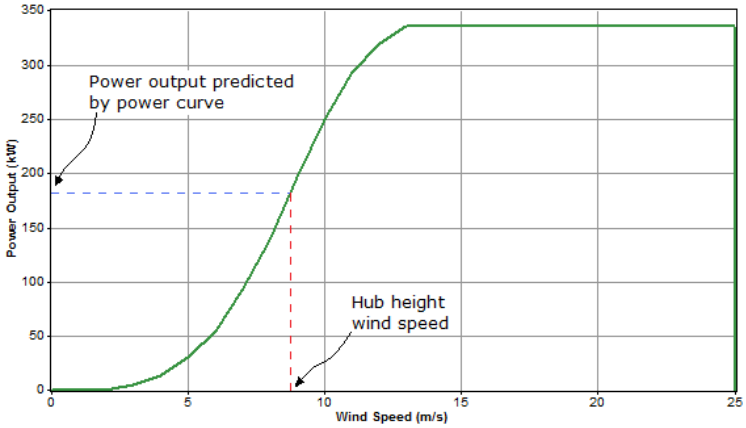

Figure 2.20 Predicted wind power of HOMER software (HOMER ENERGY, 2015)

Then, a density correction factor is used to calculate the wind turbine power (P_{WT}) from:

$$P_{WT} = P_{WT,STP} \times \left(\frac{\rho}{\rho_o}\right) \tag{2.38}$$

where:

ρ is the actual air density (kg/m^3)

ρ_o is the standard air density (1.225 kg/m^3).

2.8.4 HOMER Cost Estimates and Optimisation

The techno-economic analyses of the energy systems using HOMER software are conducted by assuming the same increasing rates of the prices of the system components. To perform the cost estimates using HOMER, a nominal interest rate (i') and an annual inflation rate (f) at the project site location are used along the project lifetime (n), which can be assumed from 20 to 25 years (Abdin and Merida, 2019). These parameters are used to evaluate the annual inflation rate (i) from:

$$i = \frac{i' - f}{1 - f} \tag{2.39}$$

Then, the discount rate (i_d) can be evaluated as:

$$i_d = \frac{1}{(1+i)^n} \tag{2.40}$$

Accordingly, the capital recovery factor (CRF) representing the equal annual cash flows can be evaluated from:

$$CRF(i,n) = \frac{i(1+i)^n}{(1+i)^n - 1} \tag{2.41}$$

The Net Present Cost (NPC) of each component in HOMER is calculated as:

$$NPC(£) = \sum_{n=1}^{t} i_d \left(C_{Com} + C_{Rep} + C_{O\&M} + C_{Fuel} - C_{Sal}\right) \tag{2.42}$$

where:

NPC is the net present cost of the component (£)

i_d is the discount rate

n is the project lifetime (years)

C_{Com} is the component capital cost (£)

C_{Rep} is the component replacement cost (£)

$C_{O\&M}$ is the component operation and maintenance cost (£)

C_{Fuel} is the fuel cost (£), if needed

C_{Sal} is the salvage value of the component (£)

Then, capital recovery factor is used to calculate the annualised cost (C_{ann}) of the system components from:

$$C_{ann,tot}(£) = CRF(i,n) \times \sum NPC(£) \tag{2.43}$$

HOMER then evaluates the levelized cost of energy ($LCOE$, £/kWh) as follows:

$$LCOE\left(\frac{£}{kWh}\right) = \frac{C_{ann,tot}}{E_{served}} \tag{2.44}$$

where:

$C_{ann,tot}$ is the total annualised cost of the simulated system components (£)

E_{served} is the total electrical load served by the system (kWh)

For the simulated hydrogen production systems, HOMER evaluates the Levelized Cost of Hydrogen ($LCOH$, £/kg) as follows:

$$LCOH\left(\frac{£}{kg}\right) = \frac{C_{ann,tot} - v_{elec}\left(E_{prim,AC} + E_{prim,DC} + E_{def} + E_{grid,sales}\right)}{M_{H_2}} \quad (2.45)$$

where:

v_{elec} is the electricity price (£/kWh)

$E_{prim,AC}$ is the primary alternating current electrical load (kWh)

$E_{prim,DC}$ is the primary direct current electrical load (kWh)

E_{def} is the deferrable load (kWh)

$E_{grid,sales}$ is the total energy sold to the grid (kWh)

M_{H_2} is the total hydrogen production (kg)

The objective function, used by HOMER to optimise the designed system, is to minimise the NPC, LCOE, and LCOH of the entire project.

2.9 Summary and Research Gap for Kuwait

The energy plan 2030 in Kuwait is targeting an increase in renewable energy to meet 15% of the expected power demand (Alsayegh, 2021). Therefore, there are intensified interests and efforts to increase the electricity generation from diverse resources of renewable energy (Al-Abdullah et al., 2023; 2025). There are various projects to produce green electricity in Kuwait using renewable energy. For example, the Shagaya Renewable Energy Park initiative is aiming to generate about 4.0 GW of green electricity by 2030 using solar and wind energy. Also, there are tremendous efforts to integrate PV solar panels into buildings and consider the use of a large-scale (about 1.0 GW) solar power plant. There are also plans for decreasing carbon emissions by 7.4 % in Kuwait by 2035 from the solar energy adoption and efficiency improvements of energy systems (Olabi et al., 2025). Most of the renewable energy projects in Kuwait are based on solar energy applications with little attention to wind energy projects (Mostafaeipour et al., 2016; Razi and Dincer, 2022). The main electricity production plant operating using wind power in Kuwait is a part of the Shagaya project, which has a total wind power electricity generation capacity of 10 MW with a service life of 25 years (Khajah and Philbin, 2022).

With continuous efforts to diversify energy sources in Kuwait and to cope with the intermittent nature of renewable energy for stabilised electricity generation, green hydrogen production becomes of increased interest (Olabi and Jouhara, 2024). To comply with the green hydrogen production strategy in Kuwait, there are various projects including the Al Dibdibah pilot project to install 50 MW water electrolysers. The Al Dibdibah project would operate using 200 GWh of PV solar power annually to produce about 3000 tonnes of hydrogen per year without any wind power (Olabi et al., 2025). Since Kuwait has several promising sites of high wind speeds, there is an opportunity of using wind power to operate water electrolysers to produce green hydrogen.

In Kuwait, there are various sites of promising wind speeds such as Kuwait Airport, Wafra site, Abdaly site, etc. (Alhajri et al., 2025). These sites are promising for installing renewable energy systems such as PV or wind turbines to produce sufficient electricity to produce hydrogen using alkaline water electrolysers. Nevertheless, there is a lack of literature on this subject, as previous research has shown, for example a technical and economic assessment of using renewables in Kuwaiti (Khajah and Philbin, 2022).

The outcome of the literature survey demonstrated the presence of several research gaps for green hydrogen production using alkaline water electrolysers operated under harsh Kuwaiti weather. These gaps involve significant parameters such as:

- Design of electrolyser electrode of optimised surface area, current density, etc. during water splitting process.
- System integration with special attention to the impact of changing the input energy type such as PV solar power, wind turbine power, or both on hydrogen production rates and system efficiency.

This research was conducted to develop a basic mathematical Excel model and TRNSYS simulation models, to study the performance of off-grid wind-operated alkaline electrolysers under Kuwaiti weather conditions. Modeling alkaline water electrolyser performance when operated using wind energy under Kuwaiti harsh conditions has received limited attention, especially for small-scale localised systems. The study of alkaline electrolyser performance using simulation models is expected to add knowledge beyond the assessment of economic and environmental impact. Modelling electrolysers is important to develop adequate designs of practical versions for real-world implementation. Therefore, the accomplishments and contributions of this study were planned as:

- Developing a mathematical model, using Excel spreadsheets, to assess the performance of off-grid wind-operated alkaline water electrolysers under Kuwaiti climate
- Developing a TRNSYS model to simulate the dynamic performance of off-grid wind-operated alkaline water electrolysers under Kuwaiti climate
- Using TRNSYS dynamic hourly bases simulations to perform performance analysis of green hydrogen production systems, over a whole year, in Kuwait.
- Assessing the potential of using wind turbines to generate electricity to be used to operate alkaline electrolysers to produce hydrogen (daily, monthly, and annually).
- Evaluating the impact of wind power change from one site to another on the productivity, and levelised cost of hydrogen (LCOH) of green hydrogen production system.

The outcomes of literature review also showed a lack of techno-economic and optimisation analyses for identifying the best renewable energy configurations that can be used to operate small-scale electrolysers to produce green hydrogen under Kuwaiti weather.
The gaps involve key parameters including:

- The impact of installation site and system components on LCOE and LCOH of small-scale off-grid wind-operated hydrogen production system.
- Optimisation of system configuration to have high hydrogen production rates and system efficiency at low costs.

HOMER Pro model was developed to optimise a small-scale off-grid wind-operated green hydrogen production systems under the harsh weather conditions of Kuwait. The optimised system outcomes are expected to add to the knowledge by demonstrating the economic and environmental benefits of these systems in Kuwait. Therefore, the main contributions of this study are to include:

- Development of HOMER model to conduct a techno-economic feasibility study of small-scale off-grid wind-operated green hydrogen production system under climatic conditions of Kuwait.
- Comparing the system performance at different sites in Kuwait considering the highest possible hydrogen production and the minimum energy and hydrogen production costs.

Chapter 3: Methodology

3.1 Introduction

This chapter includes description of the methods of development of the simulation models. It starts with the description of preliminary wind-operated electrolysis mathematical model developed using Excel spreadsheets. Next is the description of the performance assessment simulation model developed using TRNSYS software. Finally, this chapter includes description of the optimisation model developed using HOMER Pro software.

3.2 Model Development of Wind-Operated Electrolysis System

Preliminary study was conducted to study the opportunity of green hydrogen production in Kuwait using alkaline water electrolysers operated by wind power. Mathematical model was developed using Excel spreadsheets to predict and compare the electrolyser performance at three different sites proposed for green hydrogen production system installation. These sites are Kuwait Airport site, Wafra site, and Abdaly site. To perform the calculations at each site, wind speed measurements, previously recorded at 10 m from the ground level, were obtained (Zou et al., 2023). The wind speed measurements were used to calculate the average daily wind speed at rotor the hub height of the selected turbine, for each month for each site, which was used to evaluate the output power to be developed by the wind turbine. Details of the modelling procedure and mathematical model assumptions are described in the next section.

3.2.1 Wind Speeds and Turbine Specifications

Mathematical model was developed to predict and assess the performance of green hydrogen production system operated by wind power. The mathematical model of the wind-operated system comprised alkaline water electrolyser and wind turbine of power production capacity sufficient to operate the electrolyser. Therefore, data on the specifications of the alkaline water electrolyser were obtained based on the work of AlRafea et al. (2016), Hussam et al. (2024), and Wang et al. (2024).

To develop the mathematical model, wind turbine of small, rated power capacity of 10 kW was selected. The specifications of the turbine, used to identify and alter the parameters and inputs of the model, are listed in Tables 3.1.

Table 3.1 Specifications of the selected wind turbine

Specification	Value
Model of the wind turbine	Bergey – BWC Excel 10
Number of rotor blades	3
Hub height of the turbine rotor	30 m
Rated power of the turbine	10 kW
Rated wind speed	11.6 m/s
Cut-in wind speed	2.5 m/s
Cut out wind speed	20 m/s
Rotor diameter of the turbine	7 m

Based on the turbine specifications in Table 3.1, certain parameters needed changes during model development. The changes included setting the wind speed data collection height as 10 m and changing the rotor hub height to 30 m to calculate the model speeds. As listed in Table 3.1, the hub height was 30 m; thus, wind speed at 10 m were used to predict the wind speeds at the hub height, using Equation (2.17) of Section (2.7.2) of the previous chapter, which is expressed as:

$$v_w = v_g \left(\frac{h}{10}\right)^{0.16} = v_g \left(\frac{30}{10}\right)^{0.16} = 1.192\, v_g \tag{3.1}$$

where v_w is the wind speed at hub height of 30 m from the ground, and v_g is the wind speed 10 m from the ground (recorded at each site).

The average daily wind speeds at each site at both heights were obtained and compared as shown in Table 3.2.

Table 3.2 Daily average wind speed (m/s) for the sites each month

Month	Airport		Wafra		Abdaly	
	@10 m	@30 m	@10 m	@30 m	@10 m	@30 m
January	5.51	6.57	4.40	5.25	3.82	4.55
February	5.53	6.59	4.42	5.27	4.05	4.83
March	5.57	6.64	4.39	5.23	4.03	4.80
April	5.98	7.13	4.48	5.34	4.23	5.04
May	6.50	7.75	4.64	5.53	4.34	5.17
June	8.22	9.80	5.57	6.64	5.57	6.64
July	6.65	7.93	5.02	5.98	4.76	5.67
August	6.05	7.21	4.48	5.34	4.53	5.40
September	5.87	7.00	4.39	5.23	4.27	5.09
October	5.06	6.03	4.02	4.79	3.81	4.54
November	5.22	6.22	4.17	4.97	3.75	4.47
December	5.35	6.38	4.06	4.84	3.61	4.30

3.2.2 Method of Wind Power Evaluation

The output power of the wind turbine is considerably dependent on the speed of the wind approaching the rotor hub. To find a relationship between the turbine power and speed for the selected turbine, the power curve of the turbine was obtained as shown in Figure 3.1.

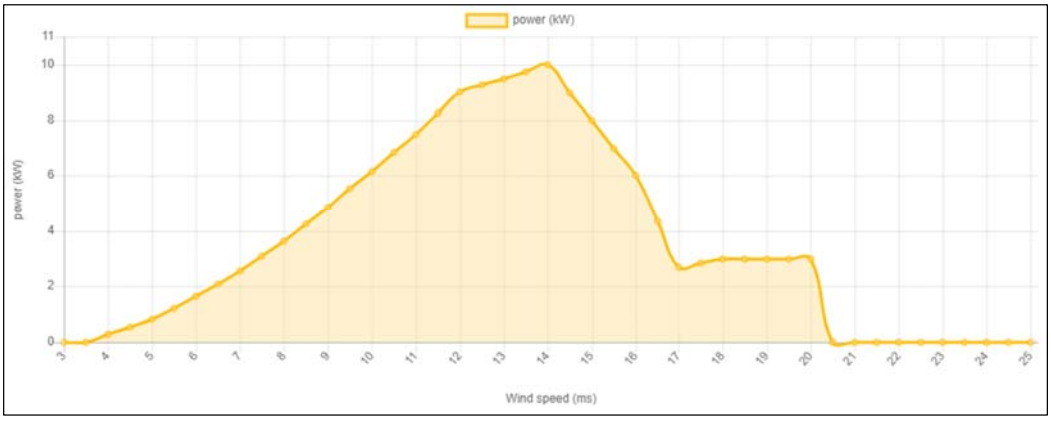

Figure 3.1 Power curve of the selected turbine (Wind-turbine-models, 2025)

From the power curve, shown in Figure 3.1, the turbine output power (P, kW) was obtained at each wind speed (v_w, m/s) in the range 3 m/s to 20 m/s, step 0.5 m/s, as listed in Table 3.3.

Table 3.3 Data points of wind power (kW) and wind speed (m/s)

v_w, m/s	P, kW		v_w, m/s	P, kW		v_w, m/s	P, kW
3.0	0.00		9.0	4.85		15.0	8.00
3.5	0.10		9.5	5.53		15.5	7.00
4.0	0.27		10.0	6.15		16.0	6.00
4.5	0.54		10.5	6.83		16.5	4.35
5.0	0.80		11.0	7.50		17.0	2.70
5.5	1.23		11.5	8.25		17.5	2.84
6.0	1.65		12.0	9.00		18.0	3.00
6.5	2.08		12.5	9.26		18.5	3.00
7.0	2.55		13.0	9.50		19.0	3.00
7.5	3.10		13.5	9.75		19.5	3.00
8.0	3.65		14.0	10.00		20.0	3.00
8.5	4.25		14.5	8.96			

The extracted data points in Table 3.3 were plotted using Excel spreadsheets for wind speeds from 0 to 12 m/s, which represented the increasing power curve shown in Figure 3.1. For the generated plot, best fitting using polynomial function was performed. The best fit equation was obtained to predict the relationship between the wind turbine output power and the wind speed, as shown in Figure 3.2.

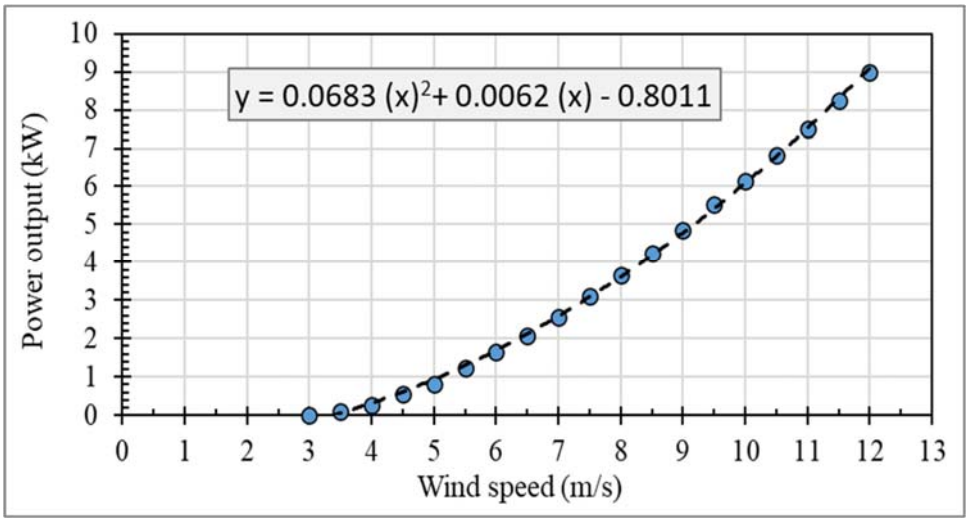

Figure 3.2 Relationship between wind turbine power output and wind speed

From the polynomial best fitting shown in Figure 3.2, the relationship between the turbine power (P, kW) and the wind speed ($v_w, m/s$), was obtained as:

$$P = 0.0683\ {v_w}^2 + 0.0062\ v_w - 0.8011 \tag{3.2}$$

3.2.3 Method of Excel Model Development

To develop an Excel mathematical model for an alkaline water electrolyser (AWE) powered by a Bergey 10kW wind turbine, the spreadsheet was structured to act as a quasi-steady-state simulator. The goal of the model was to convert the wind power (P, kW) into hydrogen mass flow ($\dot{m}_{H_2}$, kg/hr) while accounting for the electrochemical losses identified in the previous chapter. The model development steps were:

Step 1: Basic Model Inputs

The Excel sheet, as shown in Appendix-A, was set up with column headers to handle the data for each month. The model inputs included the parameters as follows:

Column-A:

It includes month of the year (from January to December)

Column-B:

It includes wind speed (m/s) using measurements recorded at 10 m

Column-C:

It includes wind speed (m/s) data at 30 m. Use the records at 10 m to calculate the speed at the turbine hub height of 30 m

Column-D:

It includes wind power output (kW). The power was calculated using the power curve fit Equation (3.2) of the wind turbine Bergey 10 k W.

Column-E:

It includes the daily average wind energy produced by the wind turbine (kWh/day). It was calculated as the Power in kW (Column-D) times 24 hrs/day.

Column-F:

It includes electrolyser operating temperature, which was assumed as 70°C for the Excel model and TRNSYS simulation. This temperature was used to calculate the temperature-dependent efficiency.

Column-G:

It includes the operating temperature in K, which was evaluated from:

$$T_{elect}(K) = T_{elect}(℃) + 273.16 \quad (3.3)$$

Step 2: Iteration for Cell Voltage

Iteration was used for cell voltage to deal with the non-linear, interdependent relationships between the voltage and other system variables, such as current and temperature (Gambou et al., 2022). During operation, the cell voltage varies with the operating temperature, but the increased temperatures decrease the overpotentials. Nevertheless, the heat generated by the electrolyser, which changes the system operating temperature, must be calculated from the difference between the operating voltage and the thermoneutral voltage of the cell. Thus, an iteration loop was needed.

First, an initial value of the cell voltage was assumed and used to calculate the current using the power output value (Column-D). Second, the current was evaluated using the power output (Column-D) and the assumed cell voltage. Third, the reversible voltage was then calculated using the operating temperature in K (Column-G). Fourth, the ohmic voltage was then calculated using the current and resistance. Sixth, the activation voltage was calculated using the operating temperature in °C (Column-F). Seventh, the concentration overpotential was assumed constant at 0.233V (Column-M).

Finally, the cell voltage was recalculated as the sum of the reversible, ohmic, activation and concentration voltage. The iteration was conducted between the assumed cell voltage and the recalculated value until both reach same value.

The excel sheet work continues as follows:

Column-H:

It includes the initial assumption of cell voltage U_{cell} (say 1.8 V as first iteration)

Column-I:

It includes the calculated stack current I (A). For number of series cells (N=20), the current I (A) was calculate from:

$$I(A) = \frac{P\ (W)}{N\ V_{cell}} = \frac{P(kW)*1000}{20\ V_{cell}} \tag{3.4}$$

The number of cells was taken as 20, for the mathematical model and TRNSYS simulation.

Column-J:

It includes the reversible voltage U_{rev} (V) calculated from:

$$U_{rev} = 1.5184 - (1.5421 \times 10^{-3}\ T) + (9.523 \times 10^{-5}\ T\ lnT) + (9.84 \times 10^{-8}\ T^2) \tag{3.5}$$

The temperature T was in K

Column-K:

It includes the ohmic voltage U_{Ohm} (V) calculated from:

$$U_{Ohm} = \frac{I(A)}{A(m^2)}\left(r_1(\Omega.m^2) + r_2\left(\frac{\Omega.m^2}{℃}\right).T(℃)\right) \tag{3.6}$$

The temperature T is in °C, r_1 and r_2 are empirical parameters of the semi-empirical Ulleberg model (Ulleberg, 2003), which is commonly used for alkaline water electrolysers. Thus, the ohmic voltage was evaluated from:

$$U_{Ohm} = \frac{I}{0.3}\left((8.05 \times 10^{-5}) + (-2.50\ \times\ 10^{-7})\ T\right) \tag{3.7}$$

Column-L:

It includes the activation voltage U_{act} (V) calculated from:

$$U_{act} = s\ .log\left[\frac{I}{A}\left(t_1 + \frac{t_2}{T(℃)} + \frac{t_3}{T^2(℃)}\right)\right] \tag{3.8}$$

In the above equation, s is referred to as the *Tafel slope* constant (V), which describes the baseline voltage needed to initiate the electrochemical reaction. In addition, $t_1, t_2,$ and t_3 are empirical temperature coefficients used to adjust the exchange current density (m^2/A). The used temperature was in K. Therefore, the activation voltage was calculated from:

$$U_{act} = 0.185\ \ log\left[\frac{I}{0.3}\left(-0.1002 + \frac{8.420}{T(℃)} + \frac{243.3}{T^2(℃)}\right)\right] \tag{3.9}$$

Column-M:

It includes the assumed constant concentration overpotential (0.233V)

Column-N:

It includes the re-calculated Cell voltage, evaluated as:

$$U_{cell} = U_{rev} + U_{Ohm} + U_{act} + U_{conc} \tag{3.10}$$

In the above equation, U_{act} is the activation voltage (V), U_{Ohm} is the Ohmic voltage (V), and U_{conc} is the concentration overpotential (V). The iteration function was implemented until cell voltage in Column-H equals cell voltage in Column-N, which indicated that the actual cell voltage was obtained.

Column-O:

It included the re-calculate current I (A) using Equation (3.4).

Column-P:

It included the calculated Faraday efficiency (η_F), which was evaluated using the current (Column-O). It is crucial for the off-grid systems where the turbine often runs at low power. The Faraday efficiency was evaluated using the empirical Equation (2.28) of Section (2.7.3) of the previous chapter.

$$\eta_F = \left(\frac{\left(\frac{I(A)}{A(m^2)}\right)^2}{f_1\left(\frac{A^2}{m^4}\right) + \left(\frac{I(A)}{A(m^2)}\right)^2} \right) f_2$$

In the above equation, A is the electrolyser cell area, which was set at 0.3 m^2 to match the entry to TRNSYS software. The empirical parameters (f_1 & f_2) were used to model how current density (I/A) and temperature affect the hydrogen gas production of the system. Therefore, the Faraday efficiency was calculated from:

$$\eta_F = \frac{\left(\frac{I}{0.3}\right)^2}{25{,}000 + \left(\frac{I}{0.3}\right)^2} \ (0.98) \tag{3.11}$$

This also ensures efficiency decrease when the Bergey turbine of small-scale power is slowly rotating in light winds.

Column-Q:

It includes the hourly hydrogen production rate ($\dot{m}_{H_2}$, kg/hr), calculated by using Faraday's law, as follows:

$$m_{H_2}\left(\frac{kg}{h}\right) = m_{H_2}\left(\frac{g}{s}\right) * 3.6 = \left(\frac{\eta_F \, N \, I(A) \, M_{H_2}\left(\frac{g}{mole}\right)}{z \, F\left(\frac{C}{mole}\right)} \right) * 3.6 \tag{3.12}$$

The parameters of the above equation are described in the previous chapter. Therefore, the mass flow rate of hydrogen was evaluated from:

$$m_{H_2}\left(\frac{kg}{h}\right) = \frac{\eta_F * 20 * I * 2.016}{2 * 96485} * 3.6 = \ 0.0007522 * \eta_F * I \tag{3.13}$$

Column-R:

It includes the daily average hydrogen production rate for each month ($\dot{m}_{H_2}$, kg/day), which was calculated as hourly hydrogen production rate ($\dot{m}_{H_2}$, kg/hr) (Column-Q) times 24 hr/day.

Column-S:

It includes the number of days for each month.

Column-T:

It includes the monthly hydrogen production ($\dot{m}_{H_2}$, kg/month), which was calculated as the daily average hydrogen production rate ($\dot{m}_{H_2}$, kg/day) (Column-R) times the number of days for each month (Column-S). The sum of the monthly hydrogen production gives the average annual hydrogen production capacity (kg/year).

Column-U:

It includes the monthly average specific energy consumption (SEC, kWh/kg), which was calculates as the ratio between the wind turbine power (kW) (Column-D) and the hourly hydrogen production rate (kg/h) (Column-Q). The average annual SEC was evaluated as the mean value of the monthly average SEC.

3.2.4 Check of Model Soundness

To ensure that the mathematical model is thermodynamically sound, its alignment was tested against the theoretical higher heating value efficiency, voltage efficiency, and low-power intermittency, as follows:

a) Check for HHV efficiency alignment

The HHV efficiency is defined (Xia et al., 2023) as the ratio between the energy content of the produced hydrogen and the consumed electrical energy. At standard conditions, the higher heating value (HHV) of hydrogen is 141.7 MJ/kg or 39.4 kWh/kg (See Table2.2)

With absence of heat exchange with the environment, the electrolyser operates at 100% HHV efficiency when the thermoneutral voltage (U_{therm}) is about 1.48 V/cell. In Excel sheet, have an individual column for HHV efficiency as follows:

Column-V:

It includes the theoretical HHV Efficiency (η_{HHV}) calculated from:

$$\eta_{HHV} = \frac{\dot{m}_{H_2}\left(\frac{kg}{h}\right).\ HHV\left(\frac{kWh}{kg}\right)}{Power\ (kW)} \times 100 = 39.4\,\frac{\dot{m}_{H_2}.}{P} \tag{3.14}$$

The check results show that the theoretical HHV efficiency never exceeded 100%. Thus, the calculated Faraday efficiency and current were physically possible.

b) Check of voltage efficiency

In Excel sheet, use an individual column for voltage efficiency as follows:

Column-W:

It includes the voltage efficiency (η_{volt}). The cell voltage (U_{cell}) was checked against the thermoneutral voltage (U_{therm}), using the voltage efficiency, described by Equation (2.29) in the previous chapter. The voltage efficiency was evaluated as:

$$\eta_{volt} = \frac{U_{therm}(V)}{U_{cell}(V)} \times 100 = \frac{1.48\,V}{U_{cell}(V)} \times 100 \tag{3.15}$$

The voltage efficiency was compared to the previously calculated HHV efficiency. They should be identical in the absence of losses, but differences were found due to the Faraday efficiency losses. The maximum value of the voltage efficiency was always less than 100%.

Column-X:

It includes the monthly average current density J, mA/cm^2. The electrolyser cell surface area was assumed as 0.3 m^2 in both Excel model and TRNSYS simulation. The current in ampere in (Column-O) was divided by 0.3 times 10 to convert from A/m^2 into mA/cm^2.

Column-Y:

It includes the monthly average wind energy produced by the wind turbine (kWh/month). It was calculated as the average daily turbine energy for each month (Column-E) times the number of days of each month (Column-S). The sum of the monthly average wind energy gives the annual amount of energy generated by the wind turbine (kWh/year).

3.2.5 Mathematical Model Verification

a) Cell voltage verification

The mathematical model developed using Microsoft Excel was verified using the calculated cell voltage. The Excel model results were compared with experimental data obtained from the study of Hug et al. (1993) conducted using 25 cells and 10 kW electrolyser. The reference values used for the comparison included the operating temperature of 70°C, atmospheric pressure, and electrolyser surface area 0.25 m^2 per cell. The verification results are shown in Table 3.4.

Table 3.4 Verification of the Excel model: Comparison of cell voltage

Current density (mA/cm^2)	Cell voltage (V)		Absolute error (V)	Percentage error (%)
	Hug et al. (1993)	Excel model		
30	1.503	1.707	0.204	12.0
40	1.545	1.737	0.192	11.1
50	1.580	1.762	0.182	10.4
60	1.614	1.784	0.170	9.5
70	1.640	1.805	0.165	9.1
80	1.660	1.824	0.164	9.0
90	1.693	1.839	0.146	8.0
100	1.717	1.855	0.138	7.5
110	1.740	1.870	0.130	7.0
120	1.761	1.886	0.125	6.6
150	1.810	1.926	0.116	6.0
200	1.882	1.988	0.106	5.3
250	1.946	2.043	0.097	4.8
300	2.006	2.095	0.089	4.3
350	2.062	2.145	0.083	3.9
400	2.115	2.194	0.079	3.6
450	2.167	2.241	0.074	3.3
500	2.217	2.287	0.070	3.1
550	2.266	2.333	0.067	2.9
600	2.313	2.378	0.065	2.7
Mean absolute percentage error (MAPE)				**6.49**

As shown in Table 3.4, the calculated Mean Absolute Percentage Error (MAPE) was 6.49%, which indicated good agreement as it is less than 10% as recommended by Rodriguez and Amores (2020) and Ashraf et al. (2025). Moreover, the model results of cell voltage and the data of Hug et al. (1993) were plotted versus the current density as shown in Figure 3.3.

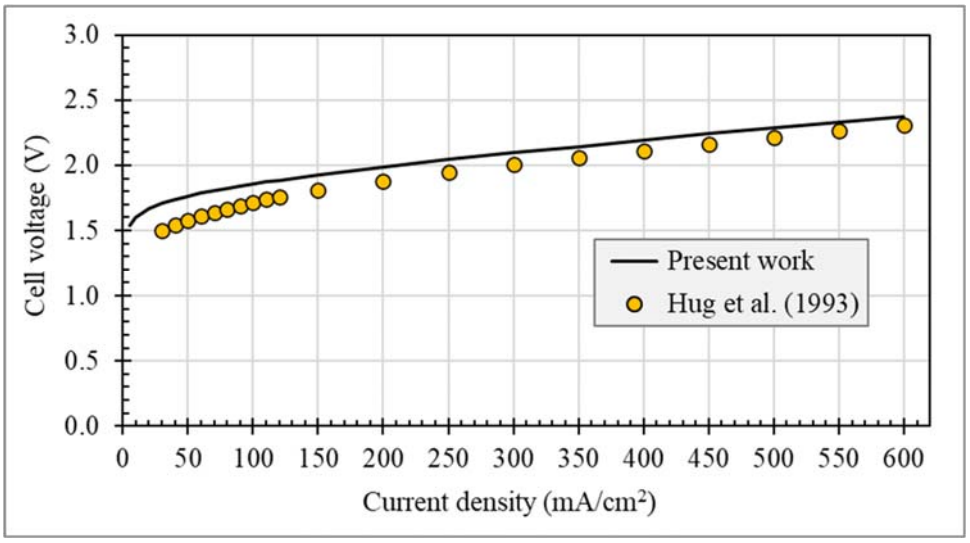

Figure 3.3 Cell voltage versus current density at temperature 70°C

As shown in Figure 3.3, the cell voltage calculated using Excel model was slightly higher than Hug et al. (1993), especially at current density lower than 200 mA/cm^2. This may be related to the assumption of high electrolyser's concentration overpotential of 0.233V in Excel model. As also shown the difference between the cell voltage of the present work and that of Hug et al. (1993) increases with the decrease of current density below 200 mA/cm^2, as reported by Jarvinen et al. (2022) as well.

b) Faraday efficiency verification

Faraday efficiency was verified by comparing the Excel model results against the standard curve of Ulleberg (2003). This comparison helps to assess the accuracy of the predictions of hydrogen mass loss when the electrolyser operates at low power such as the case of wind power levels in Kuwait. The comparison was conducted using the reference values operating temperature 70°C, constants f_1 250 and f_2 0.95, number of cells 20, and surface area of the cell 0.25 m^2. The comparison results are shown in Table 3.5.

Table 3.5 Faraday efficiency verification results

Current density, (mA/cm^2)	Faraday efficiency (%)		Absolute Error (%)
	Ulleberg (2003)	Excel model	
10	25.5	26.9	5.4
20	59.5	59.2	0.5
30	75.5	77.0	2.0
40	82.1	84.9	3.4
50	88.5	89.1	0.7
100	94.2	95.6	1.5
150	98.1	96.0	2.1
200	98.5	96.3	2.2
Mean absolute percentage error (MAPE)			**2.2**

As shown in Table 3.5, Faraday efficiency dropped drastically below 100 mA/cm^2. Thus, the model can capture the efficiency cliffs for the intermittent wind power. Also, the verification of Faraday efficiency supports the validity of the calculated specific energy consumption (SEC, kWh/kg) of hydrogen. In summary, the developed Excel model shows high level of reliability, with Mean Absolute Percentage Error (MAPE) of 6.49% for cell voltage and 2.2% for Faraday efficiency when compared to Hug et al.(933) and Ulleberg (2003). Thus, the model is reliable to predict hydrogen production under the fluctuating wind in Kuwait.

After developing high-fidelity mathematical model in Excel, the research continued toward a multi-stage simulation of hydrogen production system using TRNSYS and HOMER Pro. In the first stage, TRNSYS was used to conduct detailed transient analyses of the system

over a meteorological year (8,760 hours) under weather conditions of Kuwait. For these analyses, dynamic interactions between the fluctuated wind speed and the electrolyser were evaluated considering the thermal management needs of the system and the effect of wind intermittency on hydrogen production capacity and electrolyser efficiency. Method of using TRNSYS to simulate the system is described in the next section.

3.3 TRNSYS Modelling of Wind-operated Electrolysers

3.4 Overview

TRNSYS software is utilised for simulating the operation and assessing the performance of thermal and electrical energy systems. This software has comprehensive libraries containing accurate data on different components used to simulate various thermal and electrical energy systems (Benachir, 2023). TRNSYS libraries were previously tested and verified by various experimental studies including Brough et al. (2021) and Dezhdar et al. (2023) to be used to develop predictive models of thermal and electrical energy systems.

TRNSYS was used for dynamic transient simulations of the system by interconnecting the components and solving the corresponding differential equations for each connection and component. So, the complication of simulation was limited to identification of components' specifications (Izadi et al., 2022). Based on the features of TRNSYS such as the improved, fast, and successful simulation capabilities, it was used to predict and assess the performance of a wind-operated electrolyser system designed for green hydrogen production and operates under the weather conditions at different sits in Kuwait.

3.4.1 Components of TRNSYS Simulation Model

The proposed TRNSYS simulation model comprised the components shown in Figure 3.4.

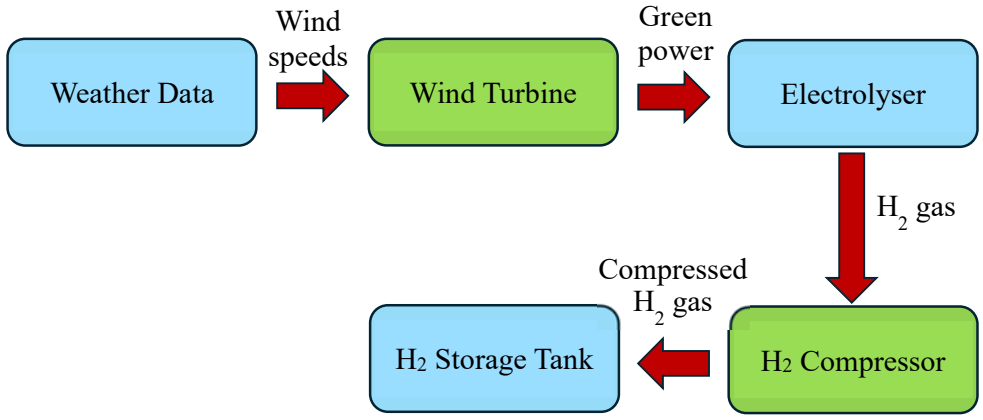

Figure 3.4 Main component of the proposed TRNSYS model

As shown in Figure 3.4, the developed TRNSYS simulation model comprised the following components:

a) Weather Data Reader

Weather data reader component was used to read and acquire accurate hourly weather data records for different sites in Kuwait. The weather data includes records of the average wind speeds that were used for evaluating the output power to be generated by the wind turbine.

b) Wind Turbine

Suitable wind turbine machine of rated output power higher than the electrolyser capacity was selected. For the selected turbine, the power curve data and other specifications were obtained and entered to the Wind Turbine TRNSYS component to predict the wind (green) output power available to operate the electrolyser.

c) Alkaline Electrolyser

Alkaline water electrolyser TRNSYS component was selected, which was operated using the wind turbine green power to split water molecules into hydrogen and oxygen.

d) Hydrogen Compressor

Hydrogen compressor TRNSYS component was selected. The hydrogen gas produced by the water electrolyser needs compression to increase the pressure and accordingly decrease the volume of the required hydrogen storage equipment (i.e. storage tank).

e) Hydrogen Storage Tank

Hydrogen storage tank TRNSYS component was selected. The compressed hydrogen gas produced by the system was stored in this tank. A specific consumption rate of the stored gas from the tank was assumed, which was used to simulate the storage tank operating cycles.

More details on the operating principles and the governing equations of each component are presented in the next section.

3.4.2 Mathematical Models of System Components

a) Wind Turbine

Wind turbine is a mechanical and electrical energy harvesting system. The turbine converters part of the kinetic energy of the oncoming wind into mechanical energy. The forces of the high-speed wind rotate the wind turbine rotor to generate mechanical power. The mechanical power is converted into electricity, which is used to operate the electrolyser to split water to

produce green hydrogen. The mathematical model to estimate the output power of the wind turbine (Oueslat, 2021) is as follows:

$$P = \frac{1}{2}\, C_p\, \rho_{air}\, A_{rotor}\, v_w^3 \tag{3.16}$$

In the above equation,

P is the output power of the wind turbine (W)

C_p is the power coefficient of the wind turbine (for modern wind turbine designs, the power coefficient is typically in the range from 0.25 to 0.45 (Oueslat, 2021)

ρ_{air} is the density of the oncoming wind stream (kg/m^3)

A_{rotor} is the swept area of the rotor blades (m^2)

v_w is the wind speed (m/s) recorded at the rotor hub height h

For professional energy yield assessment, the wind speed at the hub height of the rotor can be calculated using the Log law as follows:

$$v_w = v_g \left[\frac{ln(h/Z_0)}{ln(10/Z_0)}\right] \tag{3.17}$$

In the above equation:

v_g is the wind speed (m/s) measured at height 10 m from the ground

h is the height of the turbine rotor hub measured from the ground (m)

Z_0 is the roughness length (0.05 m)

b) Alkaline Water Electrolyser

Water electrolyser is the mechanical device that uses electricity (electric energy) to split the water molecules into hydrogen gas and oxygen gas. The governing chemical reaction of the water splitting process is described by Ulleberg (2003) and Hong (2013) as:

$$H_2O + Electric\ Energy \rightarrow H_2 + \frac{1}{2}O_2 \tag{3.18}$$

During simulation, TRNSYS subroutines of the alkaline water electrolyser component take into consideration the effect of hydrogen gas loss and electric current loss on the performance of the system. Therefore, the operation of the electrolyser is governed by the change between the low and high temperatures of the current-voltage curves. Thermodynamically speaking, Ulleberg (2003) and Brauns and Turek (2020) reported the expression of the Gibbs energy of the water splitting ($\Delta G, \mathrm{J/kg}$) as:

$$\Delta G = \Delta H - T\, \Delta S \tag{3.19}$$

In the above equation:

ΔH is the enthalpy change during water splitting process (J/kg)

T is the temperature during water splittting process (K)

ΔS is the entropy change of the water splitting proceess (J/kg K)

The water splitting reaction descried by Equation (3.18) can be initiated when the applied electrode voltage reaches a minimum value termed as the reversible voltage (U_{rev}) of the electrolyser cell (Brauns and Turek, 2020). The reversile voltage can be assessed using Gibbs energy of the water splitting reaction describeed by Equation (3.19). During water splitting, Ulleberg (2003) reported the use of 2 exchanged electrons (i.e., $z = 2$) to account for the reversible voltage of the electrloyser cell as follows:

$$U_{rev} = -\frac{\Delta G}{z\ F} \tag{3.20}$$

In the above equation:

F is Faraday constant (96,485 C/mol)

U_{rev} is the reversible cell voltage (about 1.229 V) at standard water splitting reaction temperatue of 25°C and standared pressure of 1 bar

Considering the effect of thermal and electrical energy losses during electrolyser operation, the actual voltage to be applied to the electrolyser cell must be higher than the reversible voltage. Hong (2013) reported the need to use overvoltage to activate the operation of the electrolyser. Therefore, to consider the effect of the ohmic losses ($I\ R_{ohm}$) of the system, the actual cell voltage (U_{cell}) to be applied can be calculated as:

$$U_{cell} = U_{rev} + \left(\gamma\ \frac{I_{ely}}{A}\right) + \left[S\ log\left(\frac{t\ I_{ely}}{A} + 1\right)\right] \tag{3.21}$$

In the above equation:

U_{cell} is the actual voltage to be applieed to the electrloyser cell (V)

U_{rev} is the theoretical (minimum) reversible voltage (V) needed for initiation

γ is a parameter depends on the ohmic resistance the electrolyser

I_{ely} is the electric current passing through the electrolyser cell (A)

A is the urface area of the electrolyser cell (m^2)

S, t are constants

In terms of the hydrogen production capacity, Haddad and Javani (2024) reported that the amount of hydrogen gas to be produced by the water electrolyser can be evaluated as:

$$n_{H_2} = \eta_F \; N_{cells} \; I_{ely} \; F \tag{3.22}$$

In the above equation:

n_{H_2} is the number of hydrogen gas moles to be produced (mol)

η_F is the Faraday efficiency (%)

N_{cells} is the number of series connected electrolyser cells (---)

I_{ely} is the electric current passing through the electrolyser cell (A)

F is Faraday constant (96,485 C/mol)

In addition to the hydrogen production, the amount of oxygen gas to be produced during the water splitting reaction can be evaluated as:

$$n_{O_2} = 0.5 \; n_{H_2} \tag{3.23}$$

where n_{O_2} is the number of oxygen gas moles (mol) to be produced during the process.

Regarding Faraday's efficiency, it is defined (Brauns and Turek, 2020; Haddad and Javani, 2024) as the ratio between the actual amount of hydrogen gas and the maximum theoretical amount that can be produced by the electrolyser. During electrolyser operation, more thermal energy (heat) is generated with the decreased electrical efficiency. Thus, the energy efficiency of the electrolyser system can be expressed (Elminshawy et al., 2024) as the ratio between the thermonutral voltage (U_{tn}) of the cell and the applied voltage to the electrolyser cell (U_{cell}), as early described in this chapter.

c) Electrolyser Controller

During simulation, TRNSYS controller component was used to assign the power setpoint of the hydrogen production system operated by the power produced by the wind turbine. The produced hydrogen was delivered to a storage tank after being compressed by a hydrogen compressor. Thus, one key parameter explaining the controller function of the developed model was the state of charge (SOC) of the hydrogen storage tank. The power setpoint of the controller was essential to keep feeding the produced hydrogen to the storage tank when the SOC is below 70% and to keep feeding the tank with hydrogen until SOC reaches 90%, after which it stopped the storage tank filling process.

During simulation, TRNSYS controller component performed the control algorithm as:

If SOC < 0.7, switch ON the system and enable the system operation by suppling the electrolyser with power equals the power generated by the wind turbine.

If SOC > 0.9, switch OFF the system and operate the system at idling using minimum (idle) power sufficient to overcome the losses

Therefore, when the controller code is "OFF", the electric power supplied to the system (P_{el}) was set at minimum power required for the electrolyser idling operation (P_{idle}).

d) Power Conditioning

During simulation, power conditioner TRNSYS component was used to convert the Direct Current (DC) output power produced by the wind turbine into a form of DC power suitable of to feed and operate the electrolyser. The power conditioning was important to ensure that the electrolyser operates at the constant voltage required for each cell with ability to change the current passing through the cell with the change of the electrolyser load. But the power conditioner performance was affected by the system losses, which were dependent on the applied current passing through the electrolyser. The system losses are expressed (Haddad and Javani, 2024) as:

$$P_{loss} = P_{in} - P_{out} = P_0 + \left(\frac{U_s}{U_{Out}}\right) P_{out} + \left(\frac{R_i}{U_{Out}^2}\right) P_{Out}^2 \quad (3.24)$$

In the above equation:

P_0 is the system power loss (equals the idle power P_{idle}) (W)

U_s is the set point of the electrolyser cell voltage (V)

R_i is the ohmic resistance of the conditioner component (**Ω**)

P_{out} is the output power of the power conditioning component (W)

U_{Out} is the output voltage of the power conditioning component (V)

e) Hydrogen Compressor

During simulation, the function of TRNSYS compressor component relies on the assumption that the process is polytropic for the various compression stages. During simulation, the compressor receives hydrogen gas exiting from the water electrolyser at an initial pressure (p_i) about 7 bars. The compressor duty was to increase the hydrogen gas pressure to a final pressure (p_f) of about 200 bar, to limit the required tank volume (Franco and Giovannini, 2024). The polytropic compression process work (w_{poly}, J/kg) was evaluated from:

$$w_{poly} = \frac{n}{n-1} R_{H_2} T_i \left[\left(\frac{p_f}{p_i}\right)^{\frac{n-1}{n}} - 1\right] \quad (3.25)$$

In the above equation:

n is the polytropic process index ($1.4 > n > 1.0$)

R_{H_2} is the hydrogen gas constant (4124.2 J/kg K)

T_i is the initial hydrogen temperature at the start of compression (K)

f) Storage Tank

TRNSYS hydrogen storage tank component was used to explore the tank performance. The hydrogen gas pressure inside the tank was calculated using van der Waals gas equation (real gas condition). In their study, Eté et al. (2008) reported the use of van der Waals equation to evaluate the hydrogen gas pressure inside the tank p (Pa) as follows:

$$p = \frac{n\,R\,T_{gas}}{V_{tank} - n\,b} - a\left(\frac{n^2}{V_{tank}^2}\right) \tag{3.26}$$

In the above equation:

n is the hydrogen gas molar amount (mol)

R is the universal gas constant (8.314 J/mole K)

T_{gas} is the gas temperature inside the storage tank (K)

V_{tank} is the volume (capacity) of the storage tank (m^3)

b is a constant expressing the volume of the gas molecules (m^3)

a is a constant varying with the intermolecular attraction force between molecules

The constants a and b (Sharifian and Harasek, 2013; Haddad and Javani, 2024) are:

$$a = \frac{27\ R^2\ T_{cr}^2}{64\ p_{cr}} \qquad b = \frac{R\ T_{cr}}{8\ p_{cr}} \tag{3.27}$$

In the above equations:

T_{cr} is the critical temperature of the hydrogen gas (33.18 K)

p_{cr} is the critical pressure of the hydrogen gas (1.3×10^5 Pa)

3.4.3 TRNSYS Model Components

TRNSYS model was developed to simulate, predict, and assess the performance of hydrogen production system operated using green electricity produced by wind turbine. In TRNSYS simulation modelling, the simulations were repeated several times for the three sites studied in this research. Weather data TRNSYS component was selected as wind speed free format generic data reader (Type9a), which was used as the source of the hourly records of wind speeds for each site.

The power generated by the wind turbine was used to operate the electrolyser. Therefore, a wind turbine TRNSYS component (Type90) was selected, and the specifications of the wind turbine were used to define the parameters of the wind turbine component. An alkaline water

electrolyser TRNSYS component (Type160a) was selected for producing green hydrogen through water splitting process. The specifications of the electrolyser were searched, collected, and used to change the key parameters of the component.

The system operation was controlled and tuned using a controller for the variable power electrolyser. TRNSYS controller component (Type100a) was therefore selected, and the parameters were identified. Also, a TRNSYS power conditioning component with known power INPUT (Type175a) was selected to ease the system operation and change the form of the DC power feeding the electrolyser in terms of the applied voltage and passing current.

The specifications of TRNSYS components were adjusted to suit the simulation goals. The simulated system produced hydrogen gas at a moderate pressure of 7 bars. If the gas is to be stored at moderate pressure, larger volume of the storage tank would be required. Therefore, the compressor TRNSYS component (Type167) was selected to increase the hydrogen gas pressure from 7 bars (at electrolyser outlet) to the storage tank pressure of 200 bars. For gas storage, storage tank TRNSYS component (Type164b) was selected. Also, online plotters with file of user supplied units (Type65b) were selected to show and display the simulated parameters. The simulation trials were performed using TRNSYS software version-18, using the developed model having the components and connectors shown in Figure 3.5.

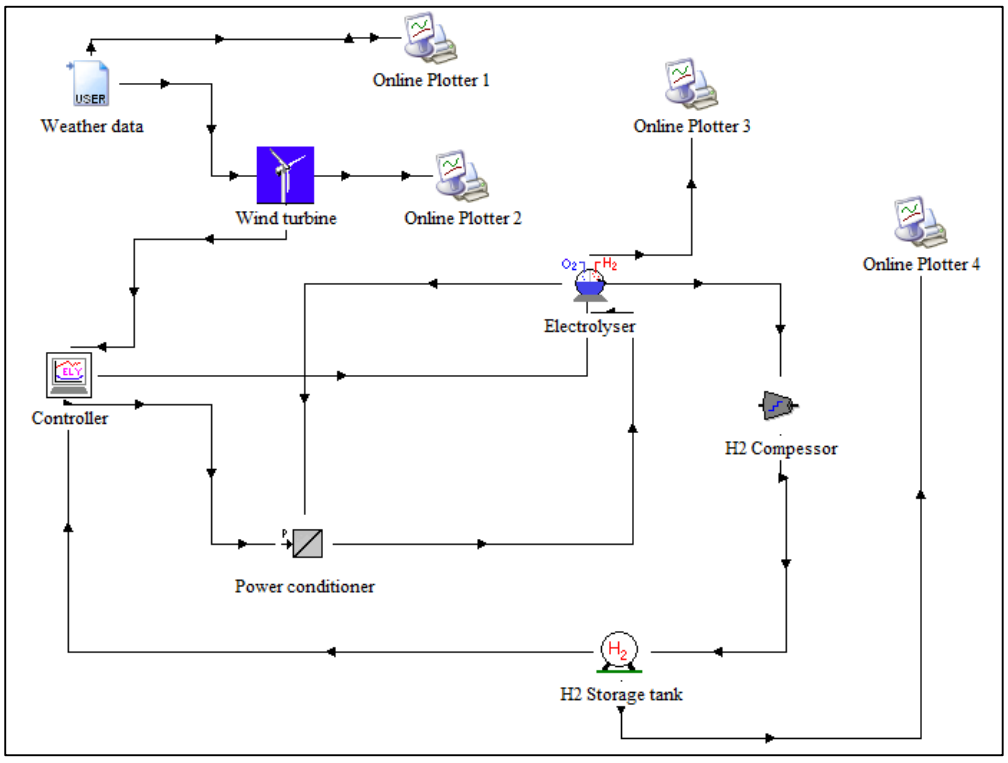

Figure 3.5 Components and connectors of the developed TRNSYS model

3.4.4 Specifications of Model Components

For the developed TRNSYS model shown in Figure 3.5, the specifications (parameters and inputs) of the different model components were identified. Some of the data were kept at the default values whereas other key parameters and inputs have been changed, as explained in the next sections.

a) TRNSYS WIND Turbine Component (Type90)

Wind turbine of power output 10 kW, which was used for developing the Excel model, was also selected for TRNSYS model. The specifications of the turbine, used to identify and alter the parameters and inputs of TRNSYS turbine component, are listed in Tables 3.1 earlier in this chapter.

Based on the turbine specifications, certain parameters and inputs needed to be changed in TRNSYS wind turbine component. The adjustments include:

- Setting the data collection height as 10 m
- Changing the rotor hub height to 30 m
- Identifying the logical unit of file containing power curve data as 36.

In addition, the inputs to the turbine TRNSYS component were adjusted as follows:

- The control signal was set to 1
- The wind speed was entered as 14 m/s
- The ambient temperature was set at 25C
- The site shear exponent was set as 0.16
- The barometric pressure was changed to 101325 Pa

b) TRNSYS Electrolyser Component (Type160a)

The power generated by the wind turbine was used to operate the alkaline water electrolyser to split water molecules to produce green hydrogen. The electrolyser component (Type160a) was the key component of the system. Therefore, it was essential to adjust the component's parameters and inputs to ensure producing meaningful simulation predictions. Some of the default values of the TRNSYS alkaline water electrolyser component were kept unchanged whereas other parameters have been changed. The parameters and input of the electrolyser component (Type160a) were adjusted as shown in Table 3.6.

Table 3.6 Parameters and inputs of the electrolyser TRNSYS component

	Specification	Value
Parameters	Temperature mode	1
	Electrolyser area	0.3 m^2
	Number of cells in series	20
	Number of stacks in parallel	1
	Maximum allowable current density	600 mA/cm^2
	Maximum allowable operating temperature	80°C
	Minimum allowable cell voltage	1.4 V
	Thermal resistance	0.167 K/W
	Thermal time constant	29 hr
	Electrolyser type	1
Inputs	Electrolyser control signal	1
	Electrolyser current	100 Amp
	Electrolyser pressure	7.0 bar
	Electrolyser environment temperature	20°C
	Cooling water inlet temperature	15°C
	Cooling water flow rate	0.25 m^3/hr
	Electrolyser operating temperature	70°C

For simulation purposes, the electrolyser area was changed, to study the impact of surface area on the system performance.

c) TRNSYS Compressor Component (Type167)

The hydrogen produced by the electrolyser was compressed to a higher pressure to limit the required storage tank volume. Therefore, the parameters and inputs of TRNSYS hydrogen compressor component (Type167) were adjusted as shown in Table 3.7.

Table 3.7 Parameters and inputs of the compressor TRNSYS component

Parameters and inputs	Value
Number of parallel compressors	1
Number of compressor stages	3
Heat capacity of gas	28.86 J/mole K
Gas inlet pressure	1 bar
Desired outlet pressure	200 bars
Low temperature	25°C
Inlet volumetric flow rate of gas	5 m^3/hr

d) TRNSYS Storage Tank Component (Type164b)

One of the key components of the green hydrogen production system is the hydrogen storage tank. During system operation, the produced hydrogen was compressed and delivered to the tank when the state of charge (SOC) of the tank was dropped below 0.9. During simulation, there was continuous hydrogen consumption (exit) from the storage tank at a predefined rate of 0.2 m^3/hr. The SOC of the tank dropped when the rate of hydrogen production (fed to the tank) was less than the consumption (exit the tank). With more gas consumption from the tank, the SOC dropped below 0.9, which initiated the system operation to produce hydrogen to feed the tank. Initially, the SOC (pressure level of the tank) was adjusted at 0.4, which means start of hydrogen production and storage when the system starts operation. The specifications of the tank were set as shown in Table 3.8.

Table 3.8 Setting the specs of the storage tank TRNSYS component

Specification	Value
Pressure mode	2
Maximum pressure	200 bars
Tank volume	**1 m^3**
Molar weight of gas	2.016 g/mol
Gas critical pressure	12.9 bars
Volumetric rate of gas entering the tank	5 m^3/hr
Volumetric rate of gas exiting the tank	**0.2 m^3/hr**
Initial pressure level	0.4

As shown in Table 3.8, the tank volume was set at 1 m^3. For simulation purposes, the tank volume was changed, to study the impact of performance.

e) TRNSYS Controller Component (Type100a)

The parameters and inputs of TRNSYS the controller component (Type100a) were adjusted as shown in Table 3.9.

Table 3.9 Adjustments of the controller TRNSYS component

	Specification	Value
Parameters	Electrolyser mode	1
	Lower SOC limit	0.7
	Upper SOC limit	0.9
	Idling power	2000 W
Inputs	Tank SOC	0.2
	Power to electrolyser	100,000 W

As listed in Table 3.9, power mode (1) was selected as it is used for simulating electrolyser with variable input power. This was the case in this study due to the intermittent nature of the power generated by the wind turbine with the remarkable hourly fluctuations of the wind speeds. The lower and upper SOC limits of the storage tank were adjusted at 0.7 and 0.9, respectively. Therefore, the water electrolyser operates when $0.7 \leq SOC \leq 0.9$ to produce hydrogen to fill the storage tank.

The idling power of the system, as shown in Table 3.9, was changed to 2000 W, which was the lowest power to be generated by the wind turbine to keep the electrolyser operating at idling condition. Regarding to the inputs of the TRNSYS controller component (Type100a), the Tank SOC was set at 0.2, to allow starting green hydrogen production with the simulation start. As also shown in Table 3.9, the power supplied to the electrolyser was changed to 100 kW. The inputs of the system were changed to enable system start, before the actual tank SOC and electrolyser power needs replaces the previous values, after every simulation step during the TRNSYS predictions.

f) TRNSYS Power Conditioner Component (Type175a)

The power conditioner TRNSYS component (Type175a) was used to ensure supplying the electrolyser with required DC power, at a specific form. The power produced by the turbine is a DC electricity of voltage and current unsuitable for the electrolyser operation. The power conditioner is essential to change the voltage and current to become suitable for electrolyser operation. The parameters and inputs of the power conditioner component were adjusted as shown in Table 3.10.

Table 3.10 Parameters and Inputs of the power conditioner TRNSYS component

	Specification	Value
Parameters	Mode	1
	Nominal power	10,000 W
	Idling constant	5.836×10^{-3}
	Set point voltage	**2.06 V**
	Ohmic constant	138.42 V^2
	Number of units in parallel	1
	Parasitic power	0 W
Inputs	Input voltage	22,000 V
	Output voltage	130 V
	Input power	10,000 W

For the power conditioning component parameters, listed in Table 3.10, the idling constant was the ratio between the power loss (constant in magnitude) and the nominal power of the simulated system. The ohmic constant was evaluated as the internal resistance of the system times the system nominal power. Also, the parasitic power was the auxiliary power needed for the system operation.

The simulation of the system performance was conducted based on 2022 wind speed data recorded at each of the three sites Kuwait Airport, WAFRA, and ABDALY. The wind speed data were obtained from the weather data library at Kuwait Institute for Scientific Research (KISR). Examples of TRNSYS output files are shown in Appendix-B.

3.4.5 Analysis Methods of Simulation Predictions

Simulation of the green hydrogen production system operation at each site started with reading the wind speed values using TRNSYS weather reading component. The wind speeds were used to evaluate the output power of the wind turbine, which was controlled before being used to operate the electrolyser to split water to produce hydrogen. The pressure of the hydrogen produced by the electrolyser is increased using compressor before being fed to the tank to be stored. The simulation trials were conducted using time step 1 hour. The simulation results were predicted for a whole year (8760 hours). The collected simulation results for the modelled system include the hourly values of the wind speed, wind turbine power, and green hydrogen production amount.

The predicted amounts of the hourly green hydrogen production were used to evaluate the monthly average production capacity and then the annual hydrogen production capacity, for each site. Moreover, the storage tank operation (charging/discharging) was assessed using the hourly predictions values of the SOC of the storage tank. The predictions were obtained, analysed and compared for the three sites. The simulation work of the system operation was repeated at different electrolyser surface area and various tank volumes, and the performance was assessed. The results were compared for the three sites.

After simulating the dynamic operation of the system with TRNSYS, the second stage of the multi-stage simulation was to conduct a techno-economic analysis of the system to optimise the system components. For this purpose, HOMER Pro was used to determine the optimum size and capacity of system components for minimised Levelised Cost of Hydrogen (LCOH). Detailed description of method of using HOMER Pro is given in the next section.

3.5 System Optimisation using HOMER Software

3.5.1 Significance of System Optimisation

To simulate the dynamic performance of thermal and electrical energy systems, TRNSYS enables collection of valuable results. But it is very difficult to optimise the components of these systems using TRNSYS. The renewable energy systems are usually optimised using optimisation algorithms (Adedoja et al., 2024). In this study, HOMER Pro software was selected to optimise the green hydrogen production system. HOMER Pro has a user-friendly interface and large library of components, which supports conducting techno-economic assessments. The adequate sizing of system components, in terms of number and capacities, is crucial for better system operation at minimised costs. The system optimisation includes sets of iterative sizing to reach the best possible size. One of the key contributions of this study the optimisation study of a green hydrogen production system, operating using wind power in harsh weather in Kuwait, using HOMER Pro software.

3.5.2 HOMER Pro for System Optimisation

HOMER software was used to conduct an hourly simulation over an entire year. The purpose of simulation was to assess the system feasibility in terms of sufficiency to serve electrical and hydrogen loads. The simulation enabled evaluating the total system costs over the project lifetime. Moreover, the system costs were essential for comparing the economics of the system at different sites in Kuwait. The method of using HOMER Pro software for system optimisation included the following steps:

Step-1: Input the Geographic Location Data

In this step, the geographical data of the sites proposed for green hydrogen production system installation were entered as inputs. The data included the latitude angle, longitude angle, and elevation above sea level. These data were obtained from Google maps and manually entered to the model.

Step-2: Input the Weather Conditions Data

For any investigated site, key weather data were required for the simulation and to conduct system optimisation. In this study, the utilised weather data included the monthly average global solar radiation (kWh/m^2/day) and the clearness index, the ambient temperature (°C), and the wind speed (m/s). The solar radiation and clearance index data were accessed from NASA website linked to HOMER Pro. Meanwhile, the daily average wind speed data for each month, previously used for Excel model simulation, were entered to HOMER.

Step-3: Input the Electrical and Hydrogen loads

In this step, the electrical load (kWh) was entered for each hour for one day (electricity load profile). Also, the hydrogen load (kg/hr) was entered on hourly basis for one day (hydrogen load profile). The methods to develop the profiles of the electrical and hydrogen loads are explained later in this chapter.

Step-4: Input the Economic Data and Constraints

After selecting the system components required for system operation. The economic data of each component were entered to HOMER Pro including the capital cost ($), replacement cost ($), O&M cost ($), etc. for each component. Flow chart, showing method of using HOMER Pro software, is shown in Figure 3.6.

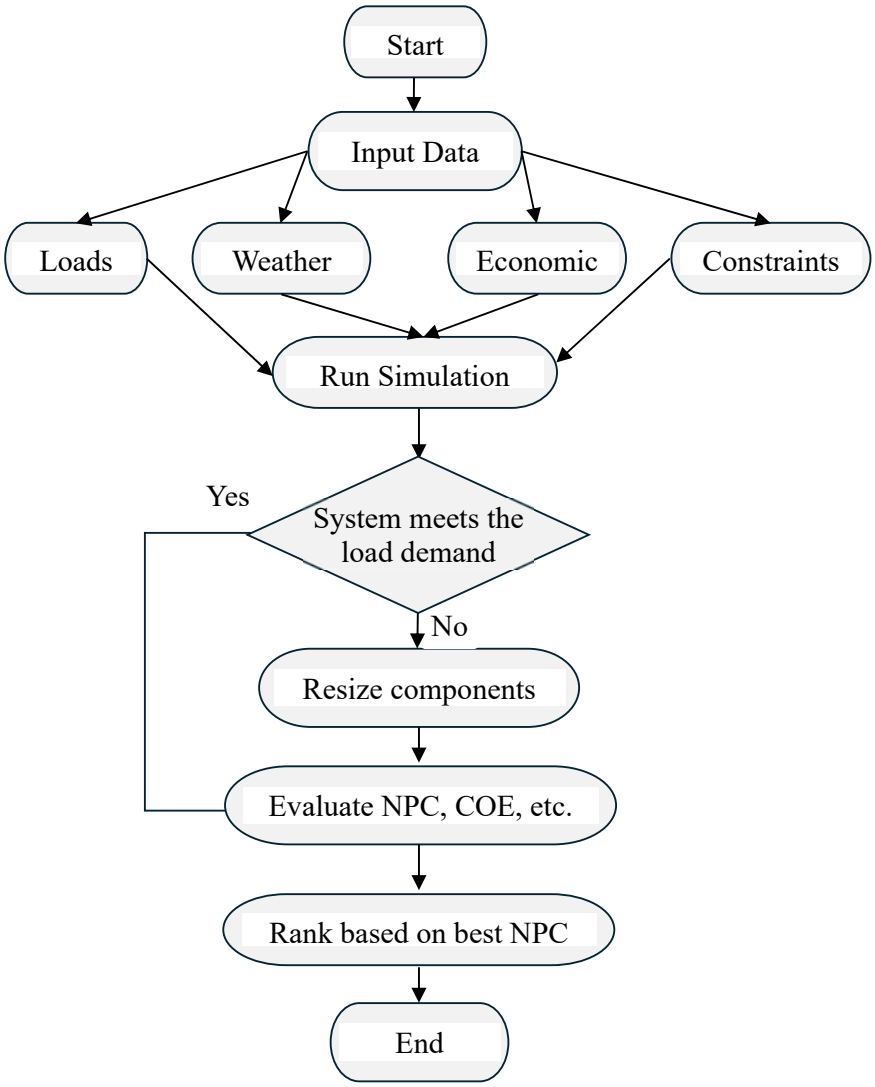

Figure 3.6 Flow chart of HOMER software utilisation steps

3.6 Geographic Data, Loads and System Resources

For all the investigated sites in Kuwait, there are preliminary data to be identified before starting the simulation and optimisation. For instance, the discount rate was set at 3.5%, the inflation rate was set at 2%, and the project lifetime was set at 25 years. Details of the optimisation process are explained in the next sections.

3.6.1 Geographic Data of the Investigated Sites

The system optimisation was conducted for the three sites used for TRNSYS simulation. These sites are Kuwait Airport site, Wafra site, and Abdaly site, which have geographic data as shown in Table 3.11.

Table 3.11 Geographical data of the investigated sites

Site	Latitude	Longitude	Elevation (m)
Airport	29.20°N	47.97°E	63
Wafra	28.59°N	48.10°E	103
Abdaly	29.98°N	47.73°E	20

3.6.2 Electrical Load of the System

The electrical load describes the AC electricity needs that the system needs to meet. This load is required for lighting, appliances, computers, industrial needs, and other needs. When the system generates less electricity than the required electrical load, HOMER identifies the case as unmet load. The hourly needs of electricity are shown in Table 3.12, the load metrics are in Table 3.13, and the load profile is shown in Figure 3.7.

Table 3.12 Hourly electrical load (kWh) of the system

hr	kWh		hr	kWh		hr	kWh
00–01	0.40		08–09	1.10		16–17	1.10
01–02	0.40		09–10	1.10		17–18	1.10
02–03	0.40		10–11	1.10		18–19	1.10
03–04	0.40		11–12	1.10		19–20	0.40
04–05	0.40		12–13	1.10		20–21	0.40
05–06	0.40		13–14	1.10		21–22	0.40
06–07	0.60		14–15	1.10		22–23	0.40
07–08	0.60		15–16	1.10		23–00	0.40

Table 3.13 Metrics of the electrical load of the system

Metric	Baseline	Scaled
Average (kWh/day)	17.7	12
Average (kW)	0.74	0.50
Peak (kW)	1.98	1.34
Load factor	0.37	0.37

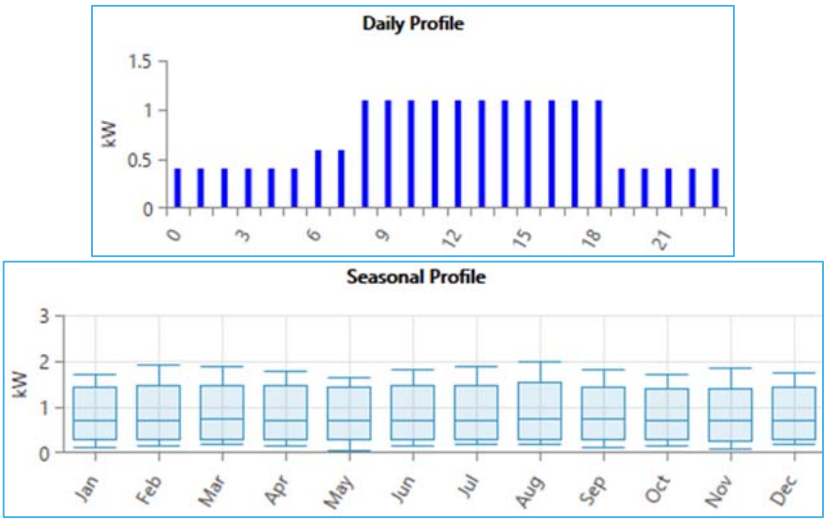

Figure 3.7 Daily and seasonal profiles of the electrical load

For the electrical load of this study, the scaled annual average was 12 kWh/day. The Day-to-day random variability was set at 10%, and the Time step random variability was set at 20%.

3.6.3 Hydrogen Load of the System

The hydrogen load presents the hydrogen gas needs that the system needs to meet. Hydrogen load describes the rates of hydrogen consumption and the hydrogen gas to be stored in the storage tank. The hourly demands of hydrogen are assumed as shown in Tale 3.14, and the metrics of the hydrogen load are shown in Table 3.15. The hourly and seasonally changes of the hydrogen load profile are shown in Figure 3.8.

Table 3.14 Hourly hydrogen load (kg/day) of the system

Period	Activity Level	Flow (kg/h)
00:00 - 06:00	Base Load (Low)	0.040
06:00 - 09:00	Morning Peak	0.180
09:00 - 17:00	Steady Day Load	0.090
17:00 - 21:00	Evening Peak	0.200
21:00 - 00:00	Night Ramp-down	0.065

Table 3.15 Metrics of the hydrogen load of the system

Metric	Baseline	Scaled
Average (kg/day)	2.49	1.00
Average (kg/h)	0.1	0.04
Peak (kg/h)	0.36	0.15
Load factor	0.28	0.28

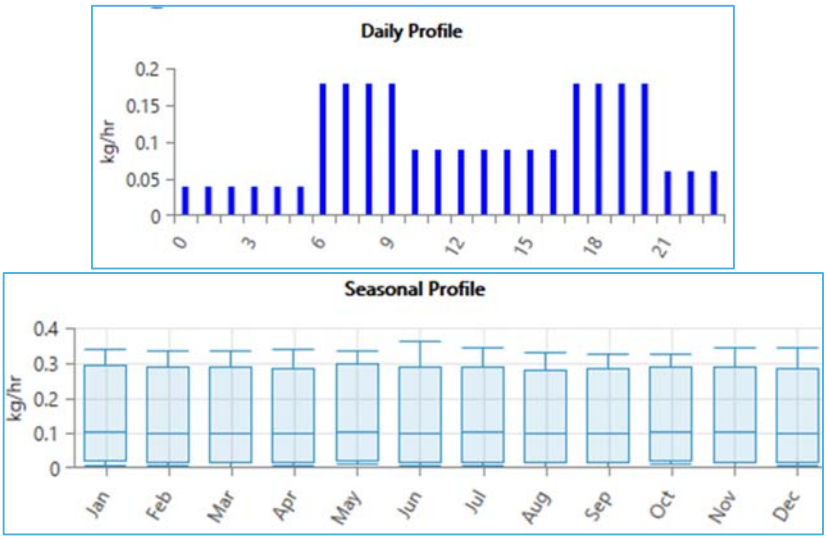

Figure 3.8 Daily and seasonal profiles of the hydrogen load

For the hydrogen load, the scaled annual average was 1.0 kg/day, which was subjected to sensitivity analysis to explore its impact on the system performance. The Day-to-day random variability was set at 10%, and the Time step random variability was set at 20%.

3.6.4 Resources of the System

The renewable resources considerably vary from one installation site to another. In this study, the wind power varies with the patterns of atmospheric circulation and the geographic effects at each site. At any site, the wind power may have significant variability both hourly and seasonally. HOMER can produce synthetic average hourly wind speed data so that there are several parameters to firstly set. For instance, Weibull shape is set at 2, autocorrelation factor is set at 0.85, diurnal pattern strength is set at 0.25, and hour of peak speed is set at 15. The anemometer height is set as 10 m above the ground. Since the turbine rotor hub height was different from the anemometer height, the hub height was entered as 30 m based on the wind turbine specifications. These parameters and setting the surface roughness at 0.01m enabled HOMER to evaluate the wind speed at the hub height using the logarithmic law.

For each investigated site, the system resources (solar radiation and ambient temperature) data were downloaded from NASA website based on the geographic location of the site. The solar radiation data included the global horizontal irradiance (GHI, kWh/m^2/day) and the clearness index (CI). The ambient temperature data included the daily average value (°C) for each month. Meanwhile, the daily average wind speed (m/s) for each month were manually entered to HOMER using the same data used for TRNSYS simulation trials.

a) Solar Radiation Resources

For the investigated sites, the clearness index (CI) and the global horizontal irradiance (GHI, kWh/m^2/day) are shown in Table 3.16 and Figure 3.9, respectively.

Table 3.16 Solar radiation data for the investigated sites

Month	Airport site		Wafra site		Abdaly site	
	CI	GHI	CI	GHI	CI	GHI
January	0.530	3.20	0.573	3.52	0.541	3.20
February	0.583	4.23	0.608	4.47	0.592	4.23
March	0.571	5.05	0.573	5.10	0.576	5.05
April	0.570	5.84	0.554	5.70	0.571	5.84
May	0.631	7.01	0.601	6.67	0.631	7.01
June	0.692	7.89	0.670	7.62	0.691	7.89
July	0.681	7.64	0.661	7.40	0.680	7.64
August	0.677	7.13	0.672	7.08	0.678	7.13
September	0.663	6.16	0.691	6.46	0.667	6.16
October	0.613	4.72	0.651	5.07	0.620	4.72
November	0.514	3.24	0.575	3.68	0.524	3.24
December	0.469	2.65	0.543	3.13	0.480	2.65

a) Airport site: scaled annual average is 5.40 kWh/m^2/day

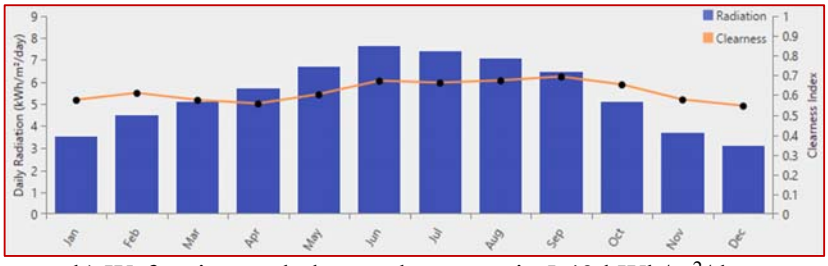

b) Wafra site: scaled annual average is 5.49 kWh/m^2/day

c) Abdaly site: scaled annual average is 5.40 kWh/m^2/day

Figure 3.9 Daily average solar radiation data for the sites

b) Ambient Temperature Resources

For the investigated sites, the daily average ambient temperatures for each month are shown in Table 3.17 and Figure 3.10, respectively.

Table 3.17 Ambient temperature (°C) data for the investigated sites

Month	Airport site	Wafra site	Abdaly site
January	12.46	13.83	12.22
February	14.43	15.27	14.30
March	18.91	19.10	18.96
April	25.10	24.62	25.35
May	31.41	30.65	31.80
June	35.38	34.69	35.86
July	37.23	36.57	37.74
August	37.05	36.43	37.51
September	33.50	33.32	33.79
October	28.17	28.58	28.24
November	20.44	21.73	20.24
December	14.48	16.08	14.14

a) Airport site: scaled annual average is 25.71°C

b) Wafra site: scaled annual average is 25.91°C

c) Abdaly site scaled annual average is 25.85°C

Figure 3.10 Daily average ambient temperature (°C) data for the sites

c) Wind Speed Resources

Wind speeds at 10 m, for the sites, are shown in Table 3.18 and Figure 3.11, respectively.

Table 3.18 Wind speed (m/s) data (at 10 m) for the investigated sites

Month	Airport site	Wafra site	Abdaly site
January	5.51	4.40	3.82
February	5.53	4.42	4.05
March	5.57	4.39	4.03
April	5.98	4.48	4.23
May	6.50	4.64	4.34
June	8.22	5.57	5.57
July	6.65	5.02	4.76
August	6.05	4.48	4.53
September	5.87	4.39	4.27
October	5.06	4.02	3.81
November	5.22	4.17	3.75
December	5.35	4.06	3.61

a) Airport site: scaled annual average is 5.96 m/s

b) Wafra site: scaled annual average is 4.50 m/s

c) Abdaly site: scaled annual average is 4.23 m/s

Figure 3.11 Daily average wind speed data, at 10 m, (m/s) for the sites

3.7 Design and Components of the System

3.7.1 Design of the System

The components of the green hydrogen production system, operated by the wind power, is shown in Figure 3.12.

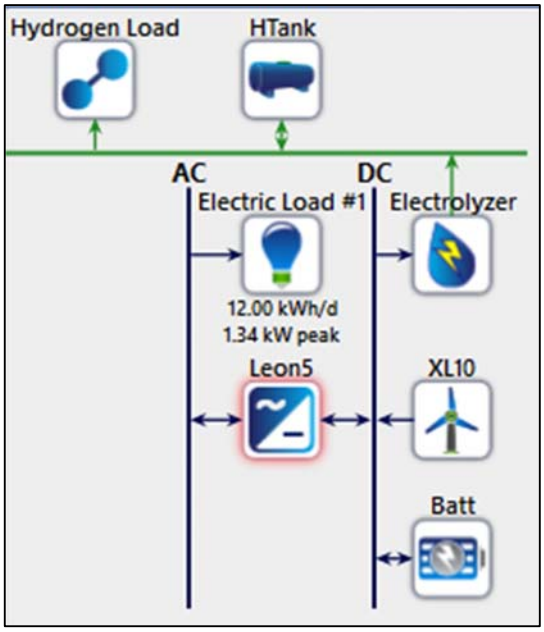

Figure 3.12 Components of the green hydrogen production system

As shown in Figure 3.12, the designed system comprised a wind turbine, an alkaline water electrolyser, storage batteries, a converter (AC/DC), a storage tank, an electrical load, and a hydrogen load. During HOMER simulation, the wind turbine produces DC electricity, which needs be converted to AC using the converter component to fulfil required AC electrical load. The excess DC electricity produced by the wind turbine is used to operate the alkaline water electrolyser to produce hydrogen to fulfil the required hydrogen load and store the remaining hydrogen in a storage tank. HOMER optimisation is therefore supportive to decide the number of wind turbines, the number of storage batteries, the converter capacity, the size of the electrolyser, and the capacity of the hydrogen storage tank. The next sections are devoted for explaining the significance, features, cost, etc. of the different components of the system.

3.7.2 Features and Economic data of System Components

a) Wind Turbine

To simulate the system performance on hourly basis, HOMER evaluates the generated wind turbine power using four steps. First, the wind speed data for each site is used to evaluate

the hourly average speed at the anemometer height of 10 m. Second, the hourly average wind speed is evaluated at the hub height of the turbine using the logarithmic law. Third, the wind turbine power curve is used to evaluate the turbine output power assuming standard air density of 1.225 kg/m^3. Fourth, the turbine power output is multiplied by the ratio of the actual density, which vary with the site elevation, to the yearly constant standard density. The selected wind turbine is Bergey Excel 10 (XL10) manufactured by Bergey Windpower. The turbine has a rotor diameter of 7 m, hub height of 30 m, and a rated capacity 10 kW of DC electricity. The typical daily production of the turbine is ranged from 37 to 75 kWh.

b) Storage Batteries

The selected battery model is the Trojan SSIG 12 120, which is a flooded lead-acid battery. The nominal voltage is 12 V, and the nominal capacity is 1.42 kWh. The battery has a maximum capacity of 118 Ah with capacity ratio of 0.417, roundtrip efficiency of 80%, and maximum charge and discharge currents of 21 A and 263 A, respectively. The string size was set at 1, the initial state of charge was set at 100% and the minimum state of charge was set at 20%. The throughput of the battery was set at 392 kWh.

c) Converter

The selected converter is Leonics S-219Cp 5kW. The inputs of the inverter were set at 96% efficiency, and that of the rectifier were set at 80% relative capacity and 94% efficiency.

d) Electrolyser

The electrolyser is a DC operated Generic electrolyser. The electrolyser efficiency was set at 85% over the entire range of input percentages. The minimum load ratio was set at 0%, which is the lowest power input to operate the electrolyser.

e) Hydrogen Storage Tank

The hydrogen tank is used to store the hydrogen generated by the electrolyser after fulfilling the hydrogen load. The tank size was optimised during simulation, and HOMER software assumes that no electricity is needed for hydrogen storage. The initial hydrogen amount inside the tank relative to the tank size was set at 40%, and the initial absolute amount was set at 0.0 kg.

The economic data of the system components, used for Homer simulation and optimisation are listed in Table 3.19.

Table 3.19 Economic data of the system components

Component	Capital ($)	Replacement ($)	O&M ($/y)	Lifetime (y)
Wind turbine	40,000	40,000	120	30
Electrolyser	500/kW	500/kW	30	10
Converter	600/kW	600/kW	00	10
Batteries	200	200	0	10
Hydrogen tank	500/kg H_2	00	00	25

3.7.3 System Simulation and Optimisation

During simulation, HOMER Pro collects the load data over a year-long (8760 hours) from the daily profiles for the installation site. Afterwards, the load data were obtained, as reported by Boait et al. (2015), by multiplying each hourly load data value by a factor (α_L), as follows:

$$\alpha_L = 1 + \delta_d + \delta_h \tag{3.28}$$

where:

δ_d is the daily perturbation factor (0.2)

δ_h is the hourly perturbation factor (0.15)

The cost comparisons were essential for the system optimisation, which were crucial for deciding the best possible system configuration capable to fulfil the required loads at lowest net present cost (NPC). The best possible configuration was decided based on the number and capacity of each component. During system optimisation, HOMER simulates the various configurations, ignores the infeasible, ranks the feasible based on the total NPC, and finally identifies the feasible configuration of lowest NPC.

The techno-economic analysis was conducted by assuming same rate of increase of the price of system components. To conduct the calculations, the nominal interest rate (i) and the annual inflation rate (f) were assumed based on the installation site considering system lifetime of 25 years. The net present cost (NPC) of each component of the energy system was evaluated using the equations previously explained in the previous chapter. The sensitivity analysis was conducted for scaled daily average hydrogen load of 1.0, 1.5, 2.0, and 2.5 kg/day. Examples of HOMER Pro optimisation results are shown in Appendix-C.

Chapter 4: Results and Discussion

4.1 Introduction

This chapter includes presentation, analyses and discussion of the simulation and modelling results of the wind operated alkaline electrolysis system. It includes results of the wind power mathematical model developed using Excel spreadsheets. It also includes the performance predictions of the simulation models developed using TRNSYS software. This chapter also includes the results of the optimisation model developed using HOMER Pro software.

4.2 Excel Mathematical Model Results

A mathematical model was developed using Excel spreadsheets to predict and compare the electrolyser performance at three sites in Kuwait: Airport site (Airport), Wafra site, and Abdaly site. The modelled wind turbine was of power output 10 kW suitable to operate an off-grid small-scale green hydrogen production system. The modelling results are presented, analysed, and discussed in the next sections.

4.2.1 Power and Energy to the Electrolyser

At each site, the power output of the wind turbine (kW) was evaluated using wind speeds assessed at the turbine rotor hub height of 30 m. Also, the daily average energy produced by the wind turbine (kWh) was calculated as shown in Table 4.1.

Table 4.1 Daily average turbine power and energy at the three sites

Month	Power (kW)				Energy (kWh/day)		
	Airport	Wafra	Abdaly		Airport	Wafra	Abdaly
January	2.19	1.11	0.64		52.48	26.66	15.45
February	2.21	1.13	0.82		53.00	27.07	19.71
March	2.25	1.10	0.81		54.04	26.45	19.33
April	2.71	1.18	0.97		65.15	28.33	23.21
May	**3.35**	**1.32**	**1.06**		**80.36**	**31.76**	**25.43**
June	**5.82**	**2.25**	**2.25**		**139.65**	**54.04**	**54.04**
July	**3.54**	**1.68**	**1.43**		**84.98**	**40.37**	**34.40**
August	2.80	1.18	1.22		67.12	28.33	29.39
September	2.59	1.10	1.00		62.09	26.45	24.01
October	1.72	0.80	0.64		41.32	19.14	15.27
November	1.88	0.92	0.59		45.18	22.03	14.20
December	2.02	0.83	0.49		48.41	19.90	11.78

The daily average electrical power generated by the wind turbine, was calculated for each month. Then, the power (kW) was multiplied by 24 hour/day to evaluate the daily average electrical energy (kWh) available to feed an electrolyser to produce hydrogen. As shown in Table 4.1, the wind speeds approaching the wind turbine rotor at the Airport site are high enough to generate more energy than at other sites. At all sites, the power was highest during June followed by July then May. In other months and at all sites, the wind turbine generated less power. Therefore, if the hydrogen production system is installed at the Airport site, it can daily produce more green hydrogen than at other sites because it has more energy. At the Airport site in June, the system receives about 140 kWh/day of energy to produce hydrogen, which was about 250% the energy (54.04 kWh/day) received at the other sites.

The comparison of the three sites shows obvious differences in wind power and wind energy, which directly affect the technical and economic feasibility of green hydrogen production in Kuwait. The Airport site appears to be the potentially feasible for an off-grid wind-operated system as it has a mean monthly power output of 5.82 kW in June, more than double the power output observed at the Wafra and Abdaly (2.25 kW) sites.

The monthly variation of the energy yield (kWh/day) shown in Table 4.1 indicates the impact of Faraday efficiency of the electrolyser as a key parameter. The operation of electrolysers in the efficiency cliff zone, less than 20% nominal load, causes more hydrogen gas crossover losses. For example, the drop in power to 0.49 kW in December at the Abdaly site decreases the current density below the safety level, which requires frequent shutdown of the system and/or critical dependence on battery storage. On the other hand, the highest energy yield of 139.65 kWh/day at the Airport site in June aligns with the summer wind season in Kuwait, which enables electrolyser operation at relatively high current density i.e. at the ohmic-dominant region of high efficiency.

For all sites, as shown in Table 4.1, there is obvious seasonal wind power instability in winter (October to December), which is a considerable techno-economic challenge. The Airport site, for instance, has a relatively stable baseline wind power above 1.72 kW whereas the Wafra and Abdaly sites have wind power below 1 kW for several months. Thus, the cost of hydrogen production at the Abdaly site is expected to be much higher than other sites due to the decreased Faraday efficiency in winter. Based on the results in Table 4.1, the Airport site was the primary candidate for off-grid wind-operated hydrogen production system, which is discussed in the next section.

4.2.2 Daily Average Hydrogen Production

The Excel model was used to evaluate the hourly hydrogen production (kg/h) using Faraday efficiency, as described Chapter 2. The daily average green hydrogen production for each month was evaluated and the results for the three sites are analysed and discussed in the following sections.

a) Daily Production at the Airport Site

The variation of the daily average hydrogen production for the wind-powered alkaline water electrolyser system at the Airport site, for each month is shown in Figure 4.1.

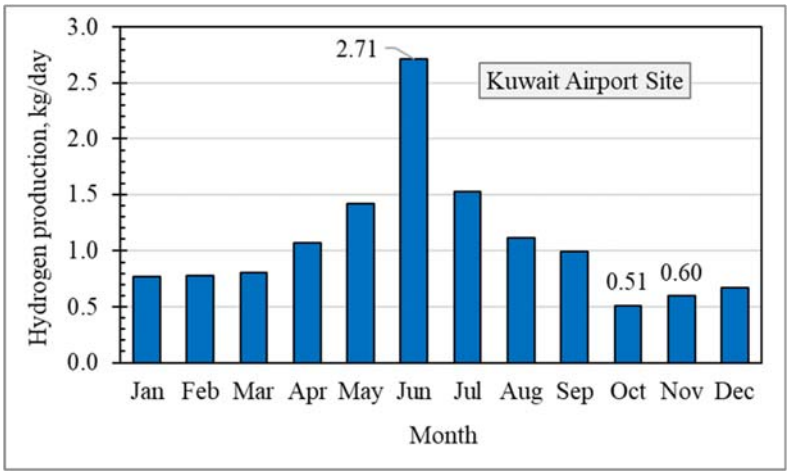

Figure 4.1 Daily average hydrogen production at the Airport site

As shown in Figure 4.1, the wind-operated green hydrogen production system at the Airport site was of highest daily average hydrogen production of 2.71 kg/day in June. The lowest hydrogen productivity was 0.51 kg/day in October. This performance can be attributed to the increased wind speeds at the Airport site in June so that the turbine produced more energy to produce more hydrogen relative to other months.

As shown in Figure 4.1, there is a distinct seasonal peak of daily average production at the Airport site, due to the fluctuation of wind patterns. In summer (May–July), the production increases sharply during this period to reach annual highest of 2.71 kg/day in June driven by the consistent high-velocity winds of Kuwaiti summer. During winter (December–March), the production remains relatively stable at low baseline of about 0.80 kg/day. Meanwhile, the system operates at its annual lowest of 0.51 kg/day in October, which reflects the seasonal transition and the lowest wind energy at the site. Therefoe, there is a significant seasonal hydrogen production mismatch as June's operation offers about five times the hydrogen production of October.

b) Daily Production at the Wafra Site

The green hydrogen production system at the Wafra site will not operate at its maximum capacity due to the relatively lower wind speeds. The variation of the daily average hydrogen production at the Wafra site is shown in Figure 4.2.

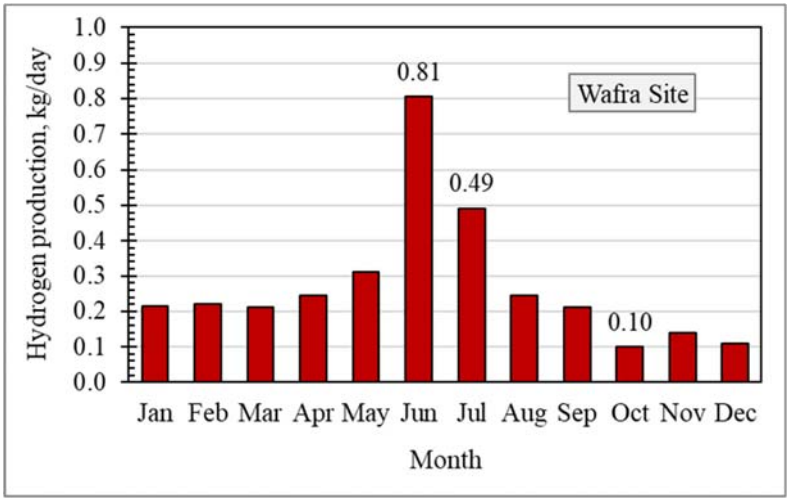

Figure 4.2 Daily average hydrogen production at the Wafra site

As shown in Figure 4.2, the highest hydrogen production at the Wafra site was 0.81 kg/day in June as well. The next highest production was 0.49 kg/day in July, which was about 60% of the daily average production in June. Meanwhile, the lowest hydrogen production of the system was 0.1 kg/day in October, which was about 12.3% of daily average production in June. The daily average hydrogen production pattern for each month at the Wafra site is characterised by a seasonal profile where the feasible hydrogen production was almost restricted to a shorter summer operation. As shown, the production rate remains remarkably suppressed for most of the year at an average about 0.28 kg/day, before it sharply increases to 0.81 kg/day in June.

As shown in Figure 4.2, the system at the Wafra site operates at very low current densities (about 10 to 15 mA/cm^2) for ten months of the year. At these low current densities, the electrolyser operation is dominant by hydrogen gas crossover losses. Accordingly, most of the hydrogen produced by the cells leaks to the oxygen side rather than being collected, which explains the comparatively low productivity of 0.10 kg/day in October. Accordingly, installing the hydrogen production system at the Wafra site, as an off-grid wind-operated system may be technically inadequate. The persistent low-production periods show that the system will be affected by high parasitic losses, which needs addition of other renewable energy sources to maintain stable current densities leading to high efficiency.

c) Daily Production at the Abdaly Site

The variations of the daily average green hydrogen production of the system at the Abdaly site, of lowest wind power potential relative to other sites, are shown in Figure 4.3.

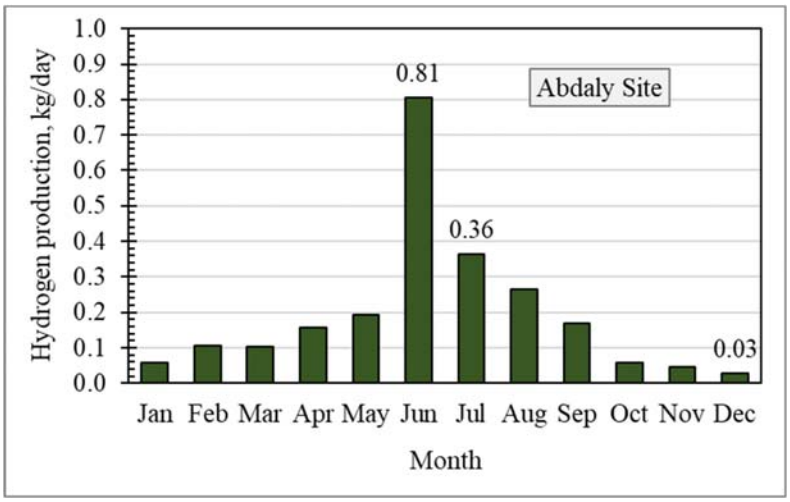

Figure 4.3 Daily average hydrogen production at the Abdaly site

As shown in Figure 4.3, the hydrogen production patterns at the Abdaly site are closer to the patterns at the other sites, except in December. During every month, the productivity of the system was affected by the low wind speed, which decreased the wind energy production. The highest daily average system production at the Abdaly site was 0.81 kg/day in June, which was the same as the highest daily production at the Wafra site (0.81 kg/day), but about 30% lower than the highest daily production at the Airport site (2.71 kg/day). The next highest daily average production at the Abdaly site was 0.36 kg/day in July whereas the lowest was 0.03 kg/day in December, which was 1.1% of the highest Abdaly's production. The daily average hydrogen production rates of the system at the three sites are compared as shown in Table 4.2.

Table 4.2 Daily average hydrogen production at the three sites

Feature	Airport	Wafra	Abdaly
Production rate	High About 2.71 kg/day	Moderate About 0.81 kg/day	Moderate About 0.81 kg/day
Winter baseline	Stable About 0.8 kg/day	Low About 0.2 kg/day	Very low <0.1 kg/day
Annual lowest	0.51 kg/day (Oct)	0.1 kg/day (Oct)	0.03 kg/day (Dec)

As shown, the system at the Airport site maintains wind energy sufficient to operate the electrolyser above the critical part-load limit (about 15% to 20%) for most of the year. But

the wind energy at the Abdaly site operates the electrolyser within the efficiency cliff region for nearly nine months. In December for example, the daily production at the Abdaly site of 0.03 kg/day suggests that nearly all the electrical energy input to the electrolyser is being consumed by parasitic currents and gas crossover. Accordingly, installing the system at the Abdaly site is the least favourable for an off-grid wind-operated small-scale system. The drop of hydrogen production from 0.81 kg/day in June to only 0.03 kg/day in December represents about 96% drop of output. It was more severe than the drop of 81% (from 2.71 to 0.51) at the Airport site in October and 87% (from 0.81 to 0.1) at the Wafra site in October.

4.2.3 Monthly and Annual Hydrogen Production

The monthly green hydrogen production was calculated for each site, by multiplying the daily average hydrogen production by the number of days of the corresponding month. The mathematical model predictions of the monthly green hydrogen production were calculated as shown in Table 4.3.

Table 4.3 Monthly and annual hydrogen production (kg) at the three sites

Month	Airport	Wafra	Abdaly
January	23.84	6.64	1.81
February	25.00	6.20	3.00
March	26.58	6.53	3.16
April	36.22	7.33	4.71
May	49.62	9.61	5.98
June	**97.73**	**24.16**	**24.16**
July	56.35	15.25	11.27
August	42.24	7.57	8.18
September	38.76	6.32	5.09
October	20.53	3.09	1.76
November	24.61	4.18	1.42
December	28.32	3.39	**0.90**
Annual	**469.80**	**100.3**	**71.46**

The results in Table 4.3 show that the monthly green hydrogen production, at any month of the year, was the highest at the Airport site relative to the other sites. At each site, the annual production was evaluated as the sum of the monthly production. As shown in Table 4.3, the highest monthly production was 97.73 kg in June at the Airport site whereas the lowest was 0.90 kg in December at the Abdaly site.

The results in Table 4.3 show highly seasonal and non-linear trend of the monthly hydrogen production data at the three sites. Compared with other sites, the Airport site consistently

outperformed Wafra and Abdaly sites by a factor of four to ten. For example, the production at the Airport site was about 98 kg in June, coinciding with the intensification of the winds. Therefore, the Airport site is the best choice to install the hydrogen production system where the wind energy is sufficient to operate the electrolyser at its high-efficiency ohmic-dominant range. With hydrogen production still exceeding 20 kg in calm October, the current density was likely higher than the value causing efficiency cliff. On the other hand, the system at the Abdaly site shows a remarkable fall in winter production, down to just 0.9 kg in December.

The drop in winter productivity at the Abdaly site shows that most of the year a notably low wind energy operates the electrolyser at the zone of activation and gas-crossover dominance at which the theoretical Faraday efficiency is the lowest. In terms of productivity, the system at the Wafra site has acceptable production but still significantly operates reliant on the mid-summer wind energy. At the Wafra site, there is significant drop of about 87% in hydrogen production, from 24.16 kg in June to 3.09 kg in October. Accordingly, the Airport site is the promising site for off-grid wind- operated hydrogen production system, compared with the other sites. To compare the annual productivity, the yearly production of the system at each site is plotted as shown in Figure 4.4.

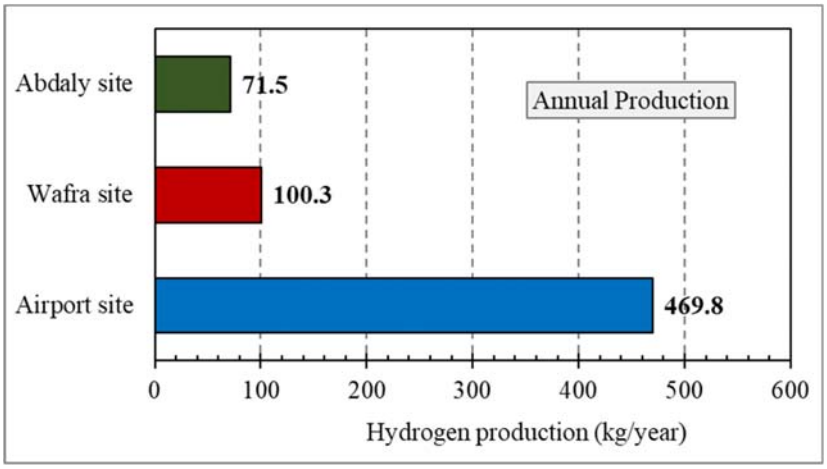

Figure 4.4 Annual green hydrogen production at the three sites

The annual hydrogen productions for the system at the three sites, as shown in Figure 4.4, have remarkable differences. The system production at the Airport site leads the other sites at 469.8 kg, followed by the Wafra site at 100.3 kg, and the Abdaly site at 71.5 kg. Thus, the annual production rates at the Wafra and Abdaly sites are about 21.3% and 15.2% the annual production at the Airport site. The variation of annual production of the system at the three sites can be attributed to the differences in wind energy potential at each site and the resulting effect on the electrolyser efficiency.

The system productivity modelled in this study is in a good alignment with broader techno-economic assessments for green hydrogen production in Kuwait. For instance, Shehabi and Dally (2021) highlighted the remarkable sensitivity of hydrogen production in Kuwait to the specific micro-climate of the installation site along with its renewable potential. The system performance at the Airport site is in a good match with the expectations for zones of high wind potential in Kuwait at which wind energy is sufficient to operate industrial-scale wind-operated electrolysis systems. Meanwhile, the low hydrogen production at the Wafra and Abdaly sites is consistent with the findings of Sebbahi et al. (2024) who reported that off-grid wind-operated systems at such sites often challenges an efficiency trap caused by wind seasonal calmness leading to low hydrogen production.

The annual production of about 470 kg for a small-scale system at the Airport is comparable to the industrial benchmarks for advanced alkaline electrolysers, which target better specific energy consumption (SEC) in the range from 45 kWh/kg H_2 to 55 kWh/kg H_2 (Ferrero et al., 2025; Nnabuife et al., 2025). The relatively poor performance of the system at the Wafra and Abdaly sites underlines IRENA's report conclusion (IRENA, 2020) that accurate selection of installation site is the most significant parameter affecting the hydrogen production at competitive prices in the Middle East. More details on SEC of the system at the three sites are given in the next section.

4.2.4 Specific Energy Consumption (SEC)

The feasibility of a hydrogen production system relies on producing more hydrogen while consuming less energy for the production. The feasibility of the system is assessed based on the specific energy consumption (SEC) expressed kWh of energy per kg of hydrogen. As explained in the previous section, the system at the Airport site has significantly higher production relative to the other sites due to the superiority of wind energy, which enables extended hours of operation of the electrolyser at high current densities.

At high current density, the system keeps operating at high Faraday efficiency, which results in economic operation with low specific energy consumption. On the other hand, the system at the Wafra and Abdaly site operates at low average wind speeds, forcing the electrolyser to mostly operate at part load. At part load, the gas crossover losses become dominant, which decreases Faraday efficiency and increases the energy required to produce the kilogram of hydrogen. With the significance of SEC, it was calculated for each month at each site and used to compare the system performance, as shown in Table 4.4.

Table 4.4 Specific energy consumption, SEC, (kWh/kg) for the sites

Month	Airport	Wafra	Abdaly
January	68.2	124.4	263.9
February	67.8	122.2	184.2
March	67.1	125.6	189.3
April	61.1	116.0	147.7
May	56.7	102.5	131.7
June	**51.4**	**67.1**	**67.1**
July	55.8	82.0	94.6
August	60.4	116.0	111.3
September	62.5	125.6	141.4
October	80.5	192.0	268.7
November	75.3	158.2	300.9
December	71.8	181.7	407.4
Annual average	**64.9**	**126.1**	**192.3**

For the green hydrogen production system, the mathematical model predictions in Table 4.4 show lowest monthly average SEC in June at all sites. The lowest SEC of 51.4 kWh/kg for the system at the Airport site demonstrated the best performance. The lowest SEC in June at the Wafra and Abdaly sites was 67.1 kWh/kg. As also shown in Table 4.4, the lowest annual average SEC was 64.9 kWh/kg at the Airport site. Meanwhile, a higher annual average SEC of 126.1 kWh/kg was found at the Wafra site, and a highest of 192.3 kWh/kg was found at the Abdaly site. Therefore, the system at the Airport site has the most efficient operation compared with the other sites.

The system at the Airport site has the most efficient and stable operation with lowest monthly average SEC of 51.4 kWh/kg in June, which was increased to 80.5 kWh/kg in October. The low SEC found in June's operation is significant because it comes closer to the theoretical efficiency limits for commercial alkaline electrolysers (Ferrero et al., 2025). The improved efficiency in June at the Airport site was possible because the strong summer wind produces more energy to move the current density to the best ohmic-dominant zone at which the Faraday efficiency is maximum.

The system at the Wafra and Abdaly sites has unstable operation at higher SEC. For example, at the Abdaly site the system has a remarkable drop of efficiency during winter months so that SEC hits a highest of 407.4 kWh/kg in December. This extreme SEC is more than ten

times the industrial standard of 50 to 55 kWh/kg (IRENA, 2020), which is caused by sharp and non-linear drop of efficiency at part-load operation. At low power input, the electrolyser operates at low current density that causes gas crossover domination, which forces the system to consume more electrical energy to supply the auxiliary loads and to keep the cell voltage at the best operational value, but it produces very little amount of hydrogen.

The SEC values at the Airport site (51.4 kWh/kg in June to 80.5 in October) align closely to IRENA (2020), which reported operating range of 50–55 kWh/kg at nominal load for state-of-the-art commercial alkaline electrolysers. The system performance at the Airport site in June (SEC is 51.4 kWh/kg) matches the 2030 advanced technology targets, which indicates the sufficiency of wind resource at this site. But the poor SEC at the Wafra and Abdaly site (exceeding 120 kWh/kg) are related to the part-load penalties. The findings of Ulleberg (2003) show exponential drop of Faraday efficiency at low current densities, which explains the high SEC at the Abdaly site in winter. Also, Shehabi and Dally (2021) reported that the economic feasibility of hydrogen production system in Kuwait depends on the installation site. As the current density is a key parameter of effect on SEC, the variation of SEC with the current density was predicted by the Excel model and plotted as shown in Figure 4.5.

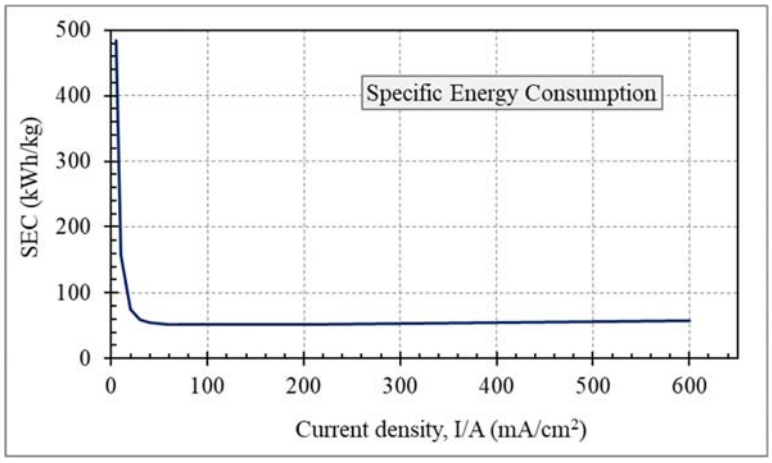

Figure 4.5 Specific Energy Consumption (kWh/kg) vs current density (mA/cm^2)

As shown in Figure 4.5, the model predictions show non-linear, quasi-U-shaped relationship between SEC and current density, which is a basis to understand electrolyser performance under fluctuating wind speeds. At very low current density (below 50 mA/cm^2), SEC shows sharp exponential increase toward a maximum of 400 to 500 kWh/kg, which is attributed mainly to the drop of Faraday efficiency. At such operating condition, the rate of hydrogen production becomes very low; the parasitic losses (such as gas crossover) and the internal shunt currents consume most of the energy supplied to the electrolyser.

As shown in Figure 4.5, SEC reaches a theoretical lowest between 45 and 55 kWh/kg with increased current density from 50 to 200 mA/cm². In this region, the system operates with a balance between the cell voltage and Faraday efficiency. Beyond 200 mA/cm², the SEC-current density curve has a gradual and linear rise, which is driven by the increased Ohmic overpotentials. The increase of operating cell voltage necessitates the use of more electrical energy to produce same mass of hydrogen. This behaviour is related to the change of Faraday efficiency so that more details on Faraday efficiency are given in the next section.

4.2.5 Faraday Efficiency and Current Density

Faraday efficiency (also termed as current efficiency) describes how the system utilises the electrical current to produce hydrogen. It is the ratio between the actual amount of produced hydrogen and the maximum theoretical amount that can be produced using same supplied current (Yodwong et al., 2020; Muthiah et al., 2024). Faraday efficiency describes the system efficacy to optimally utilise the supplied energy to produce hydrogen. The variation of the monthly average Faraday efficiency at the three sites is shown in Figure 4.6.

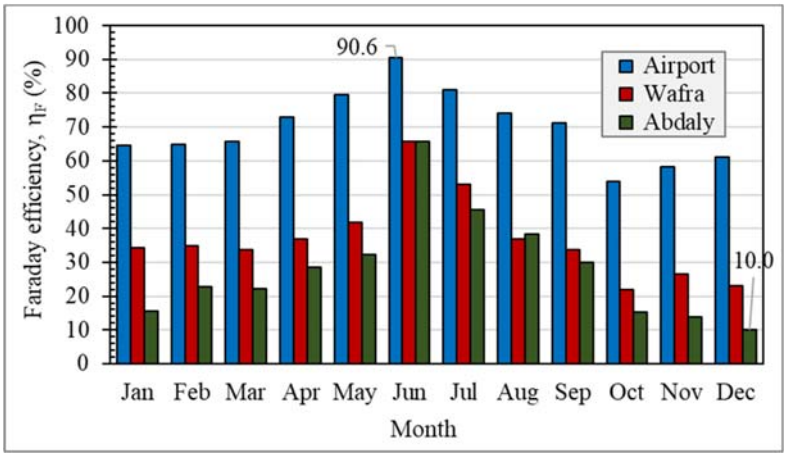

Figure 4.6 Monthly average Faraday efficiency at the three sites

In all months, as shown in Figure 4.6, Faraday efficiency was highest at Airport site followed by the Wafra then Abdaly sites. The highest efficiency was 90.6% at the Airport site in June whereas the lowest was 10% at the Abdaly site in December. The drop of Faraday efficiency was attributed to the impact of parasitic currents and the hydrogen gas crossover. The loss due to parasitic current takes place when electrical energy bypasses the electrodes and travels through the electrolyte, with less contribution to hydrogen evolution chemical reaction. The loss due to hydrogen gas crossover takes place when hydrogen gas molecules cross the membrane toward the oxygen side. The low Faraday efficiency at the three sites, as shown in Figure 4.6, is caused by the low current densities produced by low wind energy. With the

notable effect of current density on Faraday efficiency, SEC, and on hydrogen production, the monthly and annually average current densities were evaluated at the three sites and compared as shown in Table 4.5.

Table 4.5 Monthly and annual current density (mA/cm^2) at the three sites

Month	Airport	Wafra	Abdaly
January	22.0	11.6	6.9
February	22.2	11.7	8.7
March	22.6	11.5	8.5
April	27.0	12.3	10.1
May	32.9	13.7	11.1
June	**55.3**	**22.6**	**22.6**
July	34.7	17.2	14.7
August	27.7	12.3	12.7
September	25.8	11.5	10.5
October	17.5	8.5	6.8
November	19.1	9.7	6.4
December	20.4	8.8	5.3
Annual	**27.3**	**12.6**	**10.4**

At the three sites, as shown in Table 4.5, the system operates in the efficiency cliff zone. At the Airport site, the average annual current density was 27.3 mA/cm^2, which is still low, but the site is notably more productive than the other sites. At the Wafra site, the average annual current density was 12.6 mA/cm^2, so that the hydrogen production is significantly lower than the Airport site. At the Abdaly site, the average annual density was about 10.4 mA/cm^2 so that the system was hardly producing collectible hydrogen. The model predictions of the current density impact on Faraday efficiency were plotted as shown in Figure 4.7.

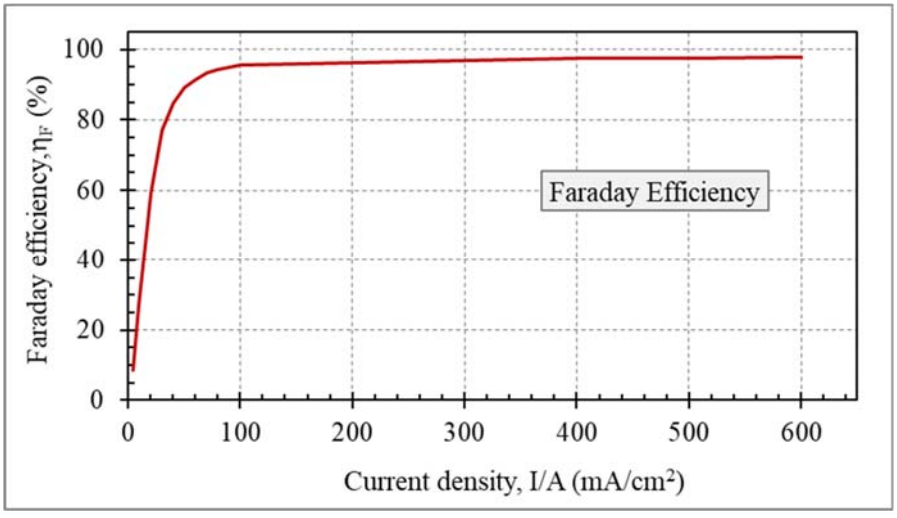

Figure 4.7 Variation of predicted Faraday efficiency with current density

The Excel model predictions in Figure 4.7 demonstrated drastic drop of Faraday efficiency at low current densities below 100 mA/cm^2. As listed before in Table 4.4, the annual average current densities were less than 100 mA/cm^2 at the three sites. At low current densities at Abdaly and Wafra sites, considerable amount of energy is lost via parasitic currents. Also, the hydrogen gas crossover rate becomes almost equal to the rate of hydrogen production. The reason for the low current density at both sites is the conversion of most of the supplied wind energy into heat with very little contribution to the hydrogen evolution reaction. The low current density caused noticeable drop of Faraday efficiency to reach a lowest of 10% at the Abdaly site in December, which necessitates shutting down the system to avoid risk of explosion with the excessive increase of hydrogen concentration in the oxygen side.

The above findings are in a good agreement with Ren et al. (2022) and Luo et al. (2024) who explained how electrolyser behaviour changes with the non-linearity relationship of voltage versus current. The increase of current density increases the ohmic and resistive losses so that more energy is needed to overcome the resistance and produce hydrogen. Therefore, high current density is required to produce more hydrogen at low efficiency. The predicted inverse relationship between SEC and productivity can be attributed to the polarisation curve behaviour of the electrolyser. This finding is in a good agreement with the model results of Ulleberg (2003) who reported the dominance of the ohmic resistance with increased current densities.

The system at the Airport site is more feasible to produce hydrogen relative to the other sites. The lower current density at the Wafra and Abdaly sites suggest that the wind potential at these sites, at the time of wind speed measurement, is not enough to efficiently operate an industrial alkaline electrolyser. At the Wafra and Abdaly sites, efficient operation may be possible with considering hybridisation of energy source with photovoltaic (PV) solar panels to increase the current density beyond 100 mA/cm^2 to operate the system at efficient zone.

The system was modelled using wind speed data recorded at 10 m from ground level, which were evaluated at the turbine height of 30 m. The wind speed was higher at 30 m than the wind speed at 10 m by about 19.2%, which affected other simulation results. The percentage change of wind speed (19.2%) was evaluated as the ratio between the difference of wind speed (wind speed at 30 m minus wind speed at 10 m) and the wind speed at 10 m. The Excel model outputs parameters such as the turbine power (kW), cell voltage (V) and cell current

(A), Faraday efficiency, mass of hydrogen (kg/year), and specific energy consumption SEC (kWh/kg) were sensitive to the change of wind speed as illustrated in Table 4.6.

Table 4.6 Change of Excel model parameters with 19.2% increase of wind speed

Parameter	Change	Airport	Wafra	Abdaly
Turbine power (kW)	Increased ↑	64.1%	103.4%	151.4%
Cell voltage (V)		2.7%	3.7%	4.7%
Cell current (A)		59.8%	96.0%	139.2%
Faraday efficiency (%)		46.9%	188.2%	408.0%
H_2 mass (kg/year)	Increased ↑	108%	294.2%	304.6%
SEC (kWh/kg)	Decreased ↓	−31.3%	−66.5%	−84.3

As shown in Table 4.6, the increase of wind speed by19.2% increased the wind turbine power output at all sites. It also increased the cell current, due to the tiny increase of cell voltage, which increased Faraday efficiency. Accordingly, there was an increase of the annual average hydrogen mass by about 108% at the Airport site, 294% at the Wafra site, and 305% at the Abdaly site. In terms of energy, SEC was decreased at all sites with the 19.2% increase in wind speed at 30 m turbine hub height.

The performance assessment of the system using the mathematical model predictions show good agreement with the literature. The SEC values at the three sites were in the range 60 to 200 kWh/kg (see Table 4.4) which agrees with Fragiacomo and Genovese (2020) and Franco and Giovannini (2023; 2024). But the model ignored the impact of electrolyser design and operating parameters on the dynamic performance. Thus, variation of the transient system performance using TRNSYS software was investigated and analysed in the next sections.

4.3 TRNSYS Model Simulation Results

TRNSYS model was developed to simulate the operation of a green hydrogen production system and to assess its performance. The components of the model included weather data reader, wind turbine, alkaline water electrolyser, compressor, and storage tank. The operation of the system was enabled and controlled using TRNSYS controller and power conditioning components. The simulation was conducted over 8760 hours to predict the performance over an entire year. Wind speed measured at 10 m from the ground at the three sites were used to evaluate the hourly wind turbine power. During simulation, a turbine operates an electrolyser to produce hydrogen by splitting water molecules. The hourly hydrogen production was predicted at the three sites. The monthly and annual green hydrogen production at each site

were predicted and used to compare the electrolyser performance at the three sites. The simulation was conducted using electrolyser having 20 cells in series with total surface are of 0.3 m^2. The simulation predictions are discussed in the next sections.

4.3.1 TRNSYS Wind Speeds and Turbine Power Output

The hourly variation of wind speeds at the three sites is shown in Figure 4.8.

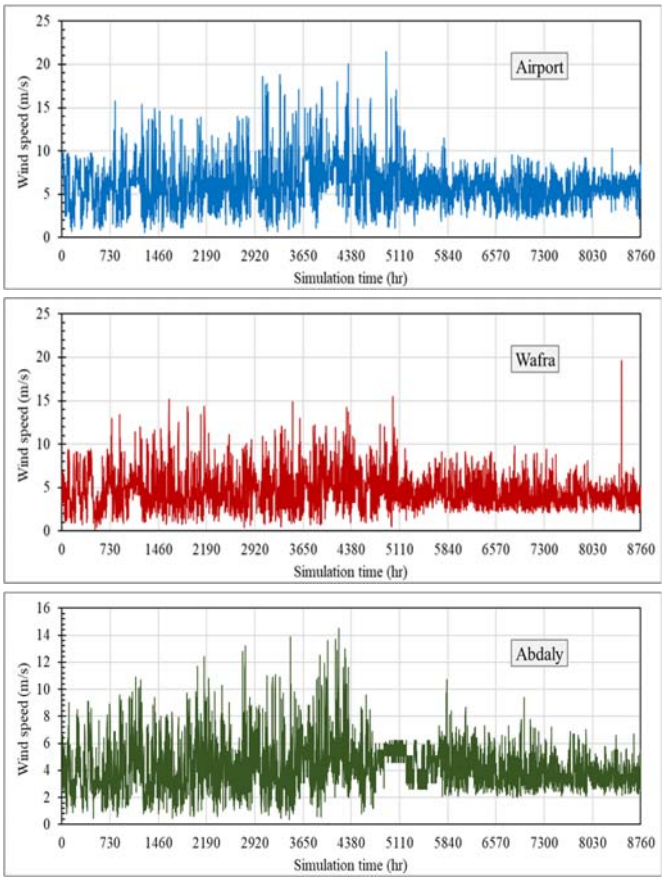

Figure 4.8 Hourly variation of the wind speed at the three sites

As shown in Figures 4.8, wind speeds were highest at the Airport site relative to other sites. At the Airport site, the highest speeds were in summer months May to August. The maximum wind speed at the turbine rotor hub height of 30 m, at the Airport site, was 21.5 m/s whereas the yearly average wind speed was 6.03 m/s. At the Wafra site, the maximum wind speed was 19.6 m/s, and the yearly average was 4.54 m/s. At the Abdaly site, the maximum wind speed was 14.50 m/s, and the yearly average was 4.23 m/s. Since the yearly average wind speed at the three sites was higher than 3 m/s, the three sites are considered (Faraz, 2024) for installing wind turbines to generate green electricity. Therefore, hourly predictions of the generated power by the Bergey 10-kW wind turbine were obtained and the hourly variations of the turbine power over the year are shown in Figure 4.9.

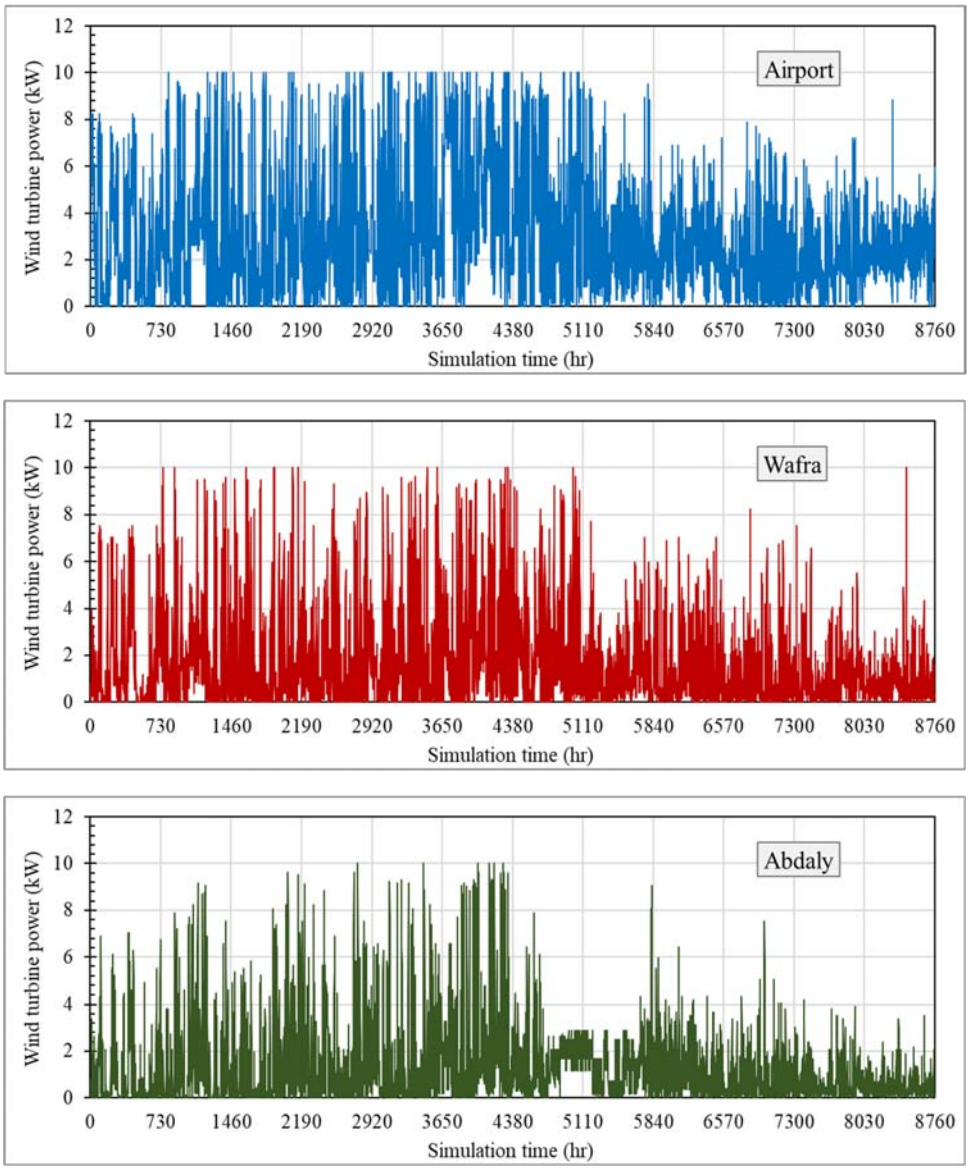

Figure 4.9 Hourly variations of wind turbine power at the three sites

As shown in Figure 4.9, the hourly wind turbine power output fluctuates with the hourly wind speed fluctuation at each site. The rated capacity of the turbine, of rotor diameter 7 m and hub height 30 m, was 10 kW. The frequency at which the turbine power output reached the 10 kW was highest at the Airport, followed by the Wafra then Abdaly sites. TRNSYS predictions show average annual energy production of 26,009 kWh for the system at the Airport site, which was about 107.8% of the Excel model predictions of 24,136 kWh. For the system at the Wafra site, TRNSYS predicted the average annual energy production as 13,598 kWh, which was 127% of the Excel model predictions of 10,654 kWh. For the system at the Abdaly site, TRNSYS predicted average annual energy production of 10,762 kWh, which was 124% the Excel predictions of 8,698 kWh.

The difference of energy predictions between Excel model and TRNSYS may be attributed to the method of assessment of each software. TRNSYS predicts hourly values and sum these values whereas Excel predicts a daily average value for each month and uses number of days of each month to obtain monthly generation before summing them to obtain an average annual. Also, TRNSYS predictions show constant wind turbine power coefficient of 0.326 at the three sites.

For the selected turbine, the 8760 hours of operation each year would produce a maximum annual energy of 87,600 kWh. Thus, installing the wind turbine at the Airport site will enable the turbine to produce about 29.7% of its maximum producible energy. Meanwhile, installing the turbine at the Wafra and Abdaly sites will result in annual energy production of 15.5% and 12.3% of the maximum producible energy, respectively.

TRNSYS predictions therefore show the preference of installing the wind turbine at the Airport site, at which the annual energy production is about twice the energy to generate at the Wafra site, and more than twice the energy to generate at the Abdaly site. Because of the relatively high wind speeds at the Airport site, the annual operational hours of the turbine were 8375 hours, which was about 96% of the 8760 hours of the year. At the Wafra site, the operational hours of the turbine were dropped to 7676 hours, which was about 88% of the total annual operating hours. At the Abdaly site, the turbine operational hours were 7644 hours, which was about 87% of the maximum annual operational hours.

The predictions in Figure 4.9 show that the turbine was able to produce the 10-kW power only for 35 hours (out of 8375 hours of operation) at the Airport site. At the Wafra and Abdaly sites, the 10-kW power output was obtained for 37 hours and 34 hours, respectively. Most of time, the turbine was unable to generate the 10-kW due to the wind speed fluctuations.

4.3.2 TRNSYS Hourly Hydrogen Production

During the simulation, TRNSYS controller component enabled and controlled the produced turbine energy fed to the electrolyser. The TRNSYS power conditioning component changed the voltage and current to suit the electrolyser operation. Power conditioning was important to change the current with the electrolyser load so that the cell voltage was also changed. When electricity was fed to the electrolyser at high current, fast water splitting took place producing more hydrogen and oxygen gases.

For simulations, the inputs and parameters of the TRNSYS electrolyser component were changed. The number of electrolyser cells was set at 20 arranged in series to form ONE parallel stack. Also, the electrolyser surface area was set at 0.3 m^2. The performance of the simulated system was assessed based on the green hydrogen production rates. The simulation was conducted on hourly basis, over a period of 8760 hours per year.

The simulation trials started with initial setting of the State of Charge (SOC) of the hydrogen storage tank to 0.4, at which the hydrogen production immediately started with the start of simulation. The produced hydrogen was then compressed and forced to fill the storage tank. Also, TRNSYS simulation starts with continuous and constant hydrogen gas consumption of 0.2 Nm^3/h from the gas stored within the tank. When the quantities of hydrogen supplied to the tank were higher than the gas consumption from the tank, SOC increased to reach 0.9, which was the upper SOC limit. When SOC reached 0.9, the green hydrogen production process stopped, and the electrolyser was kept running at idle power. The excess power of the wind turbine, beyond the electrolyser consumption, was delivered to electric batteries to be stored. Meanwhile, the continuous constant hydrogen consumption from the tank caused the tank SOC to drop below the 0.9 limit, which started the electrolyser operation to produce hydrogen and so on.

During TRNSYS simulation, the electrolyser was fed with the energy generated by the wind turbine to produce hydrogen at a low pressure of 7 bars, which was compressed to a high pressure of about 200 bars, to limit the required volume of the storage tank. The high-pressure hydrogen from the compressor was supplied to the storage tank, only when SOC of the tank is within the range between 0.7 and 0.9.

The hydrogen production rates were dependent on the wind speeds and accordingly on the wind turbine energy. At low speeds, the wind turbine produced less output energy, which operated the electrolyser at part load and produced less amounts of hydrogen. In this case, the tank SOC dropped, as the amounts of hydrogen consumed from the tank were higher than the supplied. At high speeds, the wind turbine produced more energy than the energy needed to operate the electrolyser at full load, and the excess energy was stored.

Because the electrical energy supplied to the electrolyser was intermittent due to wind speed fluctuation, the hydrogen production was intermittent and time dependent. Variations of the hourly hydrogen production rates, for the system at the three sites, are shown in Figure 4.10.

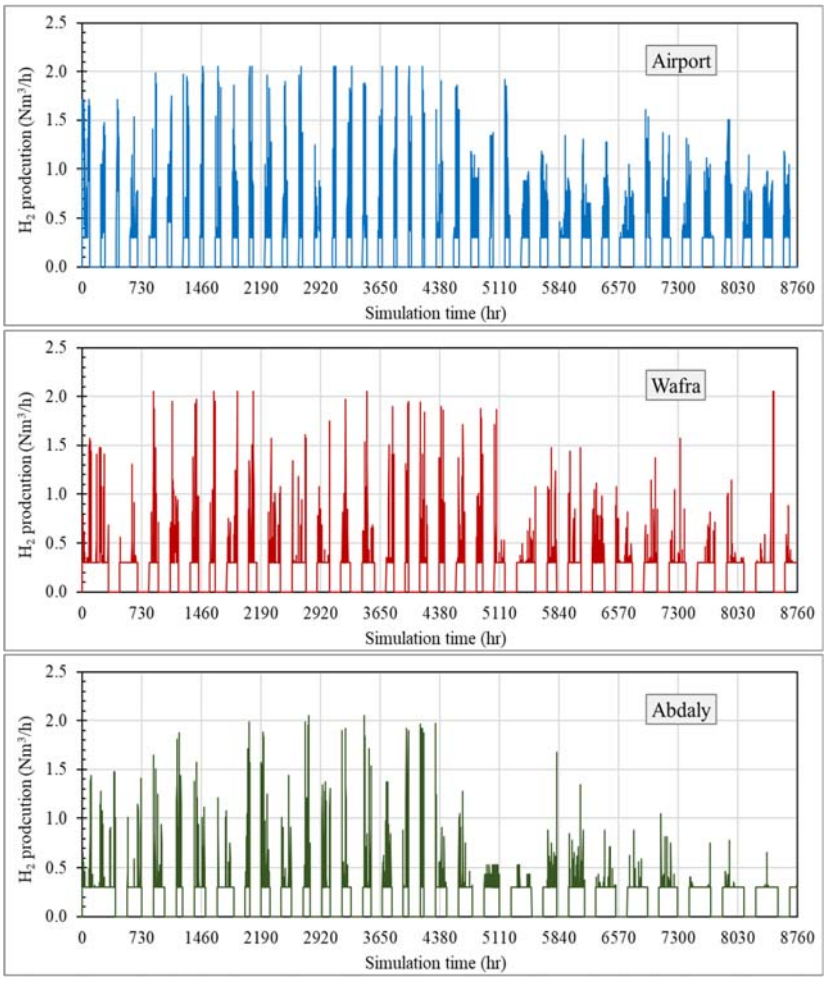

Figure 4.10 Hourly hydrogen production rates at the three sites

As depicted in Figure 4.10, the hydrogen production was unsteady as there were many hours without production. For instance, there was no production when the tank SOC reached the 0.9 limit and when the turbine stopped operations at wind speeds lower than the cut-in speed.

TRNSYS predictions showed hourly hydrogen production in Nm^3/h. The production is in Nm^3 (normal cubic metre) at temperature 273.15 K and pressure 1.01325 bar. At these conditions, the hydrogen density is 0.0899 kg/Nm^3 so that TRNSYS predictions can be converted into kg/h, to match the units used for Excel model predictions.

For the intermittent hydrogen production, TRNSYS predictions showed a maximum hourly production of 2.054 Nm^3/h (0.1847 kg/h), and an annual average production of 0.207 Nm^3/h (0.0186 kg/h) at the three sites. Examples of the hourly production for each month at the Airport site are shown in Figure 4.11, and the hourly average production rates for each month are shown in Table 4.7.

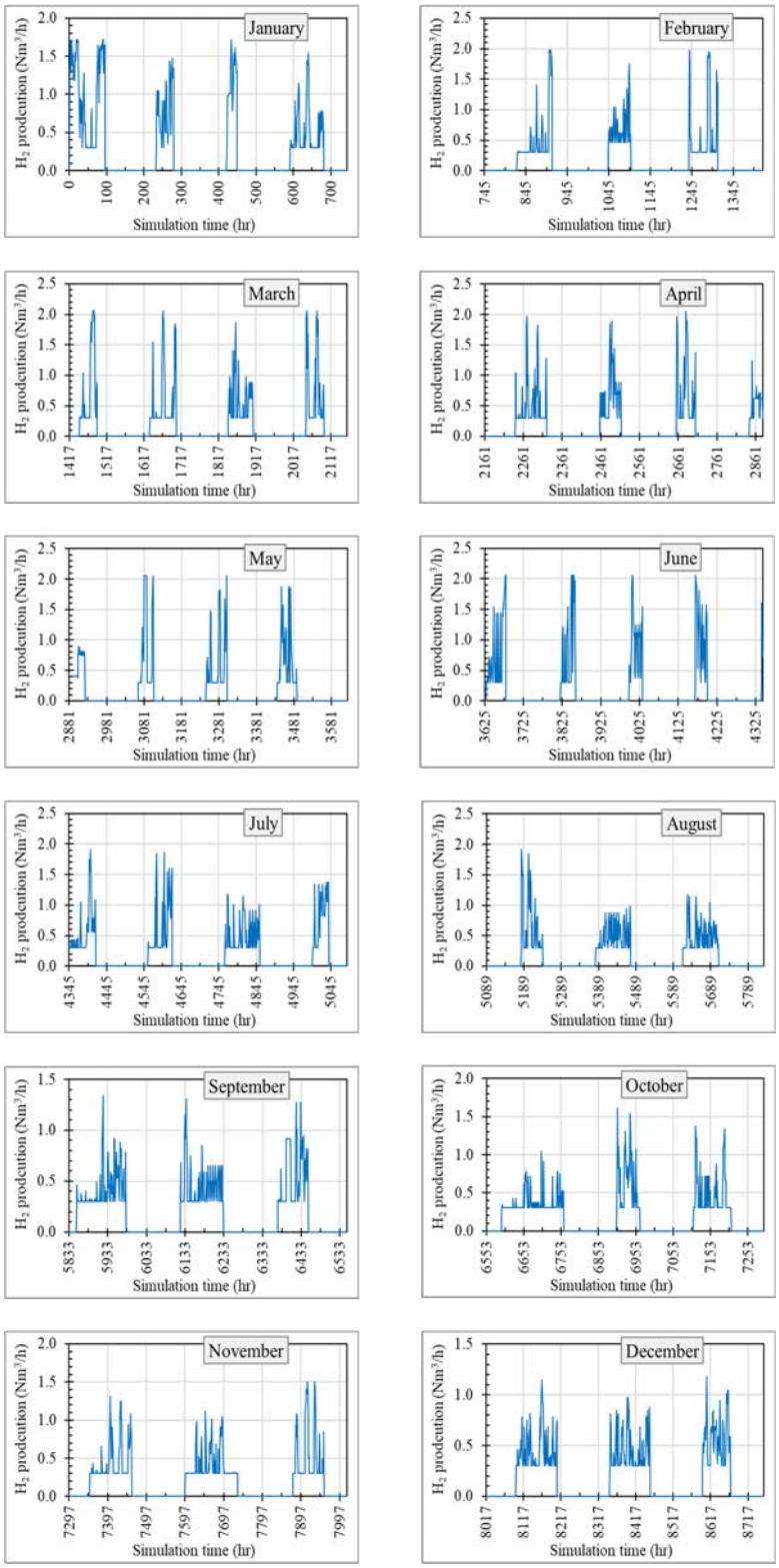

Figure 4.11 TRNSYS hourly hydrogen production (Nm^3/h) at the Airport site

Table 4.7 TRNSYS hourly average hydrogen production at the three sites

Month	Airport		Wafra		Abdaly	
	Nm^3/h	kg/h	Nm^3/h	kg/h	Nm^3/h	kg/h
January	0.284	0.0255	0.283	0.0254	0.297	0.0267
February	0.185	0.0166	0.215	0.0193	0.179	0.0161
March	0.214	0.0192	0.198	0.0178	0.194	0.0174
April	0.195	0.0175	0.167	0.0150	0.206	0.0185
May	0.185	0.0166	0.226	0.0203	0.200	0.0180
June	0.203	0.0182	0.180	0.0162	0.201	0.0181
July	0.221	0.0199	0.215	0.0193	0.217	0.0195
August	0.180	0.0162	0.210*	0.0189	0.201	0.0181
September	0.206	0.0185	0.174	0.0156	0.200	0.0180
October	0.204	0.0183	0.211	0.0190	0.204	0.0183
November	0.207	0.0186	0.206	0.0185	0.187	0.0168
December	0.193	0.0174	0.197*	0.0177	0.188	0.0169

4.3.3 TRNSYS Daily Average Hydrogen Production

For each month, the hourly hydrogen production rates were obtained and added together to evaluate the daily production at each site. The variations of the daily average production rate, for each month, at the three sites are shown in Figure 4.12.

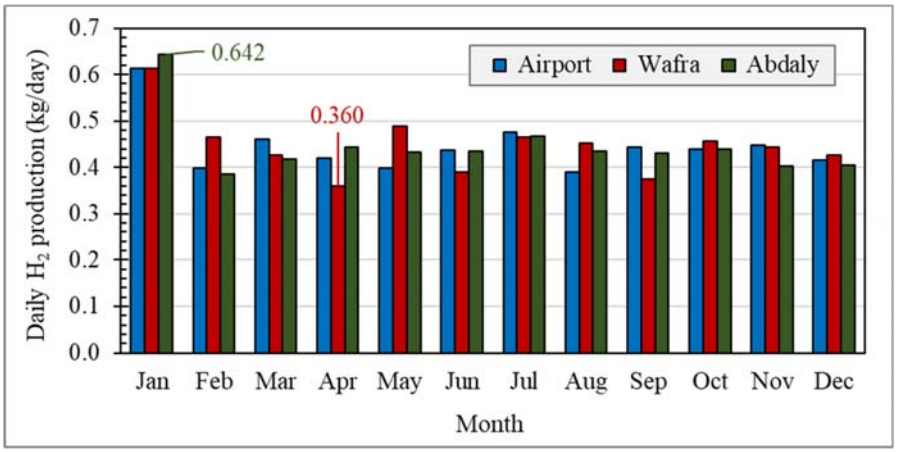

Figure 4.12 TRNSYS daily average hydrogen production (kg/day) at the sites

As shown in Figure 4.12, the daily average hydrogen production rates in January were the highest at all sites. The improvement of system productivity in January can be attributed to the increase of wind speed during this month, and the use of a low initial SOC of 0.4 for the storage tank. In January, as shown in Figure 4.12, the highest daily average production was

0.642 kg/day for the system at the Abdaly site. For the system at the Wafra or Airport sites, the daily average production was 0.613 kg/day in January. However, Figure 4.12 shows that the lowest daily average production was 0.36 kg/day in April at the Wafra site.

4.3.4 TRNSYS Monthly Average Hydrogen Production

For each month, the monthly average hydrogen production rate of the system was evaluated as the daily production capacity (kg/day) times the number of days of corresponding month. Figure 4.13 shows comparison of the monthly production rates at the three sites.

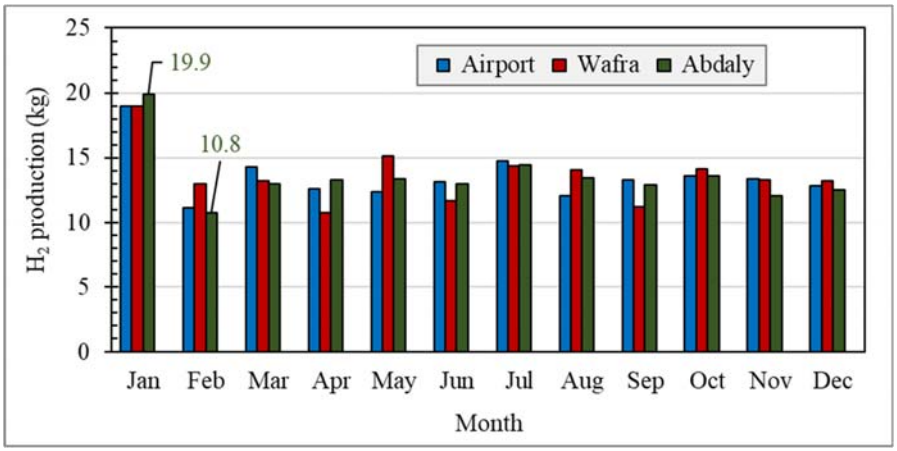

Figure 4.13 TRNSYS monthly hydrogen production capacity (kg) at the sites

As shown in Figure 4.13, the highest monthly hydrogen production capacity of 19.9 kg was obtained in January for the system at the Abdaly site. Meanwhile, the lowest production capacity of 10.8 kg was achievable in February for the system also at the Abdaly site. When the system productivity at the three sites was compared, no specific pattern of production was realised for any month. The results in Figure 4.13 show that the monthly production at the three sites was highest in January compared with other months. This may be attributed to the start of simulation in January with a tank SOC of 0.4, which resulted in producing more hydrogen to fill the tank to reach the upper SOC limit of 0.9. The production then fluctuated to keep the SOC within the range 0.7 to 0.9, as explained earlier.

In January, as shown in Figure 4.13, the monthly average hydrogen production capacity was highest at 19.9 kg for the system at the Abdaly site. The capacity was 19.0 kg for the system at the Airport and Wafra sites. As also shown, the poor performance in terms of hydrogen production was in February. The average production in February was 13.0 kg for the system at the Wafra site, followed by 11.2 kg for the system at the Airport site, then 10.8 kg for the system at the Abdaly site.

4.3.5 TRNSYS Annual Hydrogen Production

The annual hydrogen production capacity is a key metric for assessing and comparing the performance of hydrogen production systems. This parameter is important for the system designers conducting feasibility studies. It also helps the energy planners to ensure fulfilling the forecasted energy demands (Al-Douri and Groth, 2024). Due to its significant effect, the annual hydrogen production capacity was calculated for the system by summing the monthly production amounts (kg). The annual capacity of the system, at each site, was evaluated and compared as shown Figure 4.14.

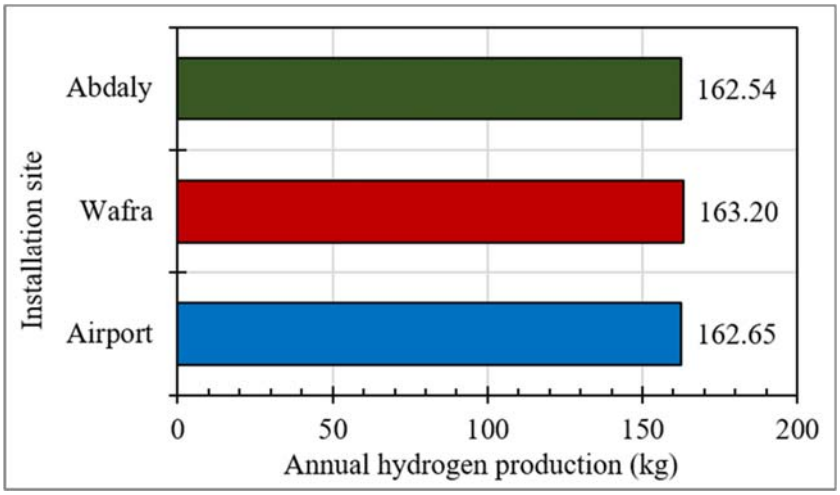

Figure 4.14 TRNSYS annual hydrogen production capacity (kg/year)

As shown in Figure 4.14, the highest annual hydrogen production capacity was 163.2 kg for the system at the Wafra site. The second highest production capacity was 162.65 kg for the system at the Airport site. The lowest annual production was 162.54 kg for the system at the Abdaly site. Based on TRNSYS simulation, the Wafra site is the promising site to install the system in terms of the annual production capacity keeping in mind that the differences in annual production at the three sites were negligible. This finding did not match the logical outcomes of the Excel model, which demonstrated the superiority of the Airport site for the annual production, see section 4.2.3. The difference between TRNSYS and Excel model predictions may be due to the use of storage method (tank) of changeable SOC during TRNSYS simulation, which was not the case for the Excel model. Also, Excel model lacks the use of storage method of excess energy.

4.3.6 Excel versus TRNSYS Annual Production

The annual hydrogen production (kg) predicted by the Excel model was compared with TRNSYS predictions as shown in Table 4.8.

Table 4.8 Comparison of annual average hydrogen production (kg)

Site	Excel	TRNSYS	Difference (%)
Airport	469.8	162.65	–65.4
Wafra	100.3	163.20	+62.7
Abdaly	71.5	162.57	+127.5

The comparison of annual hydrogen production of the static Excel model and the dynamic TRNSYS simulation shows significant differences due to the method of handling of the intermittency penalty of wind power in Kuwait. There are several probable reasons for these differences including the difference between the system constraints in TRNSYS and the idealised modeling of Excel. The Excel model works as an electrolyser-only simulation, which evaluates hydrogen production using the available raw wind data. The increased annual production at the Airport site in Excel (469.8 kg) could be related to the assumption that nearly all the captured wind energy is converted into hydrogen. On the other hand, the TRNSYS annual production remains nearly the same (about 163 kg) at all sites, which indicates that TRNSYS is probably constrained by the storage tank capacity. Once the hydrogen tank is full, TRNSYS stops production regardless of wind availability, whereas Excel model continues to calculate a theoretical production.

At the Wafra and Abdaly sites, TRNSYS predicts higher production than Excel. This could be due to the control logic and battery buffering essential for TRNSYS simulation. Excel model assumes continuous electrolyser operation even at low wind speeds where the Faraday efficiency drops and causes near-zero production. TRNSYS, however, utilises stored battery energy to keep the electrolyser at best operation and reclaim production lost in Excel model due to the parasitic crossover currents. In the Excel model, the electrolyser is usually treated as a static component, but in TRNSYS, the warm-up duration and the energy consumed by pumps and controllers are subtracted from the wind energy available to produce hydrogen, resulting in more conservative and realistic production predicted at the Airport site.

The tendency of static Excel model to overestimate the hydrogen production at the high-resource Airport site while underestimating it at the low-resource Wafra and Abdaly sites is well-documented. Ulleberg (2003), for instance, reported the importance of dynamic models such as TRNSYS for capturing the non-linear relationship between the intermittent power and the hydrogen production efficiency.

Also, Shehabi and Dally (2021) reported that the net productivity of off-grid systems, in Kuwaiti context, is often constrained by storage size and auxiliary energy needs rather in addition to the wind energy potential. The stability of annual hydrogen production predicted by TRNSYS (about 163 kg/year) aligns with the findings of Sebbahi et al. (2024) who reported the effect of storage tank capacity changes of optimised off-grid systems on the hydrogen production rates at different sites.

4.3.7 TRNSYS Predictions of Specific Energy Consumption

In addition to system productivity, it was important to assess the energy utilisation efficiency during the production process. To assess the economics of system operation, specific energy consumption (SEC) was important to consider (Al-Douri and Groth, 2024). This parameter helps comparing the system performance at the three sites and studying the feasibility and economics of hydrogen production system. For the system at the three sites, SEC was evaluated and compared as shown in Figure 4.15.

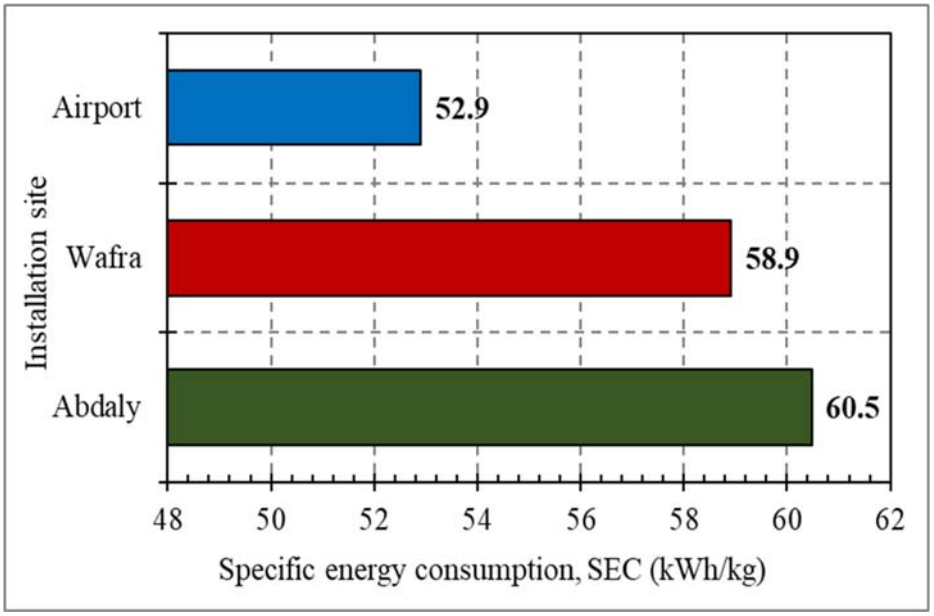

Figure 4.15 TRNSYS specific energy consumption (SEC, kWh/kg) predictions

As depicted in Figure 4.15, TRNSYS predictions show a lowest (best) SEC of 52.9 kWh/kg for the system at the Airport site, followed by 58.9 kWh/kg for the system at the Wafra site. The highest (worst) SEC was predicted as 60.5 kWh/kg for the system at the Abdaly site. Therefore, in term of the system economics, the best performance is expected for the system at the Airport site, followed by Wafra then Abdaly, which is consistent with the Excel model predictions, see section 4.2.4.

TRNSYS simulations demonstrated that the superiority of a specific installation site over the others is doubted in terms of system productivity. However, the system at the Airport site was of the best performance, in terms of the specific energy consumption. The selection of an installation site depends mainly on the operating goals. If the main target of the system is to operate at the highest possible production irrespective of the production costs, TRNSYS predictions show not much difference between the three sites. Meanwhile, if the target is the best economics, the most promising site to install the system is the Airport site.

4.3.8 Excel versus TRNSYS Specific Energy Consumption

The Specific Energy Consumption (SEC, kWh/kg) values predicted by the Excel model was compared to TRNSYS predictions as shown in Table 4.9.

Table 4.9 Comparing annual average specific energy consumption (kWh/kg)

Site	Excel	TRNSYS	Difference (%)
Airport	64.9	52.9	–18.5%
Wafra	126.1	58.9	–53.3%
Abdaly	192.3	60.5	–68.5%

The comparison of annual average SEC between the static Excel model and the dynamic TRNSYS simulation shows a remarkable difference in method of handling the intermittency penalty of wind power at the three sites. As shown, Excel overestimates the SEC at the low wind Wafra and Abdaly sites because the calculations were conducted without control limits and battery buffering adopted during TRNSYS simulation. Therefore, TRNSYS predictions are more representative of commercial electrolysers. The remarkable difference, especially at the Abdaly site (192.3 kWh/kg versus 60.5) could be attributed to the method of handling the low-wind periods.

The Excel model, as a static model, calculates the SEC for every wind speed data including operation at very low current densities which forces the system to operate into the zone of near zero Faraday efficiency, which mathematically increases the annual average SEC. In TRNSYS, the system operates with low-power cut-off so that when the wind power is low, the electrolyser shuts down or stays in standby condition. In his research, Ulleberg (2003) reported the static models' failure to capture the transient behaviour that significantly affect the specific energy consumption. Also, Sebbahi et al. (2024) reported the significance of integrating power conditioning in dynamic modelling for compromising between theoretical and actual performance of hydrogen production systems.

4.3.9 Operating Cycles of the Storage Tank

During simulation, the storage tank volume was set at 1.0 m^3 and tank pressure was set at 200 bar. At the start of the simulation, the initial SOC of the tank was set at 0.4. The upper limit of the SOC was set at 0.9 so that when the simulation started, the charging process of the tank also started. The electrolyser is supplied with turbine energy to produce hydrogen, which was compressed and forced to fill in the tank. Meanwhile, there was continuous hydrogen consumption (extraction) from the tank, which also started with the simulation, at a constant rate of 0.2 m^3/h. Therefore, there were two hydrogen streams, the first was from the electrolyser to the tank (inlet to the tank) and the second was the steady consumption (exit from the tank).

At the start of the simulation trials, the system produced high amounts of hydrogen so that the supply to the tank was higher than the consumption, which caused steady increase of the tank SOC until it reached the upper SOC limit. When the tank SOC reached 0.9, the system stopped the electrolyser from producing hydrogen while it was fed by fraction of the turbine power output (equals the idling power) to keep the electrolyser running at idling. Meanwhile, the excess power of the turbine was delivered to storage batteries, which was not included in the developed TRNSYS model.

When the electrolyser operated at idling, the hydrogen production stopped, and no hydrogen was fed to the tank. With the continuous consumption of hydrogen from the tank, the tank SOC steadily decreased to reach the lower SOC limit of 0.7. As soon as the tank SOC reached 0.7, the electrolyser operation was restarted to produce hydrogen and supply the storage tank to start another storage tank charging cycle.

At the three sites, the operating cycle of the storage tank was the same. With the start of the first tank charging, the initial SOC was 0.4 which was less than the lower SOC limit. Thus, the electrolyser started to produce hydrogen, which was compressed and supplied to the tank. Because the supply tank was higher than the consumption, the SOC of the tank increased with time to reach the upper limit of 0.9 at which the supply to the tank was stopped. When SOC reached the upper limit of 0.9, the electrolyser stopped producing hydrogen indicating the end of the first charging cycle of the tank. The duration of the first charging cycle for each site was dependent on the electrolyser production rates. The consecutive cycles of tank charging/discharging then repeated until the end of simulation, as shown in Figure 4.16.

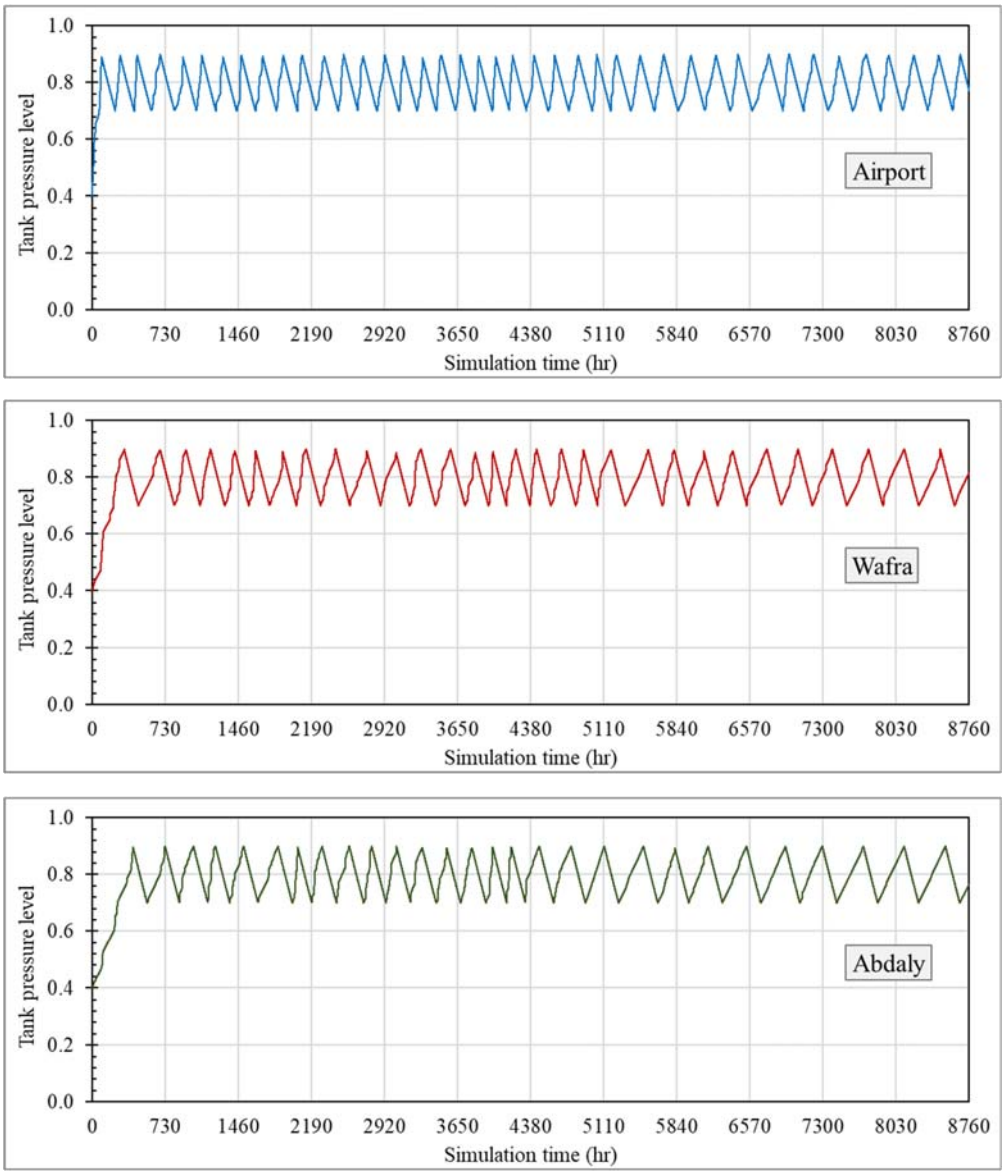

Figure 4.16 TRNSYS hourly variations of storage tank operating cycles

As shown in Figure 4.16, the duration of the first charging cycle (between SOC 0.4 and 0.9) was not the same at the three sites. For example, shortest duration of 97 hours was needed to finish the first charging cycle for the system at the Airport site. For the system at the Wafra site, the duration of the first charging cycle was increased to 322 hours. There was a further increase of first charging cycle duration to 410 hours for the system at the Abdaly site. Thus, the system of the fastest response was the system at the Airport site compared with the other sites. After the tank first charging, the operating cycles were repeated to discharge and charge the tank between the upper and lower SOC limits. But the number (frequency) of cycles was highest for the system at the Airport site due to the increased hydrogen production. But the high frequency of tank operating cycles may increase the maintenance needs of the system.

4.3.10 Impact of Electrolyser Surface Area on Performance

Electrolyser surface area is a key design parameter of significant effect on the water splitting reaction rates, operating efficiency, and hydrogen production capacity, especially for water alkaline electrolysers. The larger the surface area the higher the rates of hydrogen production due to the increased number of the active hydrogen gas formation sites and the reduction of the activation overpotential (Niblett et al., 2024). For a specific cell voltage, the electrolyser of small surface area operates at high current density, which increases the rate of hydrogen production according to Faraday's law (Luo et al., 2024) and improves the electrolyser efficiency (Madila et al., 2025). Meanwhile, the use of large surface area results in a bulky electrolyser stack size and increases the electrolyser capital costs (Yang et al., 2023). Thus, Abdelgwad et al. (2025) reported the significance of trade-off between the productivity of the system and the capital.

The effect of electrolyser surface area on the system performance was investigated. Keeping all other parameters unchanged, TRNSYS simulation trials were conducted using surface area of 0.3 m^3 before being doubled to 0.6 m^3, at the three sites. The predictions of the annual operating parameters of the electrolyser at each site are compared as shown in Table 4.10.

Table 4.10 Impact of surface area on electrolyser annual operating parameters

Simulated site	**Airport**		**Wafra**		**Abdaly**	
Surface area (m^2)	**0.3**	**0.6**	**0.3**	**0.6**	**0.3**	**0.6**
Total used current (A)	686,360	726,642	620,778	656,601	609,344	618,644
Consumed energy (kWh)	8,604	12,101	9,613	14,572	9,831	15,679
H_2 production (Nm^3)	**162.65**	**163.47**	**163.18**	**158.51**	**164.16**	**152.94**
O_2 production (Nm^3)	904.6	909.1	907.6	881.6	913.0	850.6
Generated heat (kWh)	255.6	-147.3	93.7	-397.1	67.8	-527.1
Thermal losses (kWh)	2623	2623	2623	2623	2623	2623
Cooling energy (kWh)	-660	-1458	-1264	-2391	-1370	-2858
Energy storage (kWh)	-1708	-1312	-1265	-629	-1185	-292
Minimum voltage (V)	24.7	24.7	24.7	24.7	24.7	24.7
Maximum voltage (V)	32.4	30.9	32.4	30.9	32.4	30.9
Faraday efficiency (%)	92.9	85.5	92.9	85.5	92.9	85.5
Overall efficiency (%)	84.6	81.7	84.6	81.7	84.6	81.7

As shown in Table 4.10, increasing the electrolyser surface area does not affect the minimum electrolyser voltage, which was constant at 24.7 V, at all sites. Nevertheless, the maximum

system voltage decreased from 32.4 V at surface area 0.3 m^2 to 30.9 V at area 0.6 m^2, at all sites. There was also increase of the annual current consumption by about 5.8% with the larger area at all sites.

As shown in Table 4.10, there were contradicted findings for the annual hydrogen production with doubling the electrolyser surface area. For example, the annual hydrogen production slightly increased by about 0.5% from 162.65 to 163.47 kg with doubled surface area for the system at the Airport site. Nevertheless, for the system at the Wafra or the Abdaly sites, the annual production decreased with increasing the surface area. The impact of electrolyser surface area on the SEC of the system at all sites was also assessed and compared as shown in Figure 4.17.

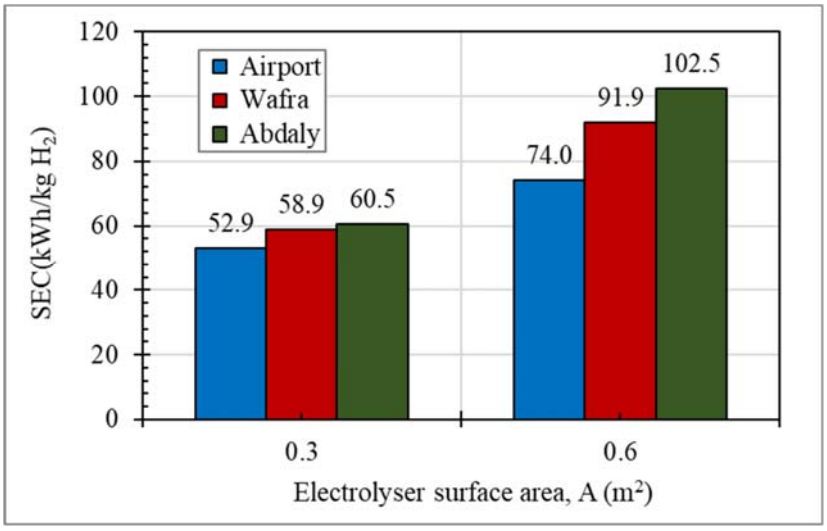

Figure 4.17 Variation of the SEC (kWh/kg) with electrolyser surface area

As shown in Figure 4.17, doubling the electrolyser surface area increased the SEC of the system at all sites, which indicated inefficient performance. There is about 40% increase in SEC (from 52.9 to 74.0 kWh/kg) with doubled surface area of the system at the Airport site. An increase of 56% in SEC (from 58.9 to 91.9 kWh/kg) was found with doubled area for the system at the Wafra site. Further increase of SEC by about 69% (from 60.5 to 102.5 kWh/kg) with doubled area was found for the system at the Abdaly site. This may be attributed to the decrease of the current density with doubling the area at same current, which was much lower than the average current density of 300 mA/cm^2 usually utilised for industrial alkaline water electrolysers (Demnitz et al., 2024). Since the system at all sites already operate at low current densities, doubling the surface area pushes the current density even further down into the efficiency cliff zone. The decreased current density slightly improves the voltage by

decreasing the ohmic resistance and activation overpotential but massively decrease the Faraday efficiency to outweigh the small voltage gain. The net effect is the increase of the system SEC, which agrees with Luo et al. (2024) and Madila et al. (2025) who demonstrated decreased overall system efficiency and Faraday efficiency with increased surface area, as shown in Figure 4.18.

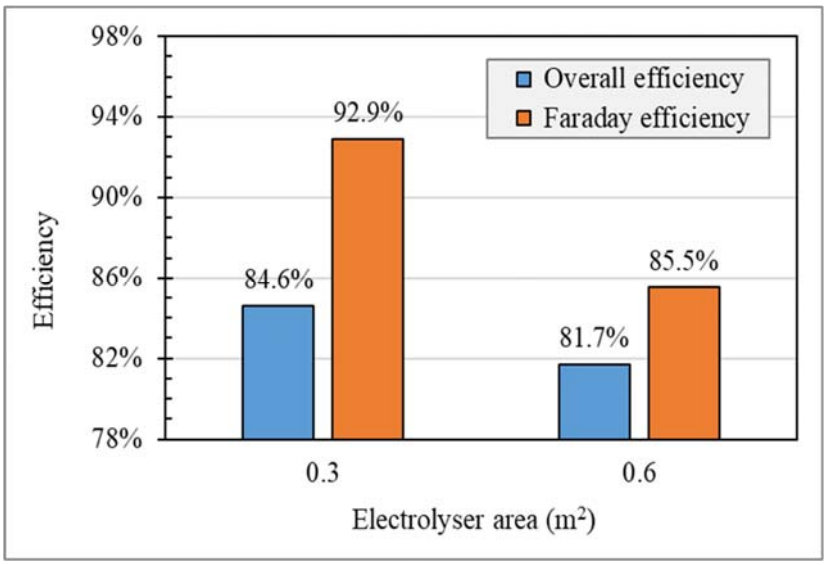

Figure 4.18 Variation of efficiencies with electrolyser surface area

Doubling the electrolyser surface area from 0.3 to 0.6 m^2 decreased Faraday efficiency and the overall system efficiency. At surface area of 0.3 m^2, as shown in Figure 4.18, Faraday efficiency was 92.9% and the overall system efficiency was 84.6%. Doubling the surface area decreased Faraday efficiency to 85.5% and the overall efficiency to 81.7%. Therefore, increasing the electrolyser surface area without means of increasing the wind turbine energy input to the electrolyser is ineffective for the system at the sites of limited wind potential. The increase of electrolyser surface area at same input energy decreases the current density, which forces the system to operate with high gas crossover causing significant increase in specific energy consumption.

4.3.11 Impact of Storage Tank Volume on Performance

During simulation, the storage tank was fed with hydrogen produced by the electrolyser, based on the SOC of the tank. Also, there was a continuous constant hydrogen consumption from the tank. To investigate the impact of storage tank volume on system performance, the volume was changed as 1.0, 2.0, 3.0, and 4.0 m^3, keeping other parameters unchanged and electrolyser surface area of 0.3 m^2. The variation of the annual hydrogen production with tank volume, for the system at the three sites is shown in Figure 4.19.

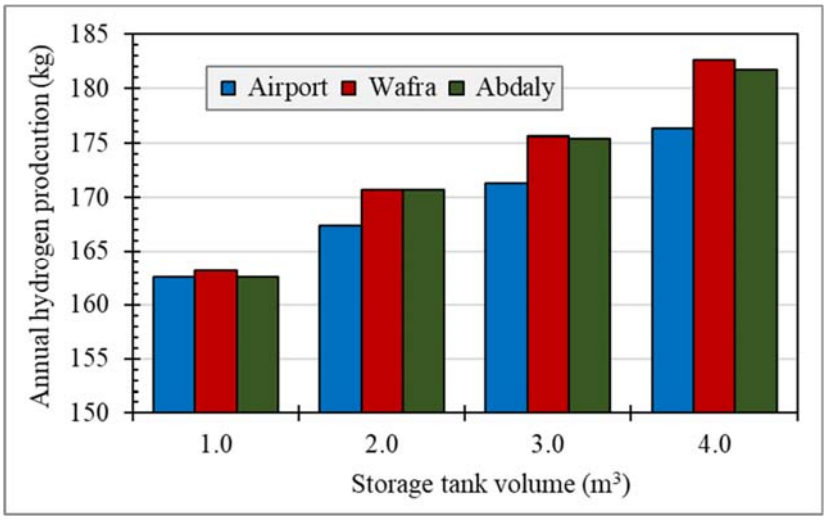

Figure 4.19 Annual hydrogen production versus tank volume

As shown in Figure 4.19, increasing the storage tank volume increased the annual production of the system at any site. Increasing the tank volume, at constant consumption of the gas from the tank provides more space (volume) for the hydrogen produced by the electrolyser to fill in the tank. Accordingly, the duration of idle operation of the electrolyser decreased and the frequency of charging/discharging cycles also decreased. An example showing the effect of tank volume on the operating cycle of the tank for the system at the Airport site is shown in Figure 4.20.

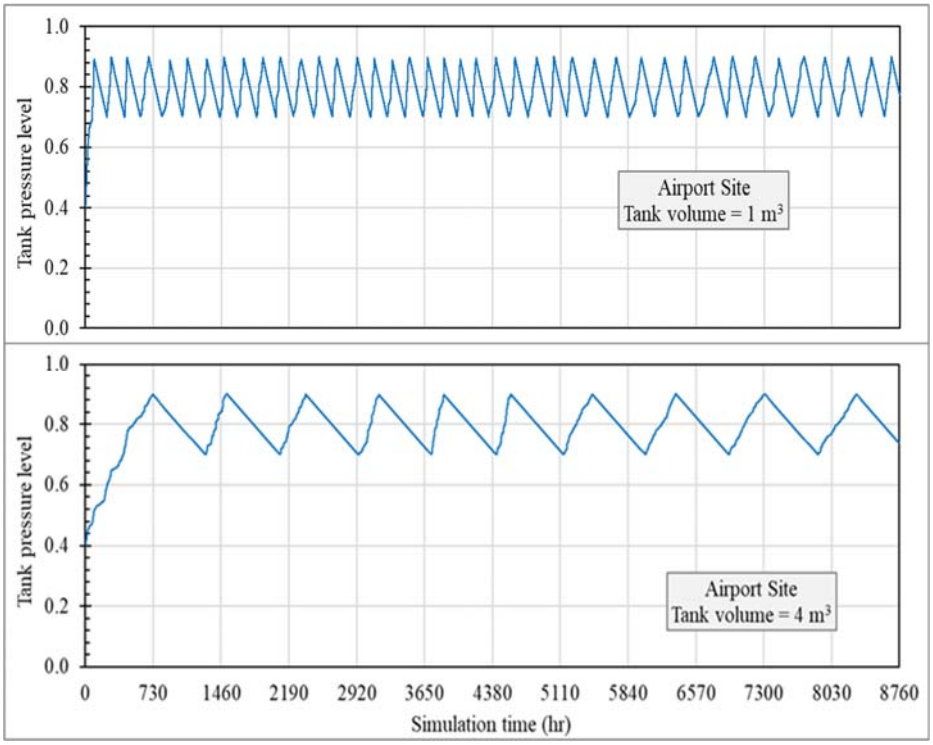

Figure 4.20 Change of storage tank operating cycle with tank volume

As shown in Figure 4.20, longer duration of the first charging process of the tank, from an initial SOC of 0.4 to a final SOC of 0.9, was found with the increase of storage tank volume. For a small tank volume of 1 m^3, the duration of the first charging process was 97 hours. Enlarging the tank volume to 4 m^3 increased the duration of the first charging process to 720 hours. With a constant hydrogen consumption from the tank, increasing the tank volume provided an extra space (volume) that can be filled with hydrogen, which needed time. Therefore, longer time was required to complete the first charging process. Meanwhile, there was no effect of increasing the tank volume on the SEC of the system at the three sites. But increasing the tank volume increases the system cost. Thus, there should be an optimisation for the size and specifications of each system component, including the tank, to ensure that the system is operating at the best possible performance. This is why it was important to optimise the system components using HOMER pro software.

4.4 HOMER Multi-Sites Optimisation Results

Homer Pro software was used to figure out the optimum economic and technical feature of each component of the hydrogen production system. HOMER was used to determine the required number of wind turbines, capacity of the electrolyser and the converter, and the storage tank size based on the wind speeds at each site.

During optimisation, HOMER matched between the hydrogen produced by the electrolyser and the required hydrogen load to evaluate the suitable size of the storage tank. Since the components of the system have different lifetimes, HOMER evaluated the LCOH over the project's lifetime of 25 years considering that the components of lifetime less than 25 years need replacement with new ones.

4.4.1 Sensitivity Analysis Results

The system components of optimised performance and adequate sizes were found using HOMER with the convergence of system constraints i.e. lowest Net Present Cost (NPC). HOMER optimised the components' sizes using minimised energy cost. During system optimisation, data on the load, weather, and economics were entered to HOMER along with optimisation constraints to evaluate the Net Present Cost (NPC, $), Levelised Cost of Energy (LCOE, $/kWh), Levelised Cost of Hydrogen (LCOH, $/kg), etc. Sensitivity analysis was conducted to assess the feasibility of the system and the reliability of the system cost by changing the required scaled daily average hydrogen production.

To link HOMER optimisation results with TRNSYS simulation, the hydrogen consumption rate from the system was set in TRNSYS at 0.2 m^3/h. In HOMER, the production capacity is expressed as kg/h, therefore TRNSYS consumption rate was converted into kg/h using hydrogen density. For an electrolyser of operating pressure 7.0 bar and operating temperature 70°C (343 K), the hydrogen density was evaluated as 0.495 kg/m^3. Therefore, the mass flow rate of consumed hydrogen was evaluated as 0.495 (kg/m^3) times 0.2 (m^3/h), which was 0.099 kg/hr. The daily average hydrogen consumption in TRNSYS was calculated as hourly mass flow rate (0.099 kg/hr) times 24 (hr/day), which was 2.38 kg/day. Therefore, sensitivity analysis was conducted using scaled daily hydrogen load (consumption) of 1.0, 1.5, 2.0, and 2.5 kg/day. The impact of scaled hydrogen load on the levelised cost of hydrogen (LCOH) was obtained for the system at all sites as shown in Table 4.11.

Table 4.11 Effect of scaled average hydrogen load on LCOH

Scaled load (kg/day)	LCOH ($/kg)		
	Airport	Wafra	Abdaly
1.0	12.5	14.9	23.7
1.5	**9.03**	13.5	19.9
2.0	9.34	14.9	19.9
2.5	7.96	13.0	18.5

The results in Table 4.11 demonstrated that the LCOH ($/kg) was lowest for scaled average hydrogen load of 1.5 kg/day. Therefore, the best performance of the optimised system in this study was for system operating at daily hydrogen consumption of 1.5 kg/day at all sites. HOMER Pro optimisation results, at daily hydrogen consumption 1.5 kg/day, including the optimised system components at the three sites are therefore presented in the next sections. Also, the next sections include comparison of the performance parameters of the system at all sites to identify the winning site. Detailed analysis of the performance and economic parameters are also included.

4.4.2 Optimised System Components

HOMER optimisation results for a scaled hydrogen consumption of 1.5 kg/day at all sites show hydrogen production capacity of about 547 kg every year. The optimisation results also show an electrolyser specific energy consumption (SEC) of 46.4 kWh/kg. The number and size of the optimised components of the system including the wind turbines, electrolyser, electricity storage batteries, converter, and storage tank at all sites are listed and compared as shown in Table 4.12.

Table 4.12 Optimised number and capacity of the components (@ 1.5 kg/day)

Component	Airport	Wafra	Abdaly
Wind turbines			
Number of turbines	2	3	5
Total capacity (kW)	20	30	50
Maximum power output (kW)	25.1	37.6	62.7
Mean power output (kW)	6.81	5.41	7.43
Annual operating hours (hr/year)	8,225	7,783	7,748
Electrolyser			
Rated capacity (kW)	7.19	9.95	8.13
Mean electrolyser input (kW)	2.92	2.91	2.9
Annual operating hours (hr/year)	7,175	6,424	6,698
Capacity Factor (CF)	40.6%	29.2%	35.7%
Maximum H_2 output (kg/hr)	0.155	0.214	0.175
Mean H_2 output (kg/hr)	0.0630	0.0627	0.0625
Battery			
Number of batteries	11	13	26
Autonomy (hours)	24.9	29.4	58.9
Nominal capacity (kWh)	15.6	18.4	36.8
Usable nominal capacity (kWh)	12.5	14.7	29.4
Lifetime throughput (kWh)	4,312	5,096	10,192
Expected life (years)	7.25	5.56	12.2
Converter			
Rated capacity (kW)	1.33	1.65	1.47
Mean output (kW)	0.5	0.5	0.5
Storage tank			
Storage tank capacity (kg)	8	14	10
Energy storage capacity (kWh)	267	467	333
Tank autonomy (hour)	533	933	667

At a scaled hydrogen load of 1.5 kg/day, as shown in Table 4.12, the optimised system at the Airport site requires 2 wind turbines whereas 3 wind turbines are needed for the system at the Wafra site and 5 wind turbines are required at the Abdaly site. At the Airport site, electrolyser of rated capacity 7.19 kW is needed, which was lower than the 9.95 kW and 8.13 kW required for the system at the Wafra and Abdaly sites, respectively. Also, smaller number of batteries (11) is needed at the Airport site whereas 13 and 26 batteries are needed

at the Wafra and Abdaly sites, respectively. Lowest rated capacity converter is needed at the Airport site relative to other sites. Finally, storage tank of small capacity (8 kg) is required at the Airport site whereas tank capacity of 14 kg and 10 kg are needed at the Wafra and Abdaly sites, respectively. These numbers and sizes clearly affect the system economics, which is explained later in this chapter, but the effect on the performance parameters is first explained in the following section.

4.4.3 Performance Parameters of the System

At all sites, the annual primary electrical load of the system was 4,379 kWh and the annual electrolyser hydrogen production was about 550 kg. Other performance parameters of the system components were evaluated at each site as shown in Table 4.13.

Table 4.13 Performance parameters of the components (@ 1.5 kg/day)

Parameter	Airport	Wafra	Abdaly
Wind turbines production (kWh/yr)	59,684	47,401	65,110
Electrolyser consumption (kWh/yr)	25,608	25,480	25,421
Excess electricity (kWh/yr)	29,382	17,156	34,940
Percentage of excess electricity	49.2%	36.2%	53.7%
Annual battery throughput (kWh/yr)	595	917	834
Tank content at end of year (kg)	4.65	1.93	0.852
Unmet hydrogen demand (kg/yr)	0.308	0.364	0.547

As shown in Table 4.13, the annual energy produced by the turbines was about 59.7 MWh for the system at the Airport site, 47.4 MWh at the Wafra site, and 65.1 MWh at the Abdaly site. The system electrolyser annually consumes energy about 25.6 MWh at the Airport site, 25.5 MWh at the Wafra site, and 25.4 MWh at the Abdaly site. The excess electricity, which is the percentage of generated wind power that cannot be used to produce hydrogen or stored in batteries was 49.2% (29.4 MWh/year) at the Airport site, 36.2% (17.2 MWh/year) at the Wafra site, and 53.7% (34.9 MWh/year) at the Abdaly site. The annual battery throughput, which is the total discharged energy by the battery during one-year, was 595 kWh at the Airport site, 917 kWh at the Wafra site, and 834 kWh at the Abdaly site. The storage tank content at end of year was 4.65 kg at the Airport site, which was decreased to 1.93 kg at the Wafra site then to 0.852 kg at the Abdaly site. The unmet hydrogen demand, which is the annual quantity of hydrogen that the system failed to deliver during low-wind periods was 0.308 kg/year at the Airport site, which was increased to 0.364 kg/year and then to 0.547 kg/year at the Wafra and Abdaly sites.

4.4.4 Economic Parameters of the System

For all sites, the economic metrices of the system are presented in Table 4.14.

Table 4.14 Economic metrices of the system (@ 1.5 kg/day)

Parameter	Airport	Wafra	Abdaly
NPC ($)	103,652	$154,307	$226,852
LCOE ($/kWh)	1.14	1.69	2.49
LCOH ($/kg)	9.03	13.5	19.9

For a scaled daily hydrogen production of 1.5 kg/day, as shown in Table 4.14, the Net Present Cost (NPC) of the system was $103,652 at the Airport site. NPC was increased to $154,307 for the system at the Wafra site, which was about 1.5 time the NPC at the Airport site. For the system at the Abdaly site, the NPC was further increased to $226,852, which was 2.2 times the NPC at the Airport site.

The analysis of the Levelised Cost of Energy (LCOE) for the three sites reveals significant economic differences that clearly varied with the wind energy profiles of Kuwait. The system at the Airport site, as shown in Table 4.14, showed most competitive energy generation cost with LCOE of $1.14/kWh. Meanwhile, the system at the Wafra site had a LCOE of about $1.69/kWh, which was about 48% higher than the cost at the Airport site. The system at the Abdaly site had a LCOE of $2.49/kWh, which was higher than the cost at the other sites; the LCOE at the Abdaly site was about 118% the LCOE at the Airport site.

The main reason for the differences of energy generation cost at the three sites is the capacity factor (CF), which is inversely proportional to the LCOE. The constant capital expenditure (CAPEX) of the system components at any site ($103,652 at the Airport site for example) makes the LCOE to directly vary with the annual energy generation at this site. At the Airport site, the better wind speeds especially during summer enabled the turbines to generate more energy (kWh) which decreased the cost of energy generation. Meanwhile, the comparatively higher LCOE at the Abdaly site of $2.49/kWh reflected the resource penalty as the low wind speeds causes infrequent turbine operation and decreases the annual generated energy. Thus, the system at the Abdaly site is over-capitalised for the available wind potential. For the system at the Abdaly site the capacity factor was low, and the system relied on expensive electric batteries for storage, which increased the energy generation costs. This proves that for off-grid wind-operated hydrogen projects in Kuwait, site selection for maximum capacity factor is the most essential element for commercial feasibility.

As shown in Table 4.14, the levelised cost of hydrogen (LCOH) at the Airport site was the lowest at 9.03 $/kg, which was increased by 49% to reach 13.8$/kg at the Wafra site. It is also increased to 2.49 $/kg at the Abdaly site, which was about 2.2 times the LCOH at the Airport site. The Levelised Cost of Hydrogen (LCOH) was dependent on the Levelised Cost of Energy (LCOE) as the energy cost was the most significant parameter of effect on the cost of hydrogen production. In alkaline water electrolysers, electricity is the main raw material required for hydrogen production; therefore, the LCOE of the wind turbines controls the hydrogen production cost. Since the specific energy consumption (SEC) of the system was in the range between 52 and 60 kWh/kg, every little increase in the LCOE triggers a real increase of the LCOH.

The economic collapse found for the system at the Abdaly site, with LCOE of $2.49/kWh and high SEC due to the decreased Faraday efficiency, caused the energy production unit (turbine) to add more to the hydrogen production cost. At the Airport site, the lower LCOE of $1.14/kWh added to the improved SEC of 52.9 kWh/kg causes the LCOH at the site to drop to the lowest of $9.03/kg shown in Table 4.14. For the 1.5 kg/day demand, Table 4.15 shows the wining site and the technical justification for being the winner.

Table 4.15 Comparative site advantages and performance winners

Category	Winning site	Justification
Lowest LCOH ($/kg)	Airport	Relatively high wind energy decreased the turbine runtime and storage size, which decreased the components' cost.
Highest system efficiency	Airport	High-velocity winds keep the electrolyser consistently operating at high current density range.
Storage reliability	Airport	Shorter periods of low wind speeds enable smaller storage tank to meet 100% autonomy.
Energy source integration	Wafra / Abdaly	Land availability enables future potential hybridisation with solar PV panels.
Energy utilisation	Airport	Lowe excess energy because hydrogen production closely fulfils the daily hydrogen demand profile.

The optimum system performance was ensured at the Airport site at any hydrogen production capacity. At the Airport site, the optimised performance was feasible for a scaled daily hydrogen production of 1.5 kg/day. The comparison in Table 4.15 proves the superiority of the Airport site over other sites. Thus, detailed system performance and analysis for the system at the Airport site are presented in the next section.

4.5 System Performance at the Airport Site

4.5.1 Electrical and Hydrogen Loads

The hourly variations of the electrical and hydrogen loads are shown in Figure 4.21.

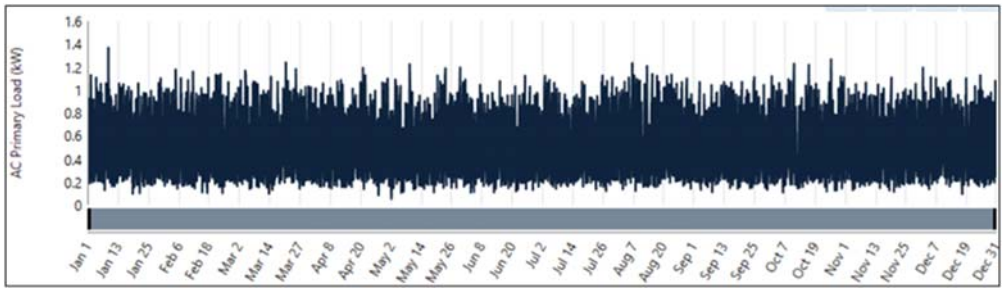

a) Electrical load

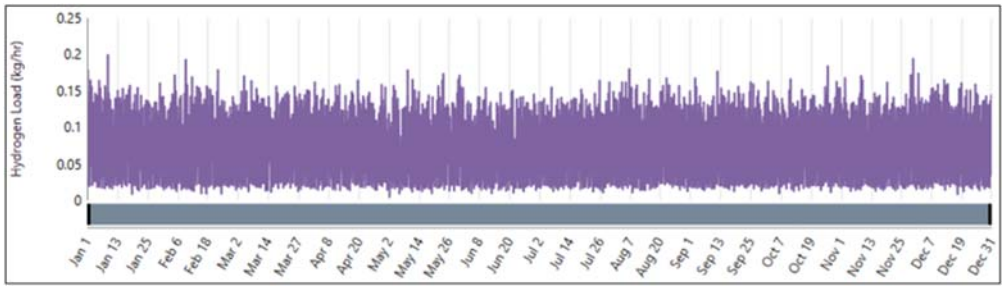

b) Hydrogen load

Figure 4.21 Hourly electrical and hydrogen loads of the system (@1.5 kg/day)

As shown in Figure 4.21a, the annual profile shows a highly unstable electrical load, which hourly fluctuates between 0.2 kW and 1.4 kW. The load significant density and frequent spikes show high intermittent electricity needs without distinct seasonal trend. The annual hydrogen load profile, shown in Figure 4.21b, shows significant stochastic instability, with hourly fluctuating needs between 0.02 kg/hr and 0.15 kg/hr. Peak spikes reaching 0.20 kg/hr occasionally took place with consistently low baseline hydrogen needs, which shows highly intermittent hydrogen consumption pattern.

4.5.2 Performance of the Wind Turbines

For the optimised system at the Airport site, two Bergy Excel 10 wind turbines were needed. The total rated capacity of the turbines was 20.0 kW with mean output of 6.81 kW. The total annual energy production of the turbines was 59, 684 kWh. The capacity factor was 34.1%, which meant operation at one third of the maximum possible wind energy. Based on the wind speeds at the site, the turbines annually operated for 8,225 hours and stopped for 535 hours every year with the drop of wind speeds below the cut-off limit of 2.5 m/s. A D-map visualisation showing the annual wind power generation profile is shown in Figure 4.22.

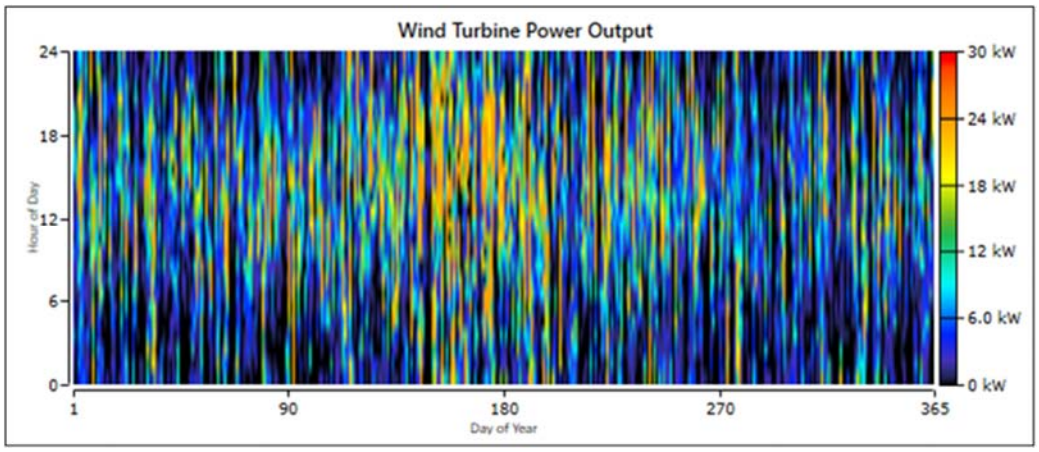

Figure 4.22 Hourly power output of the wind turbines (@1.5 kg/day)

As shown in Figure 4.22, the turbines produced highly intermittent power, with peak outputs (orange and red) frequently took place during summer (between Day 150 and 240) due to the stronger winds. For the impact on electrolyser operation, the occurrence of low-power blue zones showed frequent operation at part loads, which decreased the average Faraday efficiency and accordingly increased the Levelised Cost of Hydrogen (LCOH). The monthly average energy production of the turbines is shown in Figure 4.23.

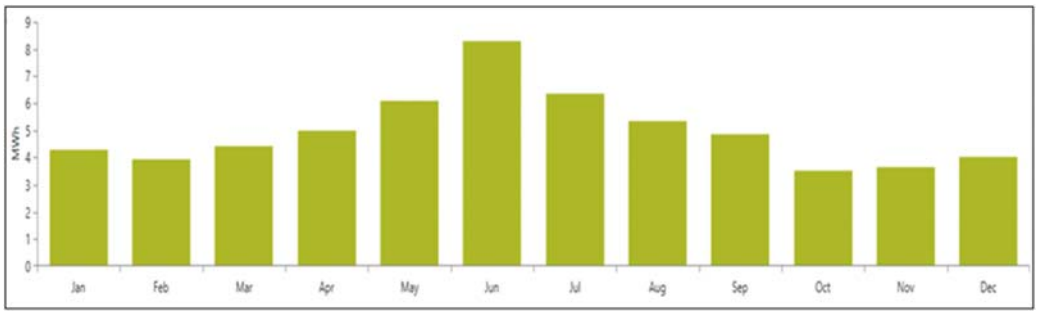

Figure 4.23 Monthly energy production of the wind turbines (@1.5 kg/day)

Figure 4.23 shows clear seasonal trend in the monthly wind energy production for the Airport site with obvious peaks during summer months May to July. The energy generation steadily increased from March to reach a maximum of about 8.3 MWh in June. On the other hand, the lowest energy generation of about 3.5 MWh took place in October. The seasonal variation of energy generation is important for the techno-economic assessment of the electrolyser. The increased energy production in summer ensured system operation close to the nominal current density, which improved Faraday efficiency. However, the low energy production in autumn and winter may require additional green source of power such as solar panels or energy storage to keep continuous hydrogen production and to avoid frequent shutdowns of the system.

4.5.3 Performance of the Electrolyser

The variation of the hourly power input to the electrolyser is shown in Figure 4.24.

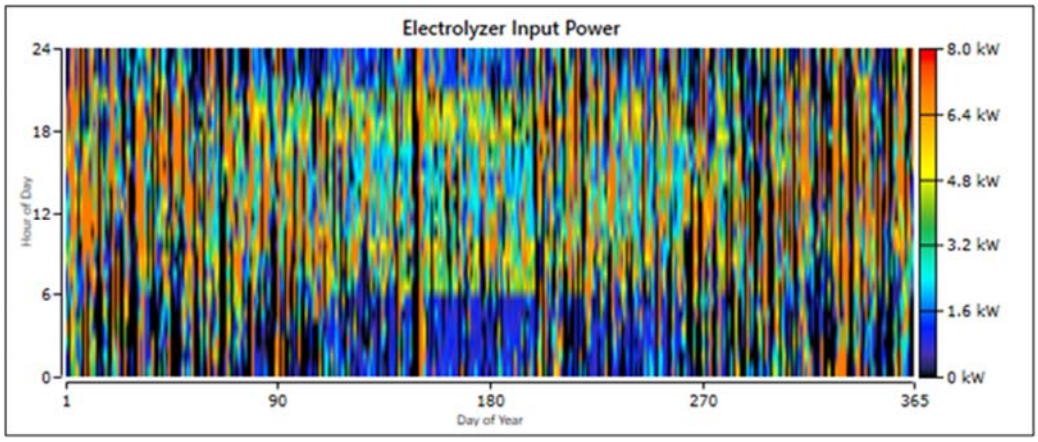

Figure 4.24 Hourly power input to the electrolyser (@1.5 kg/day)

As shown in Figure 4.24, the annual distribution of the hourly power input to the electrolyser shows highly intermittent operation. The power input to the electrolyser fluctuated between 1.6 kW and 6.4 kW, with irregular peaks (red zones) higher than 8.0 kW and frequent zero-power (black bands) showing the idle operation periods. The change of power input impacts the output of the electrolyser, as shown in Figure 4.25.

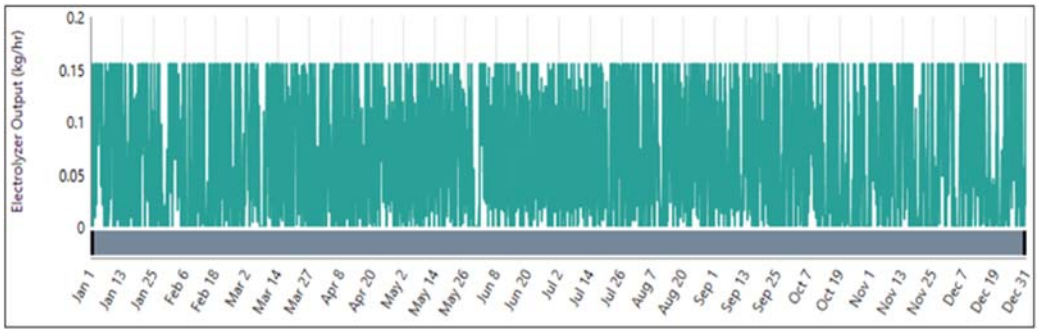

Figure 4.25 Hourly hydrogen production rate of the electrolyser (@1.5 kg/day)

The annual profile of electrolyser hydrogen output, as depicted in Figure 4.25, shows highly stochastic and intermittent production pattern, with hourly production rate fluctuated from zero production to about 0.16 kg/hr. The electrolyser output frequently reaches level near to the maximum capacity, represented by the dense horizontal alignment at the upper part of Figure 4.25. The on-off behaviour of hydrogen production directly reflects the variability of wind energy at the Airport site. The periods of zero hydrogen production are common, for example during spring months, which demonstrated the need of storage facility with the inability of the electrolyser to produce steady-state hydrogen amounts. The daily profile of the electrolyser output for each month is shown in Figure 4.26.

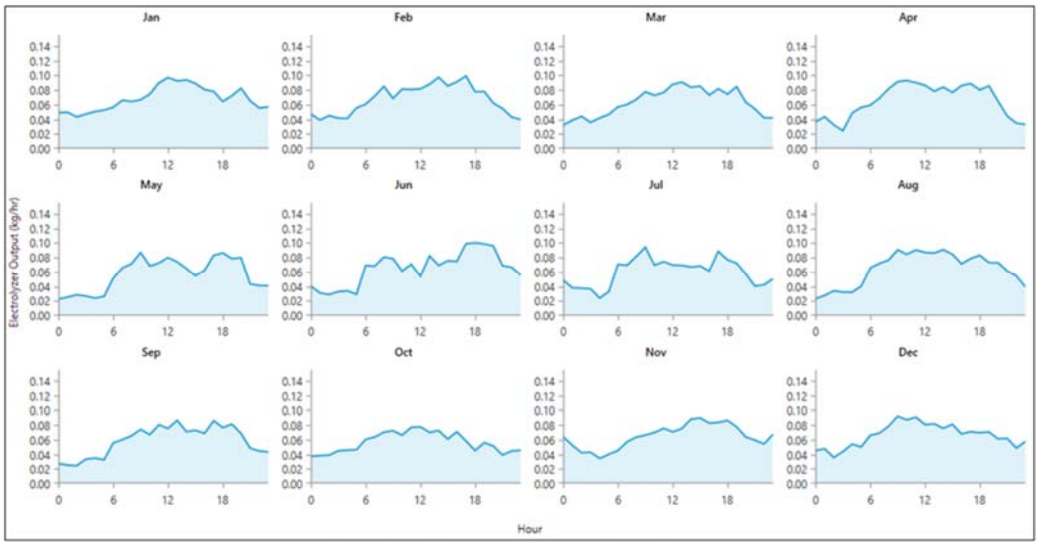

Figure 4.26 Daily profile of hydrogen production each month (@1.5 kg/day)

The daily profiles of hydrogen production for each month presented in Figure 4.26 show consistent daytime trend of hydrogen production with highest output usually takes place between hours 12:00 and 18:00. In months June and November, highest rates of hydrogen production about 0.09 to 0.1 kg/hr were found with consistent but low production took place during early morning hours (00:00–06:00). This behaviour can be attributed to the increase of wind speeds during the afternoon and evening at the Airport site.

4.5.4 Storage Level of the Hydrogen Tank

The variation of the hourly storage level (kg) of the storage tank is shown in Figure 4.27.

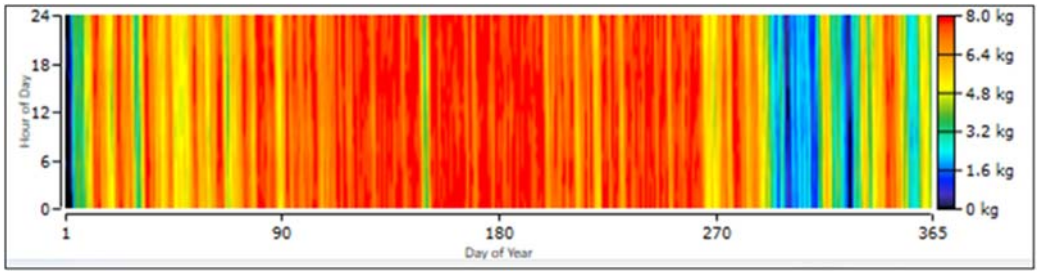

Figure 4.27 Hourly storage level of the hydrogen tank (@1.5 kg/day)

The hourly hydrogen storage levels presented in Figure 4.27 show that the system remains near its maximum capacity over the year. The red and orange zones on Figure 4.27 indicates storage level in the range from 6.4 kg to 8.0 kg, which proves the system ability to fulfil the required hydrogen load and maintain reliable and consistent storage levels. There is also significant drop of tank levels (blue/green) up to 3.2 kg during autumn due to the seasonal wind fluctuation. Therefore, the optimised 8 kg tank of the system at the Airport site was

sufficient for storage duties most of the year. Nevertheless, tank of larger volume may be required during late October operation of low wind potential. The variation of the monthly storage level of the tank is shown in Figure 4.28.

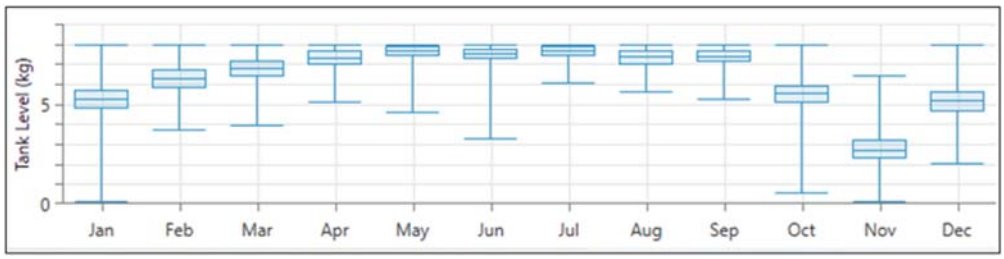

Figure 4.28 Monthly storage level of the hydrogen tank (@1.5 kg/day)

As shown in Figure 4.28, the monthly hydrogen storage levels demonstrated increased state of charge during the whole year. The hydrogen tank maintained consistent high storage level near the capacity of 8 kg during summer (April to September) due to the stable hydrogen production during summer which exceeded the hydrogen load demand. On the other hand, a decrease in storage capacity below 3 kg was found in November. Thus, the optimised tank size was sufficient for summer operation, but it reaches a critical storage level during autumn season characterised by wind energy scarcity.

4.5.5 Performance of the Storage Batteries

Storage batteries are important for the system at Airport site to bridge the gap between the intermittent wind potential and the operating needs of the electrolyser. The monthly variation of the state of charge (SOC) of the batteries is shown in Figure 2.29.

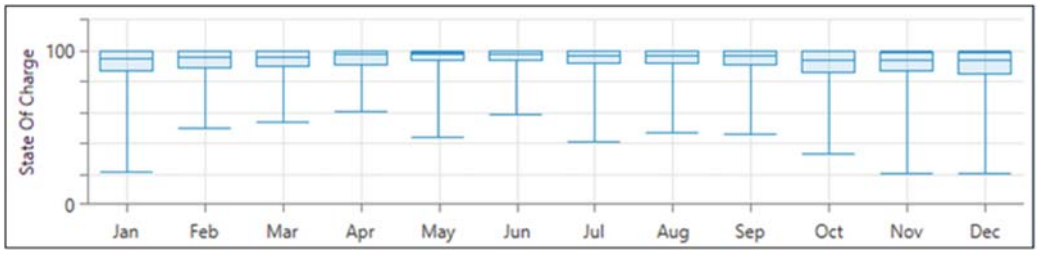

Figure 4.29 Monthly State of Charge (SOC) of the batteries (@1.5 kg/day)

The monthly SOC of the batteries show improve and reliable energy buffer. Over the year, SOC remains surprisingly stable, high, and consistent at 90% and 95%. Therefore, the wind turbines were of sufficient capacity to fulfil the required electrical load while the batteries remained nearly full. However, in months like January, October, and November, the SOC decreased to a lowest of about 20% due to seasonal wind quietens, which confirms the role of batteries in shortage prevention of wind energy generation during these periods.

4.6 System Costs at the Airport Site

The optimisation results, previously shown in Table 4.10, confirmed the capability of the green hydrogen production system at the Airport site to annually generate about 59,684 kWh of electrical energy by the wind turbines, of which the annual energy consumption of the electrolyser was about 25,608 kWh. The electrolyser at the Airport site is capable to annually produce about 547 kg of green hydrogen, which limited the specific energy consumption (SEC) of the system to about 46.82 kWh/kg. The optimised SEC value is consistent with the high-performance commercial alkaline electrolysers, which usually operate in SEC range of 47 to 58 kWh/kg (Sebbahi et al., 2024; Haoran et al., 2024; Bora, 2025). At the Airport site, the LCOH of the optimised system is 9.03 $/kg excluding gas compression costs. Details of the system costs are listed in Table 4.16.

Table 4.16 System costs at the Airport site (@ 1.5 kg/day)

Component	Cost ($)				
	Capital	Replacement	O&M	Salvage	Total
Wind turbines	80,000	0.00	4,990	9,256	75,734
Electrolyser	3,597	5,795	4,488	1,249	12,631
Batteries	2,750	6,701	2,287	1,054	10,684
Hydrogen tank	4,000	0.00	0.00	0.00	4,000
Converter	267	429	0.00	93	603
Whole system	**90,614**	**12,925**	**11,765**	**11,651**	**103,652**

As shown in Table 4.16, the total cost of the system at the Airport site is $103,652 which is significantly dominated by the initial capital cost of the wind turbines. The wind turbines are the main cost driver, which accounted for about 73% of the total system cost. No replacement cost for the wind turbines was needed as the service life of the turbines was 30 years, which resulted in a salvage value of $9,256 after the project life of 25 years. Irrespective of the decreased initial cost of the electrolyser of about $3,600, it needed high replacement and O&M costs because of its short service life of 10 years, making it the second most expensive component of the system. The batteries also were of high replacement costs due to their short service life of 10 years, which reflects the impact of battery cost on the total cost of the off-grid wind-powered electrolysis systems.

The payback period of the green hydrogen production system depends on the selling price of hydrogen. For a small-scale system feeding refuelling stations in remote areas, the selling price may reach a maximum of $20/kg. HOMER predictions of the optimised system show

an annual hydrogen production of about 550 kg. At the Airport site, the total system cost was optimised as $103,652 for the system of service life years. Simple calculations for the system payback were conducted, and the results are shown in Figure 4.30.

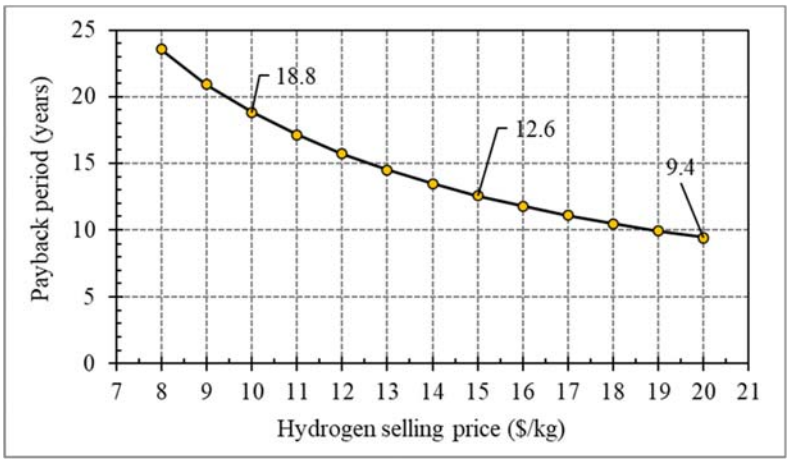

Figure 4.30 Payback period of the system vs hydrogen selling price

Although the system at the Airport site is the most productive, a payback period shorter than 25 years (project lifetime) is required to become economically feasible. The payback period for a small-scale off-grid wind-operated systems should be in the range from 7.5 to 11 years to become feasible (Ibrahim, 2025; Goel and Sharma, 2026). As depicted in Figure 4.30, the payback period of the system decreases with the hydrogen selling price. The payback period of equals the project lifetime (25 years) at hydrogen selling price of $7.55/kg. Therefore, the produced high-purity hydrogen price should exceed $7.55/kg to avoid net loss. As shown in Figure 4.30, the payback period is 18.8 years at selling price $10/kg, which can be decreased to 12.6 years at price $15/kg. When the price is $20/kg, the payback period can further be decreased to 9.4 years, which is good. Fortunately, selling high-purity hydrogen at $20/kg is possible if it is sold to specialised industrial processes, laboratory use for research, customers at remote areas, etc. Since the optimised system in this study has 25 years lifespan, there will be 15.6 years of pure profit, which means regaining the system cost in less than 40% of the project's lifetime.

.

Chapter 5: Conclusions and Future Work

5.1 Conclusions

This research shows technical feasibility and economic quantifiability of small-scale off-grid wind-operated decentralised hydrogen production system in Kuwait, important for transition towards energy sustainability. This study provides validation of the feasibility of green hydrogen production in one of the most challenging arid climates in the world. Foundational mathematical Excel model, dynamic TRNSYS simulations and HOMER optimisations have been integrated to compare the performance and economics of an off-grid small-scale green hydrogen production system at Kuwait Airport, Wafra, and Abdaly sites. A comprehensive techno-economic and multi-site performance framework was established. The results show that Airport site is the promising site for installation small-scale decentralised systems. The system at the Airport site significantly outperformed the system at the Wafra and Abdaly sites in both annual green hydrogen production and Levelised Cost of Hydrogen (LCOH).

The TRNSYS simulations show that the wind potential at the Airport site provide a more consistent daily green hydrogen production compared with the turbulent and low-velocity winds at the Wafra and Abdaly sites. The consistency of wind potential at the Airport site allowed the Bergey 10kW DC wind turbine to operate closer to its rated capacity, resulting in a Capacity Factor (CF) of about 28.4%, which was about 10% higher than CF at the Wafra and Abdaly sites.

The results of the Excel mathematical model show achievable high hydrogen production rate of about 2.71 kg/day for the system at the Airport site, relative to the moderate rates of 0.81 kg/day at the Wafra and Abdaly sites. The highest monthly production was 97.7 kg in June at the Airport site whereas the lowest was 0.9 kg in December at the Abdaly site. Annually, the production at the Airport site leads the other sites at 469.8 kg, followed by 100.3 kg at the Wafra site, and 71.5 kg at the Abdaly site. Therefore, the annual production at the Wafra and Abdaly sites was 20.3% and 15.2% the production at the Airport site. Compared with the Excel mathematical model results, TRNSYS dynamic simulations showed about the same annual production of about 163 kg at all sites. This was related to the constraints of storage tank capacity in TRNSYS, which stops the production process once the tank is full irrespective of wind energy availability. Compared with Excel model results, TRNSYS

underpredicted the annual production at the Airport site by 65.4% and overpredicted the production at the Wafra site by 62.7% and at the Abdaly site by 127.5%. The difference in annual production of the static (Excel) and dynamic (TRNSYS) models was related to the method of handling the intermittency penalty of wind energy in Kuwait.

The Excel model overpredicted the specific energy consumption (SEC) relative to TRNSYS at all sites. Excel overpredicted the SEC by 18.5% (64.9 kWh/kg versus 52.9 kWh/kg) at the Airport site, by 53.3% (126.1 kWh/kg versus 58.9 kWh/kg) at the Wafra site, and by about 68.5% (192.3 kWh/kg vs 60.5 kWh/kg) at the Abdaly site. At the Wafra and Abdaly sites of low wind speeds, Excel overestimated the SEC because it performs the calculations without considering the control limits and battery buffering considered by TRNSYS. Nevertheless, TRNSYS predictions at all sites (52.9 kWh/kg to 60.5 kWh/kg) are more representative of SEC of commercial electrolysers.

At all sites, the wind energy potential forced the system to operate at the efficiency cliff zone due to the low current density. At the Airport site, the average annual current density was 27.3 mA/cm^2, which was low, but the site was more productive than the other sites. At the Wafra site, the average annual current density was 12.6 mA/cm^2 so that the production rate was lower than that at the Airport site. At the Abdaly site, the average annual current density was 10.4 mA/cm^2 so that the system was hardly able to produce collectible hydrogen. But efficient operation at the Wafra and Abdaly sites would be possible by increasing the current density via hybridisation with other renewable energy resource such as PV solar panels.

The wind turbine at the Airport site, as predicted by TRNSYS, produced average annual energy of about 27 MWh, which was about 90.3% the energy production predicted by the Excel model. At the Wafra site, TRNSYS predicted average annual energy production of about 13.6 MWh, which was 127% of the Excel predictions. At the Abdaly site, the predicted average annual energy production by TRNSYS was 10.8 MWh, which was 1.24 times the Excel prediction. Although the turbine produced sufficient energy to operate the electrolyser, the State of Charge (SOC) of the tank forced the system to stop operation, which decreased the hydrogen productivity predicted by TRNSYS relative to the Excel model predictions.

TRNSYS simulations show that doubling the electrolyser surface area from 0.3 to 0.6 m^2 decreased Faraday efficiency from 92.9% to 85.5% and the overall system efficiency from 84.6% to 81.7%. Doubling the surface area degraded the system performance at the Airport

site by increasing SEC by about 40% whereas SEC was further increased by about 56% and 69% at the Wafra and Abdaly sites. The performance degradation at all sites with doubled surface area was attributed to the significant decrease of the current densities, which were already low.

To investigate the impact of storage tank volume on system performance, the volume was changed as 1.0, 2.0, 3.0, and 4.0 m^3 in TRNSYS, keeping other parameters unchanged. The results show increase of hydrogen production with the tank volume due to the reduction of the idle operation periods and the low frequency of charging/discharging cycles of the tank.

HOMER Pro sensitivity analysis was conducted using scaled daily hydrogen load of 1.0, 1.5, 2.0, and 2.5 kg/day. The analysis results show lowest LCOH ($/kg) at all sites for the scaled load of 1.5 kg/day. Thus, the system performance was optimised at a scaled hydrogen load 1.5 kg/day, and the results show annual hydrogen production of about 547 kg at SEC of about 46.4 kWh/kg. The number of wind turbine for the system at the Airport site was optimised as 2 whereas 3 turbines were optimised at the Wafra site and 5 turbines at the Abdaly site. At the Airport site, the optimised electrolyser rated capacity was 7.19 kW, which was increased to 9.95 kW and 8.13 kW respectively at the Wafra and Abdaly sites. Only 11 batteries were optimised for the system at the Airport site whereas 13 and 26 batteries were optimised at the Wafra and Abdaly sites. Small capacity storage tank (8 kg) was optimised for the system at the Airport site whereas higher capacities of 14 kg and 10 kg were optimised for the system at the Wafra and Abdaly sites.

Based on system lifetime of 25 years, the system Net Present Cost (NPC) at the Airport site was the lowest at $103,652 whereas NPC was $154,307 and $226,852 at the Wafra and Abdaly sites. The HOMER Pro optimisation confirmed that geographical location is a key determinant of the Levelised Cost of Hydrogen (LCOH). The system at the Airport site was of the lowest LCOH of $9.03/kg, which was risen by about 150% to reach 13.5 $/kg at the Wafra site. The highest LCOH was 19.9 $/kg at the Abdaly site, which was about 2.2 times the LCOH at the Airport site and 1.47 times the LCOH at the Wafra site. The notable rise of LCOH at the Wafra and Abdaly sites was due to the low wind potential, which necessitated the use of larger hydrogen storage tanks (up to 14.0 kg) compared with the 8.0 kg tank at the Airport site, to maintain reliable operation. Thus, the system at the Airport site outperformed the system at the Wafra and Abdaly sites, which confirmed the superiority of Airport site over the other sites.

The findings of the present study directly support Kuwait's Vision 2035 (New Kuwait) by proposing adoptable and practical solutions for carbon emission reduction and national energy mix diversification. Proving the feasibility of a small scale off-grid wind-operated system of scaled production 1.5 kg/day ensures that remote or strategically significant hubs can achieve energy autonomy without reliance on the national grid. Eventually, the findings of this research establish that site-specific wind-operated electrolysis is not a theoretical concept but a high-performance and scalable solution ready to drive toward a cleaner and more resilient industrial future in Kuwait.

5.2 Contributions to Knowledge

The key novelty of this research lies in proving that bigger is not always the only way by showing how a 1.5 kg/day hydrogen production system can be technically and economically mapped across specific geography (Airport vs. Wafra vs. Abdaly) in Kuwait. While massive green hydrogen production projects are common in literature, this research provides the first technical outline for a decentralised small-scale system tailored to the unique environmental and geographical constraints in Kuwait.

This research provides the first comprehensive techno-economic analysis for a small-scale off-grid wind-operated system of 1.5 kg/day scaled hydrogen production in Kuwait. It is expected to shift the academic concentration from large-scale export models to decentralised systems essential for decarbonisation of different industrial and transportation sectors. This research offers a pioneering small-scale hydrogen production system for arid regions.

By comparing the Airport, Wafra, and Abdaly sites, this study identifies significant regional performance gaps. It establishes that wind profiles at the Airport site offer superior feasibility over other remote sites such as Wafra and Abdaly, which offers a strategic site-selection roadmap for policymakers in Kuwait.

The present study introduces a unique tri-modelling approach by linking foundational Excel mathematical models with dynamic TRNSYS simulations and HOMER Pro economic optimisation. The use of tri-modelling approach creates high reliability justification for the off-grid wind-operated alkaline water electrolysers in regions of harsh weather. Although the tri-modelling approach was worth considering, there were several limitations implicit in the Excel model compared to the TRYSYS model. The difference between the static modeling (Excel) and dynamic (TRNSYS) is mainly due to the modeling method adopted by TRNSYS

developers. In this study, TRNSYS simulation was conducted on hourly basis. Meanwhile, excel model calculations were conducted for each month using a monthly average wind speed. The Excel model can therefore be refined to perform the calculations on hourly basis to ease comparison with TRNSYS in a future work.

Eventually, this work establishes a baseline Levelised Cost of Hydrogen (LCOH) for strictly decentralised off-grid wind-operated hydrogen production systems in Kuwait. This work also quantifies the economic penalty of intermittency at a small-scale to provide a realistic financial target for future small investments.

5.3 Recommendations

5.3.1 Recommendations for Future Research

To ensure that this research remains one of the cornerstones for future energy transition in Kuwait, future research should focus on how the small-scale wind-operated off-grid design can evolve. Therefore, it is recommended for future research to:

- Investigate the feasibility of alkaline electrolysers to scale production from 1.5 kg/day upwards to match the needs of more applications. This may involve assessing whether the economies of system scale can reduce the LCOH compared with small-scale baseline established in this research.
- Study the feasibility of off-grid wind/solar hybrid systems, as this study focused on a strict off-grid wind-operated system. Integrating photovoltaic (PV) solar panels could potentially support hydrogen production during low-wind periods in Kuwait, reducing the reliance on large-scale hydrogen storage tanks. HOMER Pro can be used to identify the perfect ratio of wind to solar capacity at each site. For example, while the Airport site may remain wind-dominant, the Wafra and Abdaly sites might achieve low hydrogen production costs through large capacity solar arrays. During summer daylight hours of calm winds, solar arrays can generate more electrical power to operate the electrolyser which may lower the LCOH. The solar radiation intensity in Kuwait makes wind/solar integration a strategic pathway for lowering the LCOH by overcoming the limitations of off-grid wind-operated systems.
- Conduct a comparative study model a grid-tied version of the system at the Airport site to determine whether the use of grid power as a backup can further enhances the financial feasibility of the system.

- Simulate a linked network (clusters) of small-scale off-grid wind-operated production systems based on the findings of the multi-site analysis (Airport, Wafra, Abdaly) of this study. This may involve load-sharing models between the neighbouring sites in which surplus hydrogen production at a specific site can be shared to compensate for deficits at other sites, to ensure enhanced reliability of hydrogen supply network.

5.3.2 Recommendations for Kuwaiti Government

Based on the results and conclusions of this study, it is recommended for the governmental bodies in Kuwait to:

- Translate the technical findings of the present study into actionable steps by developing a hydrogen zoning map. Such a map is essential for guiding the investors and developers toward the sites of promising hydrogen production potential. It is important therefore to adopt flexible policies to permit off-grid wind-operated systems at minimal bureaucratic hinders and allocate funds and land for such projects.
- Encourage investments at the sites of favourable wind profiles such as the Airport site, as evident in this study, to ensure consistent green hydrogen production of small-scale off-grid wind-operated systems.
- Implement green hydrogen subsidies to encourage investors to employ these systems at remote areas of costly electricity grid extension but have sufficient wind potential. This may offset the high LCOH of the small-scale off-grid wind-operated systems.

References

Abdelgwad, M.H., Bahnasawy, A.H. and Khater, E.G. (2025). Effect of alkaline water level and electrode surface area on the hydrogen production rate as renewable energy source using electrolysis system. *Benha Journal of Applied Sciences (BJAS)*, Vol. 10, No. 3, pp. 95-105.

Abdelhaleem, A., Kuroda, Y., Kawakami, N., Souda, M., et al. (2024). Exploring the Performance of Alkaline Water Electrolyzers Under Dynamic Operational Conditions. *ECS Meeting Abstracts*, Vol. MA2024-01, Article: 1820.

Abdin, Z. and Merida, W. (2019). Hybrid energy systems for off-grid power supply and hydrogen production based on renewable energy: a techno-economic analysis. *Energy Conversion and Management*, Vol. 196, pp. 1068-1079.

Abdolmaleki, L. and Berardi, U. (2023). Dynamic simulation of a hydrogen-fueled system for zero-energy buildings using TRNSYS software. *E3S Web of Conferences*, Vol. 396, Article: 04005.

Adedoja, O.S., Sadiku, E.R. and Hamam, Y. (2024). A techno-economic assessment of the viability of a photovoltaic-wind-battery storage-hydrogen energy system for electrifying primary healthcare centre in Sub-Saharan Africa. *Energy Conversion and Management*, Vol. X23, Article: 100643.

Ajanovic, A., Sayer, M. and Haas, R. (2022). The economics and the environmental benignity of different colors of hydrogen. *International Journal of Hydrogen Energy*, Vol. 47, No. 57, pp. 24136-24154.

Akarsu, B. and Genc, M.S. (2022). Optimization of electricity and hydrogen production with hybrid renewable energy systems. *Fuel*, Vol. 324, Article: 124465.

Akdag, O. (2025). Modeling and economic evaluation of hybrid renewable energy sources for Green hydrogen production: a case study for the Mediterranean region. *Renewable Energy*, Vol. 240, Article: 122228.

Akpasi, S.O., Anekwe, I.M.S., Tetteh, E.K., Amune, U.O., et al. (2025). Hydrogen as a clean energy carrier: advancements, challenges, and its role in a sustainable energy future. *Clean Energy*, Vol. 9, No. 1, pp. 52-88.

Aktekin, M., Genc, M.S., Azgın, S.T. and Genc, G. (2024). Assessment of techno-economic analyses of grid-connected nuclear and PV/wind/battery/hydrogen renewable hybrid system for sustainable and clean energy production in Mersin-Türkiye. *Process Safety and Environmental Protection*, Vol. 190, pp. 340-353.

Al Dhahri, H., Hussain, M., Ghani, M.A.A., Inayat, A., et al. (2026). Green hydrogen production via electrolysis: Materials innovation, system integration, and global deployment pathways. *Renewable and Sustainable Energy Reviews*, Vol. 229, Article: 116617.

Al Saadi, K. and Ghosh, A. (2024). Investigating the integration of floating photovoltaics (FPV) technology with hydrogen (H2) energy for electricity production for domestic application in Oman. *International Journal of Hydrogen Energy*, Vol. 80, pp. 1151-1163.

Al-Abdullah, Y.M., Al-Qattan, Y.S., Sreekanth, K.J. and Alsayegh, O. (2025). Evaluating the energy transition for Kuwait: Modeling Kuwait's energy future and decarbonization challenges. *Energy and Climate Change*, Vol. 6, Article: 100189.

Al-Abdullah, Y.M., Al-Saffar, M., Al-Yakoob, A. and Sahraei-Ardakani, M. (2023). Impacts of Kuwait's proposed renewable energy goals on grid operations. *International Journal of Sustainable Energy*, Vol. 42, No. 1, pp. 776-792.

Alawadhi, E.M. (2023). The potential of wind energy in Kuwait: a complete feasibility investigation. *Journal of Engineering Research*, Vol. 11, No. 1, Part B, pp. 349-361.

Al-Badi, A., Al Wahaibi, A., Ahshan, R. and Malik, A. (2022). Techno-economic feasibility of a solar-wind-fuel cell energy system in Duqm, Oman. *Energies*, Vol. 15, No. 15, Article: 5379.

Al-Douri, A. and Groth, K.M. (2024). Hydrogen production via electrolysis: State-of-the-art and research needs in risk and reliability analysis. *International Journal of Hydrogen Energy*, Vol. 63, pp. 775-785.

Algburi, S., Munther, H., Al-Dulaimi, O., Fakhruldeen, H.F., et al. (2025). Green Hydrogen Role in Sustainable Energy Transformations: A Review. *Results in Engineering*, Vol. 26, Article: 105109.

Al-Ghussain, L., Ahmad, A.D., Abubaker, A.M., Hovi, K., et al. (2023). Techno-economic feasibility of hybrid PV/wind/battery/thermal storage trigeneration system: toward 100% energy independency and Green hydrogen production. *Energy Reports*, Vol. 9, 752-772.

Alhajeri, A., Ghazal, H., Olabi, V. and Jouhara, H. (2025). Technical assessment of green hydrogen production in Kuwait. *International Journal of Hydrogen Energy*, Vol. 144, pp. 924-931.

Allebrod, F. (2013). *High Temperature and Pressure Alkaline Electrolysis*. Department of Energy Conversion and Storage, Technical University of Denmark.

Al-Orabi, A.M., Osman, M.G. and Sedhom, B.E. (2023). Evaluation of green hydrogen production using solar, wind, and hybrid technologies under various technical and financial scenarios for multi-sites in Egypt. *International Journal of Hydrogen Energy*, Vol. 48, pp. 38535-38556.

AlRafea, K., Fowler, M., Elkamel, A. and Hajimiragha, A. (2016). Integration of renewable energy sources into combined cycle power plants through electrolysis generated hydrogen in a new designed energy hub. *International Journal of Hydrogen Energy*, Vol. 41, No. 38, pp. 16718-16728.

Al-Rbaihat, R. (2025). Sensitivity Analysis of a Hybrid PV-WT Hydrogen Production System via an Electrolyzer and Fuel Cell Using TRNSYS in Coastal Regions: A Case Study in Perth, Australia. *Energies*, Vol. 18, Article: 3108.

Alsaffar, M., Ardakani, M. and Al-Abdullah, Y.M. (2025). Analyzing decarbonization policies targeting interdependent electric power and water desalination infrastructure: A case study for Kuwait. *Energy for Sustainable Development*, Vol. 86, Article: 101715.

Alsayegh, O.A. (2021). Barriers facing the transition toward sustainable energy system in Kuwait. *Energy Strategy Reviews*, Vol. 38, Article: 100779.

Al-Sharafi, A., Sahin, A.Z., Ayar, T. and Yilbas, B.S. (2017). Techno-economic analysis and optimization of solar and wind energy systems for power generation and hydrogen production in Saudi Arabia. *Renewable and Sustainable Energy Reviews*, Vol. 69, pp. 33-49.

Ansari, S.A., Alam, M.W., Dhanda, N., Abbasi, M.S., et al. (2025). Sustainable Hydrogen Production, a Review of Methods, Types, Applications, Challenges, and Future Perspectives. *Global Challenges*, Vol. 9, Article: 2500086.

Arcos, J.M.M. and Santos, D.M.F. (2023). The Hydrogen Color Spectrum: Techno-Economic Analysis of the Available Technologies for Hydrogen Production. *Gases*, Vol. 3, No. 1, pp. 25-46.

Arpino, F., Canale, C., Cortellessa, G., Dell'Isola, M., et al. (2024). Green hydrogen for energy storage and natural gas system decarbonization: An Italian case study. *International Journal of Hydrogen Energy*, Vol. 49, Part D, pp. 586-600.

Ashraf, S., Kawai, E., Mae, M. and Matsuhashi, R. (2025). Advancing electrochemical modelling of PEM electrolyzers through robust parameter estimation with the weighted mean of vectors algorithm. *Multiscale and Multidisciplinary Modeling, Experiments and Design*, Vol. 8, Article: 397.

Awad, M., Said, A., Saad, M.H., Farouk, A., et al. (2024). A review of water electrolysis for green hydrogen generation considering PV/wind/hybrid/hydropower/geothermal/tidal and wave/biogas energy systems, economic analysis, and its application. *Alexandria Engineering Journal*, Vol. 87, pp. 213-239.

Bhuiyan, M.M.H. and Siddique, Z. (2025). Hydrogen as an alternative fuel: A comprehensive review of challenges and opportunities in production, storage, and transportation. *International Journal of Hydrogen Energy*, Vol. 102, pp. 1026-1044.

Bora, D.K. (2025). Green Hydrogen Production with 25 kW Alkaline Electrolyzer Pilot Plant Shows Hydrogen Flow Rate Exponential Asymptotic Behavior with the Stack Current. *Hydrogen*, Vol. 6, No. 4, Article: 75.

Brauns, J. and Turek, T. (2020). Alkaline Water Electrolysis Powered by Renewable Energy: A Review. *Processes*, Vol. 8, Article: 248.

Brauns, J., Schonebeck, J., Kraglund, M.R., Aili, D., et al. (2021). Evaluation of Diaphragms and Membranes as Separators for Alkaline Water Electrolysis. *Journal of The Electrochemical Society*, Vol. 168, Article: 014510.

Cai, Z. (2025). Feasibility of Hydrogen Energy for High-Power Aerospace Applications: A Comprehensive Assessment. *E3S Web of Conferences*, Vol. 606, Article: 01005.

Caponi, R., Bocci, E. and Del Zotto, L. (2025). On-site hydrogen refuelling station techno-economic model for a fleet of fuel cell buses. *International Journal of Hydrogen Energy*, Vol. 71, pp. 691-700.

Carmo, M. and Stolten, D. (2018). Energy Storage Using Hydrogen Produced From Excess Renewable Electricity: Power to Hydrogen. In: de Miranda, P.E.V. (Ed.), *Science and Engineering of Hydrogen-Based Energy Technologies: Hydrogen Production and Practical Applications in Energy Generation*, pp. 165-199, Academic Press, Elsevier Inc., ISBN: 978-0-12-814251-6.

Chen, Y., Liu, J. and Feng, L. (2022). Transient analysis of a green hydrogen production and storage system using Alkaline electrolyzer. *Fuel*, Vol. 324, Article: 124752.

Criollo, A., Minchala-Avila, L.I., Benavides, D., Ochoa-Correa, D., et al. (2024). Green Hydrogen Production—Fidelity in Simulation Models for Technical–Economic Analysis. *Applied Sciences*, Vol. 14, No. 22, Article: 10720.

Daoudi, C. and Bounahmidi, T. (2024). Overview of alkaline water electrolysis modeling. *International Journal of Hydrogen Energy*, Vol. 49, No. Part C, pp. 646-667.

Dash, S.K., Chakraborty, S. and Elangovan, D. (2023). A Brief Review of Hydrogen Production Methods and Their Challenges. *Energies*, Vol. 16, No. 3, Article: 1141.

Dawood, F., Martin, A. and Shafiullah, G.M. (2020). Hydrogen production for energy: An overview. *International Journal of Hydrogen Energy*, Vol. 45, No. 7, pp. 3847-3869.

Demnitz, M., van der Schaaf, J. and de Groot, M.T. (2025). Alkaline Water Electrolysis Beyond 3 A/cm^2 Using Catalyst Coated Diaphragms. *Journal of The Electrochemical Society*, Vol. 172, Article: 014504.

Demnitz, M., van Kessel, D.W., Chpilevski, K., van der Schaaf, J., et al. (2024). Catalyst coated diaphragms for enhanced alkaline water electrolysis. *International Journal of Hydrogen Energy*, Vol. 90, pp. 792-802.

Dezhdar, A., Assareh, E., Agarwal, N., bedakhanian, A., et al. (2023). Transient optimization of a new solar-wind multi-generation system for hydrogen production, desalination, clean electricity, heating, cooling, and energy storage using TRNSYS. *Renewable Energy*, Vol. 208, pp. 512-537.

Dincer, H., Yuksel, S. and Senel, S. (2018). Analyzing the global risks for the financial crisis after the great depression using comparative hybrid hesitant fuzzy decision-making models: Policy recommendations for sustainable economic growth. *Sustainability*, Vol. 10, No. 9, Article: 3126.

Dincer, I. (2000). Renewable energy and sustainable development: a crucial review. *Renewable and sustainable Energy Reviews*, Vol. 4, No. 2, pp. 157-175.

Dincer, I., Rosen, M.A. and Ahmadi, P. (2017). *Optimization of Energy Systems*. John Wiley and Sons, ISBN: 978-1118894439.

Ding, N., Wu, W., Wang, L. and Yin, H. (2024). Application of nanomaterial based alkaline electrolyzer for hydrogen production in renewable energy-driven system: multi-criteria assessment, environmental and exergoeconomic approaches. *International Journal of Hydrogen Energy*, Vol. 52, Part C, pp. 485-504.

Duffie, J.A. and Beckman, W.A. (2013). *Solar Engineering of Thermal Processes*. New York: John Wiley & Sons Inc., ISBN: 9780470873663.

Ehlers, J.C., Feidenhans, A.A., Therkildsen, K.T. and Larrazábal, G.O. (2023). Affordable Green Hydrogen from Alkaline Water Electrolysis: Key Research Needs from an Industrial Perspective. *ACS Energy Letter*, Vol. 8, pp. 1502-1509.

Elegbeleye, I., Oguntona, O. and Elegbeleye, F. (2025). Green Hydrogen: Pathway to Net Zero Green House Gas Emission and Global Climate Change Mitigation. *Hydrogen*, Vol. 6, Article: 29.

Elminshawy, N.A.S., Diab, S., Yassen, Y.El.S. and Elbaksawi, O. (2024). An energy-economic analysis of a hybrid PV/wind/battery energy-driven hydrogen generation system in rural regions of Egypt. *Journal of Energy Storage*, Vol. 80, Article: 110256.

El-Shafie, M. (2023). Hydrogen production by water electrolysis technologies: A review. *Results in Engineering*, Vol. 20, Article: 101426.

Ete, A., Hoffheinz, G., Kelly, N. and Ulleberg, Ø. (2008). Hydrogen energy systems: development and application of modelling tools. In: *10th World Renewable Energy Congress*, 2008-07-19-2008-07-25.

Fan, J., Meng, X., Tian, J., Xing, C., et al. (2023). A review of transportation carbon emissions research using bibliometric analyses. *Journal of Traffic and Transportation Engineering (English Edition)*, Vol. 10, No. 5, pp. 878-899.

Faraz, M.I. (2024). Strategic analysis of wind energy potential and optimal turbine selection in Al-Jouf, Saudi Arabia. *Heliyon*, Vol. 10, No. 20, Article: e39188.

Ferrer, A.L.C. and Thome, A.M.T. (2023). Carbon Emissions in Transportation: A Synthesis Framework. *Sustainability*, Vol. 15, No. 11, Article: 8475.

Ferrero, D., Mansourkiaei, M., Trapani, D., Consoli, D., et al. (2025). Performance evaluation and durability assessment of hybrid alkaline/membrane electrolysis cell designs. *Journal of Power Sources*, Vol. 658, Article: 238239.

Fragiacomo, P. and Genovese, M. (2020). Numerical simulations of the energy performance of a PEM water electrolysis based high-pressure hydrogen refuelling station. *International Journal of Hydrogen Energy*, Vol. 45, No. 51, pp. 27457-27470.

Franco, A. and Giovannini, C. (2023). Recent and Future Advances in Water Electrolysis for Green Hydrogen Generation: Critical Analysis and Perspectives. *Sustainability*, Vol. 15, No. 24, Article: 16917.

Franco, A. and Giovannini, C. (2024). Hydrogen Gas Compression for Efficient Storage: Balancing Energy and Increasing Density. *Hydrogen*, Vol. 5, No. 2, pp. 293-311.

Franco, A., Carcasci, C., Ademollo, A., Calabrese, M., et al. (2025). Integrated Plant Design for Green Hydrogen Production and Power Generation in Photovoltaic Systems: Balancing Electrolyzer Sizing and Storage. *Hydrogen*, Vol. 6, No. 1, Article: 7.

Gambou, F., Guilbert, D., Zasadzinski, M. and Rafaralahy, H. (2022). A Comprehensive Survey of Alkaline Electrolyzer Modeling: Electrical Domain and Specific Electrolyte Conductivity. *Energies*, Vol. 15, No. 9, Article: 3452.

Gebremariam, G.K., Jovanovic, A.Z. and Pasti, I.A. (2023). The Effect of Electrolytes on the Kinetics of the Hydrogen Evolution Reaction. *Hydrogen*, Vol. 4, No. 4, pp. 776-806.

Geotab Team (2024). *Replacing gas cars with electric could save more than 40 tons of CO2 emissions per car, replacing gas cars with electric vehicles can result in a dramatic reduction of CO2 emissions.* [Online] Accessed on 15/02/2024, available at: https://www.geotab.com/uk/blog/replacing-gas-cars/

Goel, S. and Sharma, R. (2026). Green hydrogen production from hybrid renewable energy systems: a techno-economic analysis in Rural India. *International Journal of Sustainable Energy*, Vol. 45, No. 1, Article: 2630464.

Gokcek, M. and Kale, C. (2018). Techno-economical evaluation of a hydrogen refuelling station powered by Wind-PV hybrid power system: a case study for İzmir-Çeşme. *International Journal of Hydrogen Energy*, Vol. 43, pp. 10615-10625.

Goswami, D.Y. (2015). *Principles of Solar Engineering*. Third Edition, CRC Press, Taylor & Francis Group.

Groppi, D., Garcia, D.A., Basso, G.L., Cumo, F., et al. (2018). Analysing economic and environmental sustainability related to the use of battery and hydrogen energy storages for increasing the energy independence of small islands. *Energy Conversion and Management*, Vol. 177, pp. 64-76.

Guven, D. (2024). Offshore wind-driven green hydrogen: bridging environmental sustainability and economic viability. *International Journal of Hydrogen Energy*, Vol. 72, pp. 661-676.

Haddad, M. and Javani, N. (2024). Transient analysis of a near-zero energy building with green hydrogen production integrated with energy storage systems. *Journal of Building Engineering*, Vol. 96, Article: 110541.

Haddad, M. and Javani, N. (2025). Dynamic analysis of green hydrogen production integrated with storage tanks: An economical assessment for different demands. *International Journal of Hydrogen Energy*, Vol. 140, pp. 126-1139.

Haholu, O., Duman, A.C. and Guler, O. (2025). Techno-economic analysis of off-grid residential hybrid renewable energy systems utilizing excess energy for small-scale green hydrogen production. *Process Safety and Environmental Protection*, Vol. 200, Article: 107422.

Hai, T., Ali, M.A., Dhahad, H.A., Alizadeh, A., Sharma, A., et al. (2023). Optimal design and transient simulation next to environmental consideration of net-zero energy buildings with green hydrogen production and energy storage system. *Fuel*, Vol. 336, Article: 127126.

Hamdi, M. and El Alimi, S. (2025). Performance analysis of a photovoltaic-driven hydrogen electrolyzer system for sustainable ammonia production: Seasonal and regional assessment. *Energy Conversion and Management*, Vol. 326, Article: 119538.

Hamed, H., AlEssa, A., AlKhorafi, M., AlDakheel, A., et al. (2026). Integrating renewable energy in Sabah Al-Ahmad City: A techno-economic and environmental analysis. *Journal of Engineering Research*, Vol. 14, No. 1, pp. 1029-1038.

Hamedani, E.A., Alenabi, S.A. and Talebi, S. (2024). Hydrogen as an energy source: A review of production technologies and challenges of fuel cell vehicles. *Energy Reports*, Vol. 12, pp. 3778-3794.

Haoran, C., Xia, Y., Wei, W., Yongzhi, Z., et al. (2024). Safety and efficiency problems of hydrogen production from alkaline water electrolyzers driven by renewable energy sources. *International Journal of Hydrogen Energy*, Vol. 54, pp. 700-712.

Hassan, Q., Abdulrahman, I.S., Salman, H.M., Olapade, O.T., et al. (2023). Techno-Economic assessment of green hydrogen production by an Off-Grid photovoltaic energy system. *Energies*, Vol. 16, No. 2, Article: 744.

Henkensmeier, D., Cho, W-C., Jannasch, P., Stojadinovic, J., et al. (2024). Separators and Membranes for Advanced Alkaline Water Electrolysis. *Chemical Reviews*, Vol. 124, No. 10, pp. 6393-6443.

Hermesmann, M. and Muller, T.E. (2022). Green, turquoise, blue, or grey? Environmentally friendly hydrogen production in transforming energy systems. *Progress in Energy and Combustion Science*, Vol. 90, Article: 100996.

HOMER ENERGY (2015). *HOMER2 2.8 Help Manual*. [Online] Accessed on 08/08/2025, available at: https://www.homerenergy.com/pdf/HOMER2_2.8_HelpManual.pdf

Hong, W-P. (2013). Modeling of Solar/Hydrogen/DEGS Hybrid System for Stand Alone Applications of a Large Store. *Journal of the Korean Institute of Illuminating and Electrical Installation Engineers*, Vol. 27, No. 11, pp. 57−68.

Hosseini, T., Tabatabaei-Zavareh, M., Smart, S. and Ashman, P.J. (2024). Low-emission hydrogen production from gasification of Australian coals – Process simulation and technoeconomic assessment. *International Journal of Hydrogen Energy*, Vol. 86, pp. 245-260.

Hou, J. and Yang, M. (2025). *Green Hydrogen Production by Water Electrolysis*. CRC Press, ISBN: 978-1-032-43807-8.

Hu, S., Guo, B., Ding, S., Yang, F., et al. (2022). A comprehensive review of alkaline water electrolysis mathematical modeling. *Applied Energy*, Vol. 327, Article: 120099.

Huang, C., Torres, J.L.R., Zong, Y., You, S., et al. (2025). A review of alkaline electrolyzer technology modeling and applications for decision-making optimization in energy systems. *Renewable and Sustainable Energy Reviews*, Vol. 224, Article: 116005.

Hug, W., Bussmann, H. and Brinner, A. (1993). Intermittent operation and operation modeling of an alkaline electrolyzer. *International Journal of Hydrogen Energy*, Vol. 18, No. 12, pp. 973-977.

Hug, W., Divisek, J., Mergel, J., Seeger, W., et al. (1992). Highly efficient advanced alkaline electrolyzer for solar operation. *International Journal of Hydrogen Energy*, Vol. 17, No. 9, pp. 699-705.

Hussam, W.K., Barhoumi, E.M., Abdul-Niby, M. and Sheard, G.J. (2024). Techno-economic analysis and optimization of hydrogen production from renewable hybrid energy systems: Shagaya renewable power plant-Kuwait. *International Journal of Hydrogen Energy*, Vol. 58, pp. 56-68.

Ibrahim, M.M. (2025). Techno-Economic Study of Producing Green Hydrogen with Stand-Alone Hybrid Renewable Energy System: A Case Study in Egypt. *Case Studies in the Environment*, Vol. 9, No. 1, Article: 2702538.

IRENA (2020). *Green Hydrogen Cost Reduction: Scaling Up Electrolysers to Meet the 1.5 ℃ Climate Goal*. Abu Dhabi, UAE: International Renewable Energy Agency, ISBN: 978-92-9260-295-6.

Ishaq, H., Dincer, I. and Naterer, G.F. (2018). Development and assessment of a solar, wind and hydrogen hybrid trigeneration system. *International Journal of Hydrogen Energy*, Vol. 43, pp. 23148-23160.

Izadi, A., Shahafve, M. and Ahmadi, P. (2022). Neural network genetic algorithm optimization of a transient hybrid renewable energy system with solar/wind and hydrogen storage system for zero energy buildings at various climate conditions. *Energy Conversion and Management*, Vol. 260, Article: 115593.

Izadi, A., Shahafve, M., Ahmadi, P. and Javani, N. (2022). Transient simulation and techno-economic assessment of a near-zero energy building using a hydrogen storage system and different backup fuels. *International Journal of Hydrogen Energy*, Vol. 47, No. 74, pp. 31927-31940.

Jang, D., Cho, H-S., Lee, S., Park, M., et al. (2023). Investigation of the operation characteristics and optimization of an alkaline water electrolysis system at high temperature and a high current density. *Journal of Cleaner Production*, Vol. 424, Article: 138862.

Jarvinen, L., Puranen, P., Kosonen, A., Ruuskanen, V., et al. (2022). Automized parametrization of PEM and alkaline water electrolyzer polarisation curves. *International Journal of Hydrogen Energy*, Vol. 47, No. 75, pp. 31985-32003.

Jeje, S.O., Marazani, T., Obiko, J.O. and Shongwe, M.B. (2024). Advancing the hydrogen production economy: A comprehensive review of technologies, sustainability, and future prospects. *International Journal of Hydrogen Energy*, Vol. 78, pp. 642-661.

Jiao, F., Chen, C., Liu, T., Lu, B., et al. (2024). Insights of water-to-hydrogen conversion from thermodynamics. *The Innovation Energy*, Vol. 1, No. 1, Article: 100004.

Kalinci, Y., Hepbasli, A. and Dincer, I. (2015). Techno-economic analysis of a stand-alone hybrid renewable energy system with hydrogen production and storage options. *International Journal of Hydrogen Energy*, Vol. 40, pp. 7652-7664.

Kamel, R.M., El Badawi, M. and Alanzi, S.Sh. (2024). An optimum design and economic feasibility analysis of wind farms in Kuwait using different wind generation technologies. *Journal of Engineering Research*, Vol. 12, No. 4, pp. 840-858.

Khajah. A.M.H.A. and Philbin, S.P. (2022). Techno-Economic Analysis and Modelling of the Feasibility of Wind Energy in Kuwait. *Clean Technolies*, Vol. 4, No. 1, pp. 14-34.

Khezzar, R., Zereg, M. and Khezzar, A. (2014). Modeling improvement of the four-parameter model for photovoltaic modules. *Solar Energy*, Vol. 110, pp. 452-462.

Krishnan, S., Koning, V., de Groot, M.T., de Groot, A., et al. (2023). Present and future cost of alkaline and PEM electrolyser stacks. *International Journal of Hydrogen Energy*, Vol. 48, No. 83, pp. 32313-32330.

Kumar, S.S. and Himabindu, V. (2019). Hydrogen production by PEM water electrolysis – A review. *Materials Science for Energy Technologies*, Vol. 2, No. 3, pp. 442-454.

Kumar, S.S. and Lim, H. (2022). An overview of water electrolysis technologies for green hydrogen production. *Energy Reports*, Vol. 8, pp. 13793-13813.

Kuwait Solar News (2026). *Kuwait carbon neutrality: Impressive 2060 target unveiled*. [Online] Visited 25/02/2026, available at: https://www.pvknowhow.com/news/kuwait-carbon-neutrality-impressive-2060-target-unveiled/

Lebepe, M.C., Oviroh, P.O. and Jen, T-C. (2025). Techno-economic optimisation modelling of a solar-powered hydrogen production system for green hydrogen generation. *Sustainable Energy Research*, Vol. 12, Article: 11.

Leon, M., Silva, J., Ortiz-Soto, R. and Carrasco, S. (2023). A Techno-Economic Study for Off-Grid Green Hydrogen Production Plants: The Case of Chile. *Energies*, Vol. 16, No. 14, Article: 5327.

Luo, S., Zhang, T., Xu, H., Zhang, J., et al. (2024). Optimizing Alkaline Water Electrolysis: A Dual-Model Approach for Enhanced Hydrogen Production Efficiency. *Energies*, Vol. 17, Article: 5512.

Madila, E.E.N., Makhsoos, A., Shanbhag, M.M. and Pollet, B.G. (2025). Advancements in electrolyser stack performance: A comprehensive review of Latest technologies and efficiency strategies. *International Journal of Hydrogen Energy*, Vol. 144, pp. 1168-1189.

Maestre, V.M., Ortiz, A. and Ortiz, I. (2024). Sustainable and self-sufficient social home through a combined PV-hydrogen pilot. *Applied Energy*, Vol. 363, Article: 123061.

Maka, A.O.M. and Mehmood, M. (2024). Green hydrogen energy production: current status and potential. *Clean Energy*, Vol. 8, No. 2, pp. 1-7.

Mansir, I.B., Hani, E.H.B., Farouk, N., AlArjani, A., et al. (2022). Comparative transient simulation of a renewable energy system with hydrogen and battery energy storage for residential applications. *International Journal of Hydrogen Energy*, Vol. 47, No. 62, pp. 26198-26208.

Marino, C., Nucara, A., Panzera, M.F., Pietrafesa, M., et al. (2019). Energetic and economic analysis of a standalone photovoltaic system with hydrogen storage. *Renewable Energy*, Vol. 142, Article: 316-329.

Marocco, P., Ferrero, D., Lanzini, A. and Santarelli, M. (2022). The role of hydrogen in the optimal design of off-grid hybrid renewable energy systems. *Journal of Energy Storage*, Vol. 46, Article: 103893.

Martino, M., Ruocco, C., Meloni, E., Pullumbi, P., et al. (2021). Main Hydrogen Production Processes: An Overview. *Catalysts*, Vol. 11, No. 5, Article: 547.

Massarweh, O., Al-khuzaei, M., Al-Shafi, M., Bicer, Y., et al. (2023). Blue hydrogen production from natural gas reservoirs: A review of application and feasibility. *Journal of CO2 Utilization*, Vol. 70, Article: 102438.

Mazzeo, D., Herdem, M.S., Matera, N. and Wen, J.Z. (2022). Green hydrogen production: Analysis for different single or combined large-scale photovoltaic and wind renewable systems. *Renewable Energy*, Vol. 200, pp. 360-378.

Milani, D., Ali, K. and Robbie, M.N. (2020). Renewable-powered hydrogen economy from Australia's perspective. *International Journal of Hydrogen Energy*, Vol. 45, pp. 24125-24145.

Mohsen, F.M., Mjbel, H.M., Challoob, A.F., Alkhazaleh, R., et al. (2026). Advancements in green hydrogen production: A comprehensive review of prospects, challenges, and innovations in electrolyzer technologies. *Fuel*, Vol. 404, Article: 136251.

Mosca, L., Jimenez, J.A.M., Wassie, S.A., Gallucci, F., et al. (2020). Process design for green hydrogen production. *International Journal of Hydrogen Energy*, Vol. 45, No. 12, pp. 7266-7277.

Mostafaeipour, A., Khayyami, M., Sedaghat, A., Mohammadi, K., Shamshirband, S., Sehati, M-A. and Gorakifard, E. (2016). Evaluating the wind energy potential for hydrogen production: A case study. *International Journal of Hydrogen Energy*, Vol. 41, No. 15, pp. 6200-6210.

Mucci, S., Mitsos, A. and Bongartz, D. (2023). Power-to-X processes based on PEM water electrolyzers: A review of process integration and flexible operation. *Computers & Chemical Engineering*, Vol. 175, Article: 108260.

Mukelabai, M.D., Barbour, E.R. and Blanchard, R.E. (2024). Modeling and optimization of renewable hydrogen systems: A systematic methodological review and machine learning integration. *Energy and AI*, Vol. 18, Article: 100455.

Muller, V.P. and Eichhammer, W. (2023). Economic complexity of green hydrogen production technologies - a trade data-based analysis of country-specific industrial preconditions. *Renewable and Sustainable Energy Reviews*, Vol. 182, Article: 113304.

Munther, H., Hassan, Q., Khadom, A.A. and Mahood, H.B. (2025). Evaluating the techno-economic potential of large-scale green hydrogen production via solar, wind, and hybrid

energy systems utilizing PEM and alkaline electrolyzers. *Unconventional Resources*, Vol. 5, Article: 100122.

Muthiah, M., Elnashar, M., Afzal, W. and Tan, H. (2024). Safety assessment of hydrogen production using alkaline water electrolysis. *International Journal of Hydrogen Energy*, Vol. 84, pp. 803-821.

Nasser, M., Megahed, T.F., Ookawara, S. and Hassan H. (2022b). Techno-economic assessment of clean hydrogen production and storage using hybrid renewable energy system of PV/Wind under different climatic conditions. *Sustainable Energy Technologies and Assessments*, Vol. 52, Part B, Article: 102195.

Nasser, M., Megahed, T.F., Ookawara, S. and Hassan, H. (2022a). A review of water electrolysis–based systems for hydrogen production using hybrid/solar/wind energy systems. *Environmental Science and Pollution Research*, Vol. 29, pp. 86994-87018.

Nguyen, E., Olivier, P., Pera, M-C., Pahon, E., et al. (2024). Impacts of intermittency on low-temperature electrolysis technologies: A comprehensive review. *International Journal of Hydrogen Energy*, Vol. 70, pp. 474-492.

Niblett, D., Delpisheh, M., Ramakrishnan, S. and Mamlouk, M. (2024). Review of next generation hydrogen production from offshore wind using water electrolysis. *Journal of Power Sources*, Vol. 592, Article: 233904.

Nnabuife, S.G., Hamzat, A.K., Whidborne, J., Kuang, B., et al. (2025). Integration of renewable energy sources in tandem with electrolysis: A technology review for green hydrogen production. *International Journal of Hydrogen Energy*, Vol. 107, pp. 218-240.

Nnabuife, S.G., Quainoo, K.A., Hamzat, A.K., Darko, C.K., et al. (2024). Innovative strategies for combining solar and wind energy with green hydrogen systems. *Applied Sciences*, Vol. 14, No. 21, Article: 9771.

Nnabuife, S.G., Ugbeh-Johnson, J., Okeke, N.E. and Ogbonnaya, C. (2022). Present and Projected Developments in Hydrogen Production: A Technological Review. *Carbon Capture Science & Technology*, Vol. 3, Article: 100042.

Okonkwo, P.C., Nwokolo, S.C., Barhoumi, E., Mansir, I.B., et al. (2025). Technical and economic feasibility assessment for hybrid energy system electricity and hydrogen generation: A case study. *Global Energy Interconnection*, Vol. 8, pp. 62-81.

Okundamiya, M.S. (2021). Size optimization of a hybrid photovoltaic/fuel cell grid connected power system including hydrogen storage. *International Journal of Hydrogen Energy*, Vol. 46, No. 59, pp. 30539-30546.

Olabi, V. and Jouhara, H. (2024). An assessment of current hydrogen supply chains in the Gulf Cooperation Council (GCC). *Energy*, Vol. 299, Article: 131576.

Olabi, V., Alhajeri, A. and Jouhara, H. (2025). Designing a sustainable hydrogen supply chain network in the Gulf Cooperation Council (GCC) region: Multi-objective optimisation using a Kuwait case-study. *International Journal of Hydrogen Energy*, Vol. 142, pp. 994-1013.

Osei, L.K., Odoi-Yorke, F., Opoku, R., Baah, B., et al. (2024). Techno-economic viability of decentralised solar photovoltaic-based green hydrogen production for sustainable energy transition in Ghana. *Solar Compass*, Vol. 9, Article: 100068.

Oueslat, F. (2021). Hybrid renewable system based on solar wind and fuel cell energies coupled with diesel engines for Tunisian climate: TRNSYS simulation and economic assessment. *International Journal of Green Energy*, Vol. 18, No. 4, pp. 402-423.

Phillips, R. (2019). *Zero Gap Cell Design for Alkaline Electrolysis*. PhD Thesis, Energy Safety Research Institute, Swansea University.

Pinheiro, F.P., Gomes, D.M., Tofoli, F.L., Sampaio, R.F., et al. (2025). Techno-economic analysis of green hydrogen generation from combined wind and photovoltaic systems based on hourly temporal correlation. *International Journal of Hydrogen Energy*, Vol. 97, pp. 690-707.

Prasetyo, S.D., Trisnoaji, Y., Arifin, Z. and Mahadi, A.A. (2025). Harnessing unconventional resources for large-scale green hydrogen production: An economic and technological analysis in Indonesia. *Unconventional Resources*, Vol. 6, Article: 100174.

Qadeer, M.A., Zhang, X., Farid, M.A., Tanveer, M., et al. (2024). A review on fundamentals for designing hydrogen evolution electrocatalyst. *Journal of Power Sources*, Vol. 613, Article: 234856.

Qayoom, A., Ahmad, M.S., Fayaz, H., Qazi, A., et al. (2024). Recent advances in anion exchange membrane technology for water electrolysis: a review of progress and challenges. *Energy Science & Engineering*, Vol. 12, pp. 5328-5352.

Qazi, U.Y. (2022). Future of Hydrogen as an Alternative Fuel for Next-Generation Industrial Applications; Challenges and Expected Opportunities. *Energies*, Vol. 15, No. 13, Article: 4741.

Qolipour, M., Mostafaeipour, A. and Tousi, O.M. (2017). Techno-economic feasibility of a photovoltaic-wind power plant construction for electric and hydrogen production: a case study. *Renewable and Sustainable Energy Reviews*, Vol. 78, pp. 113-123.

Ram, K., Chand, S.S., Prasad, R., Mohammadi, A., et al. (2024). Microgrids for Green hydrogen production for fuel cell buses – a techno-economic analysis for Fiji. *Energy Conversion and Management*, Vol. 300, Article: 117928.

Ramadan, A. and Gabbar, H.A. (2024). Evaluation of hydrogen generation with hybrid renewable energy sources. *Applied Sciences*, Vol. 14, No. 14, Article: 6235.

Ramadan, A. and Gabbar, H.A. (2024). Evaluation of Hydrogen Generation with Hybrid Renewable Energy Sources. *Applied Sciences*, Vol. 14, Article: 6235.

Rambhujun, N., Salman, M.S., Wang, T., Pratthana, C., et al. (2020). Renewable hydrogen for the chemical industry. *MRS Energy and Sustainability*, Vol. 7, Article: E33.

Razi, F. and Dincer, I. (2022). Renewable energy development and hydrogen economy in MENA region: A review. *Renewable and Sustainable Energy Reviews*, Vol. 168, Article: 112763.

Reda, B., Elzamar, A.A., AlFazzani, S. and Ezzat, S.M. (2024). Green hydrogen as a source of renewable energy: a step towards sustainability, an overview. *Environment, Development and Sustainability*, https://doi.org/10.1007/s10668-024-04892-z.

Ren, Z., Wang, J., Yu, Z., Zhang, C., et al. (2022). Experimental studies and modeling of a 250-kW alkaline water electrolyzer for hydrogen production. *Journal of Power Sources*, Vol. 544, Article: 231886.

Riaz, M.A., Trogadas, P., Ayme-Perrot, D., Sachs, C., et al. (2025). Water electrolysis technologies: the importance of new cell designs and fundamental modelling to guide industrial-scale development. *Energy & Environmental Science*, Vol. 18, pp. 5190-5214.

Riemer, M. and Duscha, V. (2023). Carbon capture in blue hydrogen production is not where it is supposed to be - Evaluating the gap between practical experience and literature estimates. *Applied Energy*, Vol. 349, Article: 121622.

Rizk-Allah, R.M., Hassan, I.A., Snasel, V. and Hassanien, A.E. (2024). An optimal standalone wind-photovoltaic power plant system for green hydrogen generation: Case study for hydrogen refuelling station. *Results in Engineering*, Vol. 22, Article: 102234.

Rodriguez, J. and Amores, E. (2020). CFD Modeling and Experimental Validation of an Alkaline Water Electrolysis Cell for Hydrogen Production. *Processes*, Vol. 8, No. 12, Article: 1634.

Roy, D., Bhowmik, M. and Roskilly, A.P. (2024). Technoeconomic, environmental and multi criteria decision making investigations for optimisation of off-grid hybrid renewable energy system with green hydrogen production. *Journal of Cleaner Production*, Vol. 443, Article: 141033.

Roy, R., Antonini, G., Hayibo, K.S., Rahman, M.M., et al. (2025). Comparative techno-environmental analysis of grey, blue, green/yellow and pale-blue hydrogen production. *International Journal of Hydrogen Energy*, Vol. 116, pp. 200-210.

Saadat, Z., Farazmand, M. and Sameti, M. (2024). Integration of underground green hydrogen storage in hybrid energy generation. *Fuel*, Vol. 371, Part A, Article: 131899.

Sadeq, A.M., Homod, R.Z., Hussein, A.K., Togun, H., et al. (2024). Hydrogen energy systems: Technologies, trends, and future prospects. *Science of The Total Environment*, Vol. 939, Article: 173622.

Sahin, M.E. (2024). An Overview of Different Water Electrolyzer Types for Hydrogen Production. *Energies*, Vol. 17, No. 19, Article: 4944.

Saleem, M.S. and Abas, N. (2024). Optimizing renewable polygeneration: A synergetic approach harnessing solar and wind energy systems. *Results in Engineering*, Vol. 21, Article: 101743.

Sanchez, M., Amores, E., Rodriguez, L. and Clemente-Jul, C. (2018). Semi-empirical model and experimental validation for the performance evaluation of a 15-kW alkaline water electrolyzer. *International Journal of Hydrogen Energy*, Vol. 43, No. 45, pp. 20332-20345.

Sanfilippo, A., Vermeersch, M. and Benito, V.B. (2024). Energy transition strategies in the Gulf Cooperation Council countries. *Energy Strategy Reviews*, Vol. 55, Article: 101512.

Santos, D.M.F., Sequeira, C.A.C. and Figueiredo, J.L. (2013). Hydrogen production by alkaline water electrolysis. *Quimica Nova*, Vol. 36, No. 8, pp. 1176-1193.

Sayer, M., Ajanovic, A. and Haas, R. (2024). Economic and environmental assessment of different hydrogen production and transportation modes. *International Journal of Hydrogen Energy*, Vol. 65, pp. 626-638.

Sebbahi, S., Assila, A., Belghiti, A.A., Laasri, S., et al. (2024). A comprehensive review of recent advances in alkaline water electrolysis for hydrogen production. *International Journal of Hydrogen Energy*, Vol. 82, pp. 583-599.

Shafiee, Z., Samani, B.H. and Taki, K. (2024). Simulation of a Combined Solar-Wind-Hydrogen System for Energy Supply to a Dried Fruit Factory in Iran. *Journal of Renewable Energy and Environment*, Vol. 12, No. 1, pp. 54-66.

Sharifian, S. and Harasek, M. (2015). Dynamic Simulation of Hydrogen Generation from Renewable Energy Sources. *Chemical Engineering Transactions*, Vol. 45, pp. 409-414.

Shash, A.Y., Abdeltawab, N.M., Hassan, D.M., Darweesh, M., et al. (2025). Computational Methods, Artificial Intelligence, Modeling, and Simulation Applications in Green Hydrogen Production Through Water Electrolysis: A Review. *Hydrogen*, Vol. 6, No. 2, Article: 21.

Shehabi, M. and Dally, B. (2021). *Opportunity and Cost of Green Hydrogen in Kuwait: a preliminary assessment*. OIES-KFAS workshop 2021, Oxford Institute for Energy Studies. [Online] Visited on 20/04/2026, available at: https://www.oxfordenergy.org/wpcms/wp-content/uploads/2021/04/Opportunity-and-Cost-of-Green-Hydrogen-in-Kuwait-A-Preliminary-Assessment.pdf

Shehzad, B., Latif, S., Wahab, A., Shafique, M.U., et al. (2026). Progress and challenges in alkaline water electrolysis for sustainable hydrogen production. *Discover Chemistry*, Vol. 3, Article: 118.

Shin, H., Jang, D., Lee, S., Cho, H.S., et al. (2023). Techno-economic evaluation of green hydrogen production with low-temperature water electrolysis technologies directly coupled with renewable power sources. *Energy Conversion and Management*, Vol. 286, Article: 117083.

Simunovic, J., Pivac, I. and Barbir, F. (2022) Techno-economic assessment of hydrogen refueling station: A case study in Croatia. *International Journal of Hydrogen Energy*, Vol. 47, No. 57, pp. 24155-24168.

Singh, A., Baredar, P. and Gupta, B. (2017). Techno-economic feasibility analysis of hydrogen fuel cell and solar photovoltaic hybrid renewable energy system for academic research building. *Energy Conversion and Management*, Vol. 145, pp. 398-414.

Sorgulu, F. and Dincer, I. (2022). Analysis and techno-economic assessment of renewable hydrogen production and blending into natural gas for better sustainability. *International Journal of Hydrogen Energy*, Vol. 47, No. 46, pp. 19977-19988.

Squadrito, G., Maggio, G. and Nicita, A. (2023). The green hydrogen revolution. *Renewable Energy*, Vol. 216, Article: 119041.

Srettiwat, N., Safari, M., Olcay, H. and Malina, R. (2023). A techno-economic evaluation of solar-powered green hydrogen production for sustainable energy consumption in Belgium. *International Journal of Hydrogen Energy*, Vol. 48, No. 100, pp. 39731-39746.

Stenina, I. and Yaroslavtsev, A. (2023). Modern Technologies of Hydrogen Production. *Processes*, Vol. 11, Article: 56.

Superchi, F., Papi, F., Mannelli, A., Balduzzi, F., et al. (2023). Development of a reliable simulation framework for techno-economic analyses on green hydrogen production from wind farms using alkaline electrolyzers. *Renewable Energy*, Vol. 207, pp. 731-742.

Tatti, R., Petrollese, M., Lucariello, M., Serra, F., et al. (2024). Hydrogen storage integrated in off-grid power systems: a case study. *International Journal of Hydrogen Energy*, Vol. 79, pp. 164-176.

Temiz, M. and Dincer, I. (2021). Techno-economic analysis of Green hydrogen ferries with a floating photovoltaic based marine fuelling station. *Energy Conversion and Management*, Vol. 247, Article: 114760.

Tijani, A.S., Yusup, N.A.B. and Abdol Rahim, A. H. (2014). Mathematical modelling and simulation analysis of advanced alkaline electrolyzer system for hydrogen production. *Procedia Technology*, Vol. 15, pp. 799-807.

Tuysuz, H. (2024). Alkaline Water Electrolysis for Green Hydrogen Production. *Accounts of Chemical Research*, Vol 57, No. 4, pp. 558-567.

Tye, M.R., Haupt, S.E., Gilleland, E., Kalb, C., et al. (2019). Assessing Evidence for Weather Regimes Governing Solar Power Generation in Kuwait. *Energies*, Vol. 12, No. 23, Article: 4409.

Ulleberg, Ø. (2003). Modeling of advanced alkaline electrolyzers: a system simulation approach. *International Journal of Hydrogen Energy*, Vol. 28, No. 1, pp. 21-33.

Vedrtnam, A., Kalauni, K. and Pahwa, R. (2025). Water Electrolysis Technologies and Their Modeling Approaches: A Comprehensive Review. *Eng*, Vol. 6, Article: 81.

Verma, R. and Taneja, T. (2024). Hydrogen Fuel Cell Technology: Applications in Automotive Industry. *Journal of Advanced Research in Automotive Technology & Transportation System*, Vol. 8, No. 1, pp. 7-13.

Vincent, I. and Bessarabov, D. (2018). Low-cost hydrogen production by anion exchange membrane electrolysis: A review. *Renewable and Sustainable Energy Reviews*, Vol. 81, No. 2, pp. 1690-1704.

Wallnofer-Ogris, E., Grimmer, I., Ranz, M., Hoglinger, M., et al. (2024). A review on understanding and identifying degradation mechanisms in PEM water electrolysis cells: Insights for stack application, development, and research. *International Journal of Hydrogen Energy*, Vol. 65, pp. 381-397.

Wang, J., Wen, J., Wang, J., Yang, B., et al. (2024). Water electrolyzer operation scheduling for green hydrogen production: A review. *Renewable and Sustainable Energy Reviews*, Vol. 203, Article: 114779

Wang, T., Cao, X. and Jiao, L. (2022). PEM water electrolysis for hydrogen production: fundamentals, advances, and prospects review. *Carbon Neutrality*, Vol. 1, Article: 21.

Wei, D., Zhang, L., Alotaibi, A.A., Fang, J., et al. (2022). Transient simulation and comparative assessment of a hydrogen production and storage system with solar and wind energy using TRNSYS. *International Journal of Hydrogen Energy*, Vol. 47, No. 62, pp. 26646-26653.

Wind-turbine-models (2025). *Nordex N117 Gamma*. [Online] Visited on 15/09/2024, at: https://en.wind-turbine-models.com/turbines/96-nordex-n117-gamma

Wu, Q. and Li, C. (2022). Economy-environment-energy benefit analysis for green hydrogen based integrated energy system operation under carbon trading with a robust optimization model. *Journal of Energy Storage*, Vol. 55, Part B, Article: 105560.

Xia, Y., Cheng, H., He, H. and Wei, W. (2023). Efficiency and consistency enhancement for alkaline electrolyzers driven by renewable energy sources. *Communications Engineering*, vol. 2, Article: 22.

Xu, Q., Zhang, L., Zhang, J., Wang, J., et al. (2024). Anion Exchange Membrane Water Electrolyzer: Electrode Design, Lab-Scaled Testing System and Performance Evaluation. *EnergyChem*, Vol. 4, No. 5, Article: 100087.

Yaici, W. and Longo, M. (2025). Microgrid hybrid renewable energy systems with hydrogen and battery storage options for residential buildings: A feasibility analysis in Canada. *Journal of Cleaner Production*, Vol. 519, Article: 145974.

Yang, B., Zhang, R., Shao, Z. and Zhang, C. (2023). The economic analysis for hydrogen production cost towards electrolyzer technologies: Current and future competitiveness. *International Journal of Hydrogen Energy*, Vol. 48, No. 37, pp. 13767-13779.

Yates, J., Daiyan, R., Patterson, R., Egan, R., et al. (2020). Techno-economic analysis of hydrogen electrolysis from Off-Grid Stand-Alone photovoltaics incorporating uncertainty analysis. *Cell Reports Physical Science*, Vol. 1, No. 10, Article: 100209.

Yodwong, B., Guilbert, D., Phattanasak, M., Kaewmane, W., et al. (2020). Faraday's Efficiency Modeling of a Proton Exchange Membrane Electrolyzer Based on Experimental Data. *Energies*, Vol. 13, No. 18, Article: 4792.

Zghaibeh, M., Barhoumi, E.M., Okonkwo, P.C., Ben Belgacem, I., et al. (2022). Analytical model for a techno-economic assessment of green hydrogen production in photovoltaic power station case study Salalah city-Oman. *International Journal of Hydrogen Energy*, Vol. 47, pp. 14171-14179.

Zhou, Z., Wang, X., Yu, Z., Bian, J., et al. (2024). Capacity Configuration and Economic Analysis of Integrated Wind-Solar-Hydrogen-Storage System. *3rd International Conference on Energy, Power and Electrical Technology (ICEPET)*, pp. 417-423.

Zhu, X., Zhang, Y., Bin, S., Chen, Z., et al. (2024). Effects of key design and operating parameters on the performance of the PEM water electrolysis for hydrogen production. *Renewable Energy*, Vol. 235, Article: 121290.

Zou, Z., Dastafkan, K., Shao, Y., Zhao, C., et al. (2024). Electrocatalysts for alkaline water electrolysis at ampere-level current densities: a review. *International Journal of Hydrogen Energy*, Vol. 51, Part A, pp. 667-684.

Appendix-A: **Excel Model Spreadsheets**

A.1 Airport Site

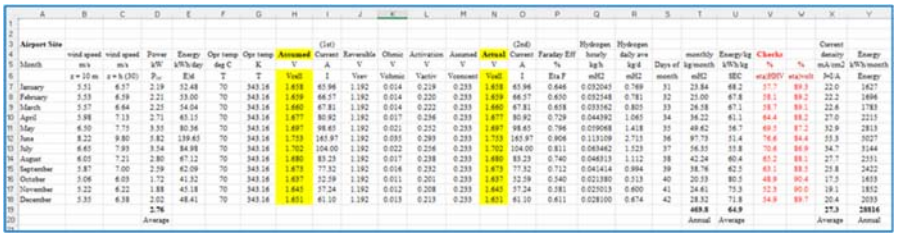

Airport Site	wind speed	wind speed	Power	Energy	Opr temp	Opr temp	Assumed	(1st) Current	Reversible	Ohmic	Activation	Assumed	Actual	(2nd) Current	Faraday Eff	Hydrogen hourly	Hydrogen daily ave		monthly	Energy/kg	Checks		Current density	Energy
Month	m/s	m/s	kW	kWh/day	deg C	K	V	A	V	V	V	V	V	A	%	kg/h	kg/d	Days of month	kg/month	kWh/kg	%	%	mA/cm2	kWh/month
	z = 10 m	z = h (30)	P_{kW}	Etd	T	T	Vcell	I	Vrev	Vohmic	Vactiv	Vconcent	Vcell	I	Eta F	mH2	mH2	month	mH2	SEC	eta/HHV	eta/volt	J=I/A	Energy
January	5.51	6.57	2.19	52.48	70	343.16	1.658	65.96	1.192	0.014	0.219	0.233	1.658	65.96	0.646	0.092043	0.769	31	23.84	68.2	37.7	89.3	22.0	1627
February	5.53	6.59	2.21	53.00	70	343.16	1.659	66.57	1.192	0.014	0.220	0.233	1.659	66.57	0.650	0.092548	0.781	32	25.00	67.8	38.1	89.2	22.2	1696
March	5.57	6.64	2.25	54.04	70	343.16	1.660	67.81	1.192	0.014	0.222	0.233	1.660	67.81	0.658	0.093562	0.803	33	26.58	67.1	38.7	89.1	22.6	1783
April	5.98	7.13	2.71	65.15	70	343.16	1.677	80.92	1.192	0.017	0.236	0.233	1.677	80.92	0.729	0.044392	1.065	34	36.22	61.1	64.4	88.2	27.0	2215
May	6.50	7.75	3.35	80.36	70	343.16	1.697	98.65	1.192	0.021	0.252	0.233	1.697	98.65	0.796	0.059068	1.418	35	49.62	56.7	69.5	87.2	32.9	2813
June	8.22	9.80	5.82	139.65	70	343.16	1.753	165.97	1.192	0.035	0.289	0.233	1.753	165.97	0.906	0.113109	2.713	36	97.73	51.4	76.6	84.4	55.3	3027
July	8.65	7.93	5.54	84.98	70	343.16	1.702	104.00	1.192	0.022	0.256	0.233	1.702	104.00	0.811	0.083462	1.523	37	56.35	53.8	70.6	84.9	34.7	3144
August	8.05	7.21	2.80	67.12	70	343.16	1.680	83.23	1.192	0.017	0.238	0.233	1.680	83.23	0.740	0.046313	1.112	38	42.24	60.4	65.2	88.1	27.7	2351
September	5.87	7.00	2.59	62.09	70	343.16	1.673	77.32	1.192	0.016	0.232	0.233	1.673	77.32	0.712	0.041414	0.994	39	38.76	62.5	63.1	88.3	25.8	2422
October	5.06	6.03	1.72	41.32	70	343.16	1.637	52.59	1.192	0.011	0.201	0.233	1.637	52.59	0.540	0.021980	0.513	40	20.53	80.5	48.9	90.4	17.5	1410
November	5.22	6.22	1.88	45.14	70	343.16	1.645	57.24	1.192	0.012	0.208	0.233	1.645	57.24	0.581	0.025013	0.600	41	24.61	75.3	52.3	90.0	19.1	1852
December	5.35	6.38	2.02	48.41	70	343.16	1.651	61.10	1.192	0.013	0.213	0.233	1.651	61.10	0.611	0.028100	0.674	42	28.32	71.8	54.9	89.7	20.4	2033
			2.76																**469.8**	**64.9**			**27.3**	**28816**
			Average																Annual	Average			Average	Annual

A.2 Wafra Site

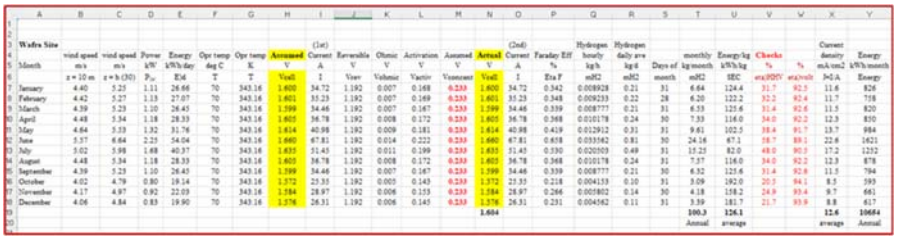

Wafra Site	wind speed	wind speed	Power	Energy	Opr temp	Opr temp	Assumed	(1st) Current	Reversible	Ohmic	Activation	Assumed	Actual	(2nd) Current	Faraday Eff	Hydrogen hourly	Hydrogen daily ave		monthly	Energy/kg	Checks		Current density	Energy
Month	m/s	m/s	kW	kWh/day	deg C	K	V	A	V	V	V	V	V	A	%	kg/h	kg/d	Days of month	kg/month	kWh/kg	%	%	mA/cm2	kWh/month
	z = 10 m	z = h (30)	P_{kW}	Etd	T	T	Vcell	I	Vrev	Vohmic	Vactiv	Vconcent	Vcell	I	Eta F	mH2	mH2	month	mH2	SEC	eta/HHV	eta/volt	J=I/A	Energy
January	4.40	5.25	1.11	26.66	70	343.16	1.600	34.72	1.192	0.007	0.168	0.233	1.600	34.72	0.342	0.058928	0.21	31	6.64	124.4	31.7	92.5	11.6	828
February	4.42	5.27	1.13	27.07	70	343.16	1.601	35.23	1.192	0.007	0.169	0.233	1.601	35.23	0.348	0.059233	0.22	28	6.20	122.2	32.2	92.4	11.7	758
March	4.39	5.23	1.10	26.43	70	343.16	1.599	34.46	1.192	0.007	0.167	0.233	1.599	34.46	0.339	0.058777	0.21	31	6.53	125.6	31.4	92.6	11.5	820
April	4.48	5.34	1.18	28.33	70	343.16	1.605	36.78	1.192	0.008	0.172	0.233	1.605	36.78	0.368	0.010178	0.24	30	7.33	116.0	34.0	92.2	12.3	870
May	4.64	5.53	1.32	31.78	70	343.16	1.614	40.98	1.192	0.009	0.181	0.233	1.614	40.98	0.419	0.012912	0.31	31	9.61	102.5	38.4	91.7	13.7	984
June	5.57	6.64	2.25	54.04	70	343.16	1.660	67.81	1.192	0.014	0.222	0.233	1.660	67.81	0.658	0.033562	0.81	30	24.16	67.1	38.7	89.1	22.6	1621
July	5.02	5.98	1.68	40.37	70	343.16	1.635	51.43	1.192	0.011	0.199	0.233	1.635	51.43	0.330	0.020503	0.49	31	15.25	82.0	48.0	90.3	17.2	1232
August	4.48	5.34	1.18	28.33	70	343.16	1.605	36.78	1.192	0.008	0.172	0.233	1.605	36.78	0.368	0.010178	0.24	31	7.57	116.0	34.0	92.2	12.3	878
September	4.39	5.23	1.10	26.43	70	343.16	1.599	34.46	1.192	0.007	0.167	0.233	1.599	34.46	0.339	0.008777	0.21	30	6.32	125.6	31.4	92.6	11.5	794
October	4.02	4.79	0.80	19.14	70	343.16	1.572	25.35	1.192	0.005	0.143	0.233	1.572	25.35	0.218	0.004153	0.10	31	3.09	192.0	20.5	94.1	8.5	593
November	4.17	4.97	0.92	22.03	70	343.16	1.584	28.97	1.192	0.006	0.153	0.233	1.584	28.97	0.266	0.005802	0.14	30	4.18	158.2	24.9	93.4	9.7	661
December	4.06	4.84	0.83	19.90	70	343.16	1.576	26.31	1.192	0.006	0.145	0.233	1.576	26.31	0.231	0.004562	0.11	31	3.39	181.7	21.7	93.9	8.8	617
							1.604												**100.3**	**126.1**			**12.6**	**10684**
																			Annual	average			average	Annual

A.3 Abdaly Site

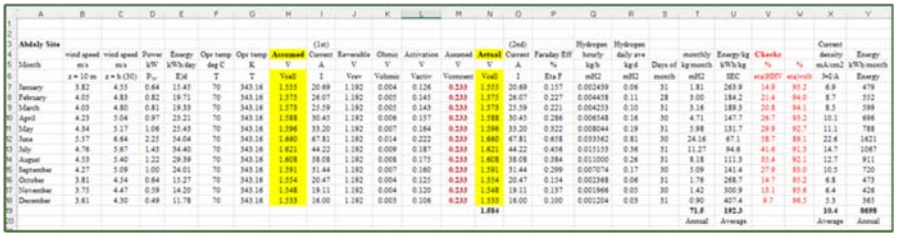

Abdaly Site	wind speed	wind speed	Power	Energy	Opr temp	Opr temp	Assumed	(1st) Current	Reversible	Ohmic	Activation	Assumed	Actual	(2nd) Current	Faraday Eff	Hydrogen hourly	Hydrogen daily ave		monthly	Energy/kg	Checks		Current density	Energy
Month	m/s	m/s	kW	kWh/day	deg C	K	V	A	V	V	V	V	V	A	%	kg/h	kg/d	Days of month	kg/month	kWh/kg	%	%	mA/cm2	kWh/month
	z = 10 m	z = h (30)	P_{kW}	Etd	T	T	Vcell	I	Vrev	Vohmic	Vactiv	Vconcent	Vcell	I	Eta F	mH2	mH2	month	mH2	SEC	eta/HHV	eta/volt	J=I/A	Energy
January	3.82	4.55	0.64	15.45	70	343.16	1.555	20.69	1.192	0.004	0.126	0.233	1.555	20.69	0.157	0.002439	0.06	31	1.81	263.9	14.9	93.2	6.9	479
February	4.01	4.83	0.82	19.71	70	343.16	1.575	26.07	1.192	0.005	0.145	0.233	1.575	26.07	0.227	0.004458	0.11	28	3.00	184.2	21.4	94.0	8.7	552
March	4.03	4.80	0.81	19.33	70	343.16	1.573	25.59	1.192	0.005	0.143	0.233	1.573	25.59	0.221	0.004253	0.10	31	3.16	189.3	20.8	94.1	8.5	599
April	4.23	5.04	0.97	23.21	70	343.16	1.588	30.45	1.192	0.006	0.157	0.233	1.588	30.45	0.286	0.006548	0.16	30	4.71	147.7	26.7	93.2	10.1	696
May	4.34	5.17	1.06	25.43	70	343.16	1.596	33.20	1.192	0.007	0.164	0.233	1.596	33.20	0.322	0.008044	0.19	31	5.98	131.7	29.9	92.7	11.1	788
June	5.57	6.64	2.25	54.04	70	343.16	1.660	67.81	1.192	0.014	0.222	0.233	1.660	67.81	0.658	0.033562	0.81	30	24.16	67.1	38.7	89.1	22.6	1621
July	4.76	5.67	1.43	34.40	70	343.16	1.621	44.22	1.192	0.009	0.187	0.233	1.621	44.22	0.456	0.015153	0.36	31	11.27	94.6	41.6	91.3	14.7	1067
August	4.53	5.40	1.22	29.39	70	343.16	1.608	38.08	1.192	0.008	0.175	0.233	1.608	38.08	0.384	0.011000	0.26	31	8.18	111.3	35.4	92.1	12.7	911
September	4.27	5.09	1.00	24.01	70	343.16	1.591	31.44	1.192	0.007	0.160	0.233	1.591	31.44	0.299	0.007074	0.17	30	5.09	141.4	27.9	93.0	10.5	720
October	3.81	4.54	0.64	15.27	70	343.16	1.554	20.47	1.192	0.004	0.125	0.233	1.554	20.47	0.154	0.002368	0.06	31	1.76	268.7	14.7	93.2	6.8	473
November	3.75	4.47	0.59	14.20	70	343.16	1.548	19.11	1.192	0.004	0.120	0.233	1.548	19.11	0.137	0.001966	0.05	30	1.42	300.9	13.1	93.6	6.4	426
December	3.61	4.30	0.49	11.78	70	343.16	1.535	16.00	1.192	0.003	0.106	0.233	1.535	16.00	0.100	0.001204	0.03	31	0.90	407.4	9.7	94.3	5.3	365
							1.584												**71.8**	**192.3**			**10.4**	**8698**
																			Annual	Average			Average	Annual

A.4 Change of Current Density

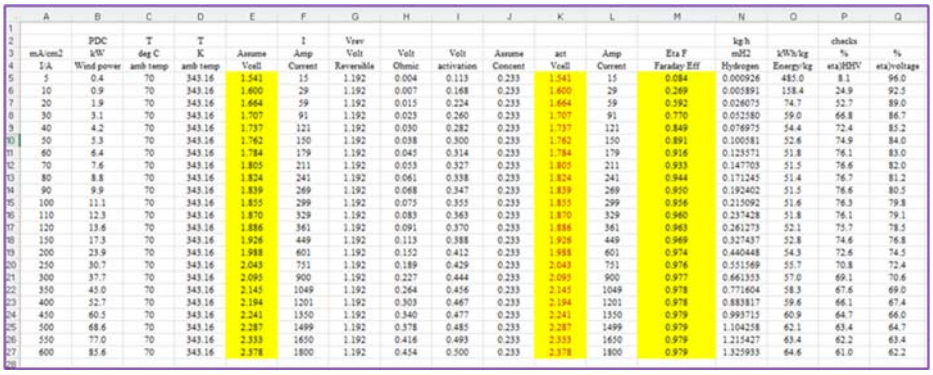

	PDC	T	T		I	Vrev									kg/h		checks	
mA/cm2	kW	deg C	K	Assume	Amp	Volt	Volt	Volt	Assume	act	Amp	Eta F	mH2	kWh/kg	%	%
I/A	Wind power	amb temp	amb temp	Vcell	Current	Reversible	Ohmic	activation	Concent	Vcell	Current	Faraday Eff	Hydrogen	Energy/kg	eta/HHV	eta/voltage
5	0.4	70	343.16	1.541	15	1.192	0.004	0.113	0.233	1.541	15	0.084	0.000926	485.0	8.1	96.0
10	0.9	70	343.16	1.600	29	1.192	0.007	0.168	0.233	1.600	29	0.269	0.005891	158.4	24.9	92.5
20	1.9	70	343.16	1.664	59	1.192	0.015	0.224	0.233	1.664	59	0.592	0.026075	74.7	52.7	89.0
30	3.1	70	343.16	1.707	91	1.192	0.023	0.260	0.233	1.707	91	0.770	0.052580	59.0	66.8	86.7
40	4.2	70	343.16	1.737	121	1.192	0.030	0.282	0.233	1.737	121	0.849	0.076975	54.4	72.4	85.2
50	5.3	70	343.16	1.762	150	1.192	0.038	0.300	0.233	1.762	150	0.891	0.100581	52.6	74.9	84.0
60	6.4	70	343.16	1.784	179	1.192	0.045	0.314	0.233	1.784	179	0.916	0.123571	51.8	76.1	83.0
70	7.6	70	343.16	1.805	211	1.192	0.053	0.327	0.233	1.805	211	0.933	0.147703	51.5	76.6	82.0
80	8.8	70	343.16	1.824	241	1.192	0.061	0.338	0.233	1.824	241	0.944	0.171245	51.4	76.7	81.2
90	9.9	70	343.16	1.839	269	1.192	0.068	0.347	0.233	1.839	269	0.950	0.192402	51.5	76.6	80.5
100	11.1	70	343.16	1.855	299	1.192	0.075	0.355	0.233	1.855	299	0.956	0.215092	51.6	76.3	79.8
110	12.3	70	343.16	1.870	329	1.192	0.083	0.363	0.233	1.870	329	0.960	0.237428	51.8	76.1	79.1
120	13.6	70	343.16	1.886	361	1.192	0.091	0.370	0.233	1.886	361	0.963	0.261273	52.1	75.7	78.5
130	17.3	70	343.16	1.926	449	1.192	0.113	0.388	0.233	1.926	449	0.969	0.327437	52.8	74.6	76.8
200	23.9	70	343.16	1.988	601	1.192	0.152	0.412	0.233	1.988	601	0.974	0.440448	54.5	72.6	74.5
250	30.7	70	343.16	2.043	751	1.192	0.189	0.429	0.233	2.043	751	0.976	0.551569	55.7	70.8	72.4
300	37.7	70	343.16	2.095	900	1.192	0.227	0.444	0.233	2.095	900	0.977	0.661353	57.0	69.1	70.6
350	45.0	70	343.16	2.145	1049	1.192	0.264	0.456	0.233	2.145	1049	0.978	0.771604	58.3	67.6	69.0
400	52.7	70	343.16	2.194	1201	1.192	0.303	0.467	0.233	2.194	1201	0.978	0.883817	59.6	66.1	67.4
450	60.5	70	343.16	2.241	1350	1.192	0.340	0.477	0.233	2.241	1350	0.979	0.993715	60.9	64.7	66.0
500	68.6	70	343.16	2.287	1499	1.192	0.378	0.485	0.233	2.287	1499	0.979	1.104258	62.1	63.4	64.7
550	77.0	70	343.16	2.333	1650	1.192	0.416	0.493	0.233	2.333	1650	0.979	1.215427	63.4	62.2	63.4
600	85.6	70	343.16	2.378	1800	1.192	0.454	0.500	0.233	2.378	1800	0.979	1.325933	64.6	61.0	62.2

Appendix-B: **TRNSYS Output Files**

B.1 Airport Site

Kuwait Airport		
Turbine		
Rotor Height:	30	[m]
Rotor Diameter:	7	[m]
Rated Power:	10	[kW]
Rated Windspeed:	15.6	[m/s]
Turbine Type:	Bergey BWC Excel 10	
Total Energy Generated:	26008.901	[kWh]
Peak Instantaneous Absolute Value:	10	[kW]
Run time:	8375	[hrs]
Power Coefficient:		
Minimum Value of Power Coefficient:	0	[0..1]
Time of Minimum Value:	48	[hrs]
Maximum Value of Power Coefficient:	0.326	[0..1]
Time of Maximum Value:	35	[hrs]
|----------		
| Unit ID 11 (Type:160) Equipment Tag: Electrolyser		
|----------		
Electrode Area:	0.3	[cm2]
Number of Cells in Series:	0	[-]
Number of Stacks in Parallel:	0	[-]
Operating Temperature Mod	Given as input	
Total Current Drawn by Electrolyzer:	686135.494	[A]
Peak Instantaneous Absolute Value:	318.899	[A/h]
Run time:	8760	[hrs]
Total Electrolyzer Power Drawn:	860378	[kWh]
Peak Instantaneous Absolute Value:	8.465	[kW]
Run time:	3063	[hrs]
Total Hydrogen Production:	1809.228	[Nm3]
Peak Instantaneous Absolute Value:	2.055	[Nm3/h]
Run time:	3063	[hrs]
Total Oxygen Production:	904.614	[Nm3]
Peak Instantaneous Absolute Value:	1.027	[Nm3/h]
Run time:	3063	[hrs]
Total Heat Generated:	2519.2	[kWh]
Peak Instantaneous Absolute Value:	0.768	[kW]
Run time:	1557	[hrs]
Total Thermal Energy Losses:	2622.754	[kWh]
Peak Instantaneous Absolute Value:	0.299	[kW]
Run time:	8760	[hrs]
Total Auxiliary Cooling Energy:	-665.146	[kWh]
Peak Instantaneous Absolute Value:	0.469	[kW]
Run time:	304	[hrs]
Total Energy Storage Rate:	-1705.689	[kWh]
Peak Instantaneous Absolute Value:	0.299	[kW]
Run time:	0	[hrs]
Electrolyzer Voltage:		
Minimum Value of Electrolyzer Voltage:	24.701	[V]
Time of Minimum Value:	96	[hrs]
Maximum Value of Electrolyzer Voltage:	32.439	[V]
Time of Maximum Value:	4170	[hrs]
Overall Efficiency:		
Minimum Value of Overall Efficiency:	0	[0..1]
Time of Minimum Value:	96	[hrs]
Maximum Value of Overall Efficiency:	0.846	[0..1]
Time of Maximum Value:	2684	[hrs]
Energy Efficiency:		
Minimum Value of Energy Efficiency:	0	[0..1]
Time of Minimum Value:	96	[hrs]
Maximum Value of Energy Efficiency:	1.006	[0..1]
Time of Maximum Value:	4169	[hrs]
Faraday Efficiency:		
Minimum Value of Faraday Efficiency:	0	[0..1]
Time of Minimum Value:	96	[hrs]
Maximum Value of Faraday Efficiency:	0.929	[0..1]
Time of Maximum Value:	4170	[hrs]
Cooling Water Outlet Temperature:		
Minimum Value of Cooling Water Outlet Temperature:	13.929	[C]
Time of Minimum Value:	4169	[hrs]
Maximum Value of Cooling Water Outlet Temperature:	16.622	[C]
Time of Maximum Value:	4170	[hrs]

|----------		
| Unit ID 19 (Type:164) Equipment Tag: H2 Storage tank		
|----------		
Maximum Allowable Pressure:	200	[bar]
Tank Volume:	1	[m3]
Gas Molar Weight:	2.016	[kg/mol]
Gas Critical Temperature:	-240	[C]
Gas Critical Pressure:	1290000	[bar]
Gas Mode:	Real Gas	
Total Volume of Gas Dumped to Prevent Overpressure:	0	[Nm3]
Peak Instantaneous Absolute Value:	0	[Nm3/h]
Run time:	0	[hrs]
Volumetric Flow Rate Into Tank:		
Minimum Value of Volumetric Flow Rate Into Tank:	0	[Nm3/h]
Time of Minimum Value:	96	[hrs]
Maximum Value of Volumetric Flow Rate Into Tank:	2.055	[Nm3/h]
Time of Maximum Value:	4170	[hrs]
Volumetric Flow Rate Out of Tank:		
Minimum Value of Volumetric Flow Rate Out of Tank:	0.2	[Nm3/h]
Time of Minimum Value:	1	[hrs]
Maximum Value of Volumetric Flow Rate Out of Tank:	0.2	[Nm3/h]
Time of Maximum Value:	1	[hrs]
Gas Temperature:		
Minimum Value of Gas Temperature:	20	[C]
Time of Minimum Value:	1	[hrs]
Maximum Value of Gas Temperature:	20	[C]
Time of Maximum Value:	1	[hrs]
Gas Volume:		
Minimum Value of Gas Volume:	70.533	[Nm3]
Time of Minimum Value:	1	[hrs]
Maximum Value of Gas Volume:	144.841	[Nm3]
Time of Maximum Value:	6963	[hrs]
Gas Pressure:		
Minimum Value of Gas Pressure:	81.278	[bar]
Time of Minimum Value:	1	[hrs]
Maximum Value of Gas Pressure:	179.985	[bar]
Time of Maximum Value:	6963	[hrs]

B.2 Wafra Site

Wafra		
Turbine		
Rotor Height:	30	[m]
Rotor Diameter:	7	[m]
Rated Power:	10	[kW]
Rated Windspeed:	15.6	[m/s]
Turbine Type:	Bergey BWC Excel 10	
Total Energy Generated:	13597.808	[kWh]
Peak Instantaneous Absolute Value:	10	[kW]
Run time:	7676	[hrs]
Power Coefficient:		
Minimum Value of Power Coefficient:	0	[0..1]
Time of Minimum Value:	42	[hrs]
Maximum Value of Power Coefficient:	0.326	[0..1]
Time of Maximum Value:	37	[hrs]
|----------		
| Unit ID 11 (Type:160) Equipment Tag: Type160a		
|----------		
Electrode Area:	0.3	[cm2]
Number of Cells in Series:	0	[-]
Number of Stacks in Parallel:	0	[-]
Operating Temperature Mod	Given as input	
Total Current Drawn by Electrolyzer:	620393.603	[A]
Peak Instantaneous Absolute Value:	299.223	[A/h]
Run time:	8760	[hrs]
Total Electrolyzer Power Drawn:	9619.866	[kWh]
Peak Instantaneous Absolute Value:	8.465	[kW]
Run time:	4547	[hrs]
Total Hydrogen Production:	1815.376	[Nm3]
Peak Instantaneous Absolute Value:	2.055	[Nm3/h]
Run time:	4547	[hrs]
Total Oxygen Production:	907.688	[Nm3]
Peak Instantaneous Absolute Value:	1.027	[Nm3/h]
Run time:	4547	[hrs]
Total Heat Generated:	91.754	[kWh]
Peak Instantaneous Absolute Value:	0.768	[kW]
Run time:	847	[hrs]
Total Thermal Energy Losses:	2622.754	[kWh]
Peak Instantaneous Absolute Value:	0.299	[kW]
Run time:	8760	[hrs]
Total Auxiliary Cooling Energy:	-1269.623	[kWh]
Peak Instantaneous Absolute Value:	0.469	[kW]
Run time:	146	[hrs]
Total Energy Storage Rate:	-1261.377	[kWh]
Peak Instantaneous Absolute Value:	0.299	[kW]
Run time:	0	[hrs]
Electrolyzer Voltage:		
Minimum Value of Electrolyzer Voltage:	24.701	[V]
Time of Minimum Value:	322	[hrs]
Maximum Value of Electrolyzer Voltage:	32.439	[V]
Time of Maximum Value:	8470	[hrs]
Overall Efficiency:		
Minimum Value of Overall Efficiency:	0	[0..1]
Time of Minimum Value:	322	[hrs]
Maximum Value of Overall Efficiency:	0.846	[0..1]
Time of Maximum Value:	3993	[hrs]
Energy Efficiency:		
Minimum Value of Energy Efficiency:	0	[0..1]
Time of Minimum Value:	322	[hrs]
Maximum Value of Energy Efficiency:	1.006	[0..1]
Time of Maximum Value:	1	[hrs]
Faraday Efficiency:		
Minimum Value of Faraday Efficiency:	0	[0..1]
Time of Minimum Value:	322	[hrs]
Maximum Value of Faraday Efficiency:	0.929	[0..1]
Time of Maximum Value:	8470	[hrs]
Cooling Water Outlet Temperature:		
Minimum Value of Cooling Water Outlet Temperature:	13.929	[C]
Time of Minimum Value:	1	[hrs]
Maximum Value of Cooling Water Outlet Temperature:	16.622	[C]
Time of Maximum Value:	8470	[hrs]

|----------		
| Unit ID 19 (Type:164) Equipment Tag: Type164b		
|----------		
Maximum Allowable Pressure:	200	[bar]
Tank Volume:	1	[m3]
Gas Molar Weight:	2.016	[kg/mol]
Gas Critical Temperature:	-240	[C]
Gas Critical Pressure:	1290000	[bar]
Gas Mode:	Real Gas	
Total Volume of Gas Dumped to Prevent Overpressure:	0	[Nm3]
Peak Instantaneous Absolute Value:	0	[Nm3/h]
Run time:	0	[hrs]
Volumetric Flow Rate Into Tank:		
Minimum Value of Volumetric Flow Rate Into Tank:	0	[Nm3/h]
Time of Minimum Value:	322	[hrs]
Maximum Value of Volumetric Flow Rate Into Tank:	2.055	[Nm3/h]
Time of Maximum Value:	8470	[hrs]
Volumetric Flow Rate Out of Tank:		
Minimum Value of Volumetric Flow Rate Out of Tank:	0.2	[Nm3/h]
Time of Minimum Value:	1	[hrs]
Maximum Value of Volumetric Flow Rate Out of Tank:	0.2	[Nm3/h]
Time of Maximum Value:	1	[hrs]
Gas Temperature:		
Minimum Value of Gas Temperature:	20	[C]
Time of Minimum Value:	1	[hrs]
Maximum Value of Gas Temperature:	20	[C]
Time of Maximum Value:	1	[hrs]
Gas Volume:		
Minimum Value of Gas Volume:	69.592	[Nm3]
Time of Minimum Value:	1	[hrs]
Maximum Value of Gas Volume:	144.943	[Nm3]
Time of Maximum Value:	3285	[hrs]
Gas Pressure:		
Minimum Value of Gas Pressure:	80.125	[bar]
Time of Minimum Value:	1	[hrs]
Maximum Value of Gas Pressure:	180.133	[bar]
Time of Maximum Value:	3285	[hrs]

B.3 Abdaly Site

Abdaly		
Turbine		
Rotor Height:	30	[m]
Rotor Diameter:	7	[m]
Rated Power:	10	[kW]
Rated Windspeed:	15.6	[m/s]
Turbine Type:	Bergey BWC Excel 10	
Total Energy Generated:	10762.404	[kWh]
Peak Instantaneous Absolute Value:	10	[kW]
Run time:	7644	[hrs]
Power Coefficient:		
Minimum Value of Power Coefficient:	0	[0..1]
Time of Minimum Value:	1	[hrs]
Maximum Value of Power Coefficient:	0.326	[0..1]
Time of Maximum Value:	34	[hrs]
|----------		
| Unit ID 11 (Type:160) Equipment Tag: Type160a		
|----------		
Electrode Area:	0.3	[cm2]
Number of Cells in Series:	0	[-]
Number of Stacks in Parallel:	0	[-]
Operating Temperature Mod	Given as input	
Total Current Drawn by Electrolyzer:	607928.635	[A]
Peak Instantaneous Absolute Value:	318.899	[A/h]
Run time:	8760	[hrs]
Total Electrolyzer Power Drawn:	9758.376	[kWh]
Peak Instantaneous Absolute Value:	8.461	[kW]
Run time:	4794	[hrs]
Total Hydrogen Production:	1808.346	[Nm3]
Peak Instantaneous Absolute Value:	2.054	[Nm3/h]
Run time:	4794	[hrs]
Total Oxygen Production:	904.173	[Nm3]
Peak Instantaneous Absolute Value:	1.027	[Nm3/h]
Run time:	4794	[hrs]
Total Heat Generated:	61.469	[kWh]
Peak Instantaneous Absolute Value:	0.768	[kW]
Run time:	750	[hrs]
Total Thermal Energy Losses:	2622.754	[kWh]
Peak Instantaneous Absolute Value:	0.299	[kW]
Run time:	8760	[hrs]
Total Auxiliary Cooling Energy:	-1373.86	[kWh]
Peak Instantaneous Absolute Value:	0.468	[kW]
Run time:	111	[hrs]
Total Energy Storage Rate:	-1187.425	[kWh]
Peak Instantaneous Absolute Value:	0.299	[kW]
Run time:	0	[hrs]
Electrolyzer Voltage:		
Minimum Value of Electrolyzer Voltage:	24.701	[V]
Time of Minimum Value:	410	[hrs]
Maximum Value of Electrolyzer Voltage:	32.437	[V]
Time of Maximum Value:	3457	[hrs]
Overall Efficiency:		
Minimum Value of Overall Efficiency:	0	[0..1]
Time of Minimum Value:	410	[hrs]
Maximum Value of Overall Efficiency:	0.846	[0..1]
Time of Maximum Value:	3185	[hrs]
Energy Efficiency:		
Minimum Value of Energy Efficiency:	0	[0..1]
Time of Minimum Value:	410	[hrs]
Maximum Value of Energy Efficiency:	1.006	[0..1]
Time of Maximum Value:	1	[hrs]
Faraday Efficiency:		
Minimum Value of Faraday Efficiency:	0	[0..1]
Time of Minimum Value:	410	[hrs]
Maximum Value of Faraday Efficiency:	0.929	[0..1]
Time of Maximum Value:	3457	[hrs]
Cooling Water Outlet Temperature:		
Minimum Value of Cooling Water Outlet Temperature:	13.929	[C]
Time of Minimum Value:	1	[hrs]
Maximum Value of Cooling Water Outlet Temperature:	16.619	[C]
Time of Maximum Value:	3457	[hrs]

|----------		
| Unit ID 19 (Type:164) Equipment Tag: Type164b		
|----------		
Maximum Allowable Pressure:	200	[bar]
Tank Volume:	1	[m3]
Gas Molar Weight:	2.016	[kg/mol]
Gas Critical Temperature:	-240	[C]
Gas Critical Pressure:	1290000	[bar]
Gas Mode:	Real Gas	
Total Volume of Gas Dumped to Prevent Overpressure:	0	[Nm3]
Peak Instantaneous Absolute Value:	0	[Nm3/h]
Run time:	0	[hrs]
Volumetric Flow Rate Into Tank:		
Minimum Value of Volumetric Flow Rate Into Tank:	0	[Nm3/h]
Time of Minimum Value:	410	[hrs]
Maximum Value of Volumetric Flow Rate Into Tank:	2.054	[Nm3/h]
Time of Maximum Value:	3457	[hrs]
Volumetric Flow Rate Out of Tank:		
Minimum Value of Volumetric Flow Rate Out of Tank:	0.2	[Nm3/h]
Time of Minimum Value:	1	[hrs]
Maximum Value of Volumetric Flow Rate Out of Tank:	0.2	[Nm3/h]
Time of Maximum Value:	1	[hrs]
Gas Temperature:		
Minimum Value of Gas Temperature:	20	[C]
Time of Minimum Value:	1	[hrs]
Maximum Value of Gas Temperature:	20	[C]
Time of Maximum Value:	1	[hrs]
Gas Volume:		
Minimum Value of Gas Volume:	69.592	[Nm3]
Time of Minimum Value:	1	[hrs]
Maximum Value of Gas Volume:	144.951	[Nm3]
Time of Maximum Value:	2569	[hrs]
Gas Pressure:		
Minimum Value of Gas Pressure:	80.125	[bar]
Time of Minimum Value:	1	[hrs]
Maximum Value of Gas Pressure:	180.144	[bar]
Time of Maximum Value:	2569	[hrs]

Appendix-C: **HOMER Pro Results**

C.1 Airport Site

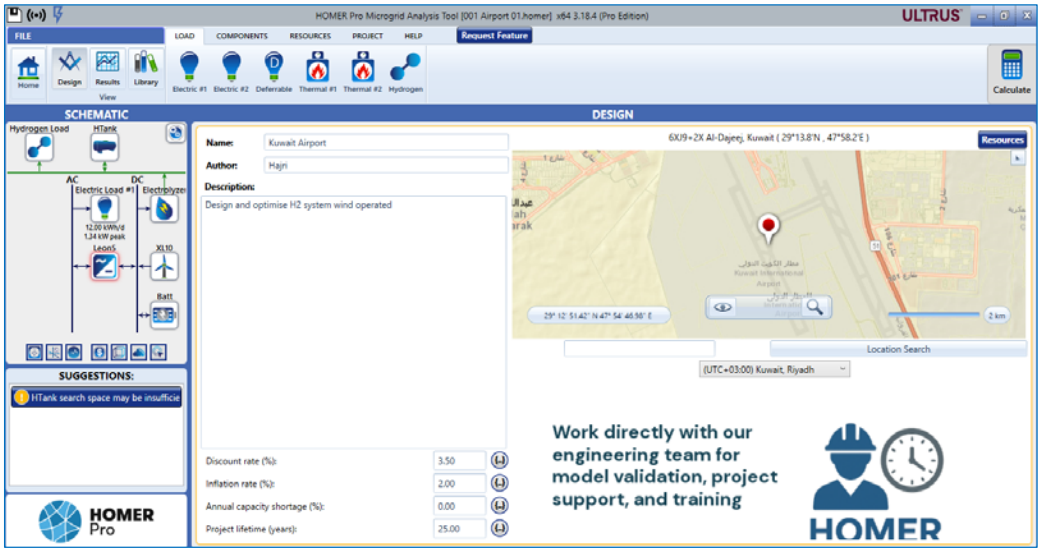

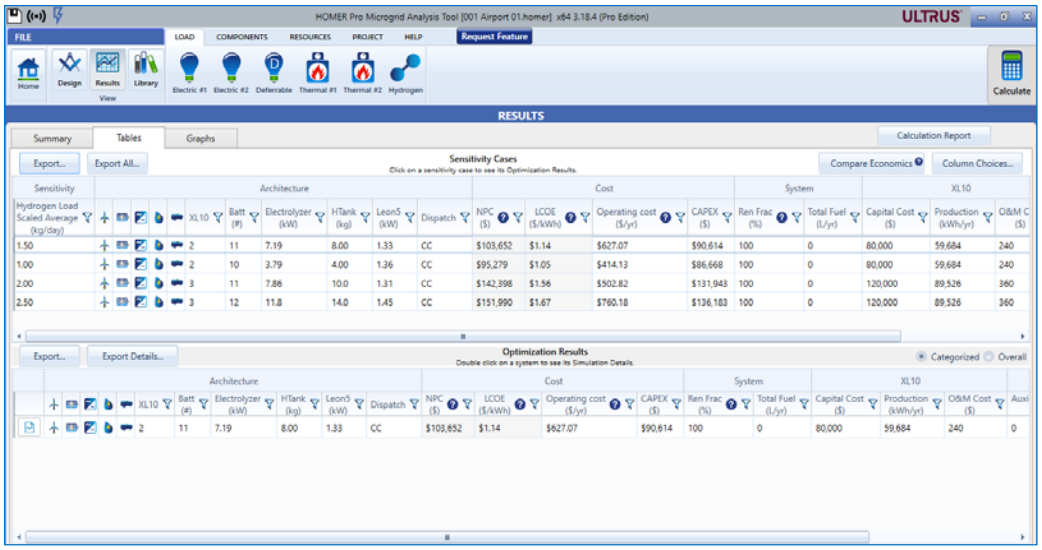

C.2 Wafra Site

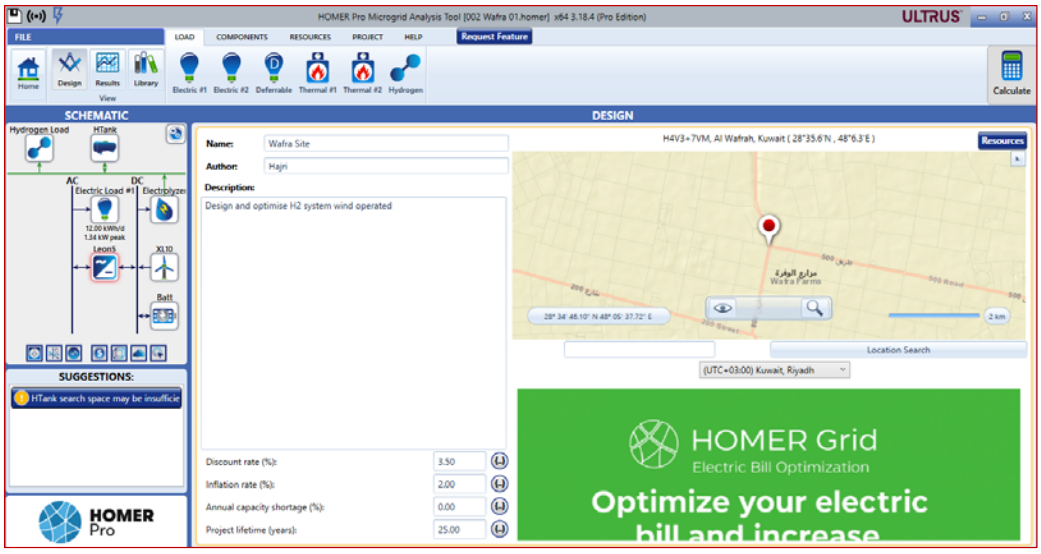

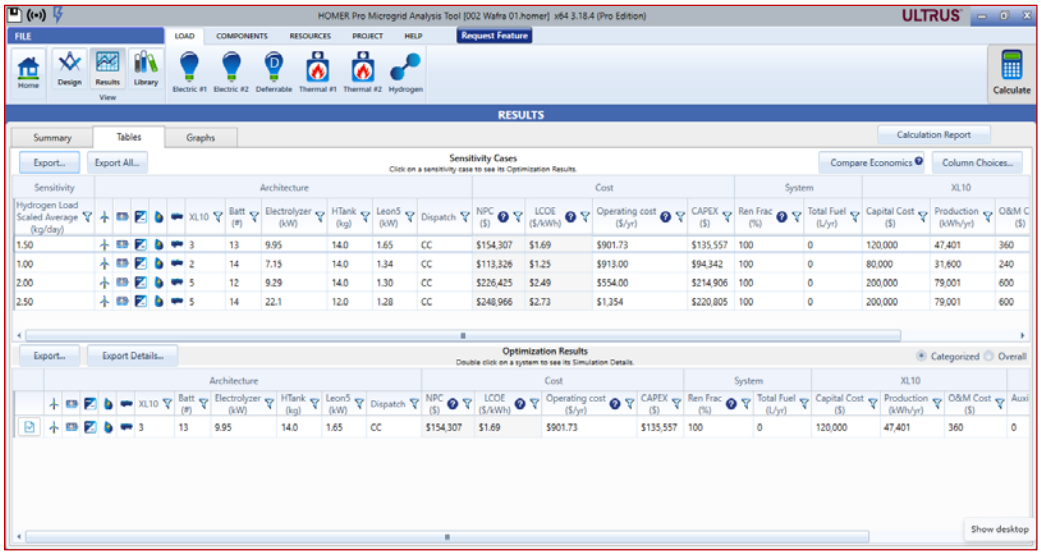

C.3 Abdaly Site